



HAL
open science

Effect of the support on the activity and morphology of hydrodesulfurization catalysts

Elizabeth Dominguez Garcia

► **To cite this version:**

Elizabeth Dominguez Garcia. *Effect of the support on the activity and morphology of hydrodesulfurization catalysts*. Organic chemistry. Normandie Université, 2017. English. NNT : 2017NORMC258 . tel-01729093

HAL Id: tel-01729093

<https://theses.hal.science/tel-01729093>

Submitted on 12 Mar 2018

HAL is a multi-disciplinary open access archive for the deposit and dissemination of scientific research documents, whether they are published or not. The documents may come from teaching and research institutions in France or abroad, or from public or private research centers.

L'archive ouverte pluridisciplinaire **HAL**, est destinée au dépôt et à la diffusion de documents scientifiques de niveau recherche, publiés ou non, émanant des établissements d'enseignement et de recherche français ou étrangers, des laboratoires publics ou privés.



Normandie Université

THESE

Pour obtenir le diplôme de doctorat

Spécialité CHIMIE

Préparée au sein de l'ENSICAEN et de l'UNICAEN

EFFECT OF THE SUPPORT ON THE ACTIVITY AND MORPHOLOGY OF HYDRODESULFURIZATION CATALYSTS

Présentée et soutenue par
Elizabeth DOMINGUEZ GARCIA

Thèse soutenue publiquement le 19 Décembre 2017
devant le jury composé de

M. Frédéric RICHARD	Maître de Conférences, HDR / Université de Poitiers	Rapporteur
M. Jeppe V. LAURITSEN	Professeur / Université d'Aarhus / Danemark	Rapporteur
Mme. Barbara GARCIA PAWELEC	Directrice de recherche / Université de Madrid	Rapporteur
Mme. Carole LAMONIER	Professeur des Universités / Université de Lille	Examineur
M. Arnaud TRAVERT	Professeur des Universités / Université Caen Normandie	Examineur
Mme. Françoise MAUGÉ	Directrice de recherche CNRS / Université Caen Normandie	Codirecteur de thèse
Mme. Laetitia OLIVIERO	Maître de Conférences, HDR / Université Caen Normandie	Directeur de thèse

Thèse dirigée par Laetitia OLIVIERO et Françoise MAUGÉ, Laboratoire Catalyse et Spectrochimie (LCS)



UNIVERSITÉ
CAEN
NORMANDIE

 **ENSICAEN**
ÉCOLE PUBLIQUE D'INGÉNIEURS
CENTRE DE RECHERCHE



to my parents

*“All geniuses are crazy
but not all crazies are geniuses”*

LIZ-

Acknowledgement

This section is dedicated to all people who in one or another way have been part of this long journey.

Firstly, I would like to thank my supervisors, Dr. Laetitia Oliviero and Dr. Françoise Maugé for giving me this great opportunity that has made me grow professionally and personally. I would also like to thank Dr. Jianjun Chen and Luz Zavala. Next, I would like to thank the members of the jury, Dr. Frédéric Richard, Dr. Carole Lamonier, Dr. Jeppe V. Lauritsen, Dr. Arnaud Travert and Dr. Bárbara Garcia Pawelec for agreeing to be participants of this moment.

Secondly, I would like to thank all LCS members where I have spent these three years. And especially I would like to thank those people who have been like my family during my stay in Caen, the members of the "Trappist team". Shashu, Juju, Dudu, Eddu, Kaka and of course my Paloma. Thanks to them, I did not feel alone being so far from my loved ones. Also I would like to thank Gitana because he was standing with me in the craziest moment and Stijn for the great moments on sulfur room.

Thirdly, I would like to thank all those people who have strongly influenced my professional life before the thesis. Dr. José Antonio Odriozola, Dr. Francisca Romero, Dr. Maribel Dominguez and Dr. Svetlana Ivannova. They do chemistry in a special way. Of course, I did not forget Dr. Cecilio Carreras. Finally I would like to thank some of the people, who unknowingly influenced me and thanks to their chemistry devotion, I started this long journey thanks to you, Federico Habela.

And finally, but not less extent, I would like to thank my family for their support and unconditional love during these three years and throughout our lives. Especially I would like to thank my parents for the education they taught me. Thanks to that I have overcome all the obstacles that have arisen along the way and will be presented in the future. Last but not least, I wanted to thank Manuel, for his great support, understanding and affection throughout all this time. And, Isabel Rodriguez who is always there for me.

Esta sección de la memoria va dedicada a todas aquellas personas que, de una u otra manera, han formado parte de este largo camino.

En primer lugar, me gustaría agradecer a mis directoras de tesis, Dra. Laetitia Oliviero y Dra. Françoise Maugé por darme esta gran oportunidad que me ha hecho crecer profesional y personalmente. También me gustaría agradecer al Dr. Jianjun Chen y a Luz Zavala. Seguidamente, me gustaría agradecer a los miembros del tribunal, Dr. Frédéric Richard, Dra. Carole Lamonier, Dr. Jeppe V. Lauritsen, Dr. Arnaud Travert y Dra. Bárbara Garcia Pawelec por aceptar ser partícipes de este momento.

En Segundo lugar, me gustaría agradecer a todos los miembros del LCS dónde he pasado estos tres años. Y especialmente a aquellas personas que han sido como mi familia durante mi estancia en Caen, los miembros del “Trappist team”. Shashu, Juju, Dudu, Eddu, Kaka y por supuesto mi Paloma. Ellos han hecho que no me sintiera sola estando tan lejos de mis seres queridos. También me gustaría agradecer a Rafa por soportarme incluso cuando estaba rozando la locura y a Stijn por los grandes momentos vividos en “sulfur room”.

En tercer lugar, me gustaría agradecer a todas aquellas personas que han influido fuertemente en mi vida profesional antes del doctorado. Dr. José Antonio Odriozola, Dra. Francisca Romero, Dra. Maribel Domínguez y Dra. Svetlana Ivanova. Ellos hacen química de una forma especial. Por supuesto al Dr. Cecilio Carreras en la que su pasión por la enseñanza hizo que realmente disfrutara trabajando. Por último, me gustaría agradecer a unas de las personas, que sin saberlo, más me influyó y que gracias a su devoción por la química hizo que comenzara este largo camino, Federico Habela.

Y finalmente, pero no en menor medida, me gustaría agradecer a mi familia por su apoyo y amor incondicional durante estos tres años y toda la vida. Especialmente me gustaría agradecer a mis padres por la educación que me inculcaron, gracias a ello he sabido superar todos los obstáculos que se han presentado en mi vida. Y finalmente, quería darle las gracias a Manuel, por su gran apoyo, comprensión y cariño a lo largo de todo este tiempo. Y a Isabel Rodríguez quien siempre ha confiado que conseguiría todas mis metas.

Table of contents

General Introduction	1
Chapter I: INTRODUCTION	9
Chapter II: CHARACTERIZATION TECHNIQUES	39
Chapter III: SUPPORT EFFECT ON NON-PROMOTED CATALYSTS ...	69
Chapter IV: SUPPORT EFFECT ON PROMOTED CATALYSTS	113
Chapter V: METAL LOADING EFFECT ON NON- AND PROMOTED CATALYSTS USING SILICA AS SUPPORT	151
Chapter VI: DRYING AND CALCINATION EFFECT ON THE STRUCTURE AND ACTIVITY OF SULFIDE (Co)Mo CATALYSTS	189
Annex I: SUPPORTED DATA FOR SUPPORT EFFECT ON NON- PROMOTED CATALYSTS	219
Annex II: Mo LOADING EFFECT ON HDS CATALYSTS SUPPORTED ON MCM-41 AND TOF CALCULATIONS FOR Mo/SiO₂ CATALYSTS	227
Annex III: EFFECT OF Mo LOADING AND TITANIA STRUCTURE ON THE MoS₂ MORPHOLOGY OF Mo/TiO₂ CATALYSTS	245
Annex IV: DECOMPOSITION	261
General Conclusion	265

General introduction

Nowadays, a lot of efforts are put into the development of energy with low environmental impact. The energy sources can be classified into renewable as solar, hydraulic, wind or biomass and non-renewable as nuclear and fossil (coal, oil and natural gas). The fossil fuel is still the most largely used currently, since it constitutes around 87% of the total energy consumed in the world [1]. Although crude oil contains the same principal components i.e. hydrocarbons and to a lesser extent, heterocompounds (sulfur, nitrogen, oxide compounds...) and metals (Table 1), it can present different characteristics depending of its geographic origin.

Table 1. Elements in crude oil [2]

Element in fuel	Percentage in wt%
Carbon	82 – 87
Hydrogen	12 – 15
Sulfur	0.1 - 5.5
Nitrogen	0.1 - 1.1
Oxygen	0.1 - 4.5

Crude oil can be classified into light or heavy oil following some important properties such as (i) API gravity (inverse of density) which is thus directly linked with the density of the crudes and (ii) sulfur percentage, since a greater amount of heterocompound is found in heavy oils.

Table 2. Properties of crude oils (API and sulfur amount) [10]

Crude oil class	Property Range	
	Gravity (°API)	Sulfur (wt. %)
Light	35-60	> 0.5
Medium	26-35	> 1.1
Heavy	10-26	> 1.1

The negative impact on environment of fuel combustion is a very big concern. In addition to global warming due to CO₂ release, emissions of particles and toxic gases as NO_x and SO_x lead also to drastic consequences on air quality, human health and environmental preservation. Hence, in most of the countries, governments implement or make more drastic the regulations as the regulations for the sulfur amount in land transportation fuel. Regulations of the sulfur amount in the sea transportation fuel will be also implemented in the coming years.

Hence, improvement of hydrotreatment processes as hydrodesulfurization (HDS), hydrodenitrogenation (HDN), hydrodeoxygenation (HDO), and hydrodemetallization (HDM), that are the main process for removal of sulfur, nitrogen, oxygen and metal, are of crucial importance. Conventional hydrotreatment catalysts are formed by molybdenum sulfide supported on alumina carrier with cobalt or nickel added as promoter. Nowadays, considering that crude oil tend to get heavier and heavier, meaning that the heterocompound containing molecules are bigger and bigger and thus more refractory, research is going on to still improve the hydrotreating catalyst activity. Thus, understanding the formation of active sites, their structures as well as their role in the reaction is necessary.

The present PhD thesis deals with a deep molecular insight into oxidic and sulfided phase of hydrotreatment catalyst. In this work, a special effort was made to understand the factors that affect the sulfided phase morphology and the consequence of the morphological changes on the catalytic activity. The main parameters we analyzed are:

- the influence of the support nature - Mo and CoMo catalysts deposited on alumina, silica and titania with a constant Mo and Co coverage were studied in Chapter III and IV
- the effect of Mo and Co loading on silica (Chapter V and Annex II), and titania (Annex III)
- the effect of pretreatment as drying and calcination, on sulfided catalysts supported on silica, alumina and titania (Chapter VI)

In this work, the catalysts are deeply (but not exclusively) characterized by CO adsorption at about 100K followed by FTIR spectroscopy (IR/CO). Indeed, it was previously shown that IR/CO is a very powerful tool that accounts for the nature, the amount of sulfided sites as well as their structure (M-edge or S-edge, sulfur coordination) and thus account for

the morphology of sulfided phase. Parallel were done between spectroscopic data and thiophene HDS activity.

References

- [1] [Http://euanmearns.com/global-energy-trends-bp-statistical-review-2014/](http://euanmearns.com/global-energy-trends-bp-statistical-review-2014/), (n.d.).
- [2] A. Strahler, *Physical Geology*, Omega, Barcelona, 1992.
- [3] A. Stanislaus, A. Marafi, M.S. Rana, *Catal. Today* 153 (2010) 1–68.
- [4] I. V Babich, J.A. Moulijn, *Fuel* 82 (2003) 607–631.
- [5] S. Brunet, D. Mey, G. Perot, C. Bouchy, F. Diehl, *Appl. Catal. a-General* 278 (2005) 143–172.
- [6] P. Grange, X. Vanhaeren, *Catal. Today* 36 (1997) 375–391.
- [7] I. Mochida, K.H. Choi, *J. Japan Pet. Inst.* 47 (2004) 145–163.
- [8] C.S. Song, *Catal. Today* 86 (2003) 211–263.
- [9] H. Topsoe, B.S. Clausen, N.Y. Topsoe, E. Pedersen, *Ind. Eng. Chem. Fundam.* 25 (1986) 25–36.
- [10] MathPro, *Int. Counc. Clean Transp.* (2011) 45.

Table of contents – I Chapter

I. CHAPTER.....	7
1.1 Hydrodesulfurization catalysts	8
1.1.1 Active sites on HDS non-promoted catalysts.....	10
1.1.1.1 MoS ₂ structure	10
1.1.1.2 MoS ₂ morphology	11
1.1.2. Active sites on HDS promoted catalysts	15
1.1.2.1 Co promotion: CoMoS morphology	17
1.1.3. Support effect in HDS catalysts	19
1.1.3.1. Anchorage nature on support surface	20
1.1.3.1.1. Aluminum oxide (γ-Al ₂ O ₃).....	20
1.1.3.1.2. Silicon oxide (SiO ₂ - silica gel)	21
1.1.3.1.3. Titanium oxide (anatase- and rutile-TiO ₂ phases)	22
1.1.3.2. Anchorage mode	23
1.1.3.3. Support effect on the MoS ₂ morphology	24
1.1.3.4. Support effect on the activity	25
1.2 Hydrodesulfurization model reactions	26
1.2.1 Mechanism of hydrodesulfurization of Thiophene	27
1.2.2 Mechanism of hydrodesulfurization of Dibenzothiophene	28
1.3 Scope of the thesis	29
1.4 References	30

***I. CHAPTER
INTRODUCTION***

1.1 Hydrodesulfurization catalysts

Typical hydrodesulfurization (HDS) catalysts are formed by transition metal sulfide (molybdenum or tungsten) supported on alumina and promoted by a second metal, normally cobalt, nickel or both together to improve the catalytic activity. The conventional preparation procedure for Co-promoted HDS catalyst supported on alumina may be divided in two different stages as shows Figure I.1: metal oxide dispersion on the support surface and the oxide species transformation to sulfide species. The metal deposition on the support surface normally is performed by wetness impregnation method. The impregnation solution is formed by metal precursors dissolved in water with a volume equal to the pore volume of the support. The metallic species diffuse inside the support pores and interactions occur between these species and the support surface sites. Finally, the sulfide species are created by the transformation of the metal oxides under H_2S/H_2 flow.

However, these transformation phenomena are not so simple, and there are several influences during the different steps as:

- i) Physicochemical phenomena during the impregnation: metal diffusion into pores, acid-base reaction (controlled by acid constant of the species in solution and support surface), adsorption, complexation or precipitation, etc.
- ii) Formation of different oxide species during drying and calcination process from the species presents in the initial solution.
- iii) The temperature and the ratio between H_2S and H_2 in sulfidation procedure, which can modify the sulfide species nature.

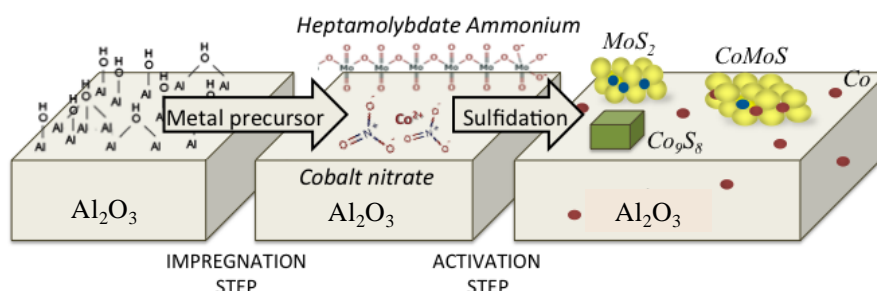


Figure I.1. Scheme of preparation from oxide to sulfide in a conventional HDS catalyst

For that reason, the studies of HDS catalysts in “so-called” oxide form, as well as, the transition products during sulfidation procedure are fundamental to understand sulfide species formation.

It is well known that active CoMoS sites are obtained by sulfidation of oxidic species, which are well dispersed on the surface of the support, whereas the bulk oxide crystallites are difficult to sulfide or give rise to phase segregation. The bulk oxide crystallites present on promoted catalyst surfaces are MoO_3 , Co_3O_4 , and CoMoO_4 . The activation stage enabling the transition from oxidic precursors to the active catalyst is considered as a key step. It has a direct influence on the level of activity of the catalysts and on their stability during the reaction. Therefore, obtaining catalysts with higher performances by controlling this stage requires a deep understanding of the transition from the oxide state to the sulfide state. It is well accepted that the majority of the CoMoS active sites may only be obtained from optimized oxidic precursors, i.e. having Co^{2+} and Mo^{6+} ions perfectly dispersed on the surface of the support (in 2D arrangement rather than in 3D).

The oxide surface on promoted catalyst is more complex than on monometallic catalyst. CoMo / Al_2O_3 oxide catalyst is formed by molybdenum oxide (MoO_x), cobalt oxide (Co_3O_4), mixture of cobalt and molybdenum oxide (CoMoO_4), and cobalt in interaction with alumina surface forming CoAl_2O_4 spinel. There are several molybdenum oxidic species reported in the literature that can be presented on Al_2O_3 surface as $\text{Mo}_7\text{O}_{24}^{6-}$, $\text{Mo}_2\text{O}_7^{2-}$, $\text{Mo}_6\text{O}_{19}^{2-}$ or isolated Molybdate, MoO_4^{2-} . All these oxomolybdate structure are collected in Figure I.2. Normally, molybdenum oxide species have been detected with two different coordinations: fourfold coordinated (MoO_4) or sixfold coordinated (MoO_6) [1]. Fourfold coordinated are linked to isolated molybdenum oxide (detected for low molybdenum loading dispersed on alumina), while sixfold coordinated are characteristic of polymerized molybdenum oxide species (detected for high molybdenum loading dispersed on alumina) [2].

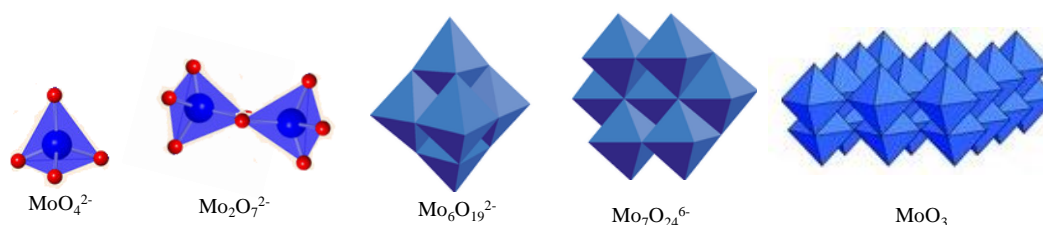


Figure I.2. Structures of molybdenum oxidic species

1.1.1 Active sites on HDS non-promoted catalysts

The active sites in non-promoted catalyst are formed by molybdenum atoms at the edge of MoS₂ clusters in interaction with the support surface.

1.1.1.1 MoS₂ structure

The structure of MoS₂ clusters is described as the one of the most stable ionic MoS₂ crystal. Thus, molybdenum disulfide is a layered compound consisting of stacks of S-Mo-S slabs held together by van der Waals interactions. Each slab is composed of two hexagonal planes of S atoms and an intermediate hexagonal plane of Mo atoms, which are trigonal prismatic coordinated to S atoms (Figure I.3). MoS₂ particles can show different length, from 2 to 6 nm, and different stacking of MoS₂ slabs, from 1 to 5 [3,4].

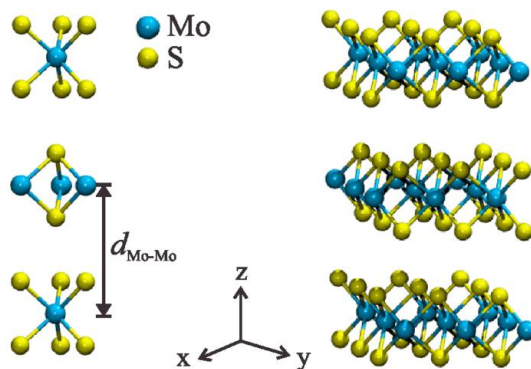


Figure I.3. Structure crystalline of MoS₂ clusters

Figure I.4 shows the MoS₂ clusters viewed by above, the most stable edges being formed by direct cleavage of the basal plane without considering further rearrangement. The structure of MoS₂ slabs leads to distinguish Mo located in different regions: basal plane, edge sites, corner sites or brim sites. All parts are clearly showed in Figure I.3, which do not represent the MoS₂ slabs taking in consideration the different sulfur coverage that the edges can adopt. In a general point of view, the basal plane is formed by Mo (IV) hexacoordinated with sulfur atoms, i.e. these atoms are perfectly stable, and therefore inactive from a catalytic insight [5]. However, edge part is formed by Mo (IV) penta- or tetraordinated with sulfur atoms depending on the sulfur coverage. Thus, Mo atoms in the corner are characterized by being formed by a coordination number smaller than the Mo on the edge. And finally, brim sites are the ones located between Mo-edge and Mo-basal. This way, Mo located on the edge or on the corner participates in the catalytic activity due to the creation of some CUS sites [6–

11]. However, the implication of brim sites in the catalytic activity is a recent hypothesis proposed by *Topsøe et al.* and coworkers [12,13]. They determine that brim sites are formed by a more metallic edge state [14]. STM combined with DFT studies showed that these sites may play a role in adsorption, hydrogenation, and C-S scission even if they are fully S saturated.

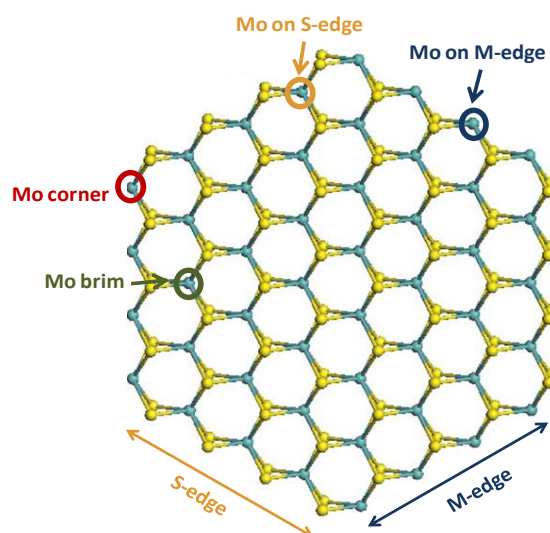


Figure I.4. Representation of MoS₂ slab with hexagonal shape. Sulfur atoms are represented by yellow balls and molybdenum atoms by blue balls

1.1.1.2 MoS₂ morphology

Kasztelan et al. was the first to propose a geometric model for the slabs morphology that is by unanimity accepted by the scientific community [15]. Several morphologies were proposed: chain, triangular, hexagonal, and orthorhombic, as shows Figure I.5 a. The particle geometries show an influence in molybdenum edge dispersion (Mo_{edge}/Mo_{slab}) as depicted in Figure I.5 b. Therefore, these particle geometries have shown an influence in the catalytic activity, i.e. there is correlation between introduced molybdenum, number of molybdenum located on the particle edges, and the catalytic activity. Then, the Mo edge dispersion depends on the slabs morphology and the slabs length as shows Figure I.5 b, getting less Mo edge when the particle size increase [10].

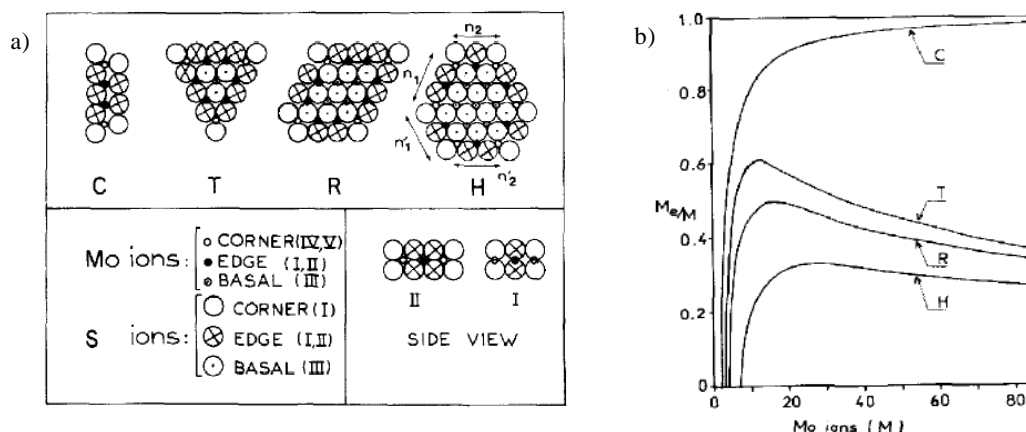


Figure I.5. Different geometry for MoS₂ slabs (a) and edge dispersion in each morphology (b) [15].

The morphology of the active phase is best described starting from a model consisting of the so-called single-layered MoS₂. The hypothetical model serves to illustrate the fact that hexagonal MoS₂ nanoparticles are expected to be terminated by two different types of low-index edge terminations. From a crystallographic insight, two plans are thermodynamically stable: the (10-10) Mo edge and the (-1010) S edge. These planes is generated by “cutting” Van der Waals interaction ensuring the cohesion of the stacked layers in the bulk structure [1]. The equilibrium shape of the MoS₂ nanoparticles is determined by the relative free-edge energies of these edges. These edge energies have been shown to be sensitive to atom incorporation, sulfidation temperature and H₂S / H₂ partial pressure ratio, which affect the slab morphology [16–18]. For instance, the observation of triangular MoS₂ nanoparticles with all three edges terminated by the same type of edge implies that the expressed edge termination is considerably more stable than the other. Hexagonal or truncated triangular nanoparticles, on the other hand, imply that the edge energies are comparable. The dispersion of the two types of edges can be quantified in detail in terms of the two dimensional Wulff construction. In this model, the shape that minimizes the total edge energies is given by the inner envelope of a surface constructed by drawing tangent lines to vectors extending from the same origin with a length proportional to the edge energies[19]. Triangular nanoparticles will result whether the free energy of one edge exceeds the other by a factor of two or more, perfect hexagon is constituted by the same vectors for both edges as shows Figure I.6. Truncated triangular nanoparticles arise for the intermediate situation, e.g. difference between edges is between one and two. Additionally to the proportion of S- and M- edge exposed, both M-edge and S-edge can show different configurations with different sulfur coverage. When the sulfur coverage on M-edge and/or S-edge is less than 100%, sulfur vacancies are created

on the edges[20–22]. Accordingly, the Mo atoms on M-edge and/or S-edge are coordinatively unsaturated sites (CUS). Thus, the morphology of MoS₂ slabs, i.e. the type and quantity of the edges exposed, is of great importance to the catalytic performance, as well as for Co-promoted MoS₂/Al₂O₃ catalyst because it was further suggested that Co atoms have different affinities towards M-edge and S-edge [23-24].

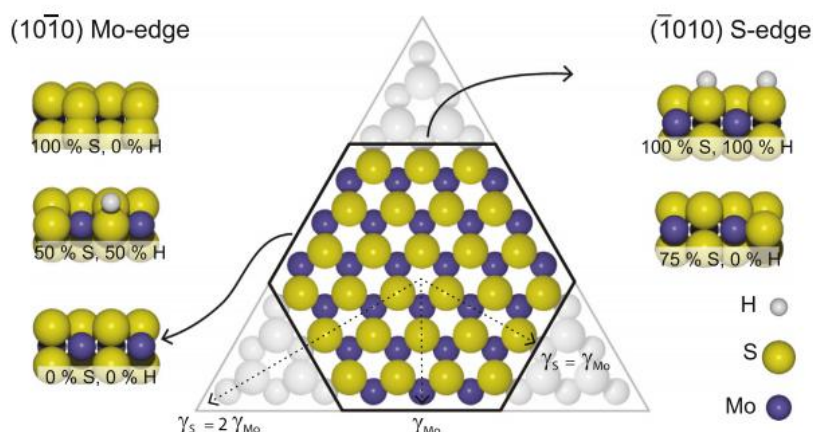


Figure I.6. Wulff construction for a hypothetical bulk-truncated MoS₂ nanoparticle with the exposed (1 0 $\bar{1}$ 0) Mo-edge and the ($\bar{1}$ 0 1 0) S-edge termination. For $Y_{Mo} = Y_S$ the particle will be a perfect hexagon, while a triangular particle with the Mo edge termination is obtained if $Y_S > 2Y_{Mo}$ [19]

The morphology of MoS₂ slabs has been investigated by several methods. One of them is density functional theory (DFT) calculations that were used by *Raybaud et. al* [22, 23, 27] to predict MoS₂ morphology under different sulfidation conditions. The stability of edge energy sites under sulfo-reductive condition were investigated by a thermodynamic model combined with DFT calculations. This thermodynamic DFT approach leads to the determination of the local structures of both edges, M- and S-edge, as a function of the chemical potential of sulfur. The chemical potential of sulfur depends on the sulfidation condition, i.e. temperature and partial pressure of H₂S and H₂. The variation of chemical potential was detailed studied for different sulfidation conditions. Thus, for typical sulfidation condition (673K and P(H₂S)/P(H₂) ~ 0.05), the chemical potential calculated is between -1 and -0.8 eV [18]. The edge energies for M- and S-edge with different sulfur coverage (0, 50 and 100%) were also calculated depending on the chemical potential of sulfur; indicating that the energy on M-edge is lower than the energy of S-edge in the wide chemical potential range, which reveals that M-edge is the most stable edge. Thus, triangular-shaped MoS₂ terminated by M-edge are observed to be the equilibrium structure under pure sulfiding condition (H₂S

pure), while the single-layer nanoparticles can become truncated with both M-edge and S-edge under sulfo-reductive conditions ($\text{PH}_2\text{S}/\text{PH}_2 \sim 0.05$). Other technique is Scanning Tunneling Microscopy (STM) that was recently introduced by *Lauritsen et al.*[23] to study the MoS_2 nanoparticles supported on Au substrate prepared by a special procedure under ultra-high vacuum (UHV) condition. The pure metal Mo was deposited on the Au(111) surface by an e-beam evaporator in the H_2S atmosphere of 1×10^{-6} mbar at 400K. Subsequently, the obtained crystal is annealed at 673K for 15 min in the same H_2S atmosphere and single-layered MoS_2 nanoparticles were formed with the basal (001) plane parallel to the Au (111) surface. It was imaged that the morphology of MoS_2 nanoparticles can vary from a triangle to a hexagon with sulfo-reductive conditions as shows Figure I.7.

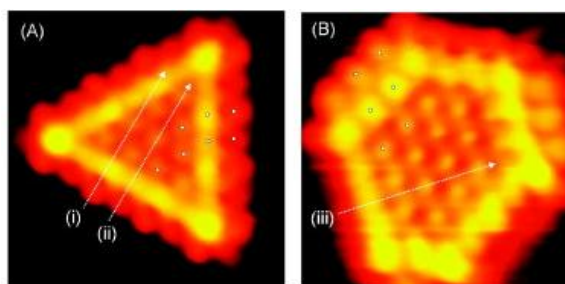


Figure I.7. STM images of single-layered MoS_2 nanoparticles synthesised under two different sulfidation conditions: a) $\text{H}_2\text{S}/\text{H}_2=500$ that gives triangular shape and b) $\text{H}_2\text{S}/\text{H}_2=0.07$ that forms hexagonal shape [23]

Finally, *Chen et al.* using CO adsorption at low temperature followed by FTIR (IR/CO) also detected the change of MoS_2 morphology. Recently, the development of IR/CO method allowed the distinction of Mo located on M- and/or S-edge. Thus, the effect on the morphology of some parameters was studied using this method. The variations of parameters carried out were Mo loading, sulfidation temperature, high pressure, even chelating agent addition. The increase of molybdenum loading and sulfidation temperature, chelating agent addition and high pressure sulfidation modify the morphology from triangular to hexagonal shape [24–27]. Such effect of various parameters could be rationalized considering that a decrease of metal-support interaction leads to change in morphology from triangular to hexagonal shape.

1.1.2. Active sites on HDS promoted catalysts

The industrial MoS₂-based HDS catalysts contain the so-called “promoters”, which cause a substantial enhancement of catalytic activity and changes in the selectivity between hydrogenation (HYD) and direct desulfurization (DDS) pathways. The promoters are small amounts of other transition metals (Co or Ni), which are introduced during the impregnation step of the molybdenum salt (co-impregnation) or on the molybdenum oxidic precursor but generally before the sulfidation step. Several models were proposed to account for the formation of CoMoS sites in a conventional catalyst (CoMo /Al₂O₃) as the contact synergy model, intercalation model, and decoration model. *Delmon* proposed the promotion role like a synergic effect between Co₉S₈ and MoS₂ that is called the contact synergy model [28–30]. But this is in contradiction with other studies that propose high addition of promoter (Co/Mo>1) results in a high number of Co₉S₈ species, which decrease the activity. Instead, Co/Mo ratio between 0.3-0.4 is well defined to reach the maximum activity in this kind of catalyst [31]. The Co intercalation between MoS₂ slabs model was proposed by *Voorhoeve and Stuiver* [32,33]. This model was followed by the pseudo-intercalation model proposed by *Farragher and Cossee* [34]. They distinguished Co in interaction with the edge and Co in interaction with the slab bulk, and they observed that energetically the Co in interaction with the bulk was not favorable. *Ledoux* also proposed another model supported by Co NMR where Co₉S₈ species are hung to the MoS₂ slab by octahedral Co species [35]. In fact, the model considers a chemical interaction between the Co₉S₈ particles and the MoS₂ slabs by a covalent bond between the sulfide atoms of the MoS₂ particles and the Co included in Co₉S₈ particles. Finally, other model and the most generally accepted, was proposed by *Topsøe et al* [31,36–41]. In this model (Figure I.8), the Co-Mo-S phase was shown to be MoS₂like structures with the promoter Co atoms located at the edge of MoS₂ called CoMoS model or decoration model. But Co is not only decorating MoS₂ particles, some Mossbauer spectroscopy experiments show three different locations of Co: i) Co in interaction with Al₂O₃ forming a kind of spinel CoAl₂O₄, ii) cobalt sulfide (Co₉S₈) that is formed for Co addition in excess, and iii) Co in promotion on MoS₂-edge slabs as shows Figure I.8. From this point, the Co-Mo-S model is similar with the pseudo-intercalation model. It should be noted that the Co-Mo-S structure is not a single bulk phase with a fixed overall CoMoS stoichiometry. Rather, it should be regarded as a family of structures with a wide range of Co concentrations, ranging from pure MoS₂ up to full coverage of the MoS₂ edges by Co. The Co atoms in Co-Mo-S may not have

identical properties due to such effects as different edge-site geometries, Co-Co interactions, and changes in sulfur coordination.

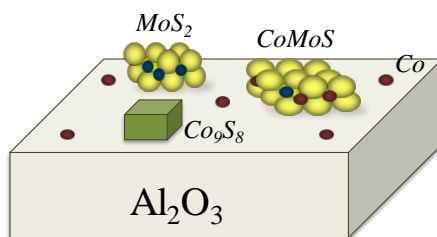


Figure I.8. Schematic view of the different species present in a conventional HDS catalyst CoMo/Al₂O₃ [39]

It is reported that several factors, such as the sulfidation temperature and pressure or support nature, can influence the structure of CoMoS sites. In particular, the formation of different types of Co-Mo-S structures, namely type I or type II, having different catalytic properties has been proposed. Indeed, in 1984, *Candia et al.* [38] proposed that if the chemical bonds between CoMoS structures and the alumina support could be eliminated, the resulting structures would have an increased intrinsic activity. These new structures were termed type II Co-Mo-S. Type-II Co-Mo-S is usually considered as a totally sulfided phase which has a higher activity than type-I (by a factor 2) [10–12]. However, for a long time, there have been limited reports on the difference between type I and type II Co-Mo-S structures. *Hinnemann et al.* showed by DFT calculations that in type I structure very specific Mo-O-Al bonds exist between the Co-Mo-S structures and support. Breaking the Mo-O-Al bonds will transform the type I into the high active type II. The difference in stacking of both Co-Mo-S structures is still controversial until now. *Shimada et al.* [44] claimed that single-layered MoS₂ slabs with Co at their edges are Co-Mo-S type I, whereas multi-layered MoS₂ slabs with Co, except the bottom layer, are Co-Mo-S type II (Figure I.9). However, *Topsøet et al.* [45] insisted that the multi-stacking may just be a “by-product” of the weak Metal-Support Interactions and that it is possible to produce single slab Co-Mo-S type II structure.

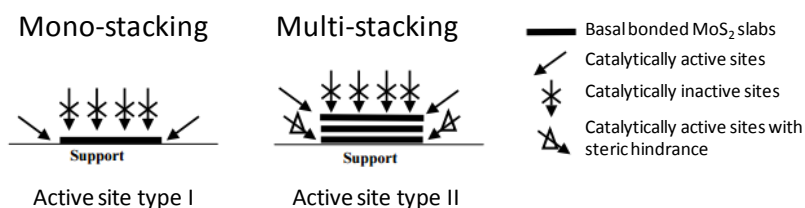


Figure I.9. Type I and II active sites as proposed by [44]

1.1.2.1 Co promotion: CoMoS morphology

The main effect of Co introduction on the morphology is seen by the fact that Co promoted MoS₂ nanoparticles present truncated hexagonal equilibrium morphology, i.e., exposing both Mo and S edges. Indeed, DFT calculations similar to the ones exposed previously for MoS₂ were also performed for Co promoted MoS₂ slabs. The affinity of Co promoter for the S-edge and for M-edge can be studied comparing the edge energies with different Co/Mo promotion ratio versus sulfidation conditions. Similar energies for both edges were obtained for high chemical potential of sulfur. On the other hand, the decrease in chemical potential in sulfur by either lowering the partial pressure of H₂S or increasing the sulfidation temperature lead to the enhancement of the affinity of Co for the S-edge at the expense of the one for M-edge site as shows Figure I.10.a [16,21,22,41]. Accordingly, the total promotion of the S-edge is favorable. In addition, Co partial decoration on M-edge (50%) leads to a significant reduction in the calculated edge energy that becomes close to the S-edge value for the same Co content. However, the partial Co decoration on S-edge becomes energetically more favorable than the total Co decoration only for chemical potential of sulfur less than -1.0 eV (conditions out of the HDS range). The calculations were performed also simulating alternated or paired configurations, i.e. Co-Mo-Co-Mo or Co-Co-Mo-Mo bonding, and similar energies were obtained. Then, in typical HDS conditions, the M-edge structure exhibits mixed Co-Mo sites (50% substitution) with 25% of sulfur coverage, the S-atom being preferentially on the top of the Mo atom, and non substituted Mo edge stabilized with 50% of sulfur coverage. The S-edge structure under HDS conditions is 100% Co substituted with 50% of sulfur coverage, Co atoms being in a tetrahedral environment. The various domains of promoter edge content and sulfur coverage are represented in Figure I.10.b with the proportion of each edge. CoMoS nanoparticles close to HDS reaction condition show to be formed by 50% of M-edge, i.e. hexagonal shape

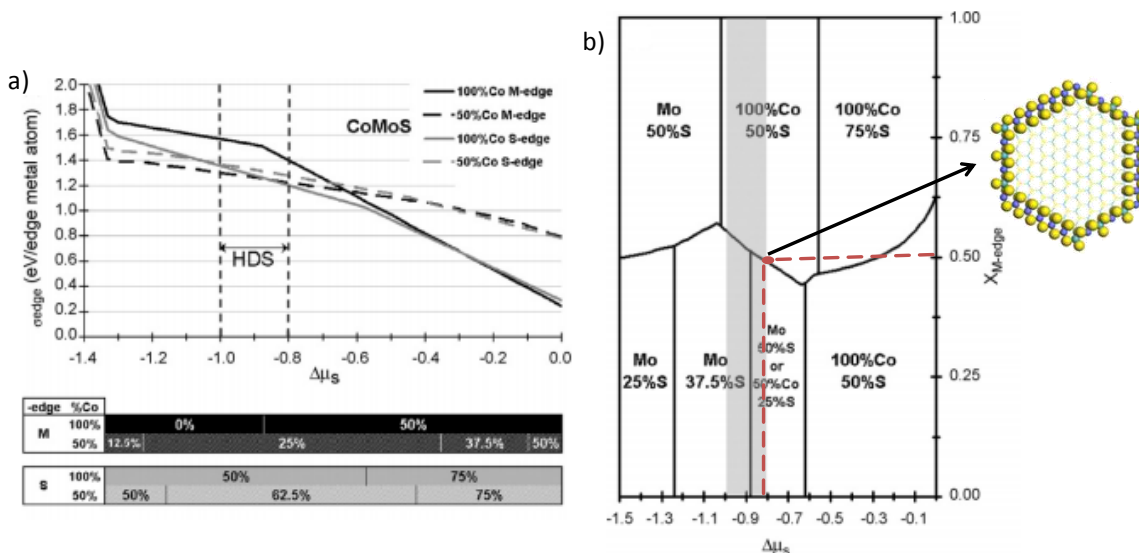


Figure I.10. a) Edge energy diagram as a function of $\Delta\mu_S$ for Co-promoted M-edge and S-edge and the most stable sulfur coverages for each edge are reported on the bar charts at the bottom of the diagrams, and b) morphology diagram for the CoMoS nano-crystallites as a function of $\Delta\mu_S$ [21]

Additionally, the morphology of Co promoted MoS_2 particles were studied by Scanning Tunneling Microscopy. The STM experiment was carried out on molybdenum deposited on an Au (111) sheet under H_2S atmosphere, leading to small Mo particles. These were then capped in a mixture of Co and Mo by co-deposition of the two metals to ensure efficient mixing of the metal. These particles were then annealed in a H_2S atmosphere to 723 K to facilitate crystallization. STM images showed truncated triangular shape for these nanoparticles. Co presence was only revealed at S edge by the detection of protrusion at this edge [19].

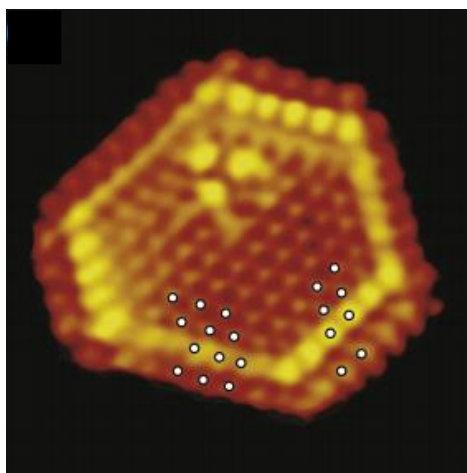


Figure I.11. STM image of Co-Mo-S nanoparticles [46]

Compared to un-promoted MoS₂ nanoparticles, where the S-edge is fully saturated with 100% S even under HDS conditions, Co promoted S edge has a reduced 50% S coverage. The reduced S coverage is a result of the preferred valence state of Co (II) compared to Mo (IV). Co promoted S-edge can therefore be thought as an active edge with already formed vacancies (CUS) with the ability to bond S containing compounds during HDS reactions, i.e. without the first requirement of vacancies formation as in the case of non promoted edge. Dealing with the selectivity, *Moses et al.* conclude that both CoMoS S-edge and unpromoted M-edge may participate in hydrogenation, whereas the CoMoS S-edge is primarily responsible for the promotion of the DDS pathway [47,48].

1.1.3. Support effect in HDS catalysts

The properties that characterize a good support can be classified in:

- i) Great textural properties such as high surface area and developed porosity relative to stable mesoporous.
- ii) High thermal stability,
- iii) Intermediate support-metal interaction that lead to good metal dispersion.
- iv) Low cost and scalability.

Several metal oxides such as Al₂O₃, SiO₂, TiO₂, ZrO₂, etc, were used as support for HDS catalysts [7,49–60]. The most used support in hydrodesulfurization catalysts is alumina, because of its great textural properties, good metal dispersion, and low cost.

The different surface properties that are characteristic of each support surface influence the metal-support interaction in the oxidic and sulfided forms and hence, the resulting metal dispersion, slab stacking, slab length and MoS₂ morphology which lead to different catalytic activity [52]. Thus, the differences in activity obtained on different support are explained in a general view by the different support-metal interaction [24,61–63]. One general way to characterize such interaction is to consider it as strong or weak according to the support. A weak interaction was reported for carbon or silica supports [19], while strong interaction was detected for MgO or TiO₂ [64,65]. This interaction can be reduced by chelating agent addition as citric acid (CA) or nitrilotriacetic acid (NTA), and increased by the addition of some additives as phosphorous. However, the interaction can be discussed according to several precise points of view: the anchorage point on the support (OH, Lewis acid sites), the

anchorage mode (edge or parallel anchorage), the nature of the anchorage (physical anchorage or chemical anchorage), the morphology of the anchored slab (with existence or not of epitaxy phenomena)... Such effects can be generalized in term of geometric effects. Also, the effect of the support can be considered as electronic... [66,67]. In this work, we have selected the usual support (Al_2O_3), a weak (SiO_2) and strong (TiO_2) interacting support. The main differences between these supports are described more precisely thereafter.

1.1.3.1. Anchorage nature on support surface

The isoelectric point (IEP) characteristic of each support and the pH of the impregnation solution of Mo play an important role in molybdenum oxide species formation and in the absorption of Molybdate anions. The impregnation solution is required to have a pH lower to the support IEP to obtain an optimum species absorption. The isoelectric point characteristic of Al_2O_3 , TiO_2 , and SiO_2 are 8, 6, and 2 respectively [68]. Hence, catalysts prepared using different supports but with same impregnation condition and the same metal loading cannot have the same dispersion.

1.1.3.1.1. Aluminum oxide ($\gamma\text{-Al}_2\text{O}_3$)

Gamma alumina is the most used support in HDS catalyst. There are several interesting factors that makes the alumina the support of choice: high surface area (100-400 m^2/g), porous with meso- size, thermal stability, high capacity to catalyst regeneration and good metal dispersion. The alumina surface is composed by acid Lewis sites, Al^{3+} , and hydroxyl group which can have basic, neutral or acid character as represented in Figure I.12.

Since alumina is the most used catalyst support in many applications, the well understanding of the surface is required. For that, many studies have been performed to know the characteristic of it surface and its interaction with the metal precursors. Thus, many studies show the alumina-molybdate interaction is first with basic hydroxyl group from alumina surface [2,66,69]. However, some interactions with neutral or acid hydroxyl group and Lewis acid sites (Al^{3+}) are also detected for higher metal loading. Moreover, gamma alumina surface were study by DFT calculations to predict the more stable planes, and study some influences in its chemistry properties to later study the interaction between MoS_2 nanoparticles and the alumina surface. For that, four different plans were studied and two were obtained energetically stable under HDS condition, (110) and (100) surface. γ -alumina (100) surface was not hydroxylated under HDS conditions. Moreover, the γ -alumina (110) surface was hydroxylated with 8.8 OH/nm^2 and both not sulfided [70].

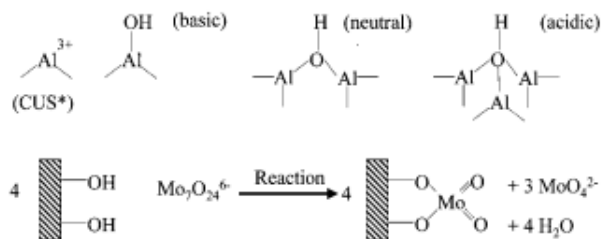


Figure I.12. Scheme of adsorption sites and molybdate adsorption mode [66,69]

1.1.3.1.2. Silicon oxide (SiO₂- silica gel)

Silica is an inert material that presents high thermal stability (higher than 1000°C) and high surface area (300-1000 m²/g). These qualities make interesting the use of silica as support for HDS catalysts. Silica surface is formed by acid hydroxyl group as is represented in Figure I.13. Silica surface is really sensitive to heating treatment, since it is formed by OH groups and it can be dehydrated to form siloxane. On the other hand, the surface can be hydrated forming germinal silanol and vicinal silanol interacting through H bonding [71]. The presence of only hydroxyl groups on the surface leads to weak interaction with the metal and then to a poor metal dispersion as revealed by the formation of MoO₃ species after calcination treatment [72].

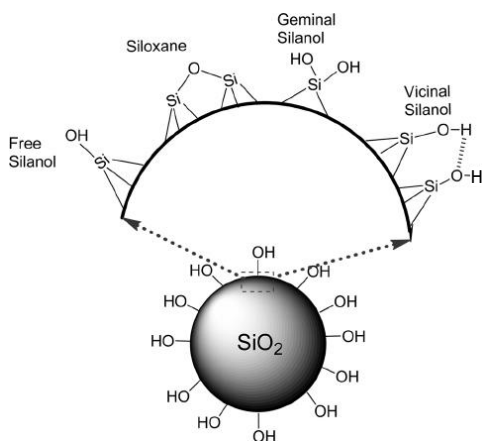


Figure I.13. Scheme of silica surface [71]

1.1.3.1.3. Titanium oxide (anatase- and rutile-TiO₂ phases)

Titanium dioxide crystallizes in three different structures: brookite (rhombohedral, a=5.436 Å, b=9.166 Å, c=5.135 Å), rutile (tetragonal, a=b=4.584 Å, c=2.953 Å) and anatase (tetragonal, a=b=3.782 Å, c=9.502 Å). But, of these three only rutile and anatase structures are

used in catalysis application, and they are the ones used in this work as support of HDS catalysts. Anatase is a metastable structure; hence it has a low thermal stability (maximum temperature, around 400°C). At high temperatures (600°C), anatase becomes rutile which is a stable structure.

Anatase and rutile unit cells are shown in Figure I.14.a. In both structures, the basic building block consists of a titanium atom surrounded by six oxygen atoms in a more or less distorted octahedral configuration. In each structure, the two bonds between the titanium and the oxygen atoms at the apices of the octahedron are slightly longer. In both structure, the stacking of the octahedra results in threefold coordinated oxygen atoms [73]. *Ramamoorthy et al.* calculated the total energy of periodic rutile TiO₂ slabs using a self-consistent ab initio method where the (110) surface has the lowest surface energy (0.31 J/m²), and (001) the highest [74]. However, (101) face is the thermodynamically most stable surface in anatase TiO₂ (0.44 J/m²) [75].

The principal reason that makes TiO₂ an interesting material in catalysis is its surface. It is full of defects and it can be categorized in step edges, oxygen vacancies, line defects, common impurities, and the manifestation of crystallographic shear planes (CSPs) at surfaces [73]. The bulk structure of reduced TiO_{2-x} crystals is quite complex with a various types of defects such as doubly charged oxygen vacancies, Ti³⁺ and Ti⁴⁺ interstitials, and planar defects such as CSPs. The defect structure varies with oxygen deficiency which depends on temperature, gas pressure, impurities, etc.

Generally, the most used titania powders are formed by pure anatase or by the mixture of rutile and anatase as the commercial titania denoted Degussa P25 which is composed by 80-90% of anatase and the complement of rutile. Since, Titania is mostly formed by anatase phase, it is interesting to study the anatase-TiO₂ surface. Thus, Costa et al. performed the study about the more stable planes in order to predict the interaction between anatase-TiO₂ surface and MoS₂ nanoparticles by DFT calculations. For that, the two principal crystallographic surfaces of anatase-TiO₂ were considered. Under HDS conditions, the (101) surface of anatase was considered dehydrated and not sulfided. The (001) anatase was found hydroxylated and partially sulfided, with a hydroxyl coverage of 3.5 OH/nm² and S coverage of 1.7 S/nm². The OH groups are Ti_{5c} (fivecoordinated) and OH monocoordinated (μ_1 -OH) types and [70].

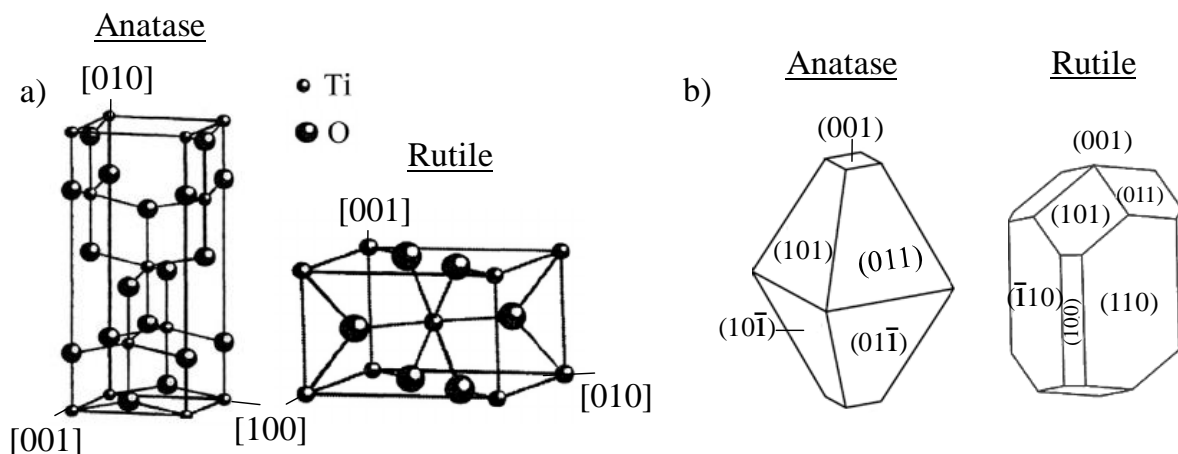


Figure I.14. a) Unit cells for anatase and rutile structure [73] and b) Wulff construction for both structures

Thus, finally, MoO_x species or MoS_2 nanoparticles can be differently anchorage in the support surface and it strongly depends on the surface nature. Gamma- Al_2O_3 surface shows different anchorage point as hydroxyl group with different acidity and Lewis acid sites, Al^{3+} . Similar anchorage can be predicted by TiO_2 surface due to it is formed by hydroxyl groups and Lewis acid sites, Ti^{4+} although this material shows a specific behavior due to the high defects numbers. And controversially SiO_2 surface shows the main anchorage with hydroxyl group.

1.1.3.2. Anchorage mode

One important aspect of the metal-support interaction is the way the slab is anchored to the surface i.e. through basal plane interaction (parallel anchorage) or through the edges (edge anchorage). Indeed, from TEM image observations, while MoS_2 was uniformly dispersed mainly through parallel anchorage on the surface of SiO_2 and Al_2O_3 . Specific slab edge-anchoring were found for TiO_2 catalysts [44,76,77]. Thus, several studies were carried out by DFT calculation on the MoS_2 -support interaction considering two supports Al_2O_3 and TiO_2 [78–80]. First, the interaction of Mo_6S_n clusters represented with M-edge termination (triangular shape) with the support was investigated [80]. Various possible types of interactions were considered which are susceptible to be formed when the particles are anchored through the edge or the corner via H bonds and van der Waals interactions, both of which may be responsible for the parallel orientation of single MoS_2 slab. In addition, an epitaxial relationship of the M-edge of MoS_2 with anatase (110) or (001) surface was found. When size effects are taken into account, particles up to 90 Å in diameter may be anchored

through the M-edge on the anatase surface. Such a strong interaction is not evidenced for alumina. Only particles with M-edge length less to 15 Å are found to interact strongly with the support and particles of larger size parallel to the surface. For this epitaxial relationship, two factors may explain the increased catalytic activity of MoS₂/anatase versus MoS₂/alumina: the stabilization of small anchored particles and the existence of a stable S-vacancy at the edge of those anchored particles. DFT calculations predicted that M-edge was energetically more stable than S-edge termination over a wide range of chemical potentials, and for this reason firstly the M-edge termination was studied. But the study about the S-edge interaction with -OH group by *Hinnemann et al.* [37] leads to the study of the interaction of S-edge termination with alumina and titania supports [78]. Wetting effect was also studied for the alumina and titania supports. The edge wetting of MoS₂ particles showed an important effect for anatase-TiO₂; instead, this effect was not so strong for alumina catalyst. Then, for Mo/Al₂O₃ catalyst, MoS₂ nanoparticles exhibit chemical interaction as Mo-O-Al bonds for M- and S-edges in small particles sizes (< 15 Å). Besides the particles showed parallel orientations stabilized by H bonds and van der Waals interactions for normal particles size, i.e. higher than 15 Å. On the other hand, Mo/TiO₂ catalyst showed an epitaxial relationship between M-edge of MoS₂ nanoparticles and the support surface at (101) and (001) plans with the formation of Mo-O-Ti-S-Mo rings. This epitaxy is not possible between the S-edge and titania surface. The wetting effect in anatase-TiO₂ leads to the formation of trapezoidal MoS₂ morphology, with two predominant M-edge and one single S-edge.

1.1.3.3. Support effect on the MoS₂ morphology

The MoS₂ morphology supported in different supports were studied by Scanning Tunneling Microscopy (STM). *Lauritsen et al.* was the pioneer to obtain an image from MoS₂ nanoparticles supported on Au (111) [81]. This study was continued using carbon or (110) rutile-TiO₂ as support using the same technique [82]. Triangular or truncated-triangular shape was obtained for MoS₂ supported on Au (111) depending on the sulfidation condition, thus hexagonal shape was detected for MoS₂ supported on graphite, and elongated hexagonal shape for MoS₂ supported on rutile-TiO₂ (110) as shows Figure I.15.

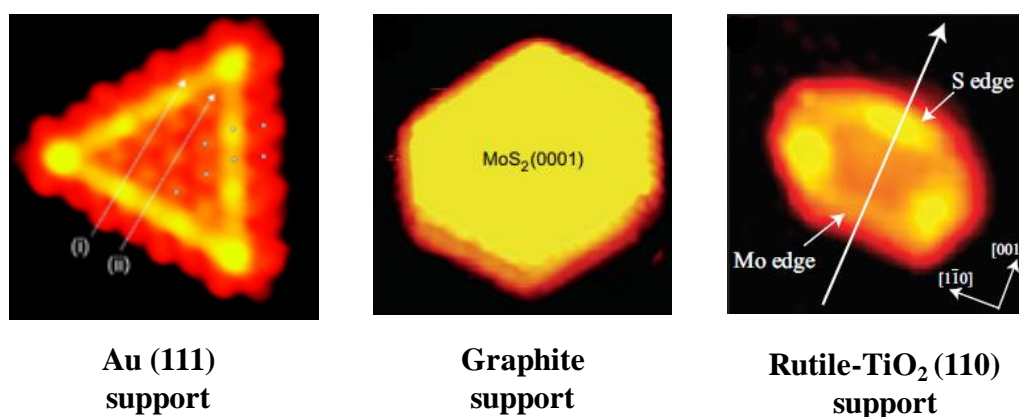


Figure I.15. STM images for MoS₂ slabs supported on Au (111), graphite and rutile-TiO₂ (110)

1.1.3.4. Support effect on the activity

The study of the support effect on the catalytic activity revealed equally that Mo/TiO₂ catalyst shows four times higher intrinsic activity than Mo/Al₂O₃ catalyst [53,58,83–86]. As well, Mo/SiO₂ catalyst shows also higher intrinsic activity than Al₂O₃. These changes in activity can be explained by the total sites available, metal-support interaction, specific MoS₂ orientation and high stacking degree. The high intrinsic activity recorded for Mo/TiO₂ catalyst can be explained by the edge-bonding interaction between the MoS₂ and the support [44], that lead to the specific epitaxial configuration detected by DFT calculations. Moreover, some authors also explained the high activity by a electronic effect, or indirect promotion by Ti [83,85,87]. Moreover, the high intrinsic activity detected for Mo/SiO₂ catalyst is explained due to the high slab stacking number forming the so-called type II active sites consequence of the weak metal-support interaction. However, the synergy between Ni(Co) and Mo in the catalysts prepared by conventional co-impregnation technique appears to be lower for TiO₂ than Al₂O₃ catalysts, and afterwards less active. Controversially, CoMo supported on silica showed be more active than CoMo supported on alumina catalyst due to the formation of CoMoS phase with high stacking number that are called CoMoS type II [88]. Instead, CoMo supported on Al₂O₃ and TiO₂ lead to the formation of CoMoS type I.

In conclusion, it is expected that a weak metal-support interaction leads to form hexagonal MoS₂ shape and highly stacked slabs on carbon and silica supports. In contrast, strong metal-support interaction should lead to form triangular MoS₂ shape and monolayer slabs [89]. Titania catalysts have a specific behavior due to the metal-support interaction

explained by the wetting effect or the so called strong ligand effect that lead them to have high intrinsic activity.

1.2. Hydrodesulfurization model reactions

The hydrodesulfurization (HDS) reaction consists in removing sulfur from sulfur-containing molecules. This reaction is carried out using hydrogen in excess and high temperature between 623 and 673 K. The fundamental transformations in HDS are the same for all mechanisms: i) adsorption of the sulfur compound to the active site, ii) hydrogenation of unsaturated C=C bonds, iii) cleavage of two carbon-sulfur bonds, iv) addition of hydrogen to the broken bonds of both sulfur and carbon, v) release of the hydrocarbon product from the catalytic site, vi) release of the H₂S from the site. The sequence of these transformations can be varied, and depends on the sulfur-containing molecule. Fuel feeds can be formed by different sulfur-containing molecules from thiols (R-S-R), which are characterized by its small molecule size, to polycyclic aromatic compounds such as methyl dibenzothiophenes that present big molecule size. The high steric hindrance presented by large molecules makes more difficult to carry out the HDS reaction as shows Figure I.16 in particular in the case of methyl substituted compounds. For that reason, catalyst enhancement is necessary since mostly these compounds form actual fuel feedstock.

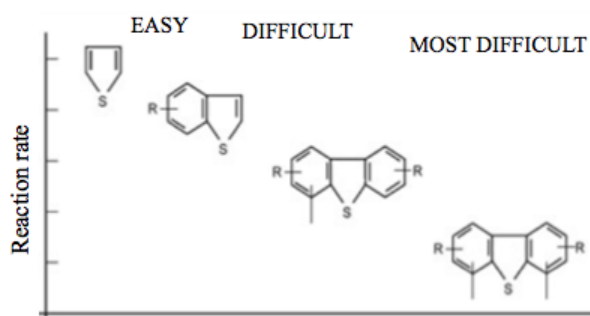


Figure I.16. Sulfur compounds feed and different reaction rate[52]

Generally, the HDS reaction takes place by the following two mechanisms: direct desulfurization pathway (DDS), in which the C-S bond is broken without preliminary hydrogenation step; and hydrogenation pathway (HYD)[90–92]. These two mechanisms occur in different ways depending on the sulfur-containing molecules, even each pathway can be performed in different active sites as the literature predicts.

Since sulfur elimination is more difficult for aromatic compounds than for linear sulfur compounds, in the present work, two different aromatics sulfur compounds were chosen as model molecules, to study the catalytic activity for HDS reaction: thiophene and dibenzothiophene. The HDS reaction scheme for thiophene and dibenzothiophene are shown below.

1.2.1 Mechanism of hydrodesulfurization of Thiophene

Thiophene is a sulfur-containing molecule with medium size. This molecule is the conventional one to study HDS reaction since it is an aromatic compound without high steric hindrance.

Thiophene molecule undergoes first a *pre-hydrogenation* of one of the double bond. Therefore, thiophene becomes dihydrothiophene that normally is just a transition product. Then, two different pathways can be carried out, hydrogenation (HYD) or direct desulfurization (DDS). DDS pathway form 1,3-Butadiene, which is a transition product is not detected because it is not a stable product. It is hydrogenated forming 1-Butene or 2-Butene, products that can be formed by both pathways direct desulfurization and hydrogenation. Moreover, HYD pathway leads to the formation of Tetrahydrothiophene, which is detected as reaction product. Then, the hydrogenation can continue forming 1-Butene or 2-Butene. The limitation of thiophene as model molecule is clearly shown, both pathways, HYD and DDS, lead to the formation of 1-Butene and 2-Butene as reaction products. Thus, Tetrahydrothiophene (THT) can be considered as hydrogenation product, and 1-Butene, 2-Butene and Butane as products of the mixture of hydrogenation and direct desulfurization pathway.

Moses *et.al* studied the thiophene reaction mechanism by DFT calculations for MoS₂ nanoparticles. The reaction selectivity was studied taking into account both M- and S-edge active sites. The product energies in reaction with M- or S-edge sites were calculated and the implication of different active sites in the different pathway was detected, i.e. C-S scission was predicted to be carried out in S-edge, while hydrogenation pathway was going on M-edge sites[93]. Additionally, the same calculations were performed for CoMoS sites, considering that Co decorates only S-edge sites. Thus, Cobalt located on S-edge showed to be the responsible of C-S scission while M-edge non-promoted was the responsible of hydrogenation pathway[94].

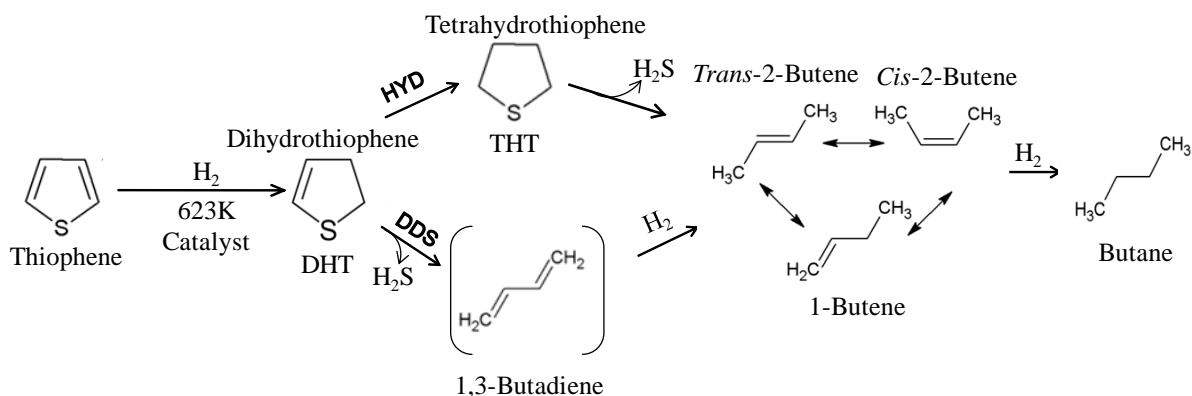


Figure I.17. Scheme of Thiophene reaction and pathway [95]

1.2.2 Mechanism of hydrodesulfurization of Dibenzothiophene

The kind of HDS model molecule has an influence in the active site behaviors, i.e. the active sites do not react in the same line for all sulfur compounds. The molecule with high steric hindrance cannot be adsorbed at single edge sulfur vacancies; likewise the hydrogenation (HYD) pathway may become the dominant route since it is less sensitive to steric effects. Thus, the HYD activity is becoming increasingly more important for heavy crude oils. For that reason, a molecule with high steric hindrance as dibenzothiophene (DBT) is considered to study the catalytic activity for some catalysts in the present work.

The Dibenzothiophene mechanism for HDS reaction is shown in Figure I.18. Two different pathways are characteristic of this reaction: Direct desulfurization (DDS) and Hydrogenation (HYD). Unlike Thiophene molecule, products from DDS or HYD can be detected after reaction, allowing a selectivity study for the active sites in HDS reaction. Biphenyl is the stable product obtained after DDS reaction pathway, while cyclohexylbenzene is the product obtained of hydrogenation pathway. It is normally considered that DDS reactions take place by sulfur removal on the so-called sulfur vacancies formed on the edges of the MoS₂ nanoparticles in interplay with edge sulfydryl groups (S–H). For the HYD pathway, on the other hand, the situation is under much more in debate [96]. Several studies have proposed a two-site model, where one or more hydrogenation steps occur on a certain type of site where adsorption is less sterically hindered prior to sulfur removal on a regular edge sulfur vacancy[97,98]. In particular, it was proposed that the so-called brim sites in close

vicinity to edge S-H groups presents a favorable geometry as active sites for the hydrogenation step during the HYD pathway [12,13].

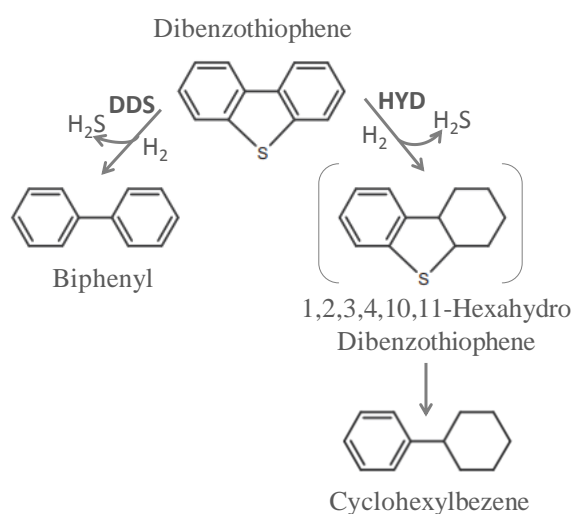


Figure I.18. Pathways of hydrodesulfurization reaction for Dibenzothiophene (DBT)

1.3. Scope of the thesis

The investigation of the active phase-support interaction is of paramount importance to make new progress in understanding the effect of the support in active phase formation and therefore its action in the HDS catalytic reaction. The support can have effects in the active phase dispersion and morphology as well as electronic effects. Recently, IR/CO method was used to distinguish Mo located on M- and S-edge for Mo/Al₂O₃ catalysts; and thus to predict the MoS₂ slab morphology on alumina support [25,26,99,100]. Several factors were studied as temperature and high-pressure sulfidation, variation in Mo loading and the addition of citric acid in the preparation step. All those factors have an effect in metal-support interaction producing a change in the MoS₂ morphology. Some influences of the support effect in the catalytic activity are already reported in the literature but without any unambiguous explanation. Hence, the goal of this work is to study mono- (Mo) and bimetallic (CoMo) catalysts supported on three different metal oxides known to have different chemistry properties: alumina, silica and titania. Therefore, MoS₂ and CoMoS nanoparticles will present different anchoring with the support surface producing changes in the catalytic activity and in the active sites nature. These different active sites have been studied by IR/CO method, which allows determining the MoS₂ slab morphology as well as the concentration of Mo edge

sites available for HDS reaction. And thus, it leads to understand the role of the active sites in the HDS reaction. The distinction of Mo located on M-edge and S-edge by IR/CO for non-promoted catalysts leads to the possibility of the study of the Co decoration affinity to M- or S-edge sites. Therefore, in the case of promoted catalysts, a new development of IR/CO method has been carried out to get information about the Co promoted sites, i.e. degree and nature. Thus, in this work, the method for these promoted catalysts will be implemented thanks to a chemiometry method in order to refine the attribution of IR bands.

1.4. References

- [1] H. Toulhoat, P. Raybaud, *Catalysis by Transition Metal Sulphides: From Molecular Theory to Industrial Application*, Editions Technip, 2013.
- [2] I.E. Wachs, *Catal. Today* 27 (1996) 437–455.
- [3] E. Payen, R. Hubaut, S. Kasztelan, O. Poulet, J. Grimblot, *J. Catal.* 147 (1994) 123–132.
- [4] J. QUARTARARO, S. MIGNARD, S. KASZTELAN, *J. Catal.* 192 (2000) 307–315.
- [5] L.S. Byskov, J.K. Norskov, B.S. Clausen, H. Topsøe, *J. Catal.* 187 (1999) 109–122.
- [6] H. Topsøe, R. Candia, N.Y. Topsøe, B.S. Clausen, *Bull. Des Soc. Chim. Belges* 93 (1984) 783–806.
- [7] C. Dujardin, M.A. Lelias, J. van Gestel, A. Travert, J.C. Duchet, F. Mauge, *Appl. Catal. A Gen.* 322 (2007) 46–57.
- [8] Y. OKAMOTO, *J. Catal.* 70 (1981) 445–448.
- [9] S.J. Tauster, T.A. Pecoraro, R.R. Chianelli, *J. Catal.* 63 (1980) 515–519.
- [10] S. Kasztelan, H. Toulhoat, J. Grimblot, J.P. Bonnelle, *Appl. Catal.* 13 (1984) 127–159.
- [11] E.J.M. Hensen, P.J. Kooyman, Y. van der Meer, A.M. van der Kraan, V.H.J. de Beer, J.A.R. van Veen, R.A. van Santen, *J. Catal.* 199 (2001) 224–235.
- [12] J. V Lauritsen, M. Nyberg, R.T. Vang, M. V Bollinger, B.S. Clausen, H. Topsøe, K.W. Jacobsen, E. Laegsgaard, J.K. Norskov, F. Besenbacher, *Nanotechnology* 14 (2003) 385–389.
- [13] J. V Lauritsen, M. Nyberg, J.K. Norskov, B.S. Clausen, H. Topsøe, E. Laegsgaard, F. Besenbacher, *J. Catal.* 224 (2004) 94–106.

- [14] M. V Bollinger, J. V Lauritsen, K.W. Jacobsen, J.K. Norskov, S. Helveg, F. Besenbacher, *Phys. Rev. Lett.* 87 (2001).
- [15] S. Kasztelan, H. Toulhoat, J. Grimblot, J.P. Bonnelle, *Bull. Soc. Chim. Belg.* 93 (1984) 807–811.
- [16] H. Schweiger, P. Raybaud, H. Toulhoat, *J. Catal.* 212 (2002) 33–38.
- [17] H. Schweiger, P. Raybaud, G. Kresse, H. Toulhoat, *J. Catal.* 207 (2002) 76–87.
- [18] P. Raybaud, J. Hafner, G. Kresse, S. Kasztelan, H. Toulhoat, *J. Catal.* 189 (2000) 129–146.
- [19] A.S. Walton, J. V Lauritsen, H. Topsoe, F. Besenbacher, *J. Catal.* 308 (2013) 306–318.
- [20] P. Raybaud, J. Hafner, G. Kresse, H. Toulhoat, *Surf. Sci.* 407 (1998) 237–250.
- [21] E. Krebs, B. Silvi, P. Raybaud, *Catal. Today* 130 (2008) 160–169.
- [22] L.S. Byskov, J.K. Norskov, B.S. Clausen, H. Topsoe, *Catal. Letters* 64 (2000) 95–99.
- [23] J. V Lauritsen, M. V Bollinger, E. Laegsgaard, K.W. Jacobsen, J.K. Norskov, B.S. Clausen, H. Topsoe, F. Besenbacher, *J. Catal.* 221 (2004) 510–522.
- [24] J. Chen, F. Maugé, J. El Fallah, L. Oliviero, *J. Catal.* 320 (2014) 170–179.
- [25] J. Chen, E. Dominguez Garcia, E. Oliviero, L. Oliviero, F. Maugé, *J. Catal.* 339 (2016) 153–162.
- [26] J. Chen, V. Labruyere, F. Mauge, A.-A. Quoineaud, A. Hugon, L. Oliviero, *J. Phys. Chem. C* 118 (2014) 30039–30044.
- [27] J. Chen, L. Oliviero, X. Portier, F. Maugé, (2015).
- [28] G. Hagenbach, P. Courty, B. Delmon, *J. Catal.* 31 (1973) 264–273.
- [29] S. Eijsbouts, *Appl. Catal. A Gen.* 158 (1997) 53–92.
- [30] B. Delmon, G.F. Froment, (1996) 37–41.
- [31] C. Wivel, R. Candia, B.S. Clausen, S. Morup, H. Topsoe, *J. Catal.* 68 (1981) 453–463.
- [32] R.J.H. Voorhoeve, J.C.M. Stuiiver, *J. Catal.* 23 (1971) 243–252.
- [33] R.J.H. Voorhoeve, *J. Catal.* 23 (1971) 236–242.
- [34] A.L. Farragher, P. Cossee, *Catal., Proc. Int. Congr.*, 5th 2 (1973) 1301–1318.

- [35] M. LEDOUX, *J. Catal.* 96 (1985) 189–201.
- [36] R. Candia, H. Topsoe, B.S. Clausen, *Actas Simp. Iberoam. Catal.*, 9th 1 (1984) 211–221.
- [37] B. Hinnemann, J.K. Norskov, H. Topsoe, *J. Phys. Chem. B* 109 (2005) 2245–2253.
- [38] R. Candia, O. Soerensen, J. Villadsen, N.Y. Topsoe, B.S. Clausen, H. Topsoe, *Bull. Des Soc. Chim. Belges* 93 (1984) 763–773.
- [39] H. Topsoe, B.S. Clausen, *Catal. Rev. Eng.* 26 (1984) 395–420.
- [40] H. Topsoe, B.S. Clausen, F.E. Massoth, *Hydrotreating Catalysis*, Springer, Berlin-Heidelberg, 1996.
- [41] L.S. Byskov, B. Hammer, J.K. Norskov, B.S. Clausen, H. Topsoe, *Catal. Letters* 47 (1997) 177–182.
- [42] H. Topsoe, B.S. Clausen, N.Y. Topsoe, E. Pedersen, *Ind. Eng. Chem. Fundam.* 25 (1986) 25–36.
- [43] [Http://www.eia.doe.gov/oiaf/servicerpt/ulsd/figd3.html](http://www.eia.doe.gov/oiaf/servicerpt/ulsd/figd3.html), (n.d.).
- [44] H. Shimada, *Catal. Today* 86 (2003) 17–29.
- [45] H. Topsoe, *Appl. Catal. a-General* 322 (2007) 3–8.
- [46] F. Besenbacher, M. Brorson, B.S. Clausen, S. Helveg, B. Hinnemann, J. Kibsgaard, J. Lauritsen, P.G. Moses, J.K. Norskov, H. Topsoe, *Catal. Today* 130 (2008) 86–96.
- [47] P.G. Moses, B. Hinnemann, H. Topsoe, J.K. Norskov, *J. Catal.* 268 (2009) 201–208.
- [48] P.G. Moses, B. Hinnemann, H. Topsoe, J.K. Norskov, *J. Catal.* 248 (2007) 188–203.
- [49] G. Perot, *Catal. Today* 86 (2003) 111–128.
- [50] C.E. Hedoire, C. Louis, A. Davidson, M. Breysse, F. Mauge, M. Vrinat, *J. Catal.* 220 (2003) 433–441.
- [51] T.D. Tang, L. Zhang, W.Q. Fu, Y.L. Ma, J. Xu, J. Jiang, G.Y. Fang, F.S. Xiao, *J. Am. Chem. Soc.* 135 (2013) 11437–11440.
- [52] T.K.T. Ninh, L. Massin, D. Laurenti, M. Vrinat, *Appl. Catal., A* 407 (2011) 29–39.
- [53] T.K.T. Ninh, D. Laurenti, E. Leclerc, M. Vrinat, *Appl. Catal. A Gen.* 487 (2014) 210–218.

- [54] S.M.A.M. Bouwens, F.B.M. van Zon, M.P. van Dijk, A.M. van der Kraan, V.H.J. de Beer, J.A.R. van Veen, D.C. Koningsberger, *J. Catal.* 146 (1994) 375–393.
- [55] C. Glasson, C. Geantet, M. Lacroix, F. Labruyere, P. Dufresne, *J. Catal.* 212 (2002) 76–85.
- [56] P. Afanasiev, *Catal. Commun.* 9 (2008) 734–739.
- [57] R.G. Leliveld, A.J. Van Dillen, J.W. Geus, D.C. Koningsberger, *J. Catal.* 171 (1997) 115–129.
- [58] P. Castillo-Villalón, J. Ramírez, R. Cuevas, P. Vázquez, R. Castañeda, *Catal. Today* 259 (2016) 140–149.
- [59] J. Ramirez, F. Sanchez-Minero, *Catal. Today* 130 (2008) 267–271.
- [60] R. Cattaneo, T. Shido, R. Prins, *J. Catal.* 185 (1999) 199–212.
- [61] M.A. Lélías, J. van Gestel, F. Maugé, J.A.R. van Veen, *Catal. Today* 130 (2008) 109–116.
- [62] M.A. Lelias, E. Le Guludec, L. Mariey, J. van Gestel, A. Travert, L. Oliviero, F. Mauge, *Catal. Today* 150 (2010) 179–185.
- [63] C. Kwak, M.Y. Kim, K. Choi, S.H. Moon, *Appl. Catal. A Gen.* 185 (1999) 19–27.
- [64] F. Cesano, S. Bertarione, A. Piovano, G. Agostini, M.M. Rahman, E. Groppo, F. Bonino, D. Scarano, C. Lamberti, S. Bordiga, L. Montanari, L. Bonoldi, R. Millini, A. Zecchina, *Catal. Sci. Technol.* 1 (2011) 123–136.
- [65] J. Ramirez, G. Macias, L. Cedeno, A. Gutierrez-Alejandre, R. Cuevas, P. Castillo, *Catal. Today* 98 (2004) 19–30.
- [66] P. Blanchard, C. Lamonier, A. Griboval, E. Payen, *Appl. Catal., A* 322 (2007) 33–45.
- [67] M.J. Vissenberg, L.J.M. Joosten, M.M.E.H. Heffels, A.J. van Welsenens, V.H.J. de Beer, R.A. van Santen, J.A.R. van Veen, *J. Phys. Chem. B* 104 (2000) 8456–8461.
- [68] D.S. Kim, K. Segawa, T. Soeya, I.E. Wachs, *J. Catal.* 136 (1992) 539–553.
- [69] J.A.R. VAN VEEN, H. DE WIT, C.A. EMEIS, P.A.J.M. HENDRIKS, 582 (1987) 579–582.
- [70] P.R. H. Toulhoat, *Catalysis by Transition Metal Sulphides*, Paris, France, 2013.
- [71] L.T. Zhuravlev, *Colloids Surfaces A Physicochem. Eng. Asp.* 173 (2000) 1–38.
- [72] Y. Okamoto, *Appl. Catal. A Gen.* 226 (2002) 115–127.

- [73] U. Diebold, *Surf. Sci. Rep.* 48 (2003) 53–229.
- [74] M. Ramamoorthy, D. Vanderbilt, R.D. King-Smith, *Phys. Rev. B* 49 (1994) 16721–16727.
- [75] C.N. Satterfield, *Heterog. Catal. Pract.* (1980) 209–467.
- [76] Y. Sakashita, Y. Araki, H. Shimada, *Appl. Catal. a-General* 215 (2001) 101–110.
- [77] K. PRATT, *J. Catal.* 124 (1990) 416–432.
- [78] D. Costa, C. Arrouvel, M. Breyse, H. Toulhoat, P. Raybaud, *J. Catal.* 246 (2007) 325–343.
- [79] S. Dzwigaj, C. Arrouvel, M. Breyse, C. Geantet, S. Inoue, H. Toulhoat, P. Raybaud, *J. Catal.* 236 (2005) 245–250.
- [80] C. Arrouvel, M. Breyse, H. Toulhoat, P. Raybaud, *J. Catal.* 232 (2005) 161–178.
- [81] J. V Lauritsen, S. Helveg, E. Laegsgaard, I. Stensgaard, B.S. Clausen, H. Topsøe, E. Besenbacher, *J. Catal.* 197 (2001) 1–5.
- [82] J. Kibsgaard, B.S. Clausen, H. Topsøe, E. Laegsgaard, J. V Lauritsen, F. Besenbacher, *J. Catal.* 263 (2009) 98–103.
- [83] J. Ramirez, S. Fuentes, G. Diaz, M. Vrinat, M. Breyse, M. Lacroix, 52 (1989).
- [84] W.H. Qian, Q. Zhang, Y. Okoshi, A. Ishihara, T. Kabe, *J. Chem. Soc. Trans.* 93 (1997) 1821–1826.
- [85] J. Ramirez, L. Cedeño, G. Busca, *J. Catal.* 184 (1999) 59–67.
- [86] M. Breyse, J.L. Portefaix, M. Vrinat, *Catal. Today* 10 (1991) 489–505.
- [87] L. Coulier, V.H.J. de Beer, J.A.R. van Veen, J.W. Niemantsverdriet, *J. Catal.* 197 (2001) 26–33.
- [88] Y. Okamoto, M. Breyse, G.M. Dhar, C. Song, *Catal. Today* 86 (2003) 1–3.
- [89] J. Kibsgaard, PhD Thesis (2008) 1–159.
- [90] M. Houalla, N.K. Nag, A. V. Sapre, D.H. Broderick, B.C. Gates, *AIChE J.* 24 (1978) 1015–1021.
- [91] A. Borgna, E.J.M. Hensen, J.A.R. van Veen, J.W. Niemantsverdriet, *J. Catal.* 221 (2004) 541–548.

- [92] M.L. Vrinat, *Appl. Catal.* 6 (1983) 137–158.
- [93] P.G. Moses, B. Hinnemann, H. Topsoe, J.K. Norskov, *J. Catal.* 260 (2008) 202–203.
- [94] Y. Okamoto, K. Hioka, K. Arakawa, T. Fujikawa, T. Ebihara, T. Kubota, *J. Catal.* 268 (2009) 49–59.
- [95] J. Leglise, L. Finot, J.N.M. van Gestel, J.C. Duchet, in: B. Delmon, G.F. Froment, P. Grange (Eds.), *Hydrotreatment Hydrocracking Oil Fractions*, 1999, pp. 51–65.
- [96] C. Song, X. Ma, *Appl. Catal. B Environ.* 41 (2003) 207–238.
- [97] M. Egorova, R. Prins, *J. Catal.* 225 (2004) 417–427.
- [98] M.C.R. Daage, *J. Catal.* 149 (1994) 414–427.
- [99] J. Chen, E. Dominguez Garcia, L. Oliviero, F. Maugé, *J. Catal.* 332 (2015) 77–82.
- [100] J. Chen, L. Oliviero, X. Portier, F. Maugé, *RSC Adv.* 5 (2015) 81038–81044.

Table of contents – II Chapter

II. CHAPTER	39
2.1 Catalyst preparation.....	40
2.2 Catalyst characterization	41
2.2.1 Structural properties: X-Ray Diffraction (XRD)	41
2.2.2 Surface properties: Nitrogen adsorption	42
2.2.3 Thermal properties: Thermogravimetry	42
2.2.4 Elemental analysis by Inductively Coupled Plasma (ICP).....	43
2.2.5 High-resolution Transmission Electron Microscopy	43
2.2.6 Spectroscopy techniques	45
2.2.6.1 UV-VIS spectroscopy	45
2.2.6.2 Raman spectroscopy	46
2.2.6.3 FTIR spectroscopy	50
2.2.6.3.1 IR setup.....	50
2.2.6.3.2 CO as probe molecule.....	52
2.2.6.3.3 Spectra treatment	54
2.2.6.3.4 Spectra decomposition.....	57
2.2.6.3.5 Metal sites quantification.....	59
2.2.6.3.6 2D infrared inversion spectroscopy (IRIS).....	60
2.3 Catalytic test.....	61
2.3.1 Thiophene test	62
2.3.1.1 Setup	62
2.4 References	63

II. CHAPTER

CHARACTERIZATION TECHNIQUES

2.1 Catalyst preparation

Catalysts present in this report are mono- or bimetallic supported on different metal oxides. First, three different commercial metal oxides (Al_2O_3 , SiO_2 , TiO_2) were chosen to carry out the study on the role of the interaction metal-support on HDS catalysts. A second study was performed with synthesized mesoporous metal oxides, MCM-41, which was chosen for their high surface area. Metal oxides properties are summarized in Table II-1.

All catalysts were prepared by wetness impregnation method. Before impregnation, the support was sieved between 0.2 - 0.5 μm and calcined (the calcination program was different for each support and depends of the structure and thermal material stability). Textural study was carried out for all supports (Table II-1).

Table II-1. Support properties.

Supports	Calcination condition	Structure	Surface area (m^2/g)	Pore volume (cm^3/g)	Pore size (nm)
Al_2O_3 (Sasol)	500°C / 3h	Gamma alumina	248	0.78	13
SiO_2 (Merck)	400°C / 4h	Amorphous	506	0.7	6
TiO_2 (Degussa)	400°C / 3h	Anatase and Rutile	59	0.18	12
		Anatase	130	0.37	11
SYNTHESIZED METAL OXIDE					
MCM-41	550°C / 6h	Ordered Hexagonal Mesoporous silica	945	1.11	4

The salts ammonium heptamolybdate tetrahydrate (AHM, $(\text{NH}_4)\text{Mo}_7\text{O}_{24} \cdot 4\text{H}_2\text{O}$, Alfa Aesar, 99%) and cobalt (II) nitrate hexahydrate ($\text{Co}(\text{NO}_3)_2 \cdot 6\text{H}_2\text{O}$, Alfa Aesar, 98%) were dissolved in proper amount of deionizer water. The volume of deionised water is calculated according to the pore volume per gram of support more 30% (to be sure the pore is full of solution). Then, the metal solution is contacted with the support surface for a maturation time of 2 hours. The impregnated material is then dried in an oven at 383K during 16 hours over stirring and then calcined at 673K with a rate of 3K/min during 5 hours for non-promoted catalysts and 723K with a rate of 3K/min during 5 hours for promoted catalysts, both over air with a flow of 100 ml/min (Figure II.1).

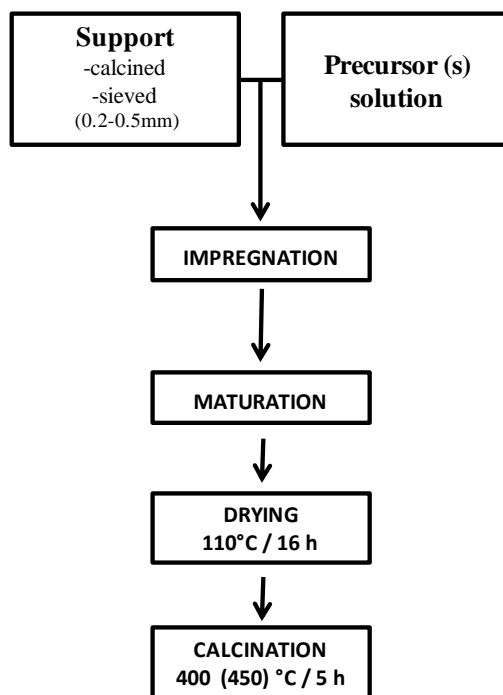


Figure II.1. Catalyst preparation scheme

2.2 Catalyst characterization

2.2.1 Structural properties: X-Ray Diffraction (XRD)

X-ray diffraction (XRD) is used to obtain information about the structure of crystalline materials based on their diffraction pattern. XRD analysis is based on constructive interference of monochromatic X-rays and a crystalline sample. The X-rays are generated by a cathode ray tube, filtered to produce monochromatic radiation, collimated to concentrate, and directed toward the sample. The interaction of the incident rays with the sample produces constructive interference and a diffracted ray, Figure II.2.

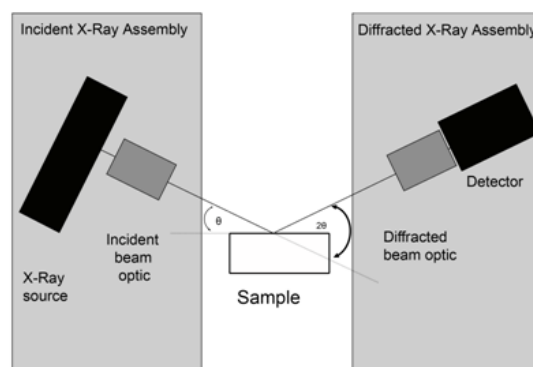


Figure II.2. Conventional XRD system

The diffraction of X-rays at crystals is described by Bragg's law ($n\lambda=2d\sin\sigma$), this law explains why the layered faces of crystals appear to reflect X-ray beams at certain angles of incidence (θ, σ).

In this work, the XRD patterns were recorded on powder, with a PANalytical X'Pert Pro diffractometer using Cu K α radiation ($\lambda = 1.5418 \text{ \AA}$, 45 kV, 40 mA).

2.2.2 Surface properties: Nitrogen adsorption

Nitrogen adsorption/desorption isotherms were measured at $-196 \text{ }^\circ\text{C}$ using Micrometrics Model ASAP 2020 volumetric adsorption analyzer. Samples were degassed at $250 \text{ }^\circ\text{C}$ under vacuum for 12 h prior to analysis. Specific surface areas were determined from the BET equation. The total volume was calculated from the volume adsorbed at $P/P_0 = 0.95$. Pore size distributions of solids were estimated by Barrett-Joyner-Halenda (BJH) method.

2.2.3 Thermal properties: Thermogravimetry

Thermal method analyses are used to determine the material changes during a temperature variation. These changes can be followed by the weight variation versus the temperature (TGA) and by differential heat flow (DSC) from ambient temperature to a maximum of 1500°C (Figure II.3). It is particularly useful in our case for the determination of thermal decomposition temperature of some template used for Mesoporous material synthesis.

Thermogravimetry analysis (TGA/DTA) measurements were carried out on a SETSYS 1750 CS evolution instrument (SETARAM). The sample (around 10 mg) was heated from 25°C to 800°C with a heating ramp of $5^\circ\text{C} / \text{min}$ over air with 40 mL/min flow rate.

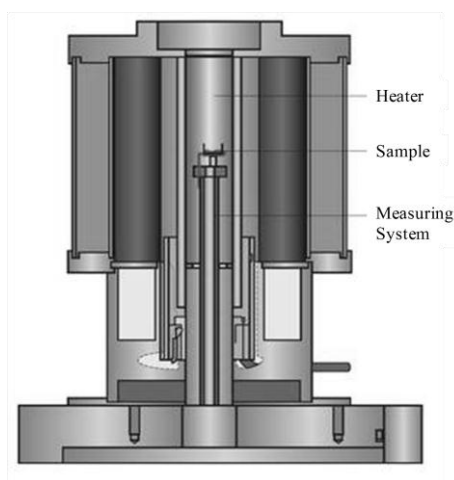


Figure II.3. Thermogravimetry system

2.2.4 Elemental analysis by Inductively Coupled Plasma (ICP)

Oxide catalysts were sulfided *ex-situ* in a glass reactor connected with 10% H₂S/H₂ (30ml/min) flow. Catalysts were sulfided at 623K with a rate of 3K/min during 2h. After, the temperature was cooled down to 298 K under N₂ flow (30 ml/min). The catalyst inside the reactor was introduced in a dry box under Ar flow, to avoid totally air contact. Then, inside the dry box, 50mg of sample was dissolved in hydrofluoric acid, aqua regia, boric acid, and water in a specific proportion with a total volume of 100 ml. Molybdenum and sulfur amount present in the catalysts was quantified by an inductively coupled plasma atomic emission spectrometry (ICP-AES) using a PerkinElmer Optima 330DV ICP instrument.

2.2.5 High-resolution Transmission Electron Microscopy

High-resolution transmission electron microscopy (HREM) was performed using a Philips CM 30T equipped with field emission gun operated at 300 kV. Samples were mounted on a microgrid carbon Quantifoil polymer supported on a copper grid by placing a few droplets of a suspension in absolute ethanol, followed by drying at ambient condition.

The samples were sulfide *ex-situ* in a glass reactor over conventional sulfidation condition (30 ml/min of H₂S/H₂ 10% at 623 K during 2 hours with a ramp at 3 K/min). After sulfidation, the sample was manipulated in a dry box over inert flow (Argon, 100 ml/min) without any air contact. The final suspension was prepared with a small amount of sulfide powder and absolute ethanol.

The measure of slabs length and stacking were determined manually by at least 300 slabs per sample from the microscopy images. The measure was done using Measurim program. Slabs length and stacking degree distributions were performed following the next equation:

$$\langle M \rangle = \frac{\sum_i M_i N_i}{N}$$

where $\langle M \rangle$ is an estimated quantity ($\langle L \rangle$, or $\langle S \rangle$), N_i in the number (frequency) of particles or slabs having the length within the discrete interval i (nm) or integer stacking i , and N total number of particles or slabs.

Total molybdenum number which forms MoS₂ slab and molybdenum located on the edges of the slabs were calculated from the “predicted” morphology using the slab length average and S-/M-edge ratio detected by IR/CO. Then, the “predicted” morphology is calculated following the next conditions:

- 1) The average slab length detected by TEM images called as L_{TEM} , is supposed to be the longer line of Mo atoms of the average MoS_2 slab as shown in Figure II.4.
- 2) The number of Molybdenum atoms which form L_{TEM} is called $N_{Mo \text{ in } L(TEM)}$, is calculated taking account the Mo-Mo distance of 3.16 \AA .
- 3) The number of Molybdenum atoms on M-edge and S-edge are called $N_{Mo \text{ in } (M-edge)}$ and $N_{Mo \text{ in } (S-edge)}$ respectively and calculated from $N_{Mo \text{ in } L(TEM)}$ with the two equation system below, Ec. II-1 and 2.

$$N_{Mo \text{ in } L(TEM)} = L_{TEM} / 3.16 + 1$$

$$N_{Mo \text{ in } L(TEM)} - 1 = N_{Mo \text{ in } (S-edge)} + N_{Mo \text{ in } (M-edge)} \quad \text{Ec. II-1}$$

$$S- / M\text{-edge ratio from IR/CO} = N_{Mo \text{ in } (S-edge)} / N_{Mo \text{ in } (M-edge)} \quad \text{Ec. II-2}$$

Thus, the prediction of MoS_2 morphology using IR/CO allows to obtain a Mo dispersion more near to the reality, since previously Mo edge dispersion were calculated with some error due to assumption of perfect triangular or hexagonal morphology [1,2]. For that reason, we propose this new calculation form using a “predicted” morphology.

Mo edge dispersion in MoS_2 nanoparticles is calculated by Ec. II-3.

$$Mo \text{ edge dispersion} = Mo \text{ located on the edges} / Total Mo \text{ in } MoS_2 \text{ slab} \quad \text{Ec. II-3}$$

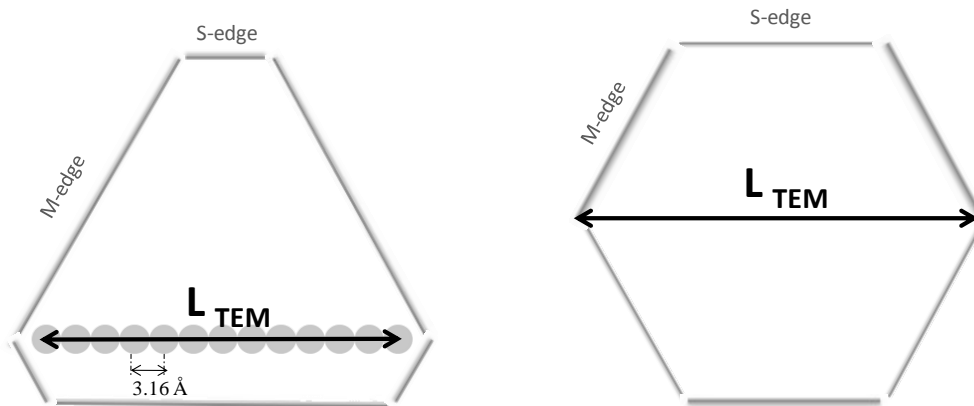


Figure II.4. Representation of MoS_2 slab for Mo edge dispersion calculation

2.2.6 Spectroscopy techniques

2.2.6.1 UV-VIS spectroscopy

Ultraviolet-visible (UV-Vis) spectra were recorded with Cary 4000 from Varian. The spectrum acquisition domain was between 800-200 nm with a speed of 300 nm/min. The analysis was done on the oxide catalysts under atmospheric conditions. Each support was used as reference knowing that some of them are active in UV-Vis creating some interferences in catalyst spectrum as shows Figure II.5 for Titania.

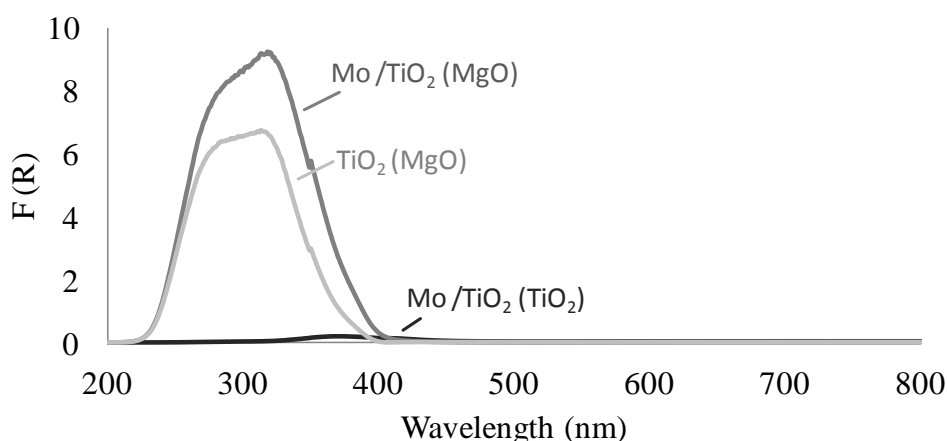


Figure II.5. Comparison of UV-Vis spectra for Mo/TiO₂ catalyst using TiO₂ or MgO as reference. In parenthesis the reference material is indicated

Several studies have been realised to investigate the average of particle domain sizes for transition metal oxides by the analysis of the optical band gap energy determined from the position of the low energy rise in the material UV-VIS spectrum [3–6]. A decrease of band gap energy is linked to greater particle domain size.

Normally, peak position is the conventional way to study electronic spectra for catalysts, but it can be limited by the influence of the vibration states of the sample structure or in our case, by the support structure [6,7]. For that reason the samples are compared through the *edge absorption energy*. This edge absorption energy is determined by finding the energy intercept of a straight line fitted through the low energy rise in the graphs of $[F(R) \cdot hv]^2$ vs hv , where $F(R)$ is the Kubelka-Munk function as shown in Figure II.6.a. Edge energy can be compared to the one obtained from results of molecular orbital calculation, but also can be compared with the average of number of nearest Mo neighbours in identified clusters. Indeed, it has been reported an empirical, linear correlation between edge energy and the local degree

of aggregation of the clusters as given by Ec. II-4. An example of graph is shown in Figure II.6 b.

$$N_{Mo} = 16 - 3.8 \cdot E$$

Ec. II-4

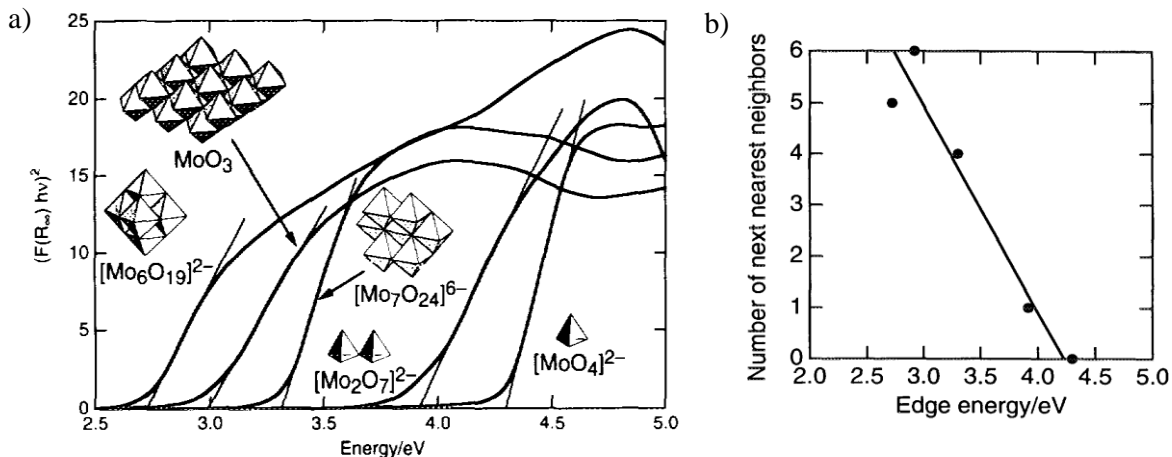


Figure II.6. Lower edge energy calculation (a) and relation with the number of nearest neighbours (b) [8]

2.2.6.2 Raman spectroscopy

In this work, Raman spectroscopy was used to study the dispersion of molybdenum oxide so all the measures were done for catalyst in oxide state. Raman spectroscopy was performed using a Jobin Yvon Labram 300 Raman spectrometer equipped with a confocal microscope, an Nd-YAG laser (frequency doubled, 532 nm) and a CCD detector (Figure II.7). Spectra were recorded at ambient conditions in the range between 100 and 1050 cm^{-1} .

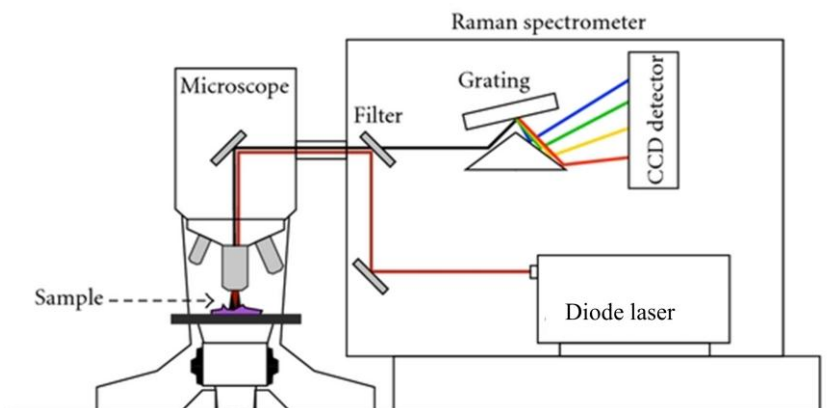


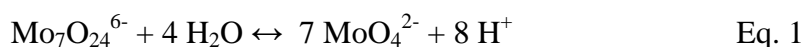
Figure II.7. Typical setup Raman spectrometer

The typical vibration range for metal oxide is below 1000 cm^{-1} which is a conflict region for FTIR spectroscopy because of the cell window absorption. It makes Raman spectroscopy; a powerful technique to study molecular vibrations of dispersed oxidic metal species.

Then, the interesting region for oxomolybdate species is between 100 and 1000 cm^{-1} where Raman vibration modes can be classified in two different types: bridge vibration (Mo-O-Mo) appears between 600 and 900 cm^{-1} and terminal vibration (Mo=O_t) between 900 and 1000 cm^{-1} [9].

The formation of oxomolybdate species depends strongly on the preparation method, pH solution, interaction with the support, metal loading, etc [4–8]. Therefore, the next paragraphs are focus in the literature Raman data on oxidic molybdenum species formed on Al₂O₃, SiO₂ and TiO₂ supports (supports studied in this work), using heptamolybdate ammonium as molybdenum precursor and prepared by wetness impregnation method.

Heptamolybdate solution, without pH modification, has a pH around 5.5 [15], and the equilibrium between Molybdate (M) and Heptamolybdate (HM) shown in Eq.1 occurs:



The direction of equilibrium changes versus the concentration and/or pH of the solution. Then, the nature of the species in solution and the temperature used to dry or calcined the sample after impregnation are the principal factors influencing the final state of the oxidic metal species formed on the catalyst surface. In order to clarify the assignment of oxomolybdate vibrations for the catalyst studied in this work, Raman vibration modes detected in aqueous solution of monomers and polymolybdate used as reference are shown in Table II-2.

Table II-2. Raman vibration modes of oxidic molybdenum species in aqueous solution [12]

Species (aq.) \ vibration mode	ν_{sym} (Mo-O _t)	ν_{asym} (Mo-O _t)	ν_{sym} (Mo-O-Mo)	(Mo-O _t) _{bend}	(Mo-O-Mo) _{deformation}
MoO ₄ ²⁻	898 cm ⁻¹	840 cm ⁻¹	-	320 cm ⁻¹	-
Mo ₇ O ₂₄ ⁶⁻	937 cm ⁻¹	900 cm ⁻¹	860 cm ⁻¹	360 cm ⁻¹	220 cm ⁻¹

The alumina support has a strong basic effect, and it can change the M/HM ratio when the solution which contains initially heptamolybdate species, is in contact with the surface in wetting condition. Indeed, at low Mo loading (corresponding to around 1 atom.nm^2),

heptamer became monomer species during wetting step as revealed by the appearance of the principal band at 898 cm^{-1} . This band has a shoulder at higher wavenumber (920 cm^{-1}) which can be due to the anchorage of the monomeric species to the surface. In the case of the preparation of catalyst with higher Mo loading (corresponding to density around 2.5 atom.nm^{-2}), the solution contains mainly heptamolybdate species but the Raman spectrum after wetting step presents two principal bands at 940 and 900 cm^{-1} which are characteristic of the presence of both molybdate and heptamolybdate species. After the drying step, the band at 940 cm^{-1} increases and the one at 900 cm^{-1} decreases, but no other modification was detected (shift or new band) in the spectrum. Instead, after calcination step MoO_3 presence is detected by the appearance of two characteristic bands of this compound at 820 and 995 cm^{-1} . Also the band characteristic of heptamolybdate at 940 is shifted to 960 cm^{-1} [12].

According to the previous results, it's possible to deduce a scheme of molybdenum oxidic species that can be found on the surface as it is shown in Figure II.8. The main conclusion is that the more bridging O in the environment of the Mo^{6+} , the higher the wavenumber associated to the Mo-O_t bond. Furthermore, there is a second factor influencing the Raman bands position that is the existence of coordinative unsaturated Mo^{6+} ions: the wavenumber associated to the Mo-O_t bond increases when the coordination number decreases [4,5].

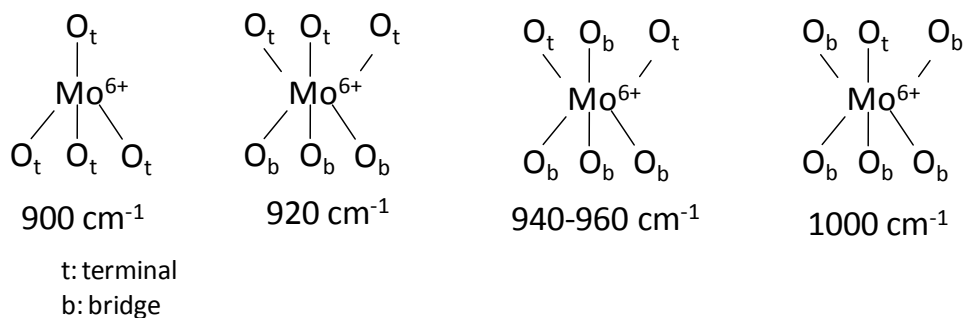


Figure II.8. Scheme of molybdenum oxide species in relation with Raman Mo-O_t vibration modes [12]

Let's now consider the other bond vibration, the Mo-O_b . Some controversies can be found in the literature to explain the band at 860 cm^{-1} corresponding to this bridge vibration that could be due either to the interaction with the support or with other Mo atoms in molybdenum oxide specie [17,18]. Moreover, there are others influences; for instance the interaction with the support depends on its nature.

One clear example of these phenomena is MoO_x supported on Titania for which a shift to higher wavenumber in both Mo-O terminal vibration and Mo-O_b is reported and can be attributed to the support interaction [11]. Also, the study of molybdenum oxide species supported on Titania is more complicated than on Alumina due to the high intensity of vibration bands coming from the Titania structure. Roughly, two bands are found in $\text{MoO}_x/\text{TiO}_2$ catalyst one characteristic of Mo=O terminal vibration around 960 cm^{-1} and another one around 870 cm^{-1} characteristic of Mo-O-Mo bridge vibration attributed to polymolybdate species which appear with Mo concentration below 4 atoms Mo/nm^2 [11]. Instead, MoO_3 formation appears with higher concentration and the main band characteristic of MoO_3 species appear at 995 and 820 cm^{-1} for terminal and bridge vibrations respectively [4,5,6].

Formation of silicomolybdic acid in silica-supported molybdenum oxide samples has been reported for several authors, and its formation requires a prolonged exposure to amount of water. Therefore it can be formed during the impregnation of aqueous solution of heptamolybdate [13,19]. Then the Raman vibration detected for silicomolybdic acid are at 980 , 963 cm^{-1} corresponding to Mo=O terminal vibrations symmetric and asymmetric respectively; at 883 cm^{-1} corresponding to Mo-O-Mo bridge symmetric vibration and the last at 250 cm^{-1} corresponding to Mo=O_{bend} terminal vibration [12]. The dehydrated Raman spectra of molybdena/silica catalysts shows the principal bands between 960 and 990 cm^{-1} that can be ascribed to silicomolybdic acid species.

The surface study becomes more complex when other metal oxide is added to the surface. This is the case of CoMo catalysts, many studies were performed in CoMo catalyst by Raman spectroscopy, and different species can be distinguished: *oxomolybdate species* were found with the same band discussed previously for Mo catalysts, *cobalt oxide* (Co_3O_4), cobalt in interaction with Al_2O_3 called *CoAl₂O₄*, and cobaltmolybdate species called *CoMoO₄*. Raman stretching for cobalt oxide species is ascribed to a band appearing at 690 cm^{-1} for CoMo/ Al_2O_3 catalyst [17]. The same band also is ascribed to *CoAl₂O₄* species. Instead, *CoMoO₄* species give a band appearing at 940 cm^{-1} [20].

2.2.6.3 FTIR spectroscopy

Material surfaces are directly involved in important catalysis procedures such as adsorption, desorption, diffusion, transformation, etc. For that reason, surface science is one of the most important branches of modern physics and chemistry. Normally, surfaces are formed by the presence of a large number of crystal lattice defects as edges, corners, brims, terraces, steps, in the dispersed material which lead to have different surface properties. The ions on the surface are characterized by a lower coordination than those in the bulk (coordinatively unsaturated sites, CUS), and the unfilled coordination of these ions make them active for molecule adsorptions, and then for catalysis.

Infrared (IR) spectroscopy gives direct information about the chemical nature of the surface and/or molecule adsorption: as an example the chemical and physical interaction between some molecules and the surface can be distinguished. For that reason, IR is a great technique to study the catalyst surface and understand the role of the active sites in catalytic reaction.

2.2.6.3.1 IR setup

The IR setup (Figure II.9) used in this work typically includes three parts: the evacuation system, the IR cell, and the spectrometer. The evacuation system allows us to get ultra high vacuum down to 10^{-3} Pa in the IR cell, as well as the introduction and evacuation of probe molecule into the cell since it is connected with pump systems and the entrance of gases used as probe molecule. The IR cell which is described more carefully below, has a specific design to carry out the activation of the sample *in situ*. The spectrometer is a Fourier Transform IR spectrometer from Nicolet, with a MCT (Mercury Cadmium Telluride) detector. The spectra were collected by 256 scans with a resolution of 4 cm^{-1} .

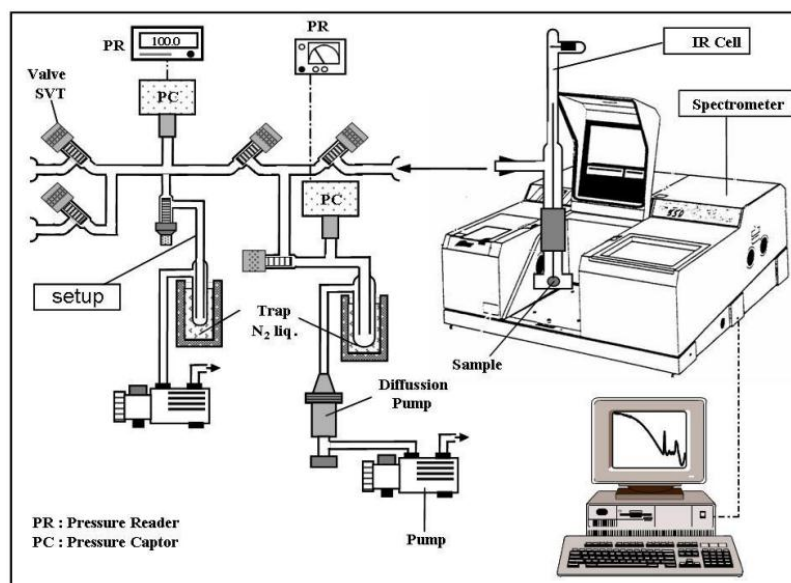


Figure II.9. Infrared setup

The IR cell used in this work is “a low temperature glass cell” (Figure II.10), where the samples can be treated at high temperature and atmospheric pressure under a controlled flow. This cell allows us to perform an *in situ* sulfidation under reaction flow followed by CO adsorption at liquid nitrogen temperature (100K).

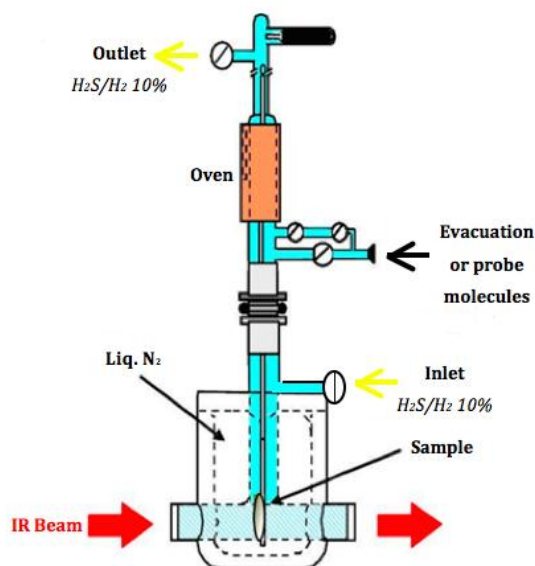


Figure II.10. IR cell at low temperature

The conventional procedure followed for all the sample is described: First, the sample is pressed in wafer form (area of 2 cm^2 , mass around 10-20 mg, precisely weighted). After, the sample is sulfided under 10% $\text{H}_2\text{S} / \text{H}_2$ flow (30ml/min) at 623 K for 2 hours with a heating

rate of 3 K/min. Then, the flow of 10% H₂S /H₂ is changed for Ar flow (30ml/min) for 10 minutes, and it is followed by evacuation at the same temperature during 1 h and then during the temperature decrease to room temperature. In the end of evacuation, the pressure of the cell must reach 10⁻³Pa. Finally, the sample is cooled down by the introduction of liquid nitrogen in the Dewar to 100 K and is ready for CO adsorption.

2.2.6.3.2 CO as probe molecule

IR spectroscopy allow the study of some stable species present in the material surface which are active to infrared as hydroxyl group, oxo-group, hydrocarbon group, amine group, etc. However, IR spectroscopy is blind with respect to the presence of CUS ions which are however decisive for catalytic properties. This problem is solved by the use of probe molecules such as CO, NO, O₂, CH₃OH, etc. Probe molecules interact with defects on the surface, and the alteration of their spectral features as a result of adsorption provide indirect information about the properties, location, or concentration of the surface sites.

The most frequently used probe molecule is carbon monoxide because it is a clean molecule (extra pure > 99%), small, which leads to non steric interactions and non-reactive adsorption. The vibrational spectrum obtained is simple and the stretching vibration is sensitive to the strength of the bond formed with the surface. Moreover, depending on the nature of the bond with the surface, CO has a high molar extinction coefficient.

CO molecule has four filled bonding orbitals, $3\sigma_n^2$, $4\sigma_n^2$, $1\pi_x^2$, $1\pi_y^2$, and one occupied weakly anti-bonding orbital, $5\sigma_n^2$. Furthermore, there are three empty molecular orbital, two $2\pi^*$ orbitals and one 6σ orbital. The highest occupied molecular orbital, HOMO, is the 5σ orbital, and the lowest unoccupied molecular orbital, LUMO, are the $2\pi^*$ orbital. As both orbitals, 4σ (at the O atom) and 5σ (at the C atom) are occupied and oriented away from the molecule along the molecular axis, CO molecule can participate in coordination bonds as a weak Lewis base. The ability to donate electrons from the two orbitals is different and depends on the orbital energies: i.e. the O atom of CO is a weaker Lewis basic center than the C atom because of the much lower orbital energy of the 4σ compared with the 5σ molecular orbital.

Then, CO interacts with metal ion by three different mechanisms: i) simple electrostatic interaction of the CO molecule with the field of the cation, ii) formation of a σ bond with CO as an electron donor, and iii) formation of a π bond with CO as an electron acceptor (Figure II.11). Electrostatic interaction denotes all effects of the metal ion that do not

include electron transfer from or to the ligand orbitals. One of these effects is the simple electrostatic interaction of the charge distribution of the CO molecule and the field of the cation. This is connected with stabilization of all orbitals of CO in the positive electrostatic potential generated by the cation and gives a positive contribution to the interaction energy. This contribution is partially compensated by the Pauli repulsion term which accounts for the repulsion between electron of the cation and the one of CO. And other effect is the polarization of the ligand molecule because the electrostatic potential is different at the position of C and O atoms of CO molecule as a consequence of the electrostatic field of the cation. Instead, according to the frontier orbital approach, the most important chemical interaction between two reacting particles occurs between their HOMO's and LUMO's when the symmetry of the corresponding orbital fits. In the case of coordination of CO to a metal ion, the first interaction proceeds between the HOMO of CO, 5σ , and a LUMO of the metal ion with a suitable spatial orientation. The second part of the frontier orbital interaction is between the occupied HOMO of the metal ion and the empty $2\pi^*$ orbitals of the ligand molecule. The formation of this π bond leads to a transfer of electron density from the cation to the ligand, and then the concept of *back-donation* appears. Therefore, these three CO- M^{n+} interactions produce some variation in C-O stretching frequency of M^{n+} -CO species, typically observed in the spectral region between 2245 and 2000 cm^{-1} . The variation of the electrostatic, σ , π contribution to the bonding of CO in M^{n+} -CO species is an important factor which accounts for the shift of its stretching frequency. And generally, the electrostatic interaction and the σ bond cause a weak frequency shifts and the π bond causes strong frequency shifts [21]. In this latter case, the greater the back-donation, the lower the frequency is detected [22]. Since π bond of M^{n+} -CO causes the strongest shift effect in CO frequency, below is described a serial of parameters associated with metal nature than makes CO frequencies vary:

- Geometry to coordination sites (linear, bridged species, etc)
- Metal coordination
- Metal oxidation state
- CO coverage
- The presence of electronic or nucleophilic compound

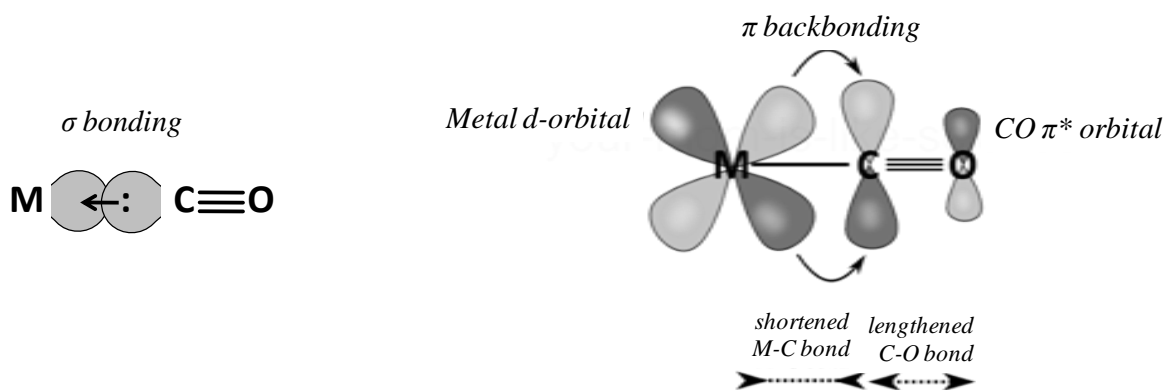


Figure II.11. Schematic representation of the orbital interactions in formation of σ and π bonds between CO and a metal ion [21]

CO adsorption depends strongly on the nature of the cations. Thus, some carbonyls are detected at low temperature only, whereas others are stable even at 670K. Then, having a preliminary idea of the surface species, one can choose the experimental condition. Although CO stretching frequency is the most informative parameter, the data determining the stabilities of the various species can be decisive for the assignment of the bands. For that, a helpful methodology (e.g. to calculate CO molar extinction coefficient) is the successive adsorption of small doses of CO pressures upon saturation. This procedure provides information about the stabilities of the various species since the most energetic sites is the first to be occupied by CO molecule.

2.2.6.3.3 Spectra treatment

In our case, CO adsorption at low temperature (100K) is carried out introducing controlled CO pressure measured by a standard volume called “small volume”, which is installed just before the entrance of the cell. This procedure allows study the nature of CO/sites interaction, calculation of the molar extinction coefficient from different species, and the quantification of adsorbed CO on different sites. Figure II.11 shows the typical CO adsorption spectra on (Co)Mo /Al₂O₃ from small doses beginning with 133 Pa of CO pressure upon saturation using equilibrium pressure (133 Pa). The first CO doses can be used to calculate the molar extinction coefficient of CO/M-edge vibration. Generally, CO interacts with sulfide clusters (MoS₂ or CoMoS) and the support surfaces as show figure II.11. CO interaction with MoS₂ or CoMoS nanoparticles is the most interesting point in this work. Recently, a combination of experimental and theoretical studies carried out for non-promoted catalysts, could distinguish CO stretching vibration of Mo located on M-edge or S-edge from MoS₂ nanoparticles. Indeed,

CO interacts with molybdenum located in M- and S-edge leading to two contributions at different wavenumbers, 2110 cm^{-1} and 2070 cm^{-1} due to their different environments [23–25]. Instead, the assignment of CO stretching vibrations for promoted catalysts is still not completely established. There are some theoretical studies about the effect of promotion nature, morphology, even about CO stretching vibrations for different promotion degree in different edges (M- and/or S-edge) [26]. But experimentally, the studies only could assign the $\nu(\text{CO})$ bands to CO interacting with non-promoted and promoted sites at 2110 cm^{-1} and $2050\text{--}2090\text{ cm}^{-1}$, respectively [27–30].

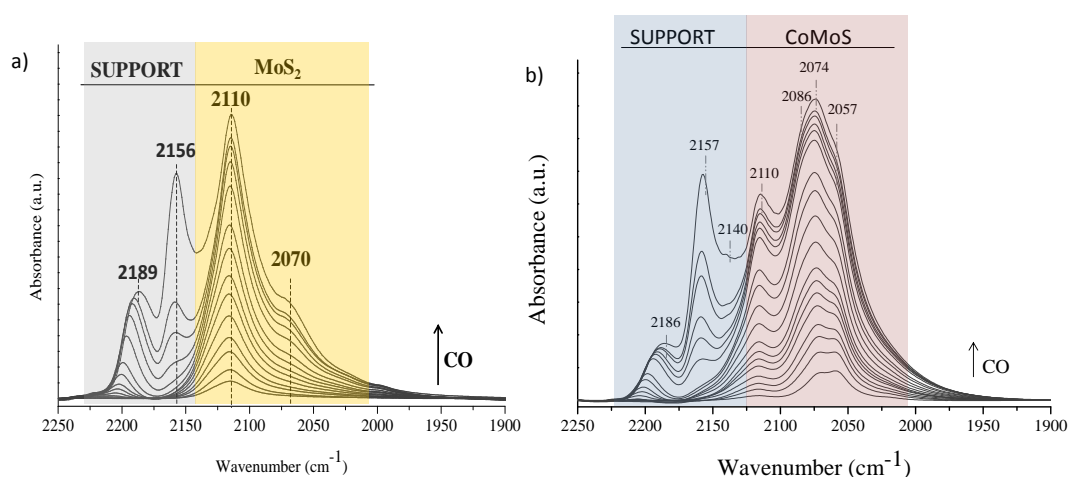


Figure II.12. CO adsorption spectra at low temperature upon saturation: a) Mo (12 % wt) / Al_2O_3 [31] and b) CoMo (12 % wt Mo, $\text{Co}/\text{Mo}+\text{Co}=0,3$) / Al_2O_3 [32]

Table II-3 shows CO stretching for non-promoted catalysts supported on Al_2O_3 . The table include CO stretching vibration obtained experimentally and calculated by DFT. The correlation between them allows the distinction and the quantification of molybdenum located in both edges on MoS_2 nanoparticles. That distinction leads to the prediction of MoS_2 morphology and then to the study about the role of the nature of edge sites on the catalytic activity.

Table II-3. CO stretching vibration assignment for non-promoted catalysts

ν (CO) band experimental (cm^{-1})	ν (CO) band calculated by DFT (cm^{-1})	Band assignment	Ref.
2130	-	Partially sulfided	[33]
2110	2110	M-edge (50% sulfur coverage)	[25,26,33,34]
2098	2087	M-edge (37.5% sulfur coverage)	[25,26,32,33]
2070	2078	S-edge (100% sulfur coverage)	[25,26,33,34]
2040	-	S-edge (sulfur coverage between 75 and 100%)	[23,34]
2020	1989	S-edge (75% sulfur coverage)	[33]
1995	-	Metallic Mo	[35]

However, Table II-4 shows the CO stretching wavenumber calculated by DFT calculation for promoted catalysts. Travert et al. calculated CO stretching wavenumber for CoMo and NiMo catalysts supported on Al_2O_3 in conventional sulfidation condition (10% $\text{H}_2\text{S} / \text{H}_2$) taking into account different promotion degree, partially with 25% and totally; as well as the promotion in different edges of MoS_2 , M- and S-edge. This big advance of CO stretching assignment for promoted catalysts could not be applied to the experimental spectra because CO stretching vibration of CO in interaction with promoted sites appears at the same range than CO stretching vibration of CO in interaction with Mo located on S-edge. This experimental limitation leads to the difficult assignment of the different components because there is no evidence of the absence of CO/S-edge contribution for promoted catalyst.

Table II-4. CO stretching calculated by DFT for promoted catalysts with different promotion degree and different MoS₂ edges [26]

Promotion degree	ν (CO) calc. by DFT (cm ⁻¹)	E _{ads} (eV)	Band assignment
100 %	2083	1.4	Co _(4C) (M-edge)
	2080	0.7	Co _(4C) (S-edge)
25%	2080	1.1	Mo _(5C) (M-edge)
	2076	1.0	Co _(4C) (M-edge)
	2054	0.7	Mo _(4C) (M-edge)
	2065	0.7	Co _(4C) (S-edge)
	2041	0.7	Mo _(4C) (S-edge)

2.2.6.3.4 Spectra decomposition

The distinction of Molybdenum located in M- and S-edge sites by IR/CO is a beneficial characteristic of this method, which allows a more precise study of sulfide catalysts. Until now, CO adsorption spectra were decomposed to distinguish the contributions of the support from the one of the sulphide clusters. A more accurate decomposition is now carried out but as shows Figure II.13.

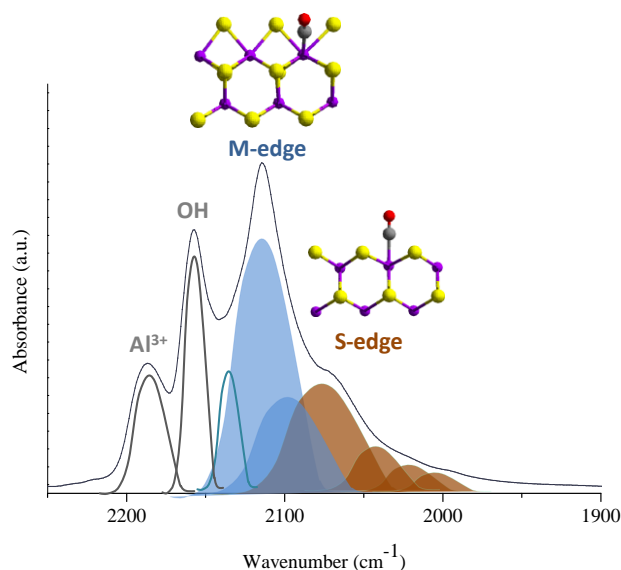


Figure II.13. Decomposition components on Mo (12 % wt) /Al₂O₃

Table II-5 shows the parameters used to decompose IR spectrum of CO adsorption in equilibrium pressure with 133 Pa. The first table correspond to all components used to fit the CO spectra for non-promoted catalysts and the second one (bellow) correspond to all components used to fit CO spectra at equilibrium pressure (133 Pa) for promoted catalysts. The decomposition of spectra for non-promoted catalysts is composed by seven components attributed to sulfided species and they can be assigned from lower wavenumber to higher wavenumber following: 1995 cm^{-1} band is ascribed to metallic Mo [36], 2020, 2040 and 2068 cm^{-1} bands are scribed to Mo located on S-edge, 2099 and 2110 cm^{-1} bands are ascribed to Mo located on M-edge, and finally 2126 cm^{-1} band is ascribed to partial sulfided species. CO bands due to its interaction with the support are added also to the decomposition but there are not shown because they are not significant to the study of MoS_2 nanoparticles. In order to advance in the investigation and understand CoMoS species formation, decomposition of IR spectra of CO at equilibrium pressure for promoted catalysts was performed due to the observation of different components from the second derivate function. As it will be explained later on, the component used to fit the spectra can be assigned from lower to higher wavenumber following: 1995 cm^{-1} band is ascribed to metallic Mo as previously, 2020 and 2038 cm^{-1} band is ascribed to Mo located on *promoted* S-edge, 2057 cm^{-1} band is ascribed to Co partially *promoted* located on S-edge, 2073 cm^{-1} band is ascribed to Co partially *promoted* located on M-edge, 2083 cm^{-1} band is ascribed to totally *promoted* located in M-edge, and finally 2098 and 2110 cm^{-1} bands are ascribed to *non-promoted* sites located on M-edge.

Table II-5. Parameters of the peak used to fit the IR spectra with OMNIC

Peak type	Peak center (cm^{-1})	FWHH (cm^{-1})
Voigt	1995 \pm 4	30 \pm 4
Voigt	2020 \pm 4	27 \pm 4
Voigt	2040 \pm 4	25 \pm 4
Voigt	2068 \pm 4	24 \pm 4
Voigt	2099 \pm 4	18 \pm 4
Voigt	2115 \pm 4	13 \pm 4
Voigt	2126 \pm 4	17 \pm 4

Peak type	Peak center (cm ⁻¹)	FWHH (cm ⁻¹)
Voigt	1995±4	27±4
Voigt	2020±4	20±4
Voigt	2038±4	16±4
Voigt	2057±4	12±4
Voigt	2065±4	10±4
Voigt	2073±4	11±4
Voigt	2083±4	11±4
Voigt	2098±4	15±4
Voigt	2110±4	12±4

2.2.6.3.5 Metal sites quantification

After the spectrum decomposition is performed the quantification of the different sites is carried out following the next equation:

$$n = \frac{Area \cdot S_{catalyst}}{\varepsilon \cdot m_{catalyst}}$$

where n is the site concentration ($\mu\text{mol g}^{-1}$), $Area$ is the IR band area of CO adsorbed on the sites (cm^{-1}), $S_{catalyst}$ is the surface of the wafer (cm^2), $m_{catalyst}$ is the wafer mass (g) and ε is the molar adsorption coefficient which is characteristic of each species that adsorbs CO ($\text{cm} \cdot \mu\text{mol}^{-1}$).

Experimentally all those parameters are known. In our case, all spectra after CO adsorption are normalised to a wafer mass of 0.01 g and 2.01 cm^2 of surface. The IR band area of adsorbed CO is calculated from the spectrum decomposition. The molar extinction coefficient depends on the species: it was calculated for Mo located on M-edge and S-edge with the values of $16 \pm 4 \text{ cm} \cdot \mu\text{mol}^{-1}$ and $35 \pm 9 \text{ cm} \cdot \mu\text{mol}^{-1}$, respectively. Maugé et al was the first to calculate the molar extinction coefficient for Mo /Al₂O₃ catalyst of CO stretching band at 2110 cm^{-1} , and CoMo /Al₂O₃ catalyst of CO stretching band at 2060 cm^{-1} with a molar extinction coefficient of $43 \pm 12 \text{ cm} \cdot \mu\text{mol}^{-1}$ [29]. Recently, an improvement of the calculation was performed by Chen et al. using a serial of (CA/Mo=x) /Al₂O₃ catalyst which present a variation of S-/M-edge ratio that allows to calculate molar extinction coefficient for Mo located on S-edge with CO stretching bands at 2020, 2040 and 2068 cm^{-1} . Then the molar extinction coefficient obtained for CO/S-edge stretching was $35 \pm 9 \text{ cm} \cdot \mu\text{mol}^{-1}$ [34].

In conclusion, values discussed previously, were used in this work to quantify different Mo sites. Moreover, in order to verify the validity of these values for the study of new materials, several molar extinction coefficient calculations were performed as shown in annex III.

2.2.6.3.6 2D infrared inversion spectroscopy (IRIS)

In collaboration with A. Travert, several experiments of CO adsorption at liquid nitrogen temperature were performed for a series of catalysts using 2D infrared inverse spectra method developed by this author.

The strong overlapping that is presented frequently in infrared spectra lead to the searching of method to study these complex case which cannot be solved by a traditional study method. For that reason, Travert et al. developed 2D Infrared Inversion Spectroscopy (2D IRIS) method which allows the simultaneous determination of surface affinities of different adsorbed species from their spectroscopic isotherm (absorbance vs. pressure). It was first performed to distinguish different carbonate species detected in CO₂ adsorption in ZrO₂ that present a strong overlapping in the 1800-1200 cm⁻¹ range. This method is described thereafter.

2D Infrared Inversion Spectroscopy (2D IRIS) is based on the inverse of the infrared spectra that consist in inverting the adsorption integral equation describing the spectroscopic isotherm which yields a 2D infrared spectrum (absorbance vs. Wavenumber) and the logarithm of adsorption equilibrium constants (ln K). The spectra of individual species are resolved in the later dimension, hence allowing the quantification of their Gibbs free adsorption energies. Therefore, the aim of the inversion method is to resolve the individual infrared spectra of adsorbed species and to extract their surface affinities from the pressure dependence of the absorbance. When the thermodynamic equilibrium is reached with the gas phase and the surface, the total IR absorbance at a given wavenumber and pressure $\alpha(\nu, p)$ can be expressed as a superposition of local isotherm $\theta(p, K)$ weighted by a distribution function $f(\nu, K)$:

$$\alpha(\nu, p) = \int_{-\infty}^{\infty} \theta(p, K) f(\nu, K) d \ln K$$

where K is the adsorption constant and ln K is proportional to the adsorption Gibbs free energy:

$$\ln K = -\Delta_{ads}G/RT$$

In first approximation, the local isotherm can be expressed by the Langmuir isotherm:

$$\theta(p, K) = \frac{K \frac{p}{p^{\circ}}}{(1 + K \frac{p}{p^{\circ}})}$$

The distribution function $f(v, K)$ is directly related to the amount of adsorption sites $N(K)$ with an adsorption constant K :

$$f(v, K)d\ln K = N(K) \in (v, K)/A$$

where $\in (v, K)$ is the adsorption coefficient of corresponding surface species and A is the geometric surface area of the pellet.

Small experimental error in the experimental isotherm $\alpha(v, p)$ can lead to large changes in the distribution function $f(v, K)$. This problem is solved using a classical procedure known as Tikhonov regularization.

Since 2D IRIS method got a good result separating components in a multiple overlapping IR spectra for CO₂ adsorption, it is used for non- and promoted sulfide catalysts to separate several component detected by the second derivate function in the promoter region between 2090-2020 cm⁻¹, and to determine the contribution of Mo in S-edge free of promotion in this promoted range.

2.3 Catalytic test

Catalytic tests were performed in all catalysts to study the role of different active sites formation in HDS reaction. Two kind of hydrodesulfurization test were performed each one with different sulfur feed: thiophene and dibenzothiophene, which differ of molecule size. The first one was used as a rapid way to evaluate the catalytic performances on different samples. And the second, more representative to sulfur compound in the actual gas-oil, leads to the possibility of study the selectivity.

2.3.1 Thiophene test

2.3.1.1 Setup

The thiophene HDS tests are performed in a stainless steel reactor. The setup is schemed in Figure II.14. Before activity test, the catalysts were sulfided under 10% H₂S/H₂ at 623 K during 2 hours with a heating ramp of 3 K /min (i.e. the same condition that for IR experiment). After that the flow is shifted to the feed flow.

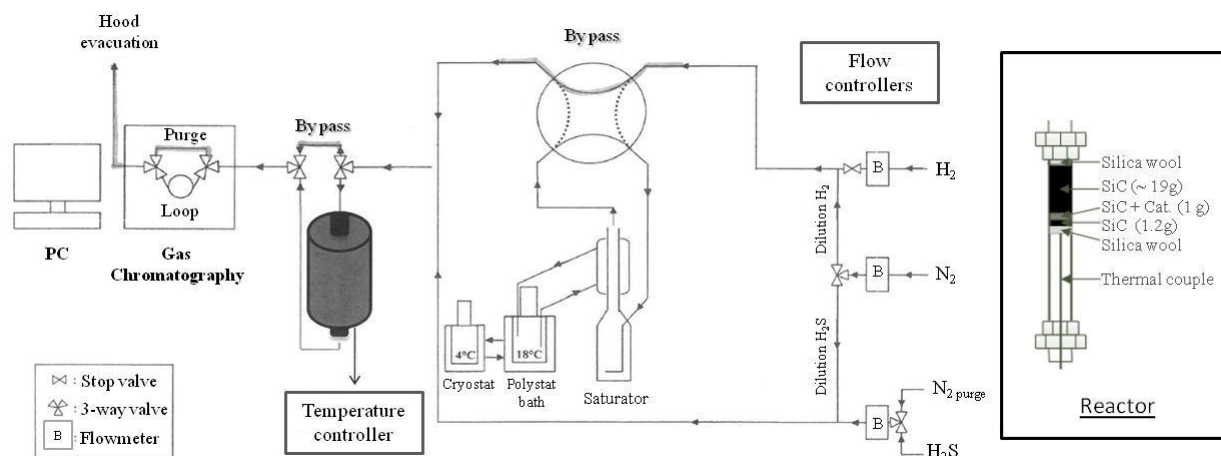


Figure II.14. Thiophene test setup

The thiophene HDS reaction was carried out at 623K using a feed (~90ml/min) consisting of 8.0 KPa thiophene, 91.2 KPa H₂ and 2.1 KPa H₂S. The gas mixture is prepared by flowing pure H₂ through a saturator containing liquid thiophene (Alfa Aesar, 99%, extra pure) kept at a constant temperature of 291K.

In all the experiments, the outlet gas was analyzed by a Varian 3900 chromatograph equipped with flam ionization (FID) detector. The concentrations of butane, 1-butene, trans-2-butene, cis-2-butene, tetrahydrothiophene (THT), as well as thiophene were recorded. In order to get a differential reactor, the conversion of thiophene is controlled below 10%.

The specific rate (r_s , mol / h.kg) was calculated using the formula as follows:

$$r_s = \frac{x \times F}{m_{cat}}$$

where χ is thiophene conversion (%), F is molar flow rate of thiophene (mol.h⁻¹), m_{cat} is the mass of the catalyst after sulfidation (corrected by the value obtained in IR experiments, kg).

Note that in this work, the formation of THT was considered when calculating the rate in thiophene HDS even if THT still contains sulfur.

2.4 References

- [1] S. Kasztelan, H. Toulhoat, J. Grimblot, J.P. Bonnelle, *Bull. Soc. Chim. Belg.* 93 (1984) 807–811.
- [2] E.J.M. Hensen, P.J. Kooyman, Y. van der Meer, A.M. van der Kraan, V.H.J. de Beer, J.A.R. van Veen, R.A. van Santen, *J. Catal.* 199 (2001) 224–235.
- [3] L.E. Brus, *J. Chem. Phys.* 80 (1984) 4403.
- [4] N. Chestnoy, R. Hull, L.E. Brus, *J. Chem. Phys.* 85 (1986) 2237.
- [5] L. Brus, *J. Phys. Chem.* 90 (1986) 2555–2560.
- [6] M. Fournier, C. Louis, M. Che, P. Chaquin, D. Masure, *J. Catal.* 119 (1989) 400–414.
- [7] E.J. Johnson, in: , 1967, pp. 153–258.
- [8] R.S. Weber, *J. Catal.* 151 (1995) 470–474.
- [9] I.E. Wachs, *Catal. Today* 27 (1996) 437–455.
- [10] D.Q. Inorgsmica, *F. De Farmacia*, (1994) 2215–2221.
- [11] S. Dzwigaj, C. Louis, M. Breyse, M. Cattenot, V. Bellière, C. Geantet, M. Vrinat, P. Blanchard, E. Payen, S. Inoue, H. Kudo, Y. Yoshimura, *Appl. Catal. B Environ.* 41 (2003) 181–191.
- [12] E. Payen, J. Grimblot, S. Kasztelan, *J. Phys. Chem. J. C. Adv. Chem. Ser* 91 (1987) 6642–6648.
- [13] W. Banares, Hu, (1994).
- [14] D. Zingg, L. Makovsky, R. Tischer, F. Brown, D. Hercules, *J. Phys. Chem.* 84 (1980) 2898–2906.
- [15] J.A.R. VAN VEEN, H. DE WIT, C.A. EMEIS, P.A.J.M. HENDRIKS, 582 (1987) 579–582.

- [16] J.G. and J.P.B. S. KASZTELAN, E. PAYEN, H. TOULHOAT, 5 (1986) 157–167.
- [17] J.G. and J.P.B. S. KASZTELAN, E. PAYEN, H. TOULHOAT, Polyhedron 5 (1986) 157–167.
- [18] I.E. Wachs, Catal. Today 27 (1996) 437–455.
- [19] J.M. Che, M., Louis, C., and Tatibouet, Polyhedron 5 (1986) 123.
- [20] L.E. Makovsky, J.M. Stencel, F.R. Brown, R.E. Tischer, S.S. Pollack, J. Catal. 89 (1984) 334–347.
- [21] K.I. Hadjiivanov, G.N. Vayssilov, Adv. Catal. 47 (2002) 307–511.
- [22] P. Bazin, O. Saur, J.C. Lavalley, M. Daturi, G. Blanchard, Phys. Chem. Chem. Phys. 7 (2005) 187.
- [23] J. Chen, Effet de La Pression de Sulfuration et D'agent Chélatant Sur La Morphologie et La Réactivité Des Phases Sulfures, 2014.
- [24] V. Labruyere, Structure Des Sites Sulfures Des Catalyseurs D'hydrotraitment: Approche Combinée Par Spectroscopie IR et Modelisation Moléculaire, 2014.
- [25] A. Travert, C. Dujardin, F. Mauge, S. Cristol, J.F. Paul, E. Payen, D. Bougeard, Catal. Today 70 (2001) 255–269.
- [26] A. Travert, C. Dujardin, F. Mauge, E. Veilly, S. Cristol, J.F. Paul, E. Payen, J. Phys. Chem. B 110 (2006) 1261–1270.
- [27] M.A. Lelias, E. Le Guludec, L. Mariey, J. van Gestel, A. Travert, L. Oliviero, F. Mauge, Catal. Today 150 (2010) 179–185.
- [28] M.A. Lélías, J. van Gestel, F. Maugé, J.A.R. van Veen, Catal. Today 130 (2008) 109–116.
- [29] F. Mauge, J.C. Lavalley, J. Catal. 137 (1992) 69–76.
- [30] C. Dujardin, M.A. Lélías, J. van Gestel, A. Travert, J.C. Duchet, F. Maugé, Appl. Catal. A Gen. 322 (2007) 46–57.
- [31] J. Chen, V. Labruyere, F. Mauge, A.-A. Quoineaud, A. Hugon, L. Oliviero, J. Phys.

- Chem. C 118 (2014) 30039–30044.
- [32] C. Dujardin, M.A. Lelias, J. van Gestel, A. Travert, J.C. Duchet, F. Mauge, *Appl. Catal. A Gen.* 322 (2007) 46–57.
- [33] V. Labruyere, *Structure Des Sites Sulfures Des Catalyseurs D'hydrotraitement: Approche Combinee Par Spctroscopie IR et Modelisation Moleculaire*, Thesis, University of Caen, 2014.
- [34] J. Chen, E. Dominguez Garcia, L. Oliviero, F. Maugé, *J. Catal.* 332 (2015) 77–82.
- [35] E.C. Decanio, D.A. Storm, *J. Catal.* 132 (1991) 375–387.
- [36] E.C. Decanio, D.A. Storm, *J. Catal.* 130 (1991) 653–656.

Table of contents – III Chapter

III. CHAPTER.....	69
3.1. Introduction	70
3.2. Experimental	72
3.3. Results	74
3.3.1. Metal oxide surface	74
3.3.1.1. Surface characterization of metal oxide used as support by IR/CO	74
3.3.1.2. Study of oxide catalysts	76
3.3.2. Sulfide catalysts.....	82
3.3.2.1. Textural and elemental analysis in sulfide catalysts	82
3.3.2.2. Catalytic activity	83
3.3.2.3. Active sites study by IR/CO: sulfo-reductive study in MoS ₂ slabs	84
3.3.2.3.1. CO adsorption on catalysts after sulfidation.....	84
3.3.2.3.2. CO adsorption on sulfide catalysts: influence of H ₂ treatment after sulfidation	87
3.3.2.3.3. CO adsorption on sulfide catalysts: influence of treatment with 2% H ₂ S/H ₂ after sulfidation	90
3.3.2.3.4. Active sites quantification	93
3.3.2.4. Slabs study by Transmission Electron Microscopy (TEM)	94
3.4. Discussion	96
3.4.1. Support-Mo interaction in oxidic catalysts	96
3.4.2. Support effect on the morphology of MoS ₂ slabs and Mo edge dispersion.....	98
3.4.2.1. Influence of the post-treatment on the sites detected by CO adsorption	98
3.4.2.2. Effect of the support on the morphology, length and stacking	99
3.4.2.3. Relation of MoS ₂ morphology with catalytic activity on sulfide catalysts ..	103
3.5. Conclusion.....	105
3.6. References	106

III. CHAPTER

SUPPORT EFFECT ON NON-PROMOTED CATALYST

Abstract: A series of Mo sulfide catalysts supported on Al₂O₃, SiO₂ and TiO₂ was prepared by wetness impregnation method using the same Mo density (3 atoms Mo/nm²) to study the role of support in MoS₂ slab formation. A thorough study was carried out from the molybdenum oxide to the molybdenum sulfide. Molybdenum edge was studied by CO adsorption followed by FTIR spectroscopy. Molybdenum located on the edges of MoS₂ slabs are the one involved in catalytic activity. A relation was found between the total Mo edge detected by IR/CO and HDS rate. Different morphologies have been detected by IR/CO method in the three different catalysts and this morphology plays a role in the catalytic activity, more exactly, a relation between S-edge/M-edge ratio and TOF was found, where a high ratio lead to a high TOF value for Mo/Al₂O₃ and Mo/SiO₂ catalysts. Moreover, specific behavior was found for Mo/TiO₂ with high TOF value and low S-/M-edge ratio. Thiophene was used as source to carry out HDS reaction which is not so efficient to distinguish DDS from HYD, but still could be detected a different in Mo/TiO₂ with respect to the others. Mo/TiO₂ presents a clear increase of THT formation which is formed by HYD pathway reaction due to be constituted mostly for M-edge characteristic of triangle morphology. Triangle truncated was predicted for MoS₂ slabs in Mo/Al₂O₃ and near to a perfect hexagon for Mo/SiO₂. Also, sulfo-reductive treatments were carried out for all three catalysts, and linear relation was found between the sensitivity to the treatment and the metal-support nature. High effect was found for catalysts which are formed by weak metal-support interaction while lightly effect was detected for catalyst formed by strong MoS₂-support interaction. MoS₂ morphologies studied by IR/CO and the slab length detected by TEM were used to predict the average morphology and study the Mo edge dispersion for each catalyst.

Keywords: Hydrodesulfurization (HDS), support effect, Molybdenum disulfide (MoS₂), Slab morphology, Sulfidation, Infrared (IR) spectroscopy, CO adsorption, Mo edge dispersion.

3.1. Introduction

Nowadays, production of ultra clean fuels is required due to the restricted governmental regulations. For that, new technologies have to be developed as well as new generation catalysts. The developments of more active HDS catalysts, which consist in both enhancing the productivity and improving product quality without negative impacts can be performed by many approaches such as changing the active component, varying preparation method, or changing the support. Indeed, the nature of the support influences the metal-support interactions at the early stage of the preparation and thus, the final active site characteristics. Understanding in details the support effect is connected with the catalyst fine structure from which originates the catalytic functionalities. Even though many studies about the understanding of the support effect were performed to understand the catalyst behaviour, there are still a lot of questions, in particular on the effect of the support on the morphology of the sulfide molybdenum slab. Indeed, non-promoted molybdenum dispersed on the surface of supports is the more simple HDS catalyst which sulfide catalyst is formed by active nanoparticles called MoS₂ [1]. MoS₂ nanoparticles are 2D clusters formed by S-Mo-S bonding [2]. In these nanoparticles; Mo atoms located in the basal plane that are catalytically inactive are distinguished from Mo atoms located at the edge of this nanoparticles that are active [3,4]. Kasztelan et al. proposed that MoS₂ slabs could adopt different morphology such as triangular, hexagonal, rhombohedral or chain; and that the percentage of molybdenum located at the edge of the particle (dispersion) directly depended on the morphology [5]. Then, the existence of two kinds of stable edges in MoS₂ slab was proposed: Mo terminated edge (Mo-edge) and sulfur terminated edge (S-edge). Both of them can show different local structure with different sulfur coverage [6–8]. First image of MoS₂ slabs morphology were recorded by Scanning Tunnelling Microscopy (STM) by Lauritsen et al. [9,10]. Single-layered of molybdenum sulfide nanoparticles dispersed on Au (111) surface was prepared to perform the experiment, thus triangular and hexagonal truncated morphology were detected versus the sulfidation conditions: triangular morphology was favoured by pure H₂S while triangular truncated morphology was favoured by more reductive conditions (conventional HDS conditions). Also, STM was used to study MoS₂ slab on rutile-TiO₂ (110), elongated hexagonal slab morphology was observed with both S-edge and Mo-edge in the longest face of the hexagon [11]. Moreover, some studies about the active phase-support interaction were performed using DFT calculations for alumina and anatase-TiO₂ surfaces [12,13]. Thus, four main plans stable in HDS conditions were obtained: hydrated (001), and non-hydrated (101) surfaces for anatase-TiO₂, and hydrated

(110), and non-hydrated (100) surfaces for gamma alumina. A single layer of MoS₂ as M-edge triangular Mo₆S_n clusters were given to study the possible interactions between the active phase and the support surfaces stable under reaction conditions. Epitaxial orientation was found favourable on anatase-TiO₂ surface and parallel orientation on alumina surface. The epitaxial orientation is formed by Mo-O-Ti-S-Mo bonds due to the partial sulfidation of titania surface. Thus, strong and specific MoS₂ anchoring with titania surface can be expected. Recently, Maugé group developed IR/CO method by FTIR spectroscopy to distinguish Mo edge sites located in the two different edges of MoS₂ nanoparticles, Mo-edge and S-edge [3,14–20]. Experimental vibrations are in agreement with theoretical vibrations determined by DFT calculation realised by Travert et al. [17,18]. The careful attribution of bands leads to get a quantification of Mo located in Mo-edge and S-edge. Extinction molar adsorption coefficient was calculated by Maugé et al for Mo-edge [14] and Chen et al. for S-edge [19]. Moreover, a linear relation between edge amounts determined from CO adsorption and catalytic activity was reported [3,4]. It is in accordance with previously mentioned fact that edges in MoS₂ slabs are directly the responsible of the activity. Finally, the proportion of Mo-edge and S-edge detected by IR/CO can be used to determine the MoS₂ morphology as was described by Chen et al. studying a morphology change with different parameters such chelating agent addition, sulfidation temperature and pressure. In an attempt to rational the effect of such parameters, the interaction between the slab and the support was pointed out as the crucial point.

Therefore, this study is focus on the determination of the influence of the support nature on MoS₂ morphology using the IR/CO method. The study is carried out using three different supports: Al₂O₃ as the reference support, TiO₂ known to lead to strong slab support interaction and SiO₂ as a weak interacting support. To clarify this notion of interaction, the supports alone and the oxidic precursors of the three catalysts were also studied by IR, Raman and UV-visible spectroscopy. Finally, the effect of observed modification of slab morphology on the activity in thiophene HDS is studied.

3.2. Experimental

3.2.1. Catalysts preparation

Catalysts were prepared by wetness impregnation method using heptamolybdate tetrahydrated salt (Alfa Aesar, 99%) as molybdenum precursor. The supports, Al₂O₃ (250 m²/g, Sasol), SiO₂ (506 m²/g, Merk) and TiO₂ (mix of anatase and rutile phases, 59 m²/g, Degussa) were first sieved between 0.2 and 0.5 μm and calcined at 673K during 3-4h for TiO₂ and SiO₂ respectively and 773K during 3h for Al₂O₃. Metal amount were determined in order to reach the same metal density (3 atoms Mo/nm²) on the different supports. After impregnation, the catalysts were dried at 383K (3K/min) during 16h and then calcined at 673K (3K/min) during 4h.

3.2.2. Elemental analysis by Inductively Coupled Plasma (ICP)

Oxide catalysts were sulfided ex-situ in a glass reactor connected with 10% H₂S/H₂ (30ml/min) flow. Catalysts were sulfided at 623K with a rate of 3K/min during 2h. After, the temperature was cooled down to 298K under N₂ flow (30ml/min). In order to avoid air contact, the reactor was introduced in a dry box under Ar flow; then, 50mg of sample was dissolved in hydrofluoric acid, aqua regia, boric acid, and water in a specific proportion with a total volume of 100 ml to quantify molybdenum and sulfur amount present in the catalysts by inductively coupled plasma atomic emission spectrometry (ICP-AES) using a Perkin Elmer Optima 330DV ICP instrument.

3.2.3. UV-VIS spectroscopy

Ultraviolet-visible (UV-Vis) spectra were recorded with a Cary 4000 from Varian equipped with a praying mantis from Harrick for diffuse reflection. The spectrum acquisition domain was between 800-200 nm with a speed of 300 nm /min. The analysis was done on the oxide catalysts under atmospheric conditions, and taken each support as reference. UV-Vis spectra (F(R) vs λ) were converted in [F(R) · hv]² vs hv in order to get the edge adsorption energy. The edge absorption energy is determined by finding the energy intercept of a straight line fitted through the low energy rise in the graphs of [F(R) · hv]² vs hv.

3.2.4. Raman spectroscopy

Raman spectroscopy was performed on the oxidic catalysts using a Jobin Yvon Labram 300 Raman spectrometer equipped with a confocal microscope, an Nd-YAG laser (frequency doubled, 532 nm) and a CCD detector. Spectra were recorded at room temperature in the region between 200 – 1000 cm^{-1} .

3.2.5. Transmission Electron Microscopy (TEM)

Transmission electron microscopy (TEM) was performed on a JEOL 2010 FEG operated at 200 kV. All studied samples were sulfided at the same condition than IR experiments, 623K during 2h at 3K/min under 10% $\text{H}_2\text{S}/\text{H}_2$ flow. After sulfurization, the samples were transported into a glove box under argon flow. The suspensions in absolute ethanol were prepared inside the box to avoid totally the air contact. TEM analyses were carried out using a few drops of the suspension on a copper grid. Slab length and stacking degree distributions of sulfide slabs were determined manually from at least 300 slabs for $\text{MoS}_2/\text{Al}_2\text{O}_3$ and $\text{MoS}_2/\text{SiO}_2$ catalysts, and 120 slabs for $\text{MoS}_2/\text{TiO}_2$ catalyst. All TEM images were recorded at the same magnification and digitised using 2kx2k CCD camera. The measurements were performed using Mesurim program.

3.2.6. CO adsorption by infrared spectroscopy (IR/CO)

Infrared characterizations were performed in a cell adapted for adsorption at liquid nitrogen temperature (100K). First, oxide catalysts in wafer form were activated in-situ with three different procedures: (i) sulfidation under 10% $\text{H}_2\text{S}/\text{H}_2$ flow, (ii) sulfidation followed by a post-treatment under H_2 flow and (iii) sulfidation followed by a post-treatment under 2% $\text{H}_2\text{S}/\text{H}_2$ flow. During the first procedure, the catalyst was sulfided at atmospheric pressure with a flow of 10% $\text{H}_2\text{S}/\text{H}_2$ (30 ml/min) at a rate of 3 K/min up to 623 K. After 2 h sulfiding at 623 K, the catalyst was flushed with Ar during 10 minutes and then let under vacuum 1 h at 623 K and finally cooled down to room temperature. For the second and third types of activation, after performing the sulfidation following the previous procedure, the Ar flush and 30 minutes under vacuum, a post-treatment was performed under pure hydrogen or 2% $\text{H}_2\text{S}/\text{H}_2$ flow (30 ml/min) at 623 K for 2 h. At the end of this treatment, Ar flow was flushed during 10 minutes and the temperature was cooled down under high vacuum until room temperature. After these activation procedures, the catalyst under high vacuum (1.10^{-4} Pa residual pressure) was cooled down to 100 K to perform CO adsorption.

Influence of the sulfidation on the support alone was checked by comparing the adsorption of CO at low temperature after the sulfidation treatment at 623K (3K/min) during 2 hours under 10% H₂S/H₂ with the one after evacuation under high vacuum at 623K.

CO adsorption experiments were performed introducing small calibrated CO doses up to an equilibrium pressure of 133 Pa. IR spectra were recorded with a Nicolet Magna 550 FT-IR spectrometer equipped with a MCT detector. All spectra were normalised to a disc of 5 mg /cm². All experiments were duplicated, with an error of 5%. For quantitative analysis, saturated spectra were decomposed using OMNIC program and pseudo-voigt function.

3.2.7. Catalytic activity: Thiophene test

Oxide catalysts were sieved again between 0.2 and 0.5 μm before to start the experiment. Then, catalysts were sulfided in situ just before reaction. Sulfurization procedure was performed at 623K with a heating rate of 3K/min, under a flow of 10% H₂S/H₂ (30ml/min) at atmospheric pressure during 2 h. After, thiophene reaction was carried out in a continuous reactor at 623K and atmospheric pressure with a thiophene partial pressure of 8 kPa in a mixture of hydrogen (91.2 kPa) and H₂S (2.1 kPa). The outlet gas was analysed by a Varian 3900 gas chromatograph equipped with flame ionization (FID) detector. The reaction rate was calculated as $r_{\text{HDS}} = (F/m) \cdot X$, where F/m is the molar flow rate of thiophene per gram of catalyst and X is thiophene conversion which is below 5%. Thiophene reaction was running during 18h to obtain the reaction rate at steady state. The initial catalyst mass was corrected by mass loss calculated during infrared experiments in order to consider the mass of the sulfided catalyst.

3.3. Results

3.3.1. Metal oxide surface

3.3.1.1. Surface characterization of metal oxide used as support by IR/CO

To understand the changes of MoS₂ morphology versus their support, a study of the support surface itself has to be done. For that, CO adsorption was used to characterize Lewis and Brønsted acid sites on alumina, silica and titania. Two different thermal treatments were performed before CO adsorption: the first one under vacuum to remove possible impurities adsorbed on the surface and the second one under sulfidation condition (the same conditions

than for catalyst sulfidation). It is well known that gamma alumina and titania surfaces present Lewis and Brønsted acid sites and that silica surface only present Brønsted acid sites. Then, CO adsorption on alumina surface gives different vibration bands (Figure III.1a): CO physisorbed presents a characteristic band around 2140 cm^{-1} ; CO interaction with OH groups is characterised by a band at 2155 cm^{-1} , and finally CO in interaction with Lewis acid sites (Al^{3+}) appears as a large band with the maximum around 2180 cm^{-1} which is the result of several bands appearing in the same region [14,15,21–23]. The experiment was performed introducing small doses of CO up to equilibrium (not showed). CO has been in interaction with Lewis acid sites and hydroxyl groups from the beginning; it indicates the strong acidity of OH group on Alumina surface. On the other hand, the saturated spectrum of CO adsorption after sulfidation doesn't show any important change in comparison with the one after heating treatment (Figure III.1a); only a shift of 3 cm^{-1} to higher wavenumber in CO/OH vibration band was detected. This shift is due to some interaction of SH species with hydroxyl group in accordance with a little decrease of basic OH band at 3775 and 3800 cm^{-1} . In conclusion, there is not a real influence of sulfidation in Al_2O_3 surface; it is in agreement with Travert et al. work [24]. In the case of silica, surface presents only hydroxyl groups, as was mentioned previously. Then, on the IR/CO spectrum, only CO physisorbed was detected through the band at 2137 cm^{-1} as well as CO in interaction with hydroxyl group through the main band around 2156 cm^{-1} and a shoulder at 2172 cm^{-1} (Figure III.1b). Figure III.1.b shows that the sulfidation treatment has no effect on the silica surface.

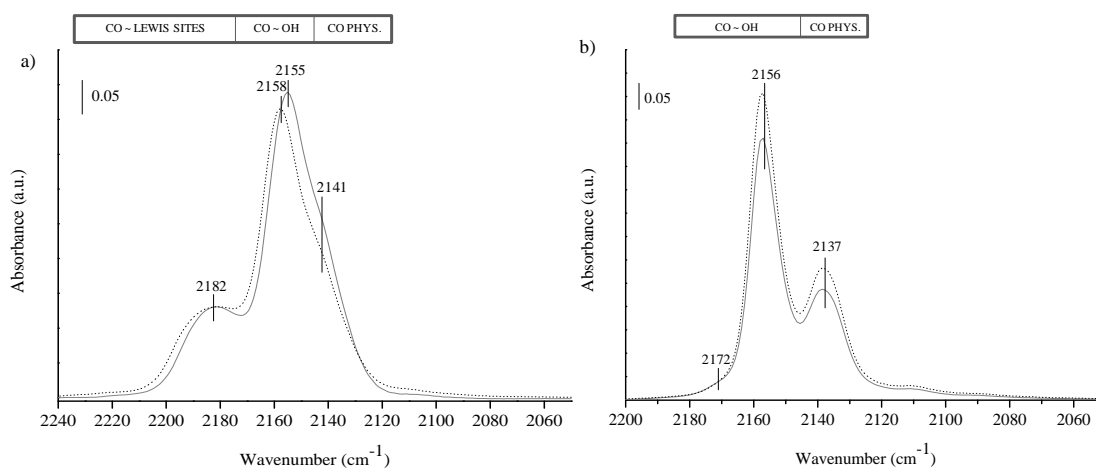
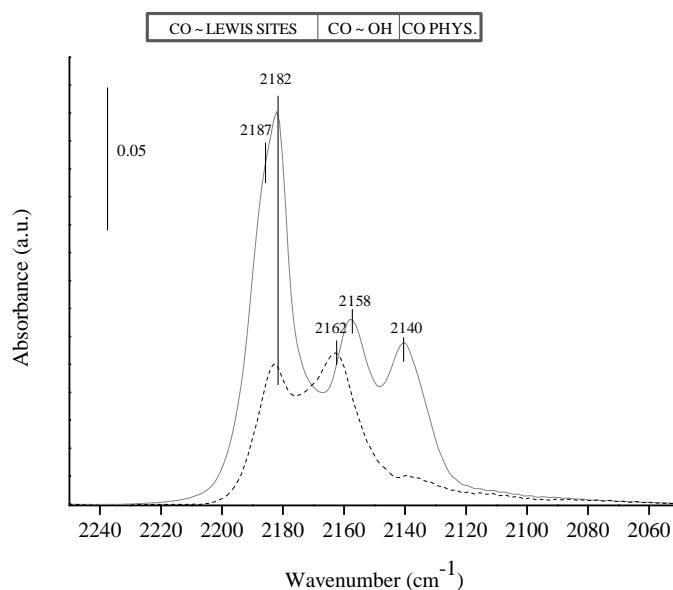


Figure III.1. IR spectra of CO adsorption (equilibrium pressure = 133 Pa) on calcined Al_2O_3 (a) and SiO_2 (b). Full line for spectrum after in-situ heating treatment (623 and 673K/2h under vacuum for Mo/ Al_2O_3 and Mo/ SiO_2 respectively), dotted line for spectrum after sulfidation (623K/2h under $\text{H}_2\text{S}/\text{H}_2$)

The same experiments were carried out on titania surface (FigureIII.2). TiO₂ surface is formed by Lewis (Ti⁴⁺) and Brønsted acid sites. These sites can be differentiated by CO interaction as was showed before in the case of alumina. CO in interaction with titania surface presents: CO physisorbed around 2140 cm⁻¹, CO/OH at 2158 cm⁻¹ i.e. at higher wavenumber in comparison with Al₂O₃ and SiO₂, and CO adsorbed in Lewis sites with several component between 2165 and 2210 cm⁻¹ with the maximum at 2182 cm⁻¹. The experiment was performed introducing small doses of CO up to equilibrium (not showed). CO has been in interaction with Lewis sites from the first doses up to saturation of these sites and then CO/OH interaction starts to appear. It indicates that titania surface is composed of strong Lewis acid sites. In FigureIII.2 is shown the high reactivity between H₂S/H₂ and titania surface. Both kind of sites (Lewis and Brønsted) are influenced by the sulfidation treatment. The intensity of bands attributed to Lewis and Brønsted sites are decreased, while CO physisorbed has disappeared. SH species in interaction with OH groups is detected by a shift of 4 cm⁻¹ to higher wavenumbers of CO/OH vibration band after sulfidation.



FigureIII.2. IR spectra of CO adsorption (equilibrium pressure = 133 Pa) on calcined TiO₂ after treatment at 623K/2h under H₂S/H₂ (discontinue line) and after heating treatment at 623K / 2h under vacuum (full line)

3.3.1.2. Study of oxide catalysts

The support surfaces were studied by CO adsorption at low temperature followed by FTIR spectroscopy (IR/CO). The CO adsorption on the support surface allows the distinction of Lewis and Brønsted acid sites for all the supports. Interesting is the possibility to study the metal-support interaction in oxide catalysts by the comparison of CO adsorption spectra at

equilibrium pressure (133 Pa) for the support and oxide catalyst as shows Figure III.3 and Figure III.4. Mo/Al₂O₃ catalyst shows an intensity decrease of the νCO band ascribed to Lewis acid sites at 2182 cm⁻¹, as well as stronger decrease of the νCO band attributed to Brønsted acid sites at 2155 cm⁻¹. Indicating that oxomolybdate species are in interaction with Lewis acid sites, Brønsted acid and basic sites, as is reported in the literature for high Mo loading [25]. Moreover, Mo/SiO₂ oxide catalyst shows a decrease of the νCO band ascribed to hydroxyl groups which are the unique species that compose silica surface.

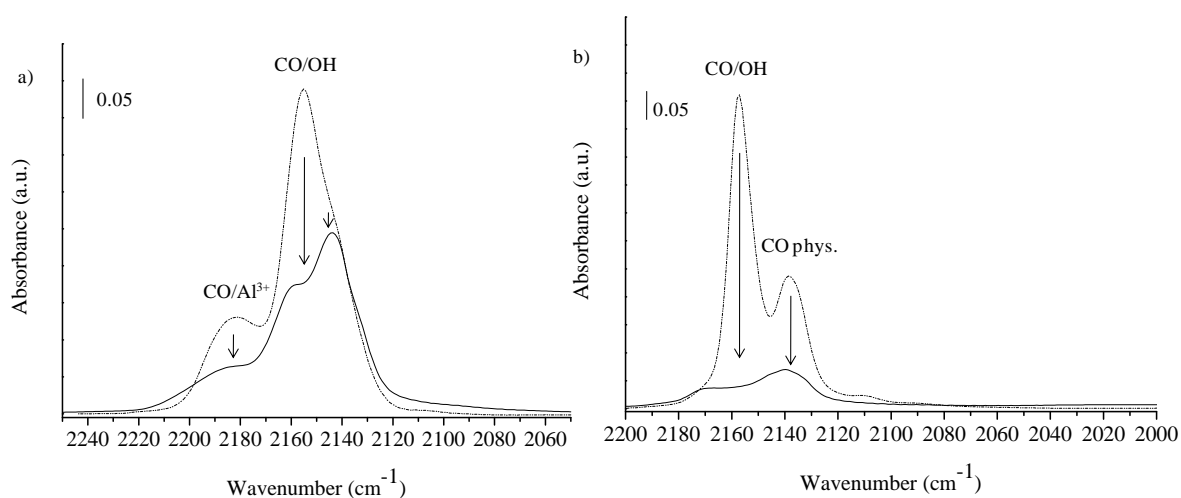


Figure III.3. IR spectra of CO adsorption at equilibrium pressure after heating treatment (623K/2h) of the support (dotted line) and catalyst in oxidic form (full line) for alumina (a), silica (b)

Finally, Figure III.4 represents IR spectra of CO adsorption on TiO₂ and Mo/TiO₂ catalyst in oxidic form. The oxide catalyst shows the intensity decrease of a νCO band that is ascribed to Lewis acid sites (Ti⁴⁺). Instead, CO vibration band of acid hydroxyl groups does not present any modification. Additionally, OH stretching band presented at 3746 cm⁻¹ (not shown) present also a decrease after the impregnation stage indicating that oxomolybdate species are in interaction with hydroxyl group. Surprisingly, this band decrease indicates that Ti⁴⁺ cations are involved in the anchoring with oxomolybdate species. Thus, titania is formed by a metastable surface that strongly depends on the environment. Generally, there are two surface energetically stable detected by DFT for anatase-TiO₂: (001) and (101). In dehydrated condition, (001) surface is formed by Lewis acid sites fivefold coordinated and Lewis basic sites two- and threefold coordinated, besides (101) surface are formed as the previous one and additionally by Lewis sites sixfolds coordinated [26]. Impregnation stage is carried out with water excess leading to the surface hydration and then form basic hydroxyl group that interact

with oxomolybdate species. The OH stretching band decreasing at 3746 cm^{-1} is ascribed by DFT calculation and FTIR spectroscopy to $\text{Ti}_{(5\text{C})-\mu_1\text{-OH}}$ basic hydroxyl group for (001) surface [27].

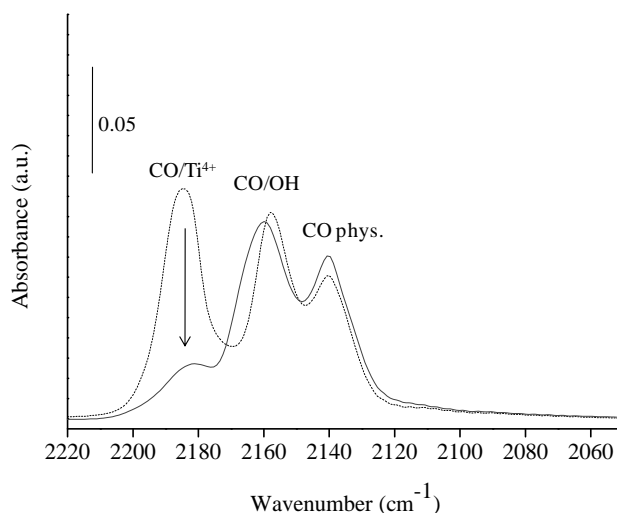


Figure III.4. IR spectra of CO adsorption at equilibrium pressure after heating treatment (473 K/2h) for TiO_2 (dotted line) and Mo/TiO_2 catalyst in oxidic form (full line)

After calcination and before sulfidation, molybdenum can be present in different species on the support surface: $(\text{MoO}_4)^{2-}$, $(\text{Mo}_7\text{O}_{24})^{6-}$, $(\text{Mo}_2\text{O}_7)^{2-}$, MoO_3 . The presence of some MoO_3 particles is characteristic of “non dispersed” molybdenum while the other correspond to dispersed ones, $(\text{Mo}_7\text{O}_{24})^{6-}$, $(\text{Mo}_2\text{O}_7)^{2-}$ being referred as polymolybdate species.

To study the nature of molybdenum species on Al_2O_3 , SiO_2 and TiO_2 surface, Raman spectra at atmospheric condition (atmospheric temperature and pressure) were performed in the oxidic catalysts.

Raman spectra are showed in Figure III.5. Raman spectrum of $\text{Mo/Al}_2\text{O}_3$ presents two bands characteristic of polymolybdate species at 956 and 856 cm^{-1} which are attributed to Mo=O and Mo-O-Mo vibrations respectively. As previously mentioned the presence of this molybdenum species is characteristic of a good dispersion of the metal on the alumina surface [28]. Similar species appear on Mo/TiO_2 , as revealed by the two bands characteristic of polymolybdate species at 965 and 874 cm^{-1} , but with a little shift around 10 cm^{-1} in comparison with polymolybdate species present in $\text{Mo/Al}_2\text{O}_3$. This shift can be related to a support effect and interpreted by the interaction between TiO_2 surface and MoO_x [29]. Conversely, on

Mo/SiO₂ surface two different molybdenum species are formed as illustrated in Figure III.5b: polymolybdate species as in the previous two cases, and molybdenum trioxide [30]. MoO₃ is a crystal phase and is characterized by two principal bands at 997 cm⁻¹ and 821 cm⁻¹ which are attributed to Mo=O and Mo-O-Mo vibrations respectively [31,32]. The presence of molybdenum trioxide means that the molybdenum is not well dispersed on silica surface.

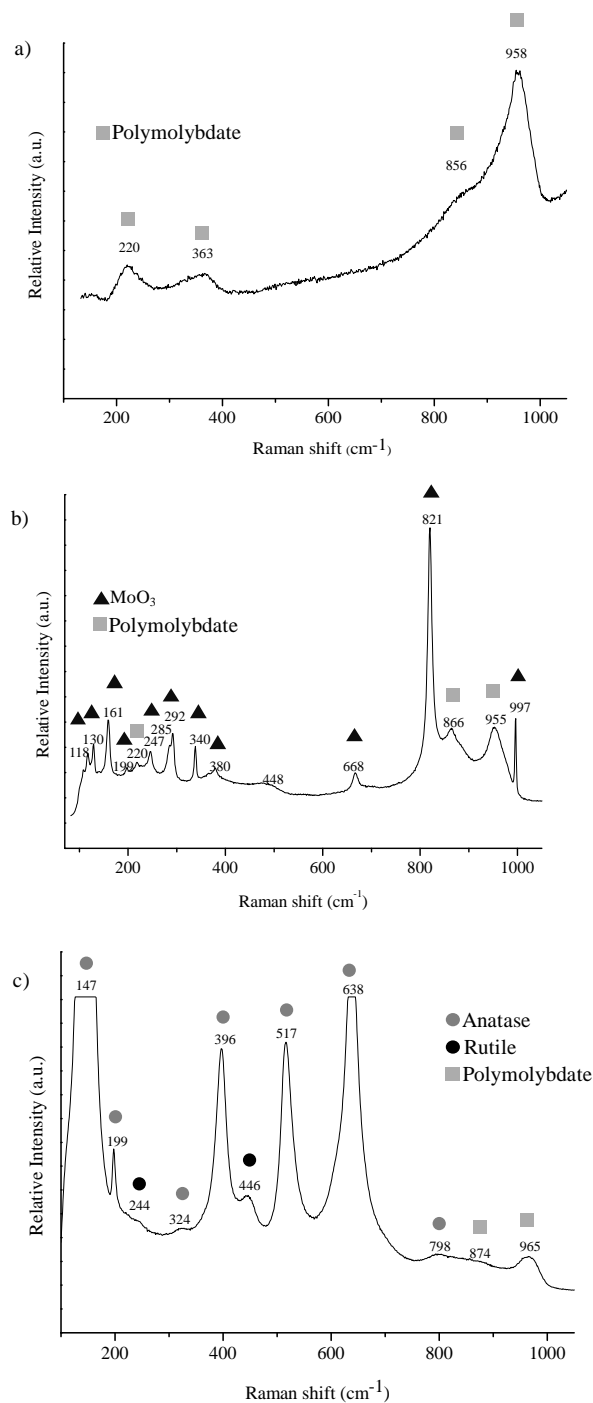


Figure III.5. Raman spectra of oxide catalysts (calcined): a) Mo/Al₂O₃, b) Mo/SiO₂ and c) Mo/TiO₂

Complementary study in oxide catalysts was done using UV-Vis spectroscopy to determine the nature of the molybdenum species present on the surface in particular to discriminate the so-called polymolybdate species (Figure III.6a). The UV-Vis spectra show for all catalysts one broad band with maximum intensity at 270, 290 and 362 nm for Mo/Al₂O₃, Mo/SiO₂ and Mo/TiO₂ respectively due to the presence of oxomolybdate species. From these spectra, the so called edge absorption energy is determined by finding the energy intercept of a straight line fitted through the low energy rise in the graphs of $[F(R) \cdot hv]^2$ vs. hv (Figure III.6.b). Indeed, UV-Vis spectroscopy can give information on the “size” of the different molybdenum anions species that can be present on the surface through the analysis of the optical bandgap energy determined from the position of the low energy rise in UV-Vis spectrum. It is reported that a decrease of band gap energy occurs when the ion size or oxide domain increases. It appears that the molybdenum species on Mo/Al₂O₃ has the highest average edge energy of 4 eV, followed by the ones on Mo/SiO₂ with 3.2 eV and finally the one on Mo/TiO₂ with 2.9 eV.

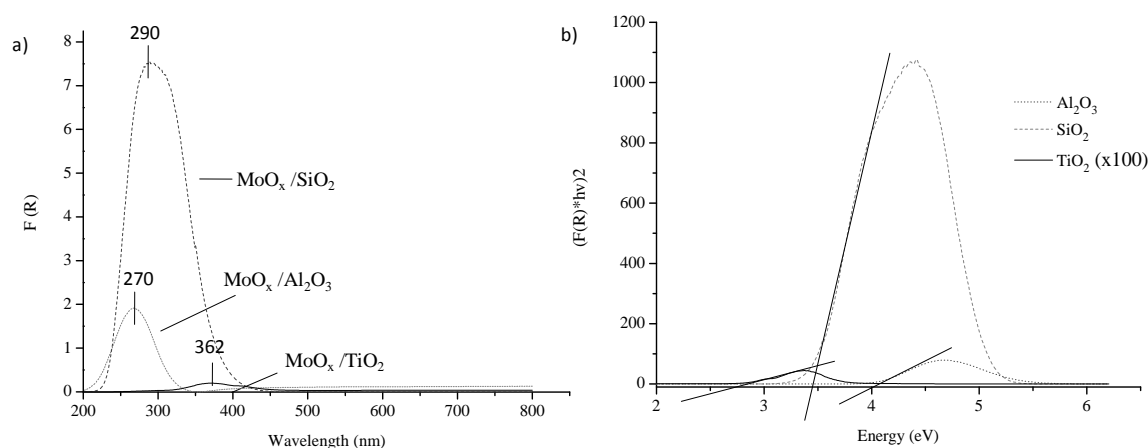


Figure III.6. UV-VIS spectra (a) and Edge energy calculation (b) on Mo/ Al₂O₃, Mo/SiO₂, and Mo/TiO₂

This edge absorption energy has been previously determined for known clusters of molybdenum and it was shown that it is linked with the average number of nearest Mo neighbours in the clusters. Thus an empirical, linear correlation between edge absorption energy (E) and the local degree of aggregation of the clusters measured by the number of nearest Mo neighbours ($N_{\text{Mo neighbours}}$) has been calculated to be: $N_{\text{Mo neighbours}} = 16 - 3.8E$ as plotted in Figure III.7-[33,34]. Then, plotting the corresponding Edge absorption energy for the Mo species formed on the three oxide catalysts, it appears that on Mo/TiO₂ polymolybdate species have a high number of Mo neighbours. Conversely, for polymolybdate species on

Mo/Al₂O₃ catalyst which records the highest band gap energy a Mo neighbour number between one and two is expected as shown in Figure III.7. This value is surprisingly low as compared to the one reported by Weber et al. [35]. On Mo/SiO₂, simultaneous presence of MoO₃ clusters and heptamolybdate species are suspected to be present on silica surface.

In conclusion, good molybdenum dispersion was detected by Raman spectra on Mo/Al₂O₃ and Mo/TiO₂ catalysts, and worse dispersion on Mo/SiO₂. Additional information from the UV-characterization was found through the calculation of the edge absorption energy for the molybdenum species present on the different support surfaces. High edge absorption energy was obtained in the case of Mo/Al₂O₃ which corresponds to small cluster formation such as Mo₂O₇²⁻. The formation of such species is in agreement with the strong intensity on the Raman spectrum of the band attributed to Mo=O terminal stretching band. Middle edge absorption energy was obtained for the species on Mo/SiO₂, which corresponds to a mixture between Mo₇O₂₄⁶⁻ and MoO₃ in agreement with the detection of both kind of species by Raman spectroscopy. And finally, the lowest edge absorption energy was obtained for the Mo species on Mo/TiO₂ which corresponds to a cluster with high number of Mo next nearest neighbours.

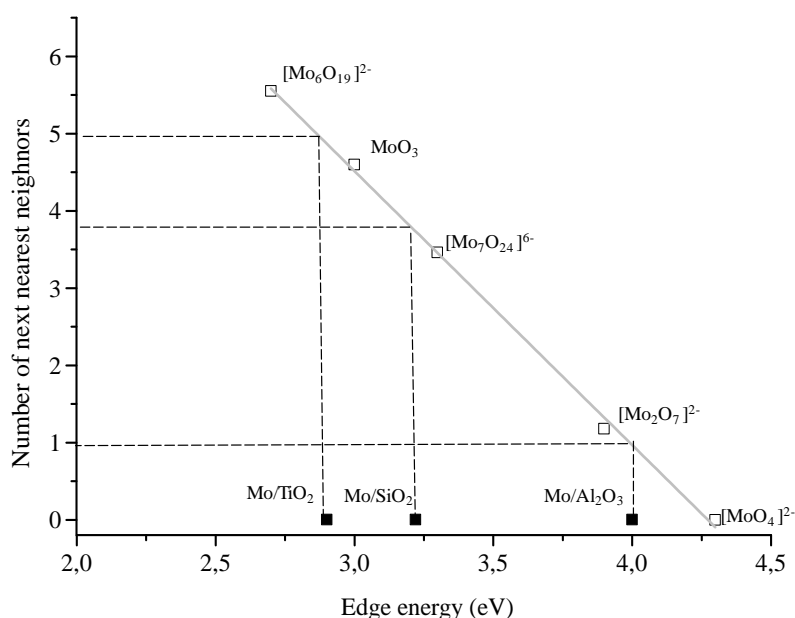


Figure III.7. Estimation of the number of Mo nearest neighbours in Mo species supported in Al₂O₃, SiO₂ and TiO₂ after calcination through the comparison with different molybdenum species in solution [33]

3.3.2. Sulfide catalysts

3.3.2.1. Textural and elemental analysis in sulfide catalysts

Surface area of the catalysts in oxidic form are summarised in Table III-1. It is worth to notice that the surface area of Mo/SiO₂ significantly decreases after the preparation step. This can be due to the low pore size of the support (around 6 nm). This decrease in surface area can explain at least partially the bad molybdenum dispersion revealed by the Raman study through the presence of MoO₃ clusters. Molybdenum and sulfur contents of the sulfide catalysts were determined by ICP analysis as shown in Table III-1. The metal content of the sulfide catalysts are in line with the metal loading used during impregnation.

Sulfur concentration in catalysts after sulfidation treatment was measured to verify if the complete formation of MoS₂ could be expected. All catalysts present indeed enough sulfur to form MoS₂ i.e. more than double molar amount of sulfur than molybdenum. Even a significantly higher S/Mo ratio of 2.8 was detected in Mo/TiO₂ catalyst even though the contribution of the sulfur present on the support alone has been deduced (The ICP analysis of the support alone after H₂S/H₂ treatment gives a wt % of sulfur of 0.16). It cannot be excluded that the presence of MoS₂ favours the sulfidation of the support.

Table III-1. Textural properties and elements present in the catalysts

Catalysts non promoted	SUPPORT Surface area (m ² /g)	CATALYST Surface area (m ² /g)	%wt Mo ^a	%wt Mo ^b	S/Mo ^b
Mo/Al ₂ O ₃	248	232	11	10.7	2.4
Mo/SiO ₂	506	305	19	16.3	2.1
Mo/TiO ₂	59	58	3	2.4	2.8*

* value corrected from the sulfur adsorbed on the support alone

^a According to catalyst preparations

^b ICP analysis

3.3.2.2. Catalytic activity

Thiophene was selected as model molecule to perform HDS reaction on non-promoted catalysts. Figure III.8 shows the thiophene HDS rate obtained on molybdenum sulfide in different supports. In this work, HDS rate is represented in two ways: per gram of catalyst (Left) and per surface area (Right) since all catalysts were prepared with the same metal density, 3 atoms Mo/nm². For HDS rate represented per gram of catalyst, it is notable the high activity in Mo/SiO₂, followed by Mo/TiO₂ and finally Mo/Al₂O₃. But this tendencies change dramatically when HDS rate is represented by surface area as Mo/TiO₂ catalyst is four times more active than the other two catalysts and Mo/SiO₂ presents the lowest rate.

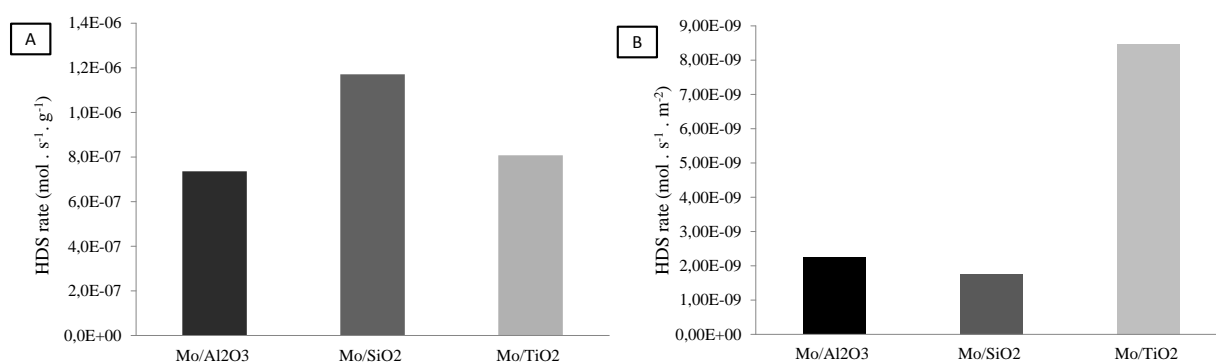


Figure III.8. Thiophene reaction rates per gram (A) and per surface area (B) on non-promoted catalysts.

It is well known that thiophene is not an optimum molecule to study the selectivity of catalysts in HDS reaction. However, a significant increase of THT product was detected for Mo/TiO₂ catalyst. THT being an intermediate product formed on HYD route (hydrogenation pathway), this result shows that hydrogenation route is favoured on Mo/TiO₂ as compared to Mo/Al₂O₃ and Mo/SiO₂ (Figure III.9).

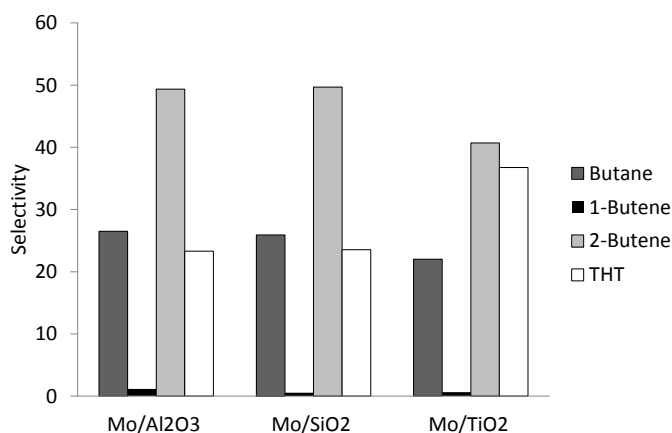


Figure III.9. Percentage of different products converted in thiophene reaction on non-promoted catalysts

As mentioned before, TiO₂ is sulfided during sulfidation process. Then, thiophene test was also carried out on sulfided TiO₂ alone to check if the extra THT formation coming from Mo/TiO₂ catalyst could be linked with sulfided TiO₂ activity. The HDS rate obtained on sulfided TiO₂ was almost zero, 0.27 mol/h.kg_{cat} instead of 2.9 mol/h.g_{cat} on Mo/TiO₂. Table III-2 shows the percentage of the products formed in Thiophene HDS reaction for both Mo/TiO₂ and TiO₂ alone. It is clear that the sulfided TiO₂ support has a lower selectivity for THT formation than the Mo/TiO₂ catalyst. Then, sulfide TiO₂ can be excluded as responsible for the favoured HYD pathway on Mo/TiO₂ catalyst.

Table III-2. Thiophene yield on Mo/TiO₂ and TiO₂

Materials	Products (%)				Conversion (%)
	Butane	1- Butene	2- Butene	THT (Tetrahydrothiophene)	
Mo/TiO ₂	0.24	0.01	0.44	0.39	1.07
TiO ₂	0.01	0.03	0.04	0.02	0.1

3.3.2.3. Active sites study by IR/CO: sulfo-reductive study in MoS₂ slabs

IR spectroscopy was used to follow CO adsorption at low temperature on Mo supported on Al₂O₃, SiO₂ and TiO₂ after in-situ sulfidation. Effect of post-treatments (after in-situ sulfidation) on CO adsorption was also studied.

3.3.2.3.1. CO adsorption on catalysts after sulfidation

CO adsorption at low temperature after in-situ sulfidation was performed on the three catalysts. Figure III.10 presents the IR spectra obtained for CO adsorption up to saturation using equilibrium pressure on Mo/Al₂O₃ catalyst. It showed the two domains of CO interactions. The first one concerns the interaction with the support and appears at higher wavenumber, between 2145 and 2240 cm⁻¹. As reported previously, on alumina, CO interacts with hydroxyl group leading to a ν(CO) band at 2157 cm⁻¹, and with Lewis acid site i.e. Al³⁺ cations, leading to several characteristic ν(CO) bands at 2235, 2221 and the principal one at

2187 cm^{-1} . The second domain corresponds to CO in interaction with MoS_2 nanoparticles. CO interacts with Mo with different coordinations leading to bands at different wavenumbers. Two kinds of CO/Mo interactions are reported: the interaction with Mo located on M-edge, appearing with $\nu(\text{CO})$ band at 2114 cm^{-1} , and Mo located on S-edge, with the principal $\nu(\text{CO})$ band at 2070 cm^{-1} . Also, others bands were detected at lower wavenumbers at about 2040, 2020, and 2000 cm^{-1} which are attributed to Mo located in S-edge with lower sulfur coverage and Mo metallic respectively [19]. In this way, Mo located on the edges of MoS_2 nanoparticles can be classified by Mo located in Mo-edge and in S-edge which are directly in relation with MoS_2 morphology.

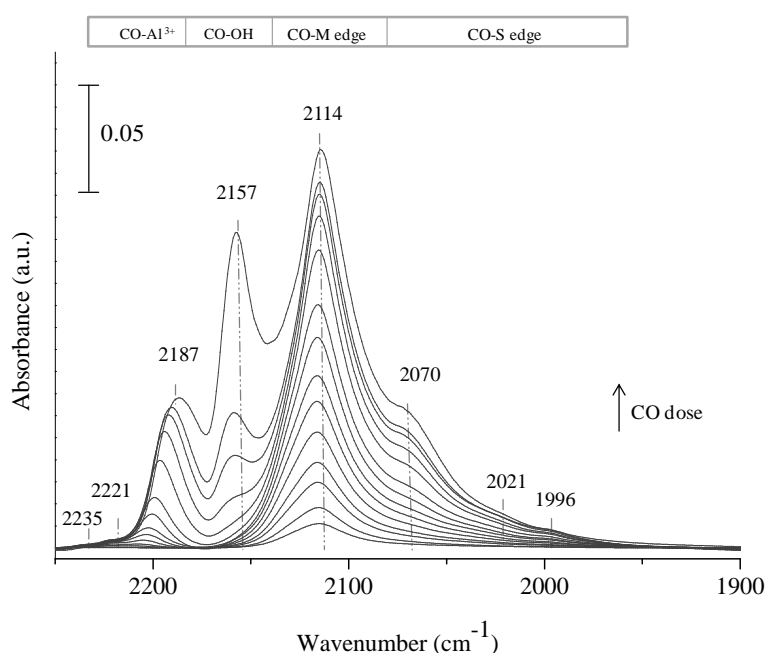


Figure III.10. IR spectra after adsorption of increasing doses of CO up to saturation using equilibrium pressure (133 Pa) on $\text{Mo}/\text{Al}_2\text{O}_3$ sulfided at 623K under 10% $\text{H}_2\text{S}/\text{H}_2$

IR spectra of CO adsorbed on sulfided Mo/SiO_2 are shown in Figure III.11 from small doses up to saturation. As previously described, the spectrum can be divided in two parts: in the first one, CO is in interaction with silica surface, i.e. with hydroxyl group and gives a $\nu(\text{CO})$ band at 2155 cm^{-1} , and physisorbed CO is also detected around 2134 cm^{-1} . In the second part of the spectrum, CO interacts with MoS_2 nanoparticles. The $\nu(\text{CO})$ band position are close to the ones obtained on $\text{Mo}/\text{Al}_2\text{O}_3$, so CO/Mo in M-edge appears at 2115 cm^{-1} and in S-edge at 2065 cm^{-1} . Some $\nu(\text{CO})$ bands appearing at lower wavenumber at 2040, 2020 and 2000 cm^{-1} increases in intensity for Mo/SiO_2 catalyst in comparison with $\text{Mo}/\text{Al}_2\text{O}_3$. Also, an increase in

S-edge/M-edge ratio was detected which means a change of the slab morphology has occurred from Mo/Al₂O₃ to Mo/SiO₂. Finally, the infrared spectrum of CO adsorption on Mo/SiO₂ also presents a distorted band at 1888 cm⁻¹ which is characteristic of Si-O-Si vibration from silica structure perturbed by CO adsorption (see annex I).

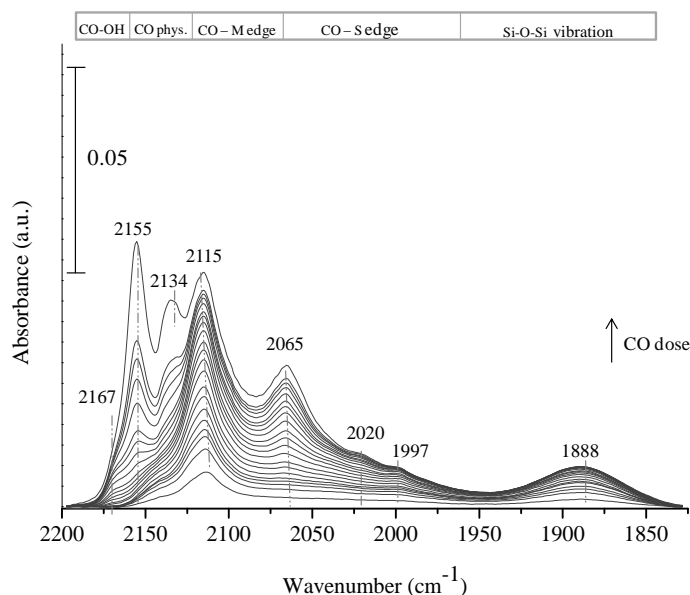


Figure III.11. IR spectra after adsorption of increasing doses of CO up to saturation using equilibrium pressure (133 Pa) on Mo/SiO₂sulfided at 623K under 10% H₂S/H₂

Finally, CO adsorption at low temperature was performed on Mo/TiO₂ catalyst from small doses up to saturation using equilibrium pressure (133 Pa) as shown in Figure III.12. As shown previously in the case of CO adsorption on titania after H₂S/H₂ treatment (Figure III.2), interaction between CO and Lewis acid sites present in titania surface is detected through the $\nu(\text{CO})$ band at 2183 cm⁻¹. For this catalyst, a small contribution of CO/OH was detected at 2155 cm⁻¹ only at CO saturation and a second band associated to CO/OH perturbed by SH species is detected at 2162 cm⁻¹. Interestingly regarding the interaction between CO and the MoS₂ phase, mostly CO in interaction with Mo located at M-edge is detected in this catalyst; with only a small-detected contribution of CO/Mo located in S-edge. CO/Mo-edge interaction appears at 2118 cm⁻¹, at higher wavenumber in comparison with the two others catalysts. This shift to higher wavenumber is due to a decrease of the back-donation of Mo to CO that implies a decrease of the electron density of Mo. This decrease of Mo electron density can be explained either by a strong interaction with the conductive support or by the increase of coordination number i.e. a high sulfur coverage at the edge. Note that a parallel with the shift of the peaks

associated with polymolybdate species observed for the catalyst in oxidic form in Raman spectrum can be made: this shift was also attributed in the literature to the metal-support interaction [29].

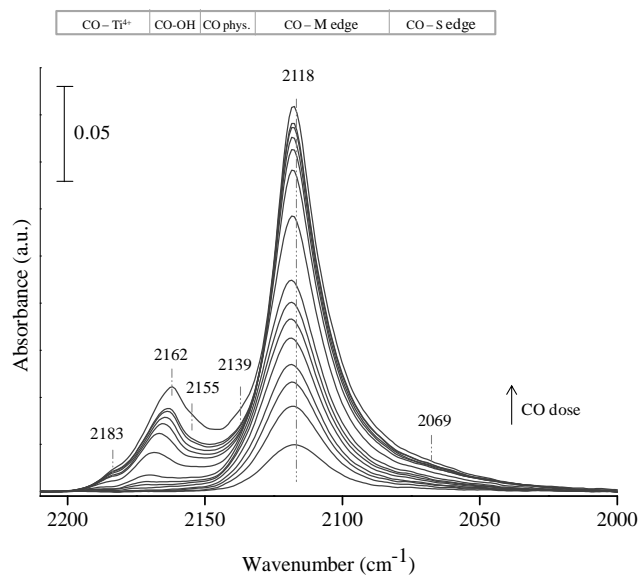


Figure III.12. IR spectra after adsorption of increasing doses of CO up to saturation using equilibrium pressure (133 Pa) on Mo/TiO₂ sulfided at 623K under 10% H₂S/H₂

In summary, mostly Mo on M-edge sites was detected by IR/CO for Mo/TiO₂ catalyst. Instead, Mo located in both edges, M- and S-edge, was detected for Mo/Al₂O₃ and Mo/SiO₂. Higher intensity of M-edge band than S-edge band was noted for Mo/Al₂O₃ while more similar (although weak) intensities between the two bands were found for Mo/SiO₂. Quantification of each site will be given later on but it can be already concluded that the support modifies the morphology of the MoS₂ slabs.

3.3.2.3.2. CO adsorption on sulfide catalysts: influence of H₂ treatment after sulfidation

The sulfur coverage at the edges of MoS₂ nanoparticles depends on the H₂S/H₂ ratio, as was explained in the introduction part. Since HDS reaction need hydrogen to remove sulfur from sulfur-compounds, and then hydrogen is still over contact with MoS₂ clusters during the reaction, the influences of H₂ on the MoS₂ edges have to be studied. For that, hydrogen treatments after sulfidation were carried out to study the reactivity of hydrogen and MoS₂ slabs supported in the three different supports.

Mo/Al₂O₃ catalyst has been studied during years by different researchers. *Dujardin et al* studied already CO adsorption at low temperature on this catalyst [3], after sulfidation and after hydrogen post-treatment. For this reason, a detailed experiment was not carried out for Mo/Al₂O₃. But a comparative experiment was done as shown in Figure III.13.a. The result obtained is in the same line that the former experiment realised by *Dujardin et al*. Indeed, an increase of the intensity of the $\nu(\text{CO})$ bands associated with CO/MoS₂ is observed. The increase factor of intensity was calculated in this experiment and compared with the one obtained by *Dujardin* and a similar value of 2 was obtained [3]. This intensity increase is explained by the decrease of sulfur coverage at the edge of MoS₂ nanoparticles i.e. the increase in CUS site concentration at the edges due to hydrogen treatment [17,36]. Also, reducing sulfur coverage lead to a shift at lowest wavenumber of the $\nu(\text{CO})$ bands attributed to CO in interaction with Mo at the edges of MoS₂ slabs. Indeed, the depletion of S at the edge leads to an increase of the electron density of the adsorbing sites that leads to a stronger back donation effect to CO. On Mo/Al₂O₃ catalyst, a small shift was detected for the $\nu(\text{CO}/\text{M-edge})$ band from 2114 to 2110 cm⁻¹ (the average sulfur coverage being 50% [37]) and another band appears at 2099 cm⁻¹ which correspond to Mo in Mo-edge with a lower sulfur coverage (37.5% sulfur coverage[37]). For the $\nu(\text{CO})$ band attributed to CO/S-edge a little shift from 2070 to 2065 cm⁻¹ due to the decrease of sulfur coverage is also observed.

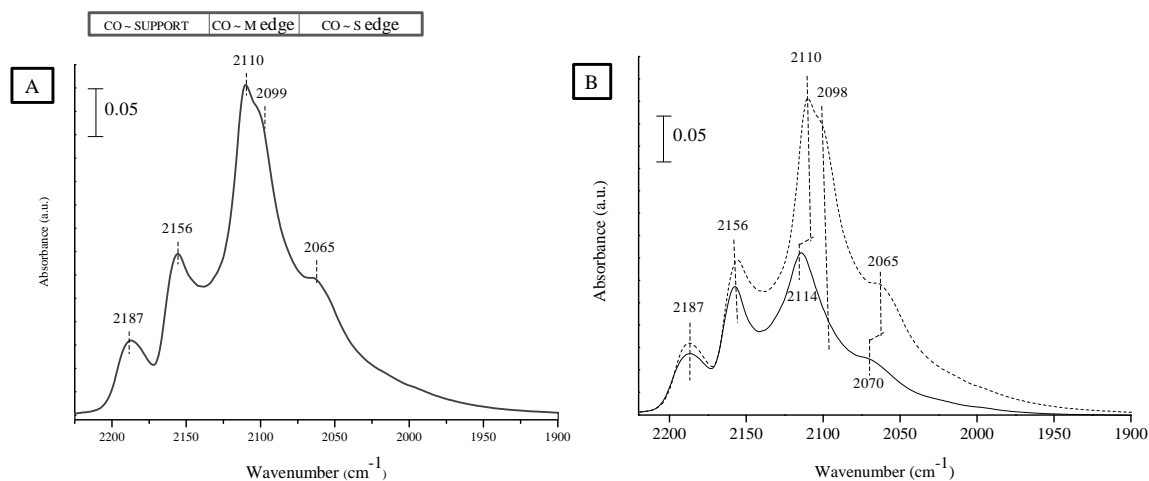


Figure III.13. IR spectra after adsorption of CO at equilibrium pressure (133 Pa) on sulfided Mo/Al₂O₃ after H₂ treatment during 2h at 623K (A) and comparison without H₂ treatment (B)

The same experiment was performed on Mo/SiO₂ and is shown in Figure III.14. For this catalyst a detailed experiment was carried out as it has not been performed before; then the experiment begin with small doses upon saturation as shown in Figure III.14.a. For Mo/SiO₂, a

big change in intensity was detected for the $\nu(\text{CO})$ bands of CO in interaction with MoS_2 phase after the H_2 treatment: the bands are five times more intense than the ones recorded after sulfidation. Besides, some changes in $\nu(\text{CO})$ band positions were recorded for CO interaction with Mo edge sites. The principal $\nu(\text{CO})$ band detected after sulfidation for CO/M-edge presents a shift from 2114 to 2112 cm^{-1} and another intense $\nu(\text{CO})$ band at 2102 cm^{-1} appears that can be attributed to CO/M-edge with lower S coverage after H_2 treatment. On the other hand, the principal CO/S-edge band does not show any modification of its position in comparison with the one observed on the spectrum after sulfidation.

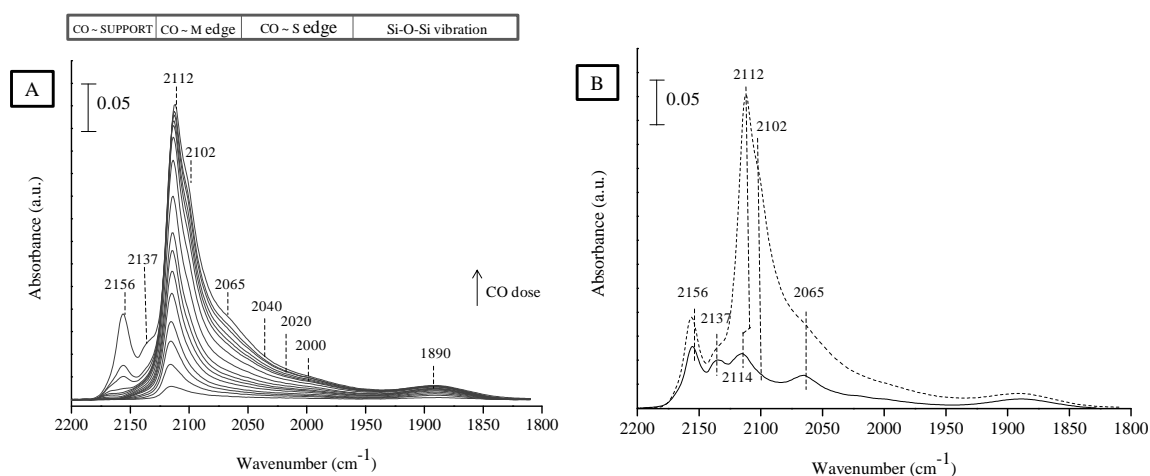


Figure III.14. IR spectra after adsorption of increasing doses of CO up to saturation of Mo/SiO_2 after H_2 treatment during 2h at 623K (a) and comparison with CO equilibrium pressure (133 Pa) spectra after sulfidation (b)

CO adsorption on Mo/TiO_2 after H_2 post-treatment is shown in Figure III.15.a. Since titania reacts with H_2S during sulfidation, hydrogen treatment has also an influence on TiO_2 surface as shown in Figure III.15.b. Thus, two $\nu(\text{CO})$ bands appear at 2181 cm^{-1} and 2157 cm^{-1} characteristic of CO in interaction with Lewis acid sites and hydroxyl groups respectively. As previously observed, the $\nu(\text{CO})$ bands ascribed to CO interaction with MoS_2 nanoparticles show a shift to lower wavenumber from 2118 to 2111 cm^{-1} and a new $\nu(\text{CO})$ band appears at 2102 cm^{-1} due to the decrease of sulfur coverage in Mo-edge. Also a shift to lower wavenumber of the CO/Mo in S-edge vibration from 2070 to 2065 cm^{-1} is observed. But, surprisingly, no strong change in intensity of $\nu(\text{CO/M-edge})$ band was detected for this catalyst, while this site is the most sensitive to H_2 post-treatment for the two others catalysts.

In summary, H_2 post-treatment leads to a decrease in sulfur coverage in both edges and then to a shift to lower wavenumber of CO/Mo edges vibrations (Mo in Mo-edge and S-edge).

CO/M-edge stretching band is more sensitive to H₂ treatment than the CO/S-edge one. Interestingly, after H₂ treatment, the position of both the $\nu(\text{CO/M-edge})$ and $\nu(\text{CO/S-edge})$ bands is close for the three samples. H₂ post-treatment produces a strong increase in the intensity of Mo sites detected by IR/CO on Mo/Al₂O₃ and Mo/SiO₂, but only a limited one on Mo/TiO₂.

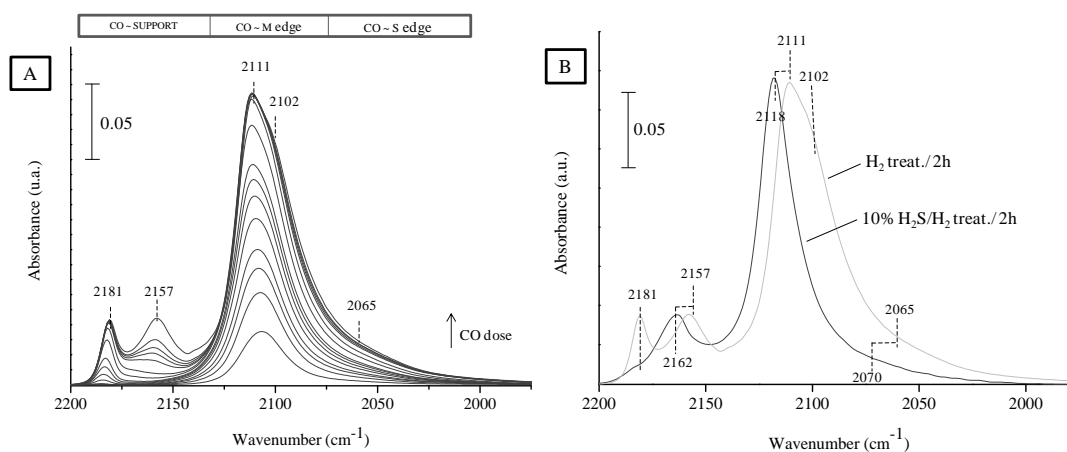


Figure III.15. CO adsorption spectra from small CO pressures up to saturation in Mo/TiO₂ after H₂ treatment during 2h at 623K (a) and comparison CO saturated spectra after sulfidation and H₂ treatment during 2 hours (b)

3.3.2.3.3. CO adsorption on sulfide catalysts: influence of treatment with 2% H₂S/H₂ after sulfidation

MoS₂ clusters under reaction are in contact with H₂ but also with H₂S that is produced during reaction. Previously MoS₂ nanoparticles were studied after sulfidation condition and after H₂ treatment while during reaction they are in intermediate atmosphere. Then, after sulfidation, MoS₂ nanoparticles were treated under a sulfur-reductive flow of 2% H₂S/H₂ i.e. similar to the one used in thiophene model reaction in this work.

After such treatment, CO adsorption spectra for Mo/Al₂O₃ from small doses up to saturation at equilibrium pressure are shown in Figure III.16.a. They do not present any significant modification in band positions in comparison with the ones after 10% H₂S/H₂ treatment: CO adsorption on hydroxyl groups and on Lewis acid sites appears at 2157 cm⁻¹, and 2187 cm⁻¹ respectively; and, CO in interaction with MoS₂ nanoparticles gives rise to CO/M-edge vibration at 2114 cm⁻¹ and CO/S-edge vibration at 2070 cm⁻¹. However, in comparison with the spectrum after 10% H₂S/H₂ (Figure III.16.b), an increase of intensity of all these bands is observed although in lesser extent than after H₂ treatment.

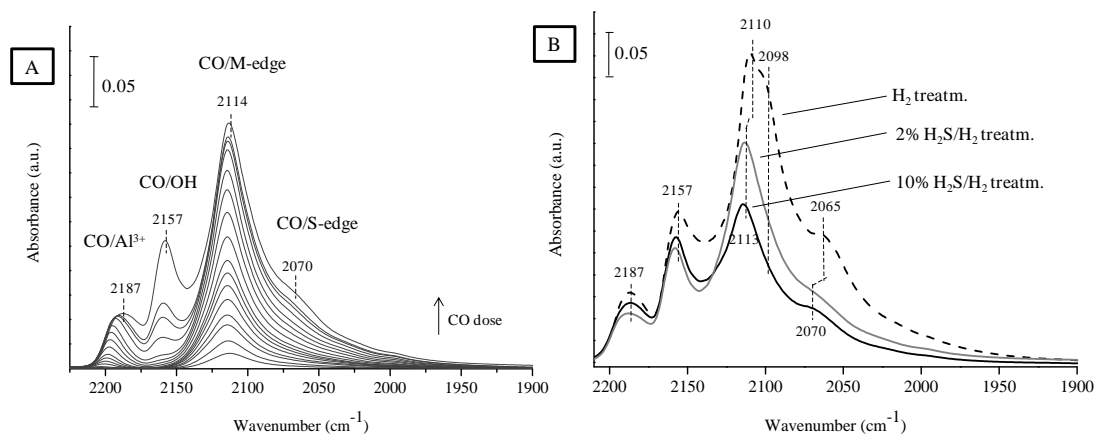


Figure III.16. CO adsorption spectra from small CO pressures up to saturation after H₂S (2%)/ H₂ (a), and comparison of sulfo-reductive treatment (b) in Mo/Al₂O₃

The same experiment was carried out on Mo/SiO₂ (Figure III.17.a). As was reported for Mo/Al₂O₃, no change in $\nu(\text{CO})$ band position was detected in CO adsorption after 2% H₂S/H₂ treatment. CO/OH appears at the same wavenumber at 2156 cm⁻¹, and CO physisorbed at 2137 cm⁻¹. CO/Mo-edge appears at 2116 cm⁻¹ and CO/S-edge appear at 2065 cm⁻¹, exactly at the same position than on the spectrum obtained after 10% H₂S/H₂ treatment. Comparison between sulfo-reductive conditions is shown in Figure III.17.b. In this comparison, the high influence of sulfo-reductive condition in MoS₂ nanoparticles supported on SiO₂ appears clearly. An increase of the band of CO/Mo sites located in M-edge is detected in comparison with the spectrum obtained after 10% H₂S/H₂ treatment in lower extent in comparison with the spectrum after H₂ treatment. Instead, the band intensity of the CO/Mo in S-edge interaction presents an intensity increase in comparison with CO saturated spectrum after 10% H₂S/H₂ treatment, but there are not comparable differences in comparison with the spectrum after hydrogen treatment.

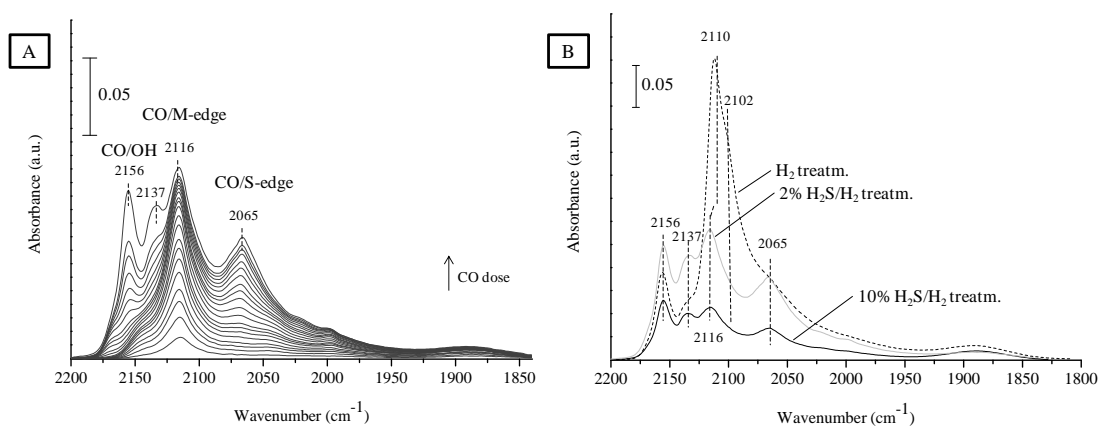


Figure III.17. CO adsorption subtraction spectra up to saturation after H₂S (2%) / H₂(a), and comparison of sulfo-reductive treatment (b) in Mo/SiO₂

Finally, the same experiment was performed in Mo/TiO₂ as shown in Figure III.18.a. CO adsorption spectra look the same after 2% H₂S/H₂ than after 10% H₂S/H₂, as shown in Figure III.18.b. Then, CO/M edge interaction appears at 2118 cm⁻¹ and CO/S-edge at 2070 cm⁻¹; and CO interaction with the support at 2162 cm⁻¹, as was discussed previously. The absence of effect can be linked to the stability of the edges due to a strong interaction between the slab and the support.

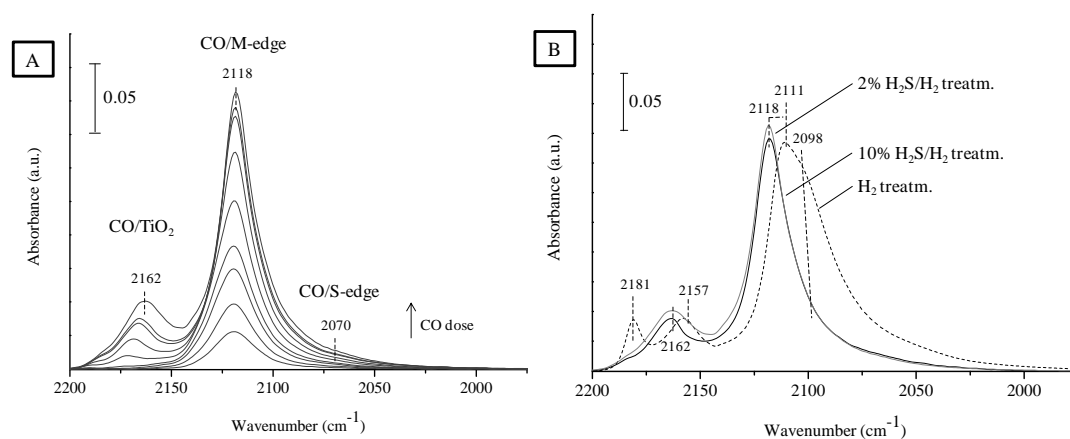


Figure III.18. IR spectra of CO adsorption increasing CO doses up to saturation after 2% H₂S/H₂ treatment (a), and comparison of sulfo-reductive treatment (b) in Mo/TiO₂

3.3.2.3.4. Active sites quantification

Quantification of Mo located in Mo-edge and S-edge was carried out using the respective CO band area obtained at saturation for each previously described treatment. All spectra were normalised to a pellet of 0.01 g of mass and a surface of 2.01 cm². The molar extinction coefficients used for the quantifications shown in Table III-3 were $16 \pm 4 \text{ mol}^{-1} \cdot \text{cm}$ for CO/Mo-edge calculated by *Maugé et al.* using Mo/Al₂O₃ catalyst [14], and $35 \pm 4 \text{ mol}^{-1} \cdot \text{cm}$ for CO/S-edge calculated by *Chen et al* using (CA/Mo=2)/Al₂O₃ (CA: citric acid) [19]. However, as was mentioned previously, Mo/TiO₂ catalyst after sulfidation with 10% H₂S/H₂, has only one contribution at the first doses, then a molar extinction coefficient can be recalculated using the first CO doses for CO/M-edge at 2118 cm⁻¹ in this catalyst. The result of the calculation was $14 \text{ mol}^{-1} \cdot \text{cm}$ (calculation shown in annex I). It is in the same order of magnitude than the one calculated for Mo/Al₂O₃ by *Maugé et al.*, $16 \pm 4 \text{ mol}^{-1} \cdot \text{cm}$ showing that the same species for all catalysts can be considered. As previously mentioned, a band appears after H₂ treatment around 2098 cm⁻¹ that is attributed to Mo located in M-edge with lower sulfur coverage. Being the same CO/Mo-edge species but with the different Mo coordination number they could have a different molar extinction coefficient. Mo/TiO₂ catalyst after H₂ treatment presents only one contribution band at 2008 cm⁻¹ for the first CO doses. Then, the molar extinction coefficient was calculated with the three first CO doses and was $21 \text{ mol}^{-1} \cdot \text{cm}$ versus $16 \text{ mol}^{-1} \cdot \text{cm}$ for the component at 2110 cm⁻¹, i. e. there is not strong difference between them. The calculated error was 4% using only one epsilon instead of two (one for each component).

The decomposition of CO saturated spectra for all samples was carried out with the Omnic software. Table III-3 shows the results obtained for the three sulfo-reductive treatments for the three catalysts. As was mentioned before, after H₂ treatment new CUS sites are detected due to the removal of sulfur in the edge of MoS₂ nanoparticles through the formation H₂S. After H₂ treatment, Mo/SiO₂ catalyst presents the strongest change, having 5 times more Mo edges sites than after sulfidation. Then, it is followed by Mo/Al₂O₃ for which the double of sites after H₂ treatment was detected. Finally, the less affected by H₂ treatment was Mo/TiO₂ which has only an increase of 30%. Both sites were affected by H₂ treatment, Mo-edge and S-edge but not in the same extent. Consequently after H₂ treatment, Mo/Al₂O₃ and Mo/TiO₂ present an increase of S-edge proportion while Mo/SiO₂ catalyst presents a decrease of S-edge percentage. After the 2% H₂S/H₂ treatment a little increase of Mo sites is recorded for Mo/Al₂O₃ and Mo/SiO₂, but any modification is recorded for Mo/TiO₂. For Mo/Al₂O₃, the increase of site concentration after the 2% H₂S/H₂ treatment does not lead to change in the percentage of Mo

edge located in Mo-edge and S-edge in comparison with one after 10% H₂S/H₂ treatment. Instead a change was detected for Mo/SiO₂ which presents a decrease of S-edge/M-edge ratio in comparison with the one after 10% H₂S/H₂ but in lower extent than after H₂ treatment.

Table III-3. Quantification by CO adsorption in Mo located in the edges of MoS₂ nanoparticles on Mo supported on Al₂O₃, SiO₂ and TiO₂ after three different sulfo-reductive treatments.

Catalysts	Conc. M-edge ($\mu\text{mol/g}$)	Conc. S-edge ($\mu\text{mol/g}$)	Total edge ($\mu\text{mol/g}$)	S-edge/M- edge
Mo/Al₂O₃	83	17	100	0.20
Mo/SiO₂	22	12	34	0.54
Mo/TiO₂	80	3	82	0.03
Sulfide catalysts after H ₂ post-treatment during 2h at 623K (*)				
Mo/Al₂O₃ *	182	52	234	0.28
Mo/SiO₂ *	125	41	166	0.32
Mo/TiO₂ *	100	7	107	0.07
Sulfide catalysts after 2% H ₂ S/H ₂ post-treatment during 2h at 623K (**)				
Mo/Al ₂ O ₃ **	120	24	144	0.20
Mo/SiO ₂ **	67	28	95	0.42
Mo/TiO ₂ **	80	3	82	0.03

3.3.2.4. Slabs study by Transmission Electron Microscopy (TEM).

MoS₂ slabs on the three different catalysts after sulfidation were studied by Transmission Electron Microscopy (TEM). Some of the pictures obtained are shown in Figure III.19 for Mo supported on Al₂O₃, SiO₂ and TiO₂.

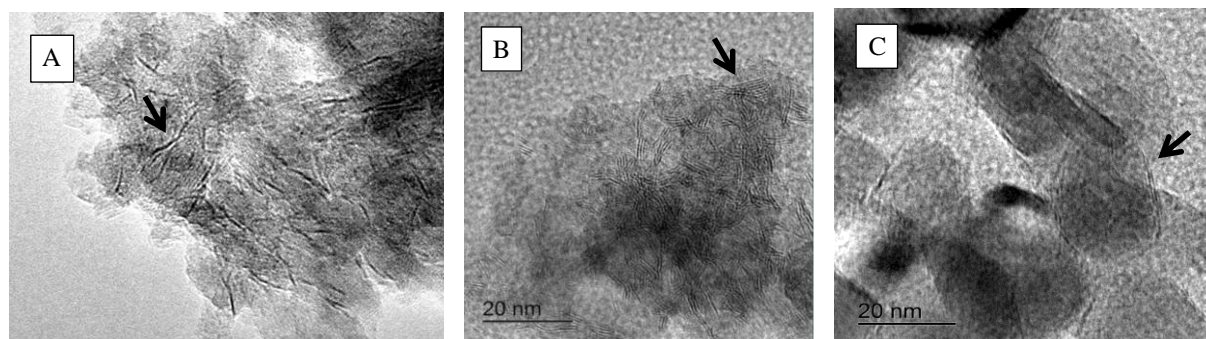
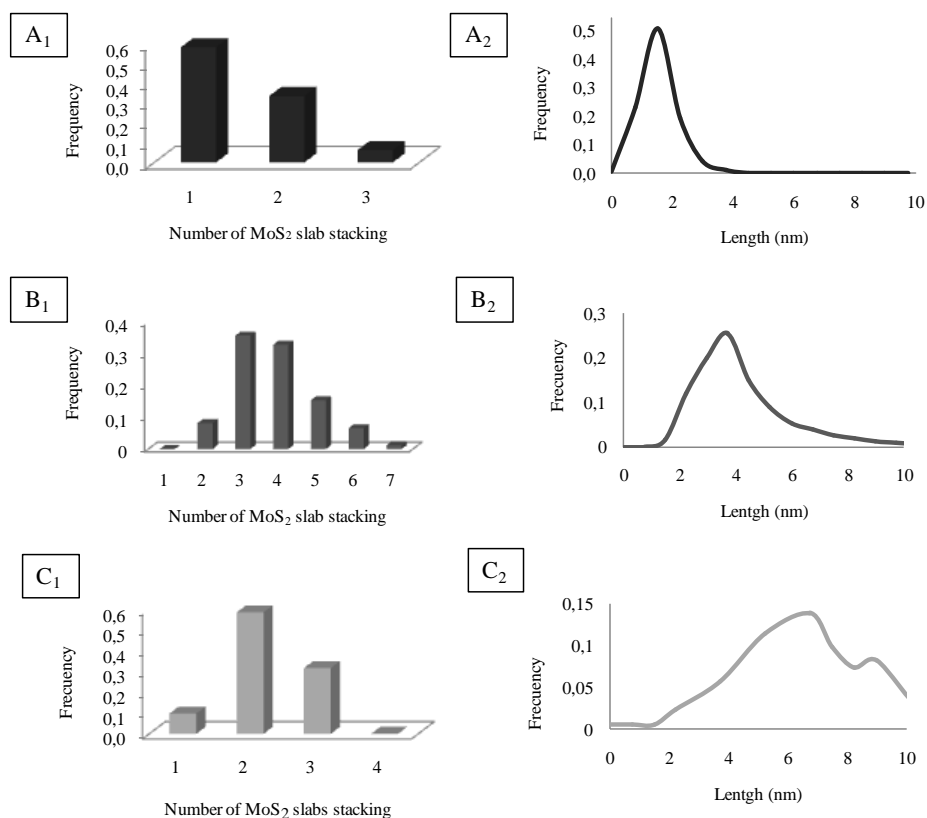


Figure III.19. TEM picture of MoS₂ slab in Mo/Al₂O₃ (a), Mo/SiO₂ (b), and Mo/TiO₂ (c)

Slab length and stacking degree distributions of sulfide slabs in the three catalysts and the summary of average results are shown in Figure III.20. Mo/Al₂O₃ presents a mono stacking and the smaller particle size of 2 nm with a narrow distribution. Mo/SiO₂ has a high stacking number near to 4 and an average length of 4.7 nm with an intermediate distribution. Finally, Mo/TiO₂ presents the bigger average slab length of 6.7 nm with a wide distribution and a stacking number of 2.



Catalysts	Stacking average	Length average (nm)
Mo/Al ₂ O ₃	1.3	2.0
Mo/SiO ₂	3.5	4.7
Mo/TiO ₂	2.0	6.7

Figure III.20. Stacking (1) and length (2) of sulfide slabs in Mo/Al₂O₃ (A), Mo/SiO₂ (B) and Mo/TiO₂ (C). And the summary result of stacking and length in the table for Mo sulfide catalysts

3.4. Discussion

The support effect on non-promoted catalysts has been studied by different techniques at different stages of the preparation route starting from the support surfaces, followed by the oxidic form of the catalysts and finally to the sulfide catalysts. Table III-4 summarises the results obtained of these studies. The goal of this approach is to study the parameters linked to the support that influence the formation of MoS₂ slabs in order to get a rational view of the so called slab-support interaction.

Table III-4. Summary of catalysts characterization

Catalysts	Catalyst Characterization						
	Raman	Sensitivity to Sulfo-reductive treatments	Morphology by IR/CO	Slab stacking	Slab length	Total sites per surface unit	Thiophene rate per area unit
Mo/SiO ₂	-Polymolybdate species -MoO ₃ species	High	Near to perfect hexagon	High	Medium	Low	Low
Mo/Al ₂ O ₃	-Polymolybdate species	Medium	Triangle truncated	Low	Low	Medium	Medium
Mo/TiO ₂	-Polymolybdate species	Low	Triangle	Medium	High	High	High

3.4.1. Support-Mo interaction in oxidic catalysts

The support surface was characterised by IR/CO to determine the acidic sites available on the surface of the three supports and then to highlight the possible differences in the interaction between the Mo precursor and the support surface during the impregnation step. The case of the alumina support has been extensively studied due to its high industrial use. It is well known that Al₂O₃ surface is constituted by hydroxyl groups with different nature, and by Lewis acid sites, Al³⁺ cations. Specific metal-support interaction has been proposed between the basic OH groups and the monomolybdate anions at low loading of Mo (< 0.6 Mo at.nm⁻²) while electrostatic interaction with Al³⁺ is considered to occur at higher loading [38,39]. Moreover, for Mo loading in the range of this study, this support is known to be reactive and to lead to the formation of the so-called AlMo₆ polyanions during the impregnation stage [28]. Blanchard et al. reported that after calcination and contact with air, these anions remain on the oxidic precursor. The characteristic Raman spectrum of such species shows mainly contributions at 952, 560 and 350 cm⁻¹. These features are close to the ones observed in this work. However, a contribution at 860 cm⁻¹ also clearly appears in our case. For this reason, from the Raman

results, we only consider that polymolybdates are formed on the oxidic precursor on alumina support with terminal vibrations ($\nu_{\text{Mo=O}}$) giving rise to the peak at 955 cm^{-1} and bridge vibrations ($\nu_{\text{Mo-O-Mo}}$) to the one at 860 cm^{-1} . From the characterization of the oxidic precursor by UV-visible, it can be infer that these polymolybdates are small anions such as $\text{Mo}_2\text{O}_7^{2-}$.

On TiO_2 surface, the strongest adsorbing sites for CO are the Lewis acid sites as confirmed by the interaction between CO and these sites at low CO coverage. van Veen et al. have reported previously that the interaction of heptamolybdate solution with TiO_2 gives rise to interaction between polymolybdate species and Ti^{4+} CUS sites [38,40]. Accordingly, the detection of the decrease of CO/Ti^{4+} stretching band for calcined catalyst in comparison with the support alone can be considered as a strong anchoring (Ti-O-Mo) between oxomolybdate and the surface by hydroxyl group formed by the hydration during the impregnation stage. Moreover, the Raman results stand the strong metal-support interaction due to the detection of the vibration bands shift at 10 cm^{-1} to higher wavenumber in comparison with the other two catalysts. Additionally, the formation of polymolybdate are confirmed with a lower Mo=O/Mo-O-Mo peak ratio than in the case of Al_2O_3 indicating that bigger anions are formed on TiO_2 . This result is confirmed by the UV-visible study. Polymolybdates with high number of Mo nearest neighbour are formed on TiO_2 .

Finally, SiO_2 surface only presents acid hydroxyl groups. Thus, specific interaction with the Mo anions is not favoured. Accordingly, the dispersion of molybdenum on SiO_2 is low and formation of MoO_3 is revealed by Raman spectroscopy. Moreover, formation of polymolybdates such as $\text{Mo}_7\text{O}_{24}^{6-}$ is proposed according to low Mo=O/Mo-O-Mo ratio detected in Raman spectrum and the UV-visible result.

In conclusion, the interaction of the Mo species in the oxidic precursor is clearly different on the three studied supports. A strong interaction between polymolybdate species and TiO_2 is explained by the presence of strong Lewis acid sites. Intermediate interaction with OH and weaker Lewis acid sites is reported to occur on alumina. And on SiO_2 , weak interaction with acid hydroxyl groups is observed. Consequently, already in the oxidic precursors, different Mo species are formed.

3.4.2. Support effect on the morphology of MoS₂ slabs and Mo edge dispersion

3.4.2.1. Influence of the post-treatment on the sites detected by CO adsorption

CO adsorption at low temperature followed by FTIR spectroscopy was used to characterize MoS₂ slabs supported on Al₂O₃, SiO₂ and TiO₂ after sulfidation and after two different post-treatments. Indeed, DFT calculations predict the influence of sulfidation conditions (temperature and H₂S/H₂ ratio) on the sulfur coverage of MoS₂ edges [8,41]. Moreover, previous studies from our group have shown the influence of post-treatment on the sulfur coverage on the edges of MoS₂ slabs supported on Al₂O₃ by IR/CO method [20,42–44]. In particular, it was shown that after the sulfidation at atmospheric pressure, the H₂ post-treatment leads to an increase of CUS sites detected by CO as well as to the formation of more S depleted sites giving rise to a shift of the main $\nu(\text{CO})$ band to lower wavenumbers and the appearance of a shoulder one on Mo/Al₂O₃ [3,4]. Accordingly, in this study, an increase of Mo sites detected by CO has been observed after the H₂ post treatment for the three catalysts. This increase is well explained by the formation of CUS sites by elimination of sulfur on the edge forming H₂S during the post-treatment. However, it appears that the magnitude of the increase varies significantly with the support nature: the strongest effect was recorded for Mo/SiO₂, followed by Mo/Al₂O₃ and finally for Mo/TiO₂. Therefore, the effect of the reductive treatment on the CUS formation is stronger for a weak metal-support interaction. The decrease of sulfur coverage was also detected by the shift of the $\nu(\text{CO/Mo})$ bands at lower wavenumbers and the appearance of a shoulder around 2100 cm⁻¹ for the three catalysts. For the main $\nu(\text{CO/M-edge})$ band, Mo/Al₂O₃ and Mo/SiO₂ catalysts showed the band shift in the same order, unlike Mo/TiO₂ catalyst showed higher band shift. Surprisingly, no increase of CUS sites was detected for this catalyst as could be expected by the high shift presented. That can indicate that the strong interaction with the support has a role in the sites stabilization, and the shift of the band to lower wavenumber is due to the reduction of Ti⁴⁺ cations to Ti³⁺. This treatment shows the stability presented by MoS₂ structure on titania surface that can be linked with the strong interaction with the support.

Considering the influence of the treatment/post-treatment on the Mo site quantification, experiments after 2% H₂S/H₂ post-treatment were also performed in order to reach closer conditions to the ones used in the catalytic test. In this case, a moderate increase of CUS

availability was detected for Mo/Al₂O₃ and Mo/SiO₂ catalysts but no influence was found for Mo/TiO₂. Moreover, any band shift was detected after 2% H₂S/H₂ post-treatment meaning that the S depletion in the environment of the adsorbing sites is indeed limited.

3.4.2.2. Effect of the support on the morphology, length and stacking

In the following only the IR/CO results obtained after the 2% H₂S/H₂ post-treatment will be considered. The comparison of the IR/CO spectra obtained for three catalysts normalised by surface area are shown in Figure III.21. Mo located in two different edge sites (M- and S-edge) was distinguished by IR/CO method. The $\nu(\text{CO/M-edge})$ band appears around 2115 cm⁻¹ for Mo/Al₂O₃ and Mo/SiO₂ and at 2118 cm⁻¹ for Mo/TiO₂. The $\nu(\text{CO/S-edge})$ band appears at 2070 cm⁻¹ for Mo/Al₂O₃ and Mo/TiO₂ and at 2065 cm⁻¹ for SiO₂. This comparison highlights the variation of the slab morphology versus the support: almost no Mo on S-edge was detected for Mo/TiO₂, while some Mo on S-edge with different ratios was found for the other two sulfide catalysts.

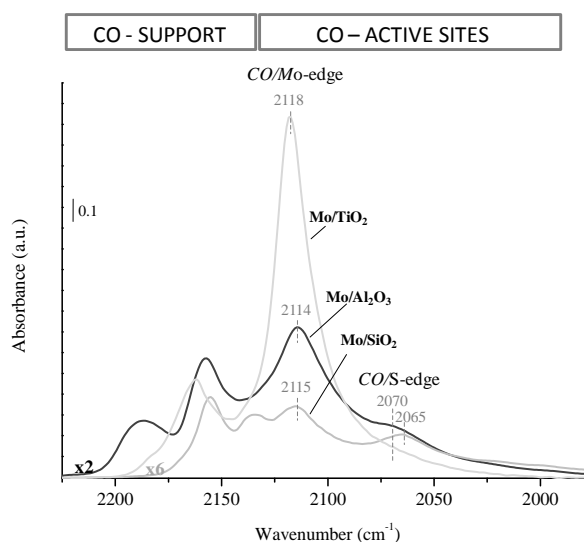


Figure III.21. IR spectra of CO in equilibrium normalised by surface area of Mo/Al₂O₃, Mo/SiO₂ and Mo/TiO₂

Accordingly, to more accurately study the change observed in the three sulfided catalysts, S-/M-edge ratio and Mo edges sites are represented in Figure III.22. Then, significative change in S- /M-edge ratio was found for the three catalysts. The ratio increases in the order Mo/TiO₂ < Mo/Al₂O₃ < Mo/SiO₂ that is in relation with the nature of metal-support interaction. The S-/M-edge ratios calculated by the quantification of Mo sites probed by CO, are used to predict the MoS₂ morphology. Then, a morphology near to a

perfect hexagon can be predict for Mo/SiO₂, truncated triangle for Mo/Al₂O₃ and near to perfect triangle for Mo/TiO₂. It is also notable the high amount of Mo sites detected on Mo/TiO₂ in comparison with the others two catalysts. In the opposite way, very low amount of Mo sites was detected for Mo/SiO₂.

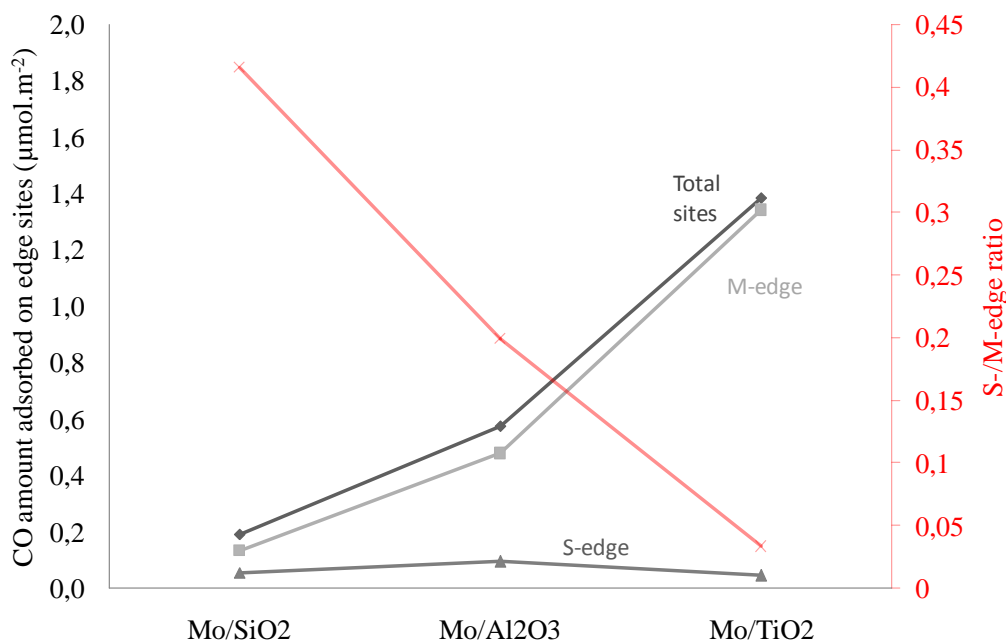


Figure III.22. Sites concentration (black line) and S- /M-edge ratio (red line) on sulfided catalysts detected by IR/CO

Also, different stacking and length of MoS₂ slabs have been recorded for the different supports. The slabs stacking increase in the order Mo/Al₂O₃ < Mo/TiO₂ < Mo/SiO₂, with 1, 2 and 4 average values, respectively. The high stacking in Mo/SiO₂ can be linked with the weak interaction metal-support in the impregnation step as it was previously described. The slab length increases in the order Mo/Al₂O₃ < Mo/SiO₂ < Mo/TiO₂, with 2.0, 4.7 and 6.7 nm average values, respectively.

The average of slab length (L_{TEM}) from TEM images and S-edge/M-edge ratio from IR/CO were then taken into account to describe the “average” MoS₂ slab in the three catalysts. Mo-Mo distance (3.16 Å) was taken to calculate the number of molybdenum atoms (n_L) forming the longer line that is detected by TEM microscopy (L_{TEM}), and S-edge/M-edge ratio from IR/CO was considered to calculate the number of molybdenum present in M- (n_M) and S-edge (n_S) in MoS₂ slab edges. The corner sites are considered half as M-edge sites and half as S-edge sites. The equations used as are:

$$n_L - 1 = n_S + n_M$$

$$S\text{-} / M\text{-edge ratio from IR/CO} = n_S / n_M$$

The result of the predicted morphologies is shown in Figure III.23 highlighting the strong differences in the slab characteristics versus the support. Then, Mo edge dispersion can be calculated from this global slab morphology for the three supports (Table III-5). Both, the slab length obtained by TEM and the morphology influence Mo edge dispersion [45]: the longer the slab the lower the Mo edge dispersion. For the same slab length, Mo edge dispersion is higher for triangular than for hexagonal shape.

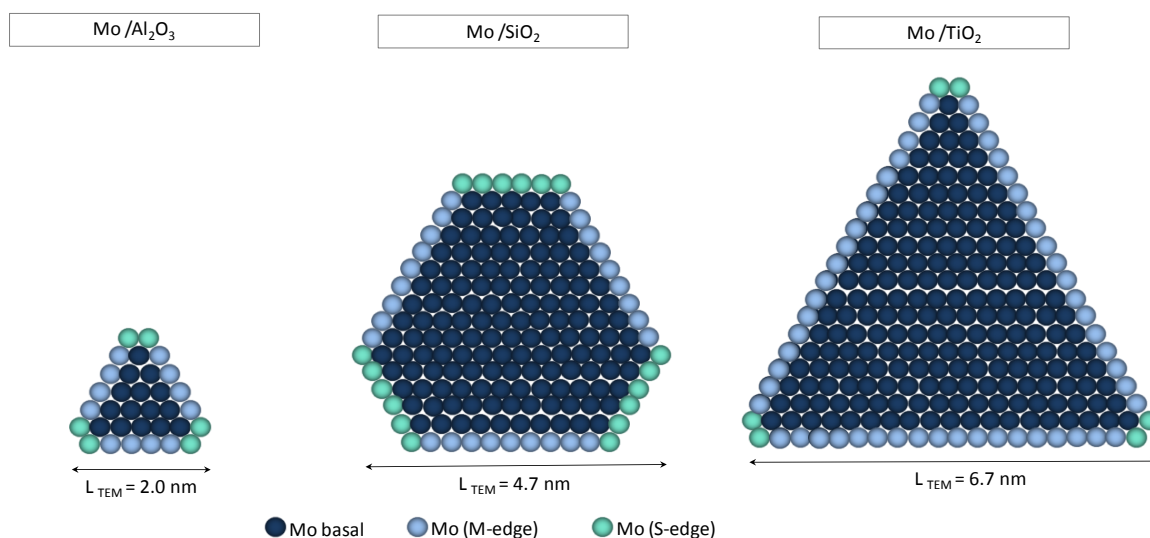


Figure III.23. MoS₂ slab imaging by combination of TEM microscopy and IR/CO spectroscopy

Then, the concentration of total Mo edge sites can be calculated taking into account the total Mo concentration obtained from ICP analysis the percentage of Mo in molybdenum sulfide form calculated by XPS from the reference [46], the slab length from TEM and the MoS₂ shape obtained by IR/CO (Table III-5). Table III-5 that high Mo edge dispersion was calculated for Mo/Al₂O₃ due to its small particle size and slab shape close to a triangle. Instead, Mo sites amount is low for Mo/SiO₂ due to the high nanoparticles size and the hexagon morphology. Although Mo/SiO₂ and Mo/TiO₂ present different particle size, calculation gives an equivalent and small amount of Mo edge dispersion for both catalysts. The similar Mo dispersion is explained by the compensation of the triangle morphology to the high average slab length for Mo/TiO₂ compared with Mo/SiO₂.

The Mo edge concentration obtained by direct quantitative IR/CO method (experimental) is compared with the one calculated from TEM given the MoS₂ shape obtained by IR/CO (calculated) in Table III-5. The ratio between experimental and calculated is around 50% for Mo supported in Al₂O₃ and SiO₂ catalysts, such values being in the usual range [3]. Conversely, the double value for experimental than calculated one is obtained for Mo/TiO₂ catalyst. Note that for this catalyst, the validity of the epsilon value has been checked.

Table III-5. Comparison between Mo edge calculated by TEM¹ results and Mo detected by IR/CO

Catalyst	Edge dispersion by TEM ¹	Total Mo by ICP (μmol/g)	Sulfuration rate (%) by XPS *	Mo edge calculated by TEM (μmol/g)	Mo edge by IR/CO (μmol/g) After H ₂ post-treatment	Mo edge exp./Mo edge calc.
Mo/Al ₂ O ₃	0.54	1115	75.6	455	234	0.51
Mo/SiO ₂	0.24	1699	73.9	301	166	0.55
Mo/TiO ₂	0.24	250	85.7	52	107	2.08

¹ the S-/M- edge ratio was considered in this calculation to determine the shape of the slab.

*% sulfidation rate was taken from reference [46].

The excess of sites detected for Mo/TiO₂ catalyst could be explained by three different hypotheses. The first hypothesis is linked with the possibility that MoS₂ nanoparticles on titania can present different morphology like elongated hexagonal shape as detected by STM using rutile-TiO₂ (110) as support [48]. This morphology was observed by *Lauritsen et al.* for a single-layer of MoS₂ supported on rutile TiO₂ (110) sulfided at 950K, that is formed by two long edge ascribed to M-edge and S-edge (Figure III.24) [49]. Considering this morphology, the Mo edge dispersion was calculated using the slab shape showed in Figure III.24, the slab length measured by TEM and the S-/M-edge ratio obtained by IR/CO. With such morphology, the Mo edge dispersion is double, i.e. 0.50 for elongated hexagonal shape versus 0.24 for triangle shape. Thus, the change in Mo edge dispersion according to the slab morphology (double for elongated hexagon) is in good relation with the difference observed between the Mo edge measured by IR/CO and the one calculated using a classical morphology. This could indicate that MoS₂ slabs on Mo/TiO₂, present elongated hexagonal morphology with the MoS₂-TiO₂ anchoring by S-edge sites since mostly M-edge sites were detected by IR/CO. *Hinnemann et al* studied the MoS₂ anchoring by M- or S-edge sites in alumina surface by DFT calculations. The anchoring by S-edge sites was more favourable energetically than M-edge sites on alumina [50]. This hypothesis is also in agreement with the calculation performed by Costa et al. which observed S-edge anchoring for small MoS₂ with alumina surface. However calculations

performed on Mo/TiO₂ show no possibility of S-edge anchoring with support surface for anatase-TiO₂ [12]. These authors studied the anchoring for MoS₂ with different lengths. For slabs with long length like is our case, their results show strong anchoring of MoS₂ with anatase-TiO₂ surface through the so-called “chemical ligand effect”, but by M-edge sites. These calculations refuse the possibility of the elongated hexagon morphology on Mo/TiO₂ catalyst. It leads to discuss other possible hypotheses as the “extra” probe of sites by CO, i.e. Mo sites that are not only located on the edges, e.g. brim sites. The brim sites are considered as Mo sites with more metallic character than Mo edge sites and full sulfur coordinated. The full sulfur coordinated indicates that CO cannot be adsorbed on these sites, but considering that the strong anchoring of MoS₂ on titania leads to the formation of Mo-O-Ti-S-Mo bonds that stabilizes MoS₂ structure creating sulfur vacancies, which in this point CO could be adsorbed. The brim sites detection by CO should lead to show a band shift to lower wavenumber due to the metallic character presented by these sites [51,52]. Then, according that $\nu_{\text{CO/M-edge}}$ band for Mo/TiO₂ appeared at 2118 cm⁻¹, i.e. at higher wavenumber than other catalysts, indicated that CO molecules are not probing brim sites. Thus, the excess of Mo sites detected for Mo/TiO₂ catalyst can be linked to the slab length value obtained by the small slabs amount observed in TEM images, influencing in the calculated value of Mo edges calc.

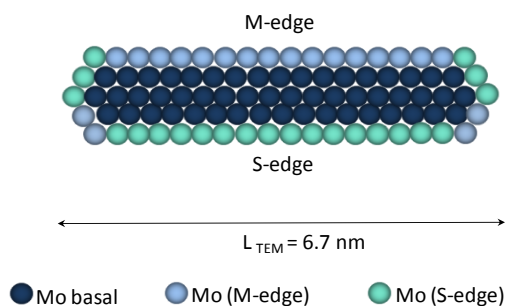


Figure III.24. Imaging elongated hexagon MoS₂ morphology given slabs length from TEM and S-/M-edge ratio from IR/CO

3.4.2.3. Relation of MoS₂ morphology with catalytic activity on sulfide catalysts

Recently, several studies showed the relation between total Mo sites, and MoS₂ morphology with the catalytic activity [17,52–54]. These two parameters were reported to be the main influence of catalytic activity. Thus, the relation between total sites detected by IR/CO and catalytic activity per surface unit, are shown in Figure III.25. Thus, a tendency between total sites and HDS rate was found, since higher Mo sites available present, higher catalytic activity present the catalyst. The high activity was found for Mo/TiO₂ catalyst, followed by

Mo/Al₂O₃ catalyst, and finally Mo/SiO₂ catalyst. Then the high activity of Mo/TiO₂ that can be linked with the high amount of Mo sites detected, confirms the reliability of the IR/CO measurements on this catalyst (that is different from the calculated one as mentioned in the previous section).

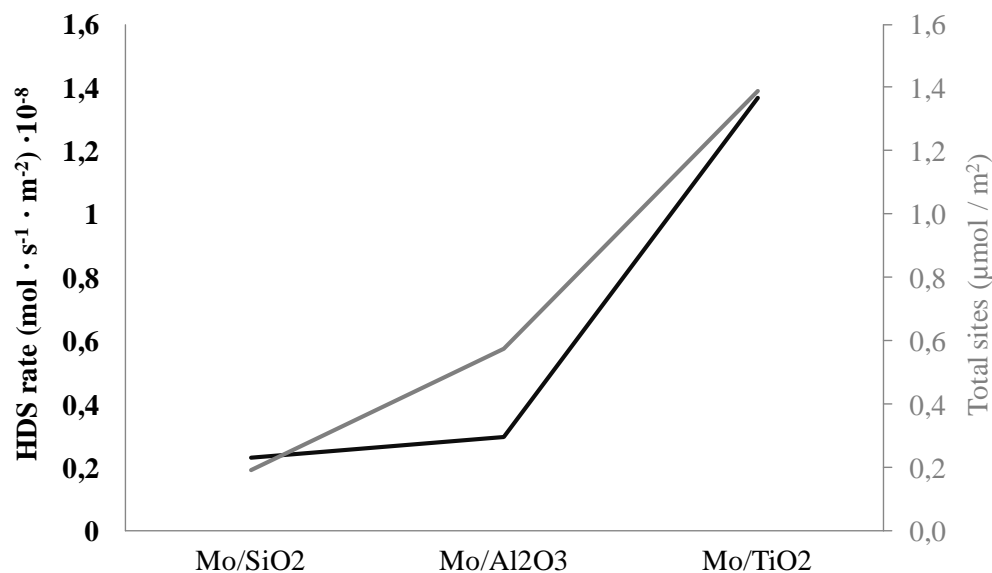


Figure III.25. Relation between total active sites detected by IR/CO (grey line) and catalytic activity (black line) for Mo/Al₂O₃, Mo/SiO₂ and Mo/TiO₂

The variations of the S-/M-edge ratio and TOF values are given in Figure III.26. For Mo/Al₂O₃ and Mo/SiO₂ an increase of TOF value was detected when there is an increase of S-/M-edge ratio as was expected from previous study [4]. It can be linked with the selectivity: Mo in S-edge favours DDS (Direct Desulfurization) pathway and Mo in M-edge favours HYD (Hydrogenation) pathway [55]. The case of Mo/TiO₂ is more complex: even if the selectivity towards HYD pathway could be explained by the presence of quasi exclusively Mo sites on the M-edge or the presence of brim sites, the high value of TOF is a particular result. Note that this TOF value is obtained even though concentration of sites detected by IR/CO was surprisingly high. It appears from this study that the active sites in the case of Mo/TiO₂ are of a particular nature. This specific behavior may be for the presence of a high concentration of brim sites on Mo/TiO₂.

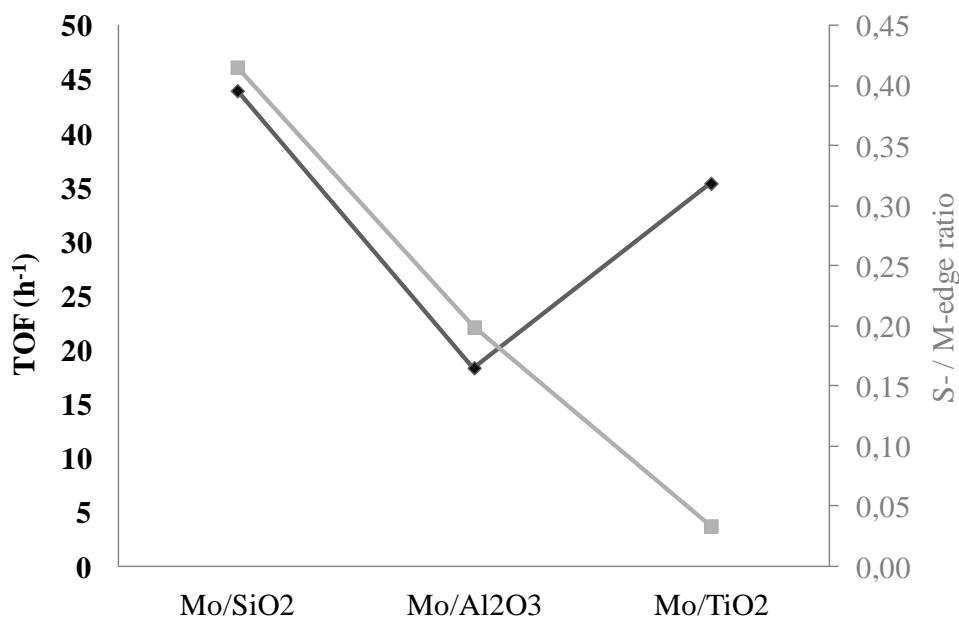


Figure III.26. Total TOF value taking into account total Mo sites detected after 2% H₂S/H₂ post-treatment for Mo supported on Al₂O₃, SiO₂ and TiO₂

3.5. Conclusion

A clear and important support effect was evidenced in MoS₂ nanoparticles formation. The metal-support interactions formed during the impregnation stage strongly impact the formation of MoS₂ slabs (dispersion, morphology, stacking length, etc) and influence the reactivity.

Indeed, when Mo precursor interacts with weakly acidic hydroxyl group as on silica, oxomolybdenum species with low dispersion are created that favored the MoO₃ species formation. If Mo precursor is in interaction with basic hydroxyl groups and Lewis acid sites as on alumina, the metal-support interactions are stronger and polymolybdate species with a large dispersion are formed as detected by Raman and UV-Vis spectroscopies. As for titania, strong metal-support interactions occur since molybdenum precursor only interacts with Lewis acid sites of titania. This strong interaction is testified by the shift to higher wavenumbers of Mo=O vibration detected by Raman (and not observed on other supports). In such a case, a good dispersion of oxo-Mo species is measured.

This first stage has a key effect on the genesis of the sulfide phase, and can strongly change the morphology, activity and selectivity of the resulting MoS₂ slabs. Near to perfect hexagonal

sulfide slabs with high stacking and high slab length were detected for Mo/SiO₂ catalyst which lead to low Mo edge dispersion. Truncated triangle sulfide slabs were observed for Mo/Al₂O₃ with mono-stacking and small slab lengths, which lead to high Mo edge dispersion. For alumina and silica supported catalysts, the activity can be related to the concentration of Mo edge sites and to the S-/M-edge ratio; the S-edge sites having a greater TOF value than M-edge sites. Thus, the more active Mo sulfided catalysts supported on silica and alumina should present both a good dispersion and a morphology that favors the S-edges. The S-/M-edge ratio: then low S-/M-edge ratio gives small TOF value. However, a different behavior was found for Mo/TiO₂ catalyst. The highest catalytic activity was found for this catalyst even though it is composed by high amount of Mo sites on M-edge. The strong interaction between MoS₂ slab and TiO₂ that gives rise to specific sites with high activity is thus confirmed by this study.

3.6. References

- [1] H. Topsoe, B.S. Clausen, F.E. Massoth, *Hydrotreating Catalysis*, Springer, Berlin-Heidelberg, 1996.
- [2] A.S. Walton, J. V Lauritsen, H. Topsoe, F. Besenbacher, *J. Catal.* 308 (2013) 306–318.
- [3] C. Dujardin, M.A. Lelias, J. van Gestel, A. Travert, J.C. Duchet, F. Mauge, *Appl. Catal. A Gen.* 322 (2007) 46–57.
- [4] J. Chen, F. Maugé, J. El Fallah, L. Oliviero, *J. Catal.* 320 (2014) 170–179.
- [5] S. Kasztelan, H. Toulhoat, J. Grimblot, J.P. Bonnelle, *Bull. Soc. Chim. Belg.* 93 (1984) 807–811.
- [6] P. Raybaud, J. Hafner, G. Kresse, S. Kasztelan, H. Toulhoat, *J. Catal.* 189 (2000) 129–146.
- [7] P. Raybaud, J. Hafner, G. Kresse, H. Toulhoat, *Surf. Sci.* 407 (1998) 237–250.
- [8] H. Schweiger, P. Raybaud, G. Kresse, H. Toulhoat, *J. Catal.* 207 (2002) 76–87.
- [9] J. V Lauritsen, M. V Bollinger, E. Laegsgaard, K.W. Jacobsen, J.K. Norskov, B.S. Clausen, H. Topsoe, F. Besenbacher, *J. Catal.* 221 (2004) 510–522.
- [10] S. Helveg, J. V Lauritsen, E. Laegsgaard, I. Stensgaard, J.K. Norskov, B.S. Clausen, H.

- Topsoe, F. Besenbacher, *Phys. Rev. Lett.* 84 (2000) 951–954.
- [11] J. Kibsgaard, PhD Thesis (2008) 1–159.
- [12] D. Costa, C. Arrouvel, M. Breysse, H. Toulhoat, P. Raybaud, *J. Catal.* 246 (2007) 325–343.
- [13] C. Arrouvel, M. Breysse, H. Toulhoat, P. Raybaud, *J. Catal.* 232 (2005) 161–178.
- [14] F. Mauge, J.C. Lavalley, *J. Catal.* 137 (1992) 69–76.
- [15] F. Mauge, C. Binet, J.C. Lavalley, *Catal. by Met. Les Houches Sch. Les Houches, Fr., Mar. 19-29, 1996 (1997)* 1–17.
- [16] A. Travert, F. Mauge, *Stud. Surf. Sci. Catal.* 127 (1999) 269–277.
- [17] A. Travert, C. Dujardin, F. Mauge, S. Cristol, J.F. Paul, E. Payen, D. Bougeard, *Catal. Today* 70 (2001) 255–269.
- [18] A. Travert, C. Dujardin, F. Mauge, E. Veilly, S. Cristol, J.F. Paul, E. Payen, *J. Phys. Chem. B* 110 (2006) 1261–1270.
- [19] J. Chen, E. Dominguez Garcia, L. Oliviero, F. Maugé, *J. Catal.* 332 (2015) 77–82.
- [20] J. Chen, V. Labruyere, F. Mauge, A.-A. Quoineaud, A. Hugon, L. Oliviero, *J. Phys. Chem. C* 118 (2014) 30039–30044.
- [21] J. Bachelier, M.J. Tilliette, M. Cornac, J.C. Duchet, J.C. Lavalley, D. Cornet, *Bull. Des Soc. Chim. Belges* 93 (1984) 743–750.
- [22] H. Nasser, A. Redey, T. Yuzhakova, Z.N. Toth, T. Ollar, *React. Kinet. Catal. Lett.* 92 (2007) 329–335.
- [23] Y. Sakashita, Y. Araki, H. Shimada, *Appl. Catal. a-General* 215 (2001) 101–110.
- [24] a. Travert, O. V. Manoilova, a. a. Tsyganenko, F. Mauge, F. Maugé, J.C. Lavalley, *J. Phys. Chem. B* 106 (2002) 1350–1362.
- [25] N.Y. Topsoe, H. Topsoe, *J. Catal.* 139 (1993) 631–640.
- [26] C. Arrouvel, M. Digne, M. Breysse, H. Toulhoat, P. Raybaud, *J. Catal.* 222 (2004) 152–166.

- [27] S. Dzwigaj, C. Arrouvel, M. Breysse, C. Geantet, S. Inoue, H. Toulhoat, P. Raybaud, J. Catal. 236 (2005) 245–250.
- [28] P. Blanchard, C. Lamonier, A. Griboval, E. Payen, Appl. Catal., A 322 (2007) 33–45.
- [29] S. Dzwigaj, C. Louis, M. Breysse, M. Cattenot, V. Bellière, C. Geantet, M. Vrinat, P. Blanchard, E. Payen, S. Inoue, H. Kudo, Y. Yoshimura, Appl. Catal. B Environ. 41 (2003) 181–191.
- [30] W. Banares, Hu, (1994).
- [31] B. Delmon, H. Knözinger, J. Phys. Chem. 98 (1994) 11269–11275.
- [32] L. Seguin, M. Figlarz, R. Cavagnat, J.C. Lassgues, Spectrochim. Acta Part A Mol. Biomol. Spectrosc. 51 (1995) 1323–1344.
- [33] R.S. Weber, J. Catal. 151 (1995) 470–474.
- [34] M. Fournier, C. Louis, M. Che, P. Chaquin, D. Masure, J. Catal. 119 (1989) 400–414.
- [35] L. van Haandel, G.M. Bremmer, E.J.M. Hensen, T. Weber, J. Catal. 351 (2017) 95–106.
- [36] A. Travert, H. Nakamura, R.A. van Santen, S. Cristol, J.F. Paul, E. Payen, J. Am. Chem. Soc. 124 (2002) 7084–7095.
- [37] V. Labruyere, Structure Des Sites Sulfures Des Catalyseurs D’hydrotraitement: Approche Combinee Par Spcetroscopie IR et Modelisation Moleculaire, Universite of Caen, 2014.
- [38] J.A.R. VAN VEEN, H. DE WIT, C.A. EMEIS, P.A.J.M. HENDRIKS, 582 (1987) 579–582.
- [39] I.E. Wachs, Catal. Today 27 (1996) 437–455.
- [40] M.J. Vissenberg, L.J.M. Joosten, M.M.E.H. Heffels, A.J. van Welsenens, V.H.J. de Beer, R.A. van Santen, J.A.R. van Veen, J. Phys. Chem. B 104 (2000) 8456–8461.
- [41] P. Raybaud, Appl. Catal. a-General 322 (2007) 76–91.
- [42] C. Dujardin, M.A. Lélías, J. van Gestel, A. Travert, J.C. Duchet, F. Maugé, Appl. Catal. A Gen. 322 (2007) 46–57.

- [43] L. Oliviero, L. Mariey, M.A. Lelias, S. Aiello, J. van Gestel, F. Mauge, *Catal. Letters* 135 (2010) 62–67.
- [44] J. Chen, E. Dominguez Garcia, E. Oliviero, L. Oliviero, F. Maugé, *J. Catal.* 339 (2016) 153–162.
- [45] S. Kasztelan, H. Toulhoat, J. Grimblot, J.P. Bonnelle, *Appl. Catal.* 13 (1984) 127–159.
- [46] T. Kim, T. Ninh, T. Kim, T. Ninh, (2013).
- [47] J. Kibsgaard, B.S. Clausen, H. Topsoe, E. Laegsgaard, J. V Lauritsen, F. Besenbacher, *J. Catal.* 263 (2009) 98–103.
- [48] J. Kibsgaard, B.S. Clausen, H. Topsøe, E. Lægsgaard, J. V. Lauritsen, F. Besenbacher, *J. Catal.* 263 (2009) 98–103.
- [49] B. Hinnemann, J.K. Norskov, H. Topsoe, *J. Phys. Chem. B* 109 (2005) 2245–2253.
- [50] E.C. Decanio, D.A. Storm, *J. Catal.* 132 (1991) 375–387.
- [51] K.I. Hadjiivanov, G.N. Vayssilov, *Adv. Catal.* 47 (2002) 307–511.
- [52] M.A. Lelias, E. Le Guludec, L. Mariey, J. van Gestel, A. Travert, L. Oliviero, F. Mauge, *Catal. Today* 150 (2010) 179–185.
- [53] M.A. Lelias, P.J. Kooyman, L. Mariey, L. Oliviero, A. Travert, J. van Gestel, J.A.R. van Veen, F. Mauge, *J. Catal.* 267 (2009) 14–23.
- [54] J. Chen, *Effet de La Pression de Sulfuration et D’agent Chélatant Sur La Morphologie et La Réactivité Des Phases Sulfures*, 2014.
- [55] P.G. Moses, B. Hinnemann, H. Topsoe, J.K. Norskov, *J. Catal.* 260 (2008) 202–203.

Table of contents – IV Chapter

IV. CHAPTER.....	113
4.1. Introduction	114
4.2. Experimental	115
4.3. Results	117
4.3.1. Effect of the support on promoted site formation	117
4.3.1.1. Oxide catalysts study by Raman spectroscopy	117
4.3.1.2. Sulfide catalysts	121
4.3.1.2.1. Elemental analysis in sulfide catalysts	121
4.3.1.2.2. Catalytic activity	122
4.3.1.2.3. Active sites study by IR/CO	123
4.3.1.2.3.1 CO adsorption on promoted sulfide catalysts	123
4.3.1.2.3.2 2D Infrared Inversion Spectra (2D-IRIS) method application in (Co) Mo catalysts	127
4.3.1.2.4. Slab study by Transmission Electron Microscopy (TEM)	132
4.4. Discussion	133
4.4.1. Attribution of the components in the CO stretching range for promoted sites	134
4.4.2. Morphology effect on CoMoS site formation	139
4.4.3 The influence of CoMoS sites on the HDS activity	142
4.5. Conclusion.....	145
4.6. References	147

IV. CHAPTER

SUPPORT EFFECT ON PROMOTED CATALYSTS

Abstract: A series of CoMo sulfide catalysts supported on Al₂O₃, SiO₂ and TiO₂ was prepared by wetness impregnation method keeping constant Mo amount (3 atoms Mo/nm²) and adding Cobalt with a molar ratio of $\text{Co}/(\text{Mo}+\text{Co}) = 0.3$ to study the role of support in CoMoS sites formation. Co promotion in Mo-edge and S-edge is studied by CO adsorption followed by IR (IR/CO) spectroscopy; and a comparison with non-promoted catalyst was carried out. The inversion of adsorption isotherms obtained by IR spectroscopy, (2D IRIS) method, was performed on promoted and non-promoted catalysts to verify that $\nu(\text{CO})$ vibration contributions from 2000-2090 cm⁻¹ can be attributed to CO/CoMoS interactions only. Then it appears that indeed this region of the infrared spectra is free of the contribution coming from CO/S-edge of MoS₂ nanoparticles. Then, a promotion study can be carried out in order to show the impact of the slab morphology on the promotion degree of the edges. IR/CO method shows Co promotion in both sites (S-edge and Mo-edge) of MoS₂ slabs. Co promotion is favored on S-edge since a lower CoMoS site formation is detected in Mo/TiO₂ which presents a triangular morphology mostly formed by Mo-edge. Instead, good promotion degree was found in CoMo/SiO₂ due to the high S-edge/Mo-edge ratio recorded in MoS₂ particles in non-promoted catalyst.

Keywords: Hydrodesulfurization (HDS), support effect, Molybdenum disulfide (MoS₂), Slab morphology, Sulfidation, Infrared (IR) spectroscopy, CO adsorption, Mo edge dispersion.

4.1. Introduction

Conventional HDS catalyst is formed by a transition metal (Mo or W) sulfide promoted by another transition metal (Co or Ni) supported on metal oxide (normally alumina) [1]. Many studies over these catalysts were performed to understand the catalyst behavior in HDS reaction. Co introduction on Mo catalysts can lead to the formation of CoMoS sites, Co_8S_9 or Co located on the support surface [2]. CoMoS sites are the one involved in the catalytic activity and are formed by the Cobalt in decoration of the MoS_2 edges [3]. The literature record upon ten times higher activity for CoMoS sites than for non promoted MoS_2 edge sites, phenomenon named the promotion effect although the role of the promotion is still in debate. Thus, two different types of CoMoS sites are reported in the literature so called CoMoS type-I and CoMoS type-II. CoMoS type-II is twice more active than type-I. *Shimada et al.* attributed this difference in activity to the high stacking that present type-II compared with type-I, however *Topsoe et al.* assure that it is possible to obtain CoMoS type-II with mono stacking [4,5]. Therefore, the origin of CoMoS site types with different catalytic activity is still in debate. This explains the importance of understanding CoMoS site formation. In this purpose, different studies using DFT calculations or Scanning Tunneling Microscopy (STM) have been performed. *Lauritsen* and co-workers showed the Co promotion is favored on S-edge of MoS_2 nanoparticles [6]. On the other hand, *Kasztelan et al.* predicted that both sites (M-edge and S-edge) of MoS_2 nanoparticles could be promoted since both sites are energetically favorable for the Co decoration although S-edge sites present lower energy than M-edge sites [7–9]. Besides, the same techniques were used to detect the morphology of promoted slabs. STM showed a change of morphology after Co addition from triangular shape for MoS_2 nanoparticles to triangular truncated shape for Co promoted MoS_2 . The change of morphology was also predicted by DFT calculations: near to a perfect hexagon shape for Co promoted slab was proposed under conventional sulfidation condition. However, all these predictions are linked to model catalyst or calculation, and then in order to study the CoMoS site formation in a catalyst under real conditions, the catalyst characterization by CO adsorption at low temperature following by FTIR spectroscopy (IR/CO) is proposed. This technique allows distinguishing non-promoted sites (MoS_2) and promoted sites (CoMoS). Recently, many studies from Chen and co-workers lead to an in depth study of non-promoted catalysts. However IR/CO technique presents one limitation for promoted catalysts since the stretching bands attributed to CO/S-edge for non-promoted catalysts appear in the same wavenumber range than the stretching bands characteristic of CO/CoMoS vibration. In order to solve this limitation, 2D Infrared Inversion Spectroscopy (2D-IRIS) is performed for non- and promoted catalysts. 2D-IRIS method consists on inverting the

adsorption integral equation describing the spectroscopic isotherm, which yields a 2D infrared spectrum (absorbance vs. Wavenumber and the logarithm of adsorption equilibrium constants ($\ln K$). The spectra of individual species are resolved in the later dimension, hence allowing the quantification of their Gibbs free adsorption energies. This 2D Infrared Inversion Spectroscopy (2D IRIS) method was developed by *Travert et al.* [10] to distinguish different adsorbed species with different affinities, i.e. different adsorption energies, by their spectroscopic isotherm (absorbance vs. pressure). It was performed to distinguish different carbonates species detected after CO₂ adsorption on ZrO₂ that present a strong overlapping in the 1800-1200 cm⁻¹ range impossible to separate by the conventional method. Thus, 2D-IRIS method is used in the present work to resolve the limitation by comparison of the adsorption energies between non- and promoted sites. After this study, CoMoS site formation was study by IR/CO method using different support and changing metals loading (Mo and Co). The change of support has a variation in the metal-support interaction that leads to the formation of MoS₂ nanoparticles with different morphology. The morphology is linked with S-/M-edge ratio and it is used as the origin point to perform the study about the prevalence of Co decoration by M- or S-edge.

4.2. Experimental

4.2.1. Catalysts preparation

CoMo catalysts were supported in different metal oxide keeping the same molybdenum density (3 atoms Mo per nm²) and the same Co/(Co + Mo) molar ratio equal to 0.3. Al₂O₃ (gamma alumina, 250 m²/g, Sasol), SiO₂ (506 m²/g, Merk) and TiO₂ (mixture of anatase and rutile phase, 59 m²/g, Degussa) were used as support. Heptamolybdate tetrahydrated salt (Alfa Aesar, 99%) and cobalt nitrate (Alfa Aesar, 98%) were used as molybdenum and cobalt precursors respectively. Both precursors were dissolved in an adjusted water volume and dispersed inside the pores of the support by a maturation step of 2 hours. Before impregnation, the supports were calcined and sieved with particle size between 0.2-0.5 μm. After impregnation, the catalysts were drying at 383 K (3 K/min) during 16 hours and then calcined at 723 K (3 K/min) during 5 hours.

4.2.2. Catalysts characterization

4.2.2.1 Elemental analysis by Inductively Coupled Plasma (ICP)

Oxide catalysts were sulfided ex-situ in a glass reactor connected with 10% H₂S/H₂ (30ml/min) flow. Catalysts were sulfided at 623 K with a rate of 3 K/min during 2 h. After, the temperature was

cooled down to 298 K under N₂ flow (30ml/min). Then the catalyst inside the reactor was introduced in a dry box under Ar flow, to avoid totally air contact. Then, inside the dry box, 50 mg of sample was taken to quantify molybdenum, cobalt and sulfur amount present in the catalysts by an Inductively Coupled Plasma Atomic Emission Spectrometer (ICP-AES) using a PerkinElmer Optima 330DV ICP instrument.

4.2.2.2 Raman spectroscopy

Raman spectroscopy was used to study the dispersion of molybdenum and cobalt oxidic species so all the measures were done on catalysts in oxide state. Raman spectroscopy was performed using a Jobin Yvon Labram 300 Raman spectrometer equipped with a confocal microscope, an Nd-YAG laser (frequency doubled, 532 nm) and a CCD detector. Spectra were recorded at room temperature in the region between 200 – 1000 cm⁻¹.

4.2.2.3 Transmission Electron Microscopy (TEM)

Transmission electron microscopy (TEM) was performed on a JEOL 2010 FEG operated at 200 kV. All cracked samples were sulfided at 623 K during 2 h at 3 K/min under 10% H₂S/H₂ flow. After sulfurization, the samples were transported into a dry box under argon flow. The suspensions in ethanol absolute for TEM analysis were prepared inside the box to avoid totally the air contact. TEM analyses were carried out using a few drops of the suspension on a copper grid. Slab length and stacking degree distributions of sulfide slabs were determined manually from at least 300 slabs. All TEM images were recorded at the same magnification and digitised using 2kx2k CCD camera. The measure was performed using Mesurim program.

4.2.2.4 Infrared spectroscopy

Infrared characterizations were performed in a low temperature cell adapted to adsorb carbon monoxide at liquid nitrogen temperature (100K). Firstly, oxide catalysts in wafer form were activated *in situ* at 623 K under 10% H₂S/H₂ flow during 2 hours with a rate of 3 K/min which is the conventional sulfidation procedure. After 2 hours under sulfidation condition, the catalyst was flushed with Ar during 10 minutes and left 1 h under vacuum at 623 K and finally it was cooled down to room temperature. Secondly, the catalyst under high vacuum (1.10⁻⁴ Pa) was cooled down to 100 K to perform CO adsorption.

CO adsorption was performed in two different ways: the conventional experiments were performed introducing small CO pressure by a calibrated volume up to sites saturation using a equilibrium pressure of 133 Pa, and isotherm experiments were carried out increasing equilibrium CO pressure up to sites saturation. All IR spectra were recorded with a Nicolet Magna 550 FT-IR

spectrometer equipped with a MCT detector. Every spectrum was normalized to a disc of 5 mg /cm² and duplicated (reproducibility error of 5%). Equilibrium/saturated spectra were decomposed using OMNIC program and pseudo-voigt function. Inversion of Infrared spectra was performed using Matlab program and a computational methodology developed by *Travert et al.*, which is described in more details in [11].

4.2.2.5 Catalytic activity: Thiophene test

Oxide catalysts were sieved between 0.2 and 0.5 μm before to start the experiment. Then, catalysts were sulfided in situ just before the reaction. Sulfidation procedure was performed at 623 K with a heating rate of 3 K/min, under a flow of 10% H₂S/H₂ (30ml/min) at atmospheric pressure during 2 h. After, thiophene reaction was carried out in a continuous reactor at 623 K and atmospheric pressure with a thiophene partial pressure of 8 kPa in a mixture of hydrogen (91.2 kPa) and H₂S (2.1 kPa). The outlet gas was analyzed by Varian 3900 gas chromatograph equipped with flame ionization (FID) detector. The reaction rate was calculated as $r_{\text{HDS}} = (F/m) \cdot X$, where F/m is the molar flow rate of thiophene per gram of catalyst and X is thiophene conversion which is below 5%. Thiophene reaction was running during 18 h to obtain a stable reaction rate. The mass after sulfurization was corrected by mass loss calculated from the infrared experiments.

4.3. Results

4.3.1. Effect of the support on promoted site formation

The complexity of the surface of Co promoted catalyst makes the study and understanding of the system quite difficult. For this reason, detailed study of the catalyst from the oxidic form to the sulfide form is required, as well as the comparison between mono- and bimetallic states.

4.3.1.1. Oxide catalysts study by Raman spectroscopy

Oxidic molybdenum can be present in different forms: crystalline MoO₃ species which is not appropriate to form MoS₂ nanoparticles and polymolybdate anions as Mo₇O₂₄²⁻, Mo₂O₇²⁻, Mo₆O₁₉²⁻. However, in the case of Co promoted catalysts in oxide form several compounds containing molybdenum and/or cobalt can exist on the support surface. Thus, the literature reports several compounds on CoMo/Al₂O₃ catalyst surface such as CoMoO₄, Co₃O₄, MoO_x, CoAl₂O₄, and Al₂(MoO₄)₃. For this reason, Raman spectroscopy was performed on promoted catalysts in oxidic form to identify the species presented on their surface and compared them with the ones on Mo

catalyst surface. Since the metal-support interaction is supposed to play a role in the formation of different oxidic species, different supports, Al_2O_3 , SiO_2 and TiO_2 were used.

Figure IV.1 shows Raman spectra for (Co)Mo/ Al_2O_3 catalysts in oxidic form where Raman spectrum for CoMo catalyst is represented by full line and the one for Mo catalyst by dotted line. Some differences are detected between both Raman spectra due to Co addition. Non-promoted catalyst shows two principal bands attributed to Mo-O vibration modes characteristic of polymolybdate species at 220, 360, 856 and 955 cm^{-1} where the two last bands are the more characteristics one and correspond to bridge vibration modes and terminal vibration modes, respectively. The main band ascribed to terminal Mo-O vibration mode between 900 and 1000 cm^{-1} , is widening for promoted catalyst due to the presence of a band at 937 cm^{-1} . This band can be attributed to the Cobalt incorporation on the surface and it is ascribed to CoMoO_4 species [12]. However, the band at 958 cm^{-1} ascribed to polymolybdate species is also detected that indicates the presence of mixture of cobalt and molybdenum oxide and oxomolybdate species. Finally an intense band is detected at 150 cm^{-1} for promoted catalyst; since the region at lower wavenumber is characteristic of metal-support interaction and it just appears after Co addition, this band can be ascribed to Cobalt in interaction with alumina surface. Cobalt in interaction with Al_2O_3 surface form a species denoted as CoAl_2O_4 and this spinel is characteristic to give several mode vibration bands at 196, 411, 483, 523, 620, 690, and 756 cm^{-1} [13,14]. Therefore the small bands detected at 515, and 637 cm^{-1} can be ascribed to this specie.

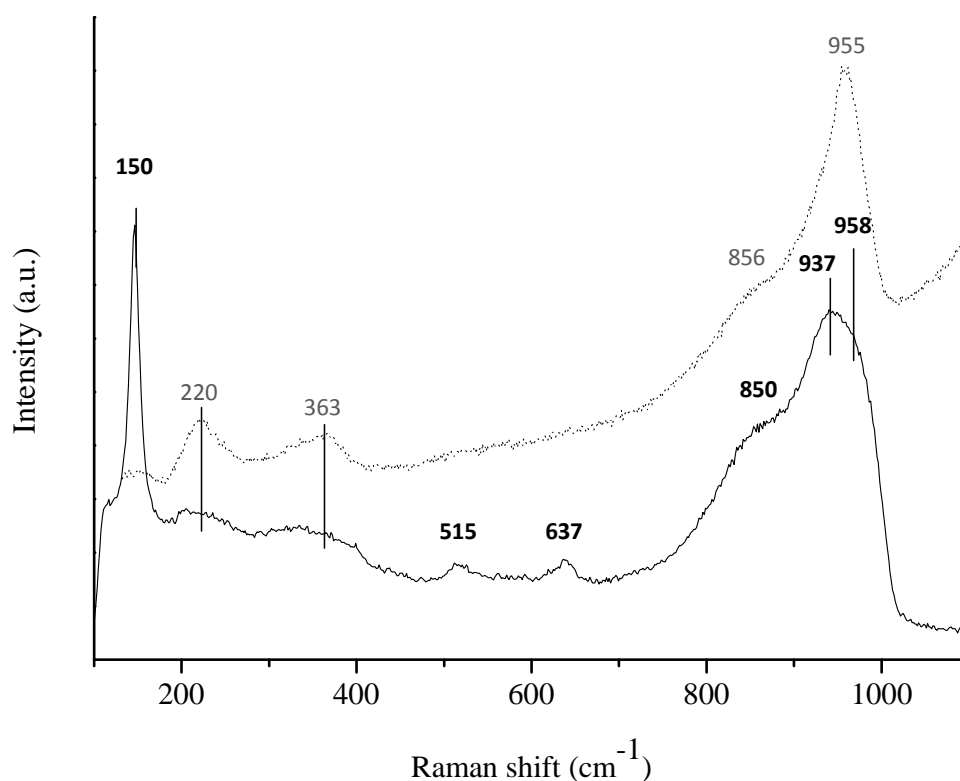


Figure IV.1. Raman spectra comparison for Mo (dotted line) and CoMo (full line) catalysts in oxidic form supported on Al_2O_3

Raman spectra of Mo and CoMo catalysts in oxidic form supported on SiO_2 are shown in Figure IV.2 where Raman spectrum for Mo catalyst is represented by dotted line and CoMo catalyst by full line. Raman spectrum of non-promoted catalyst shows several bands at the wavenumber range characteristic of Mo-O vibration modes. Two intense bands at 820 and 995 cm^{-1} are detected and are ascribed to MoO_3 species. Furthermore, two bands at 866 and 955 cm^{-1} ascribed to polymolybdate species can be detected. Thus, two different species are presented on Mo/ SiO_2 surface, MoO_3 and polymolybdate species. However, some changes are recorded for CoMo/ SiO_2 by Co addition as the appearance of one intense band at 939 cm^{-1} that is attributed to CoMoO_4 species and a band at 700 cm^{-1} , which can be attributed to Cobalt oxide deposited on the surface as Co_3O_4 [12]. On the other hand, some band characteristics of polymolybdate species detected already on non-promoted catalyst is still detected for promoted catalyst. Principally a decrease of MoO_3 species is detected on promoted catalyst surface compared with non-promoted catalyst. In conclusion, CoMo / SiO_2 catalyst surface is formed by polymolybdate species, MoO_3 , Co_3O_4 , and CoMoO_4 .

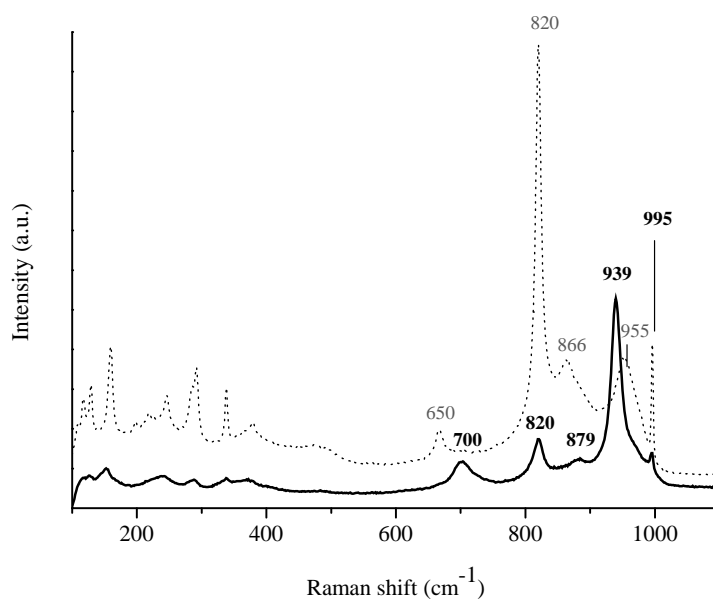


Figure IV.2. Raman spectra comparison for Mo (dotted line) and CoMo (full line) catalysts in oxidic form supported on SiO_2

Raman spectra of Mo and CoMo oxidic catalysts supported on TiO_2 are shown in Figure IV.3. Non-promoted catalyst is represented by dotted line and promoted catalyst by full line. The vibration modes characteristics of anatase and rutile structures are detected in both Raman spectra at low wavenumber range. Anatase phase present Raman vibration mode at 147, 200, 324, 396, 517, 638 and 798 cm^{-1} , and rutile phase at 244, and 446 cm^{-1} [15]. Raman spectrum of non-promoted catalyst shows two principal bands characteristic of Mo-O vibration modes at 874 cm^{-1} and 965 cm^{-1} , which are ascribed to polymolybdate species. However, Raman spectrum of CoMo catalyst shows the main vibration band at 951 cm^{-1} , which is attributed to CoMoO_4 species. Besides, other two vibration bands are detected at 846 cm^{-1} and 965 cm^{-1} that are ascribed to polymolybdate species. The specific metal- TiO_2 surface interaction leads to observe a band shift of 10 cm^{-1} to higher wavenumber for all Mo-O vibration bands compared with other two catalysts [16]. Thus, CoMo/ TiO_2 catalyst is composed by CoMoO_4 and polymolybdate species.

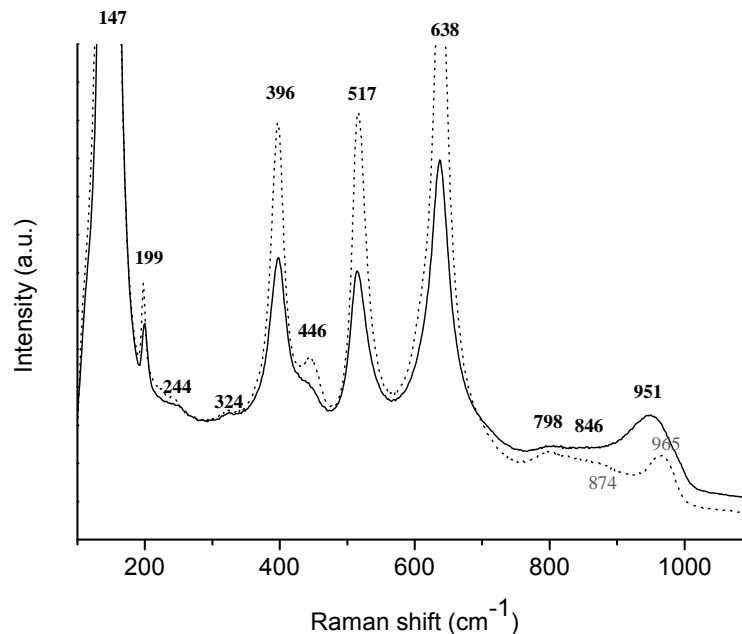


Figure IV.3. Raman spectra comparison of Mo (dotted line) and CoMo (full line) oxidic catalysts supported on TiO₂

4.3.1.2. Sulfide catalysts

4.3.1.2.1. Elemental analysis in sulfide catalysts

Surface area analysis was carried out for promoted catalysts. Since the cobalt amount introduced is not so high, any change in the surface area can be expected in comparison with non-promoted catalysts. Table IV-1 summarizes the surface area of the support, monometallic and bimetallic catalysts. In general, the surface area does not present any change after the Co addition. However, some variation in surface area can be detected in comparison with the support. CoMo/Al₂O₃ and CoMo/TiO₂ do not present any significantly surface area variation, controversially CoMo/SiO₂ catalyst loss 2/5 of the surface area presented by the support before the impregnation.

Elemental analysis was carried out on promoted sulfide catalysts by ICP analysis. The cobalt, molybdenum and sulfur wt% obtained by ICP analyses (experimental values) are summarized in Table IV-1 as well as the metal wt% introduced during the preparation (theoretical value, wt% Mo and wt% Co for the support + metals). These theoretical and experimental values are different because of the mass modification associated with the calcination and sulfidation steps. Finally, the sulfur amount presents on the catalyst after sulfidation stage was also measured by ICP analysis. Thus, CoMo /TiO₂ catalyst presents the highest sulfur/metal ratio due to the support sulfidation; it is followed by CoMo /Al₂O₃ and finally by CoMo /SiO₂ catalysts.

Table IV-1. Summary of surface properties and elemental analysis for promoted catalysts

Catalyst	Surface area support (m ² /g)	Surface area CoMo catalyst (m ² /g)	Surface area Mo catalyst (m ² /g)	%wt Mo ^a	%wt Mo ^b	%wt Co ^a	%wt Co ^b	S/Mo+Co
CoMo/Al ₂ O ₃	250	235	232	10	8	2	2	2.1
CoMo/SiO ₂	506	307	305	19	16	4	3.0	1.7
CoMo/TiO ₂	59	58	58	3	2	1	0.4	2.8

Note: (a) Catalyst preparation, and (b) ICP analysis

4.3.1.2.2. Catalytic activity

The catalytic activity for promoted catalysts was studied using Thiophene as model molecule to study the support effect in HDS reaction. Thiophene HDS rate per gram and per surface area for CoMo catalysts are presented in Figure IV.4.a and Figure IV.4.b respectively. In both cases, CoMo/Al₂O₃ catalyst presents the highest catalytic activity. However, CoMo/SiO₂ catalyst presents higher HDS rate than CoMo/TiO₂ if the HDS rate is represented per gram of catalyst, while CoMo/TiO₂ catalyst presents higher HDS rate than CoMo/SiO₂ catalyst when HDS rate is expressed per surface area.

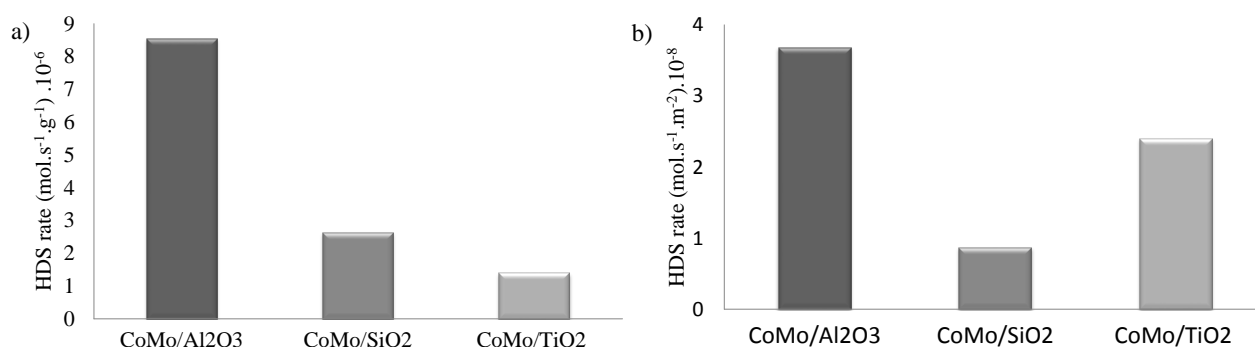


Figure IV.4. Thiophene reaction rates per gram (A) and per surface area (B) on promoted catalysts

It is well known that thiophene is not an optimum molecule to study the selectivity of HDS catalysts. However, some differences between the product distributions were found as shows Figure IV.5. In particular, it appears that CoMo/TiO₂ favors the HYD pathway as was shown for Mo/TiO₂

catalyst since the percentage of THT formed is significantly higher for this catalyst as compared to CoMo/Al₂O₃.

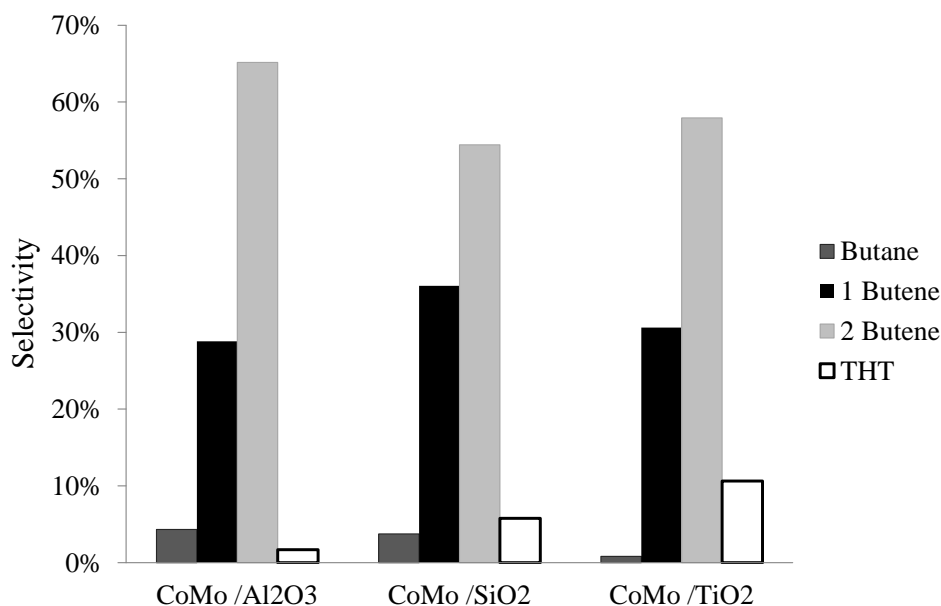


Figure IV.5. Percentage of different products converted in thiophene HDS reaction for CoMo catalysts supported on Al₂O₃, SiO₂ and TiO₂

4.3.1.2.3. Active sites study by IR/CO

The development of IR/CO method allows a great study of sulfide catalysts as was shown previously. It gives specific information about the species nature present on the catalyst surface which is directly involved in the catalytic reaction. CO adsorption at low temperature after sulfurization was carried out on CoMo sulfide catalysts supported on Al₂O₃, SiO₂ and TiO₂ in order to study the support effect on CoMoS phase formation.

4.3.1.2.3.1 CO adsorption on promoted sulfide catalysts

CO adsorption at low temperature followed by FTIR spectroscopy (IR/CO) was performed for sulfide CoMo catalysts supported on Al₂O₃, SiO₂ and TiO₂. IR/CO spectra from small CO pressures up to saturation using equilibrium pressure (133 Pa) for sulfide CoMo/Al₂O₃ catalyst are shown in Figure IV.6. IR spectra present two different CO adsorption domains: adsorption on the support surface and adsorption on the sulfide sites. Al₂O₃ surface is formed by Lewis acid sites and Brønsted sites. Accordingly, CO bands are detected at 2157 and 2186 cm⁻¹ and ascribed to hydroxyl group and Lewis acid sites, respectively. The CO vibration band at 2140 cm⁻¹ is ascribed to physisorbed CO. Because of the presence of Co, the promoted catalyst surface is more complex than the one of non-promoted catalysts. Indeed, the promoted catalyst surface can present CoMoS

sites that are the active sites but also Co_8S_9 phase that is reported non active. The distinction by IR/CO between these two species is not straightforward. Indeed, the stretching vibration of CO in interaction with CoMoS sites is reported to lead to overlapping bands with the maximum around 2070 cm^{-1} while for CO in interaction with Co_8S_9 the band is reported at 2065 cm^{-1} [17]. Therefore, the $\nu(\text{CO})$ adsorption range for promoted sites is established between 2020 and 2090 cm^{-1} as is shown in Figure IV.6.b without a priori exclusion of the contribution of Co_9S_8 . For $\nu(\text{CO})$ of CO/non-promoted sites the range is as previously described in chapter III between 2090 and 2120 cm^{-1} with the maximum around 2110 cm^{-1} [17–20]. So, CO adsorption spectra for CoMo/ Al_2O_3 catalyst present a CO band ascribed to its interaction with Mo non-promoted sites at 2115 cm^{-1} , and several components in the range ascribed to CO on promoted sites as shows the second derivate in Figure IV.6.a. Three principal components are then detected at 2057 , 2074 and 2085 cm^{-1} . Since no contribution at 2065 cm^{-1} is revealed; it can be concluded that Co_9S_8 is not formed on CoMo/ Al_2O_3 .

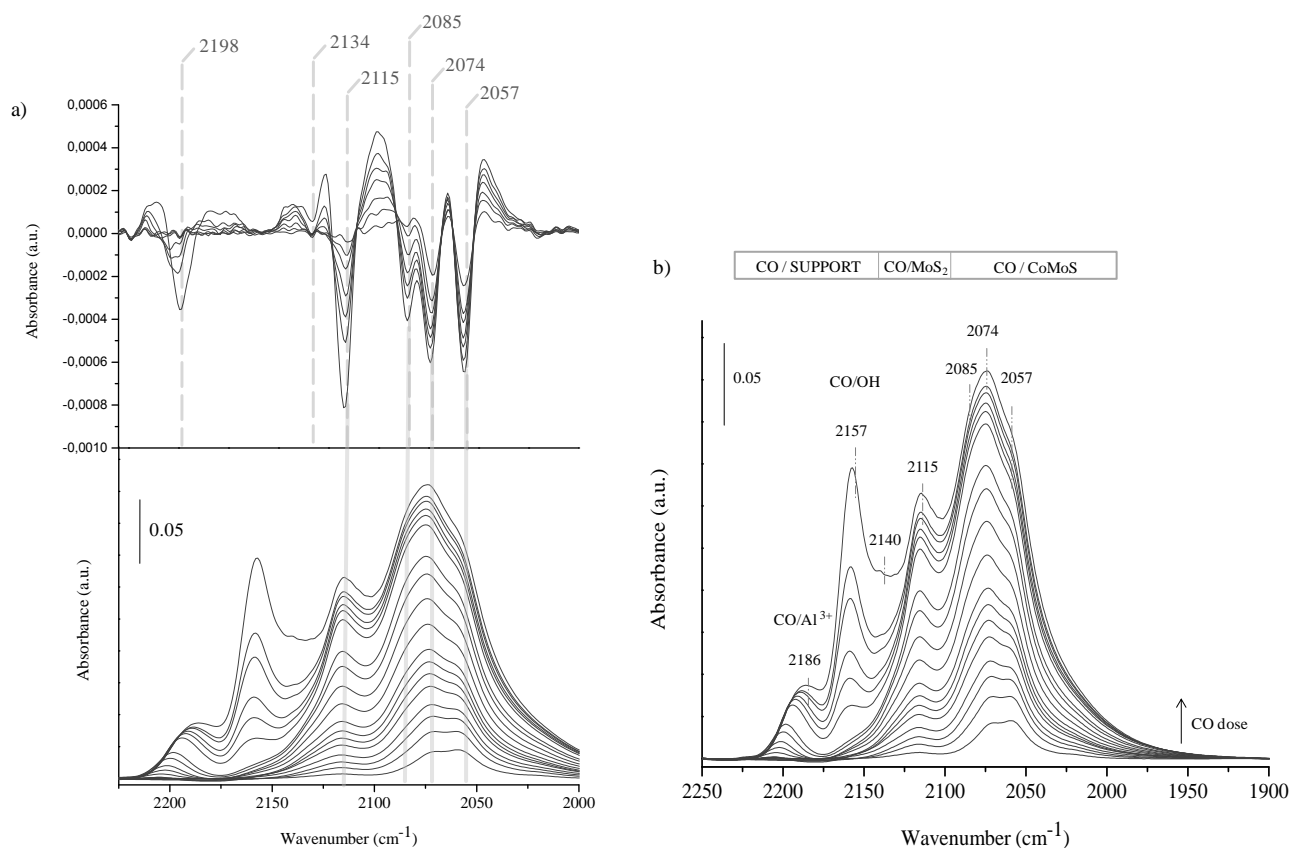


Figure IV.6. IR spectra of CO adsorption from small CO doses up to saturation at equilibrium pressure (133Pa) for sulfide CoMo/ Al_2O_3 and second derivate of small CO doses (top a)

CO adsorption at low temperature followed by FTIR spectroscopy was performed for sulfided CoMo/ SiO_2 catalyst from small CO pressures up to saturation using CO equilibrium

pressure at 133 Pa. The spectra are shown in Figure IV.7.b. The distortion band coming from structure silica vibration was detected at 1888 cm^{-1} as was reported for Mo/SiO_2 . Since silica surface is formed just by hydroxyl group, the stretching band characteristic of CO interaction with hydroxyl group is detected at 2156 cm^{-1} , and physisorbed CO at 2136 cm^{-1} . On the other hand, CO interacts with the sulfide phase giving rise to several stretching bands: νCO band characteristic of non-promoted sites at 2113 cm^{-1} , and the overlapping bands ascribed to promoted sites detected in the $2020 - 2090\text{ cm}^{-1}$ range. The components that form the overlapping bands are detected by the second derivate of the first doses as shows Figure IV.7.a. The same three components are detected for CoMo/SiO_2 than for $\text{CoMo/Al}_2\text{O}_3$ catalysts: $2060, 2073, \text{ and } 2083\text{ cm}^{-1}$. These three components can be ascribed to Cobalt on CoMoS sites with different environments; the precise attribution will be studied more in details in the discussion part. Finally, a new component is detected for CoMo/SiO_2 catalyst at 2065 cm^{-1} ascribed to Co_8S_9 formation in accordance with the poor dispersion of the metal on silica surface as shown by Raman study. This $\nu(\text{CO})$ band was detected already for $\text{Co/Al}_2\text{O}_3$ catalyst and $\text{CoMo/Al}_2\text{O}_3$ catalyst that presents a cobalt excess [17].

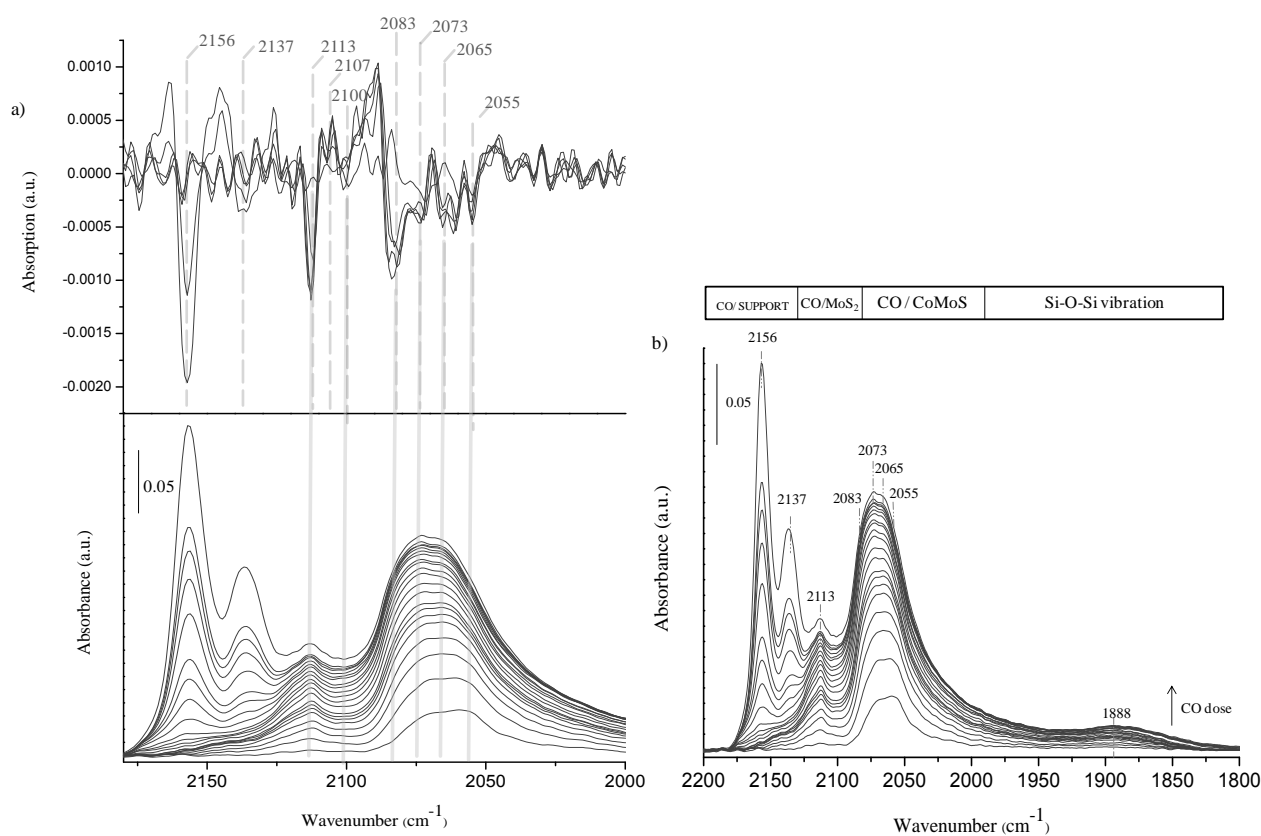


Figure IV.7. IR spectra of CO adsorption from small CO doses up to saturation at equilibrium pressure (133Pa) for CoMo/SiO_2 catalyst and second derivate of small CO doses

Finally, CO adsorption at low temperature followed by FTIR spectroscopy was performed on sulfided CoMo/TiO₂ catalyst from small CO doses up to saturation as is shown in Figure IV.8.b. A decrease of the spectra intensity was detected for this catalyst compared to previous ones in accordance with its lower surface area. CO interacts with Titania surface which is formed by Lewis acid sites and Brønsted sites. According to this interaction, $\nu(\text{CO})$ bands are detected at 2162, 2140 and 2183 cm⁻¹ and can be ascribed to CO in interaction with hydroxyl groups perturbed by SH species coming from the sulfurization process, physisorbed CO and Lewis acid sites, respectively. Moreover, CO spectra also show other CO adsorption domain corresponding to the interaction with active sites. Indeed, a $\nu(\text{CO})$ band is detected at 2116 cm⁻¹ ascribed to CO on non-promoted sites; as well as overlapping bands between 2020 and 2090 cm⁻¹ that are attributed to CO on promoted sites. The components that form the overlapping bands are detected using the second derivative as shows Figure IV.8.a. However, second derivative functions show a lot of noise and it is difficult to establish clearly the components, although still some components can be detected at 2057, 2065, 2074 and 2085 cm⁻¹.

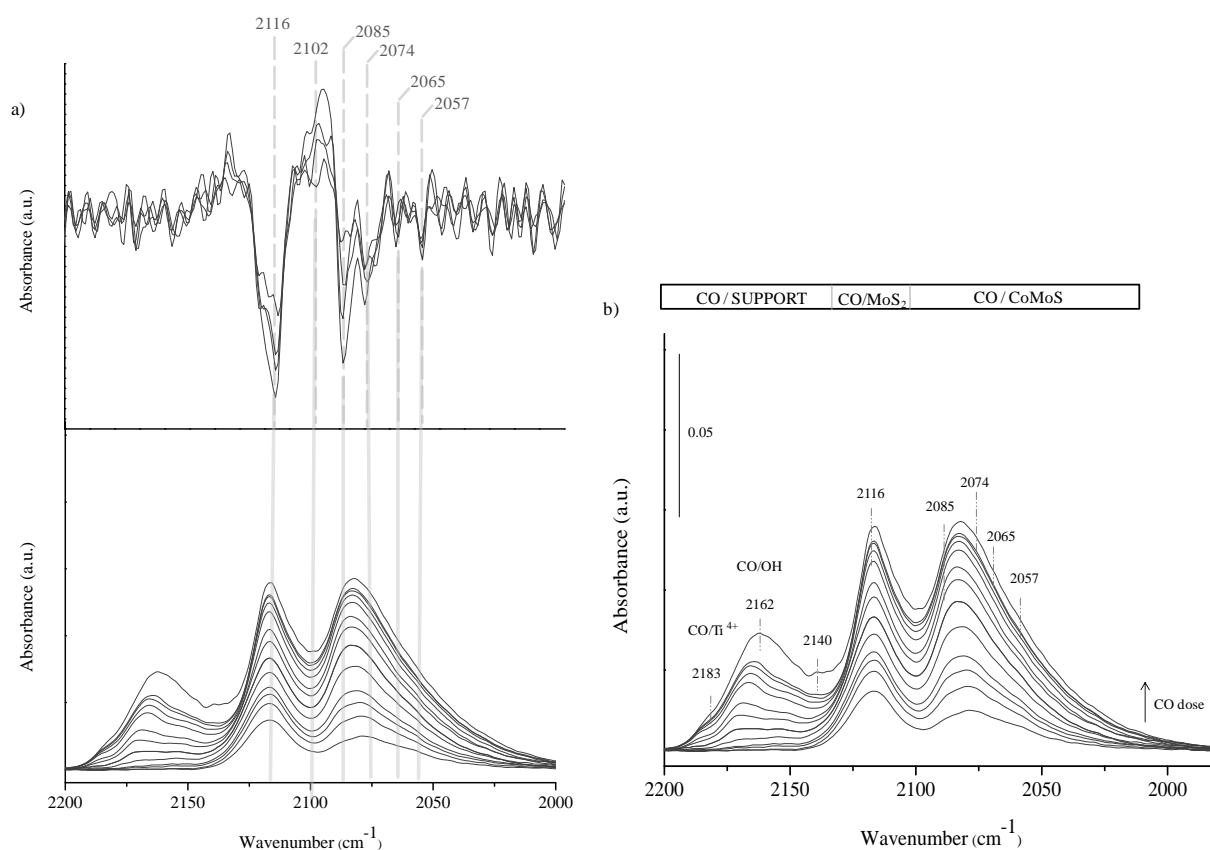


Figure IV.8. . IR spectra of CO adsorption from small CO pressures up to saturation at equilibrium pressure (133Pa) for CoMo /TiO₂ catalyst and second derivative of small CO pressure

Spectra decomposition of CO saturated spectra was carried out for promoted catalysts taking into account the components determined by the second derivative function. The decomposition was performed using OMNIC program and using pseudo-voigt function. Quantification of sites was performed distinguishing non- and promoted sites. Different molar extinction coefficients were used to carry out the calculation: $16 \pm 4 \text{ cm} \cdot \mu\text{mol}^{-1}$ for non promoted sites and $43 \pm 14 \text{ cm} \cdot \mu\text{mol}^{-1}$ for promoted sites. Both values were taken from the calculations performed by Maugé et al [17]. The quantification of all components is summarized in Table IV-2. Two components are used for non promoted sites at 2098 and 2110 cm^{-1} as is reported in the literature; and several components for promoted sites at 2083, 2073, 2065, 2057, 2038 and 2020 cm^{-1} .

Table IV-2. Sites quantification for promoted catalysts supported on Al_2O_3 , SiO_2 and TiO_2

Wavenumber (cm^{-1})	Promoted sites				Non-promoted sites		Total non-promoted sites	Total promoted sites *	Total sites
	2057	2065	2073	2083	2099	2110			
Catalysts	$\mu\text{mol edge sites} / \text{g}_{\text{catalyst}}$ detected by IR/CO								
CoMo/ Al_2O_3	17	-	19	13	28	33	61	62	123
CoMo/ SiO_2	11	5	6	11	14	12	26	38	64
CoMo/ TiO_2	3	1	2	7	9	14	23	14	37

* Total promoted sites without the contribution of Co_9S_8

4.3.1.2.3.2 2D Infrared Inversion Spectra (2D-IRIS) method application in (Co) Mo catalysts

CO adsorption at low temperature followed by FTIR spectroscopy (IR/CO) is a powerful characterization method for (Co)Mo sulfide catalysts surface. This technique has been developed satisfactorily for non-promoted catalysts leading to the distinction of Mo on M- and S-edge sites. However, the characterization of promoted catalysts by IR/CO method presents a limitation. Indeed, the νCO bands are detected in the same wavenumber range for CO on promoted sites and on Mo on non-promoted S-edge sites [18,21,22]. Two examples of this limitation are shown in Figure IV.9. Figure IV.9.a shows the comparison of IR spectra of CO adsorption at equilibrium pressure for Mo/ Al_2O_3 and CoMo/ Al_2O_3 catalysts. CO/S-edges stretching band shows a maximum at 2070 cm^{-1} , while the overlapping stretching bands of CO/CoMoS show a maximum at 2073 cm^{-1} . The same case is presented for (Co)Mo/ SiO_2 catalyst as shows Figure IV.9.b. Close wavenumber is recorded for CO/S-edge stretching band detected at 2065 cm^{-1} and CO/CoMoS stretching band with a maximum at 2073 cm^{-1} . Thus, this limitation can be extrapolated to all catalysts that are formed by MoS_2 nanoparticles with S-edge sites. Accordingly, since Mo/ TiO_2 catalyst is constituted by MoS_2

nanoparticles mostly formed by M-edge sites (97% of Mo-edge versus 3% of S-edge), CoMo/TiO₂ catalyst does not present the limitation as the two previous promoted catalysts as shows Figure IV.10. Except for this specific case, the described limitation is presented as a barrier for the catalyst study and for that reason this limitation has to be resolved for the continuous development of the characterization of Co promoted sulfide catalysts by IR/CO method.

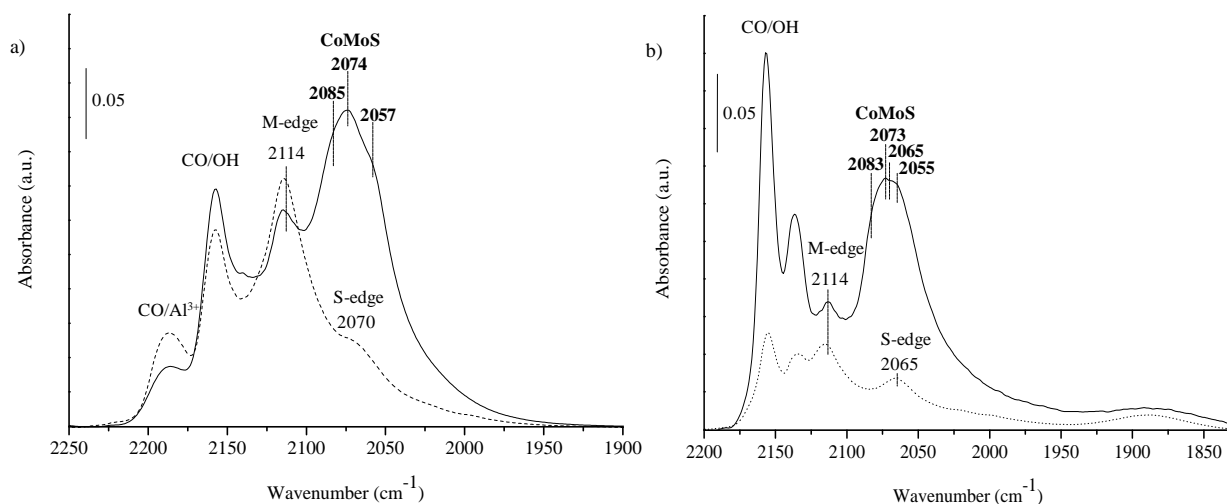


Figure IV.9. IR spectra of CO at equilibrium pressure for Mo (dotted line) and CoMo (full line) sulfide catalysts supported on Al₂O₃ (a) or SiO₂ (b)

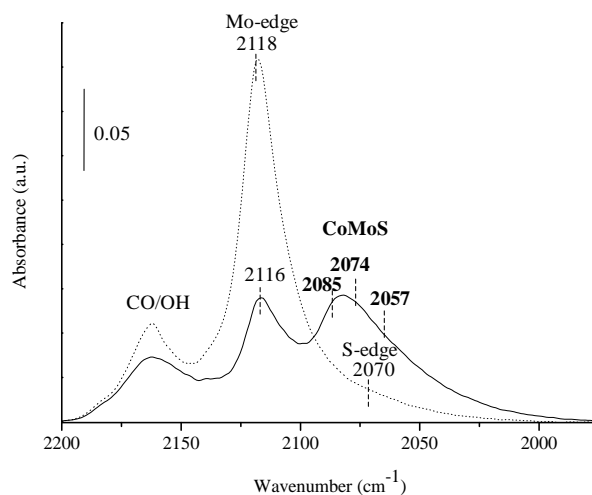


Figure IV.10. IR spectra of CO adsorption at equilibrium pressure for Mo (dotted line) and CoMo (full line) catalysts supported on TiO₂

2D IRIS method was performed for non- and promoted catalysts in order to try to solve the IR/CO limitation for promoted catalyst characterization. For that, CO adsorption at low temperature

(100K) with different CO equilibrium pressures were performed on non- and promoted catalysts. Figure IV.11 shows the IR isotherm for the CoMo/Al₂O₃ catalyst i.e. the total area of CO bands versus the equilibrium CO pressures. The plateau is recorded at 133 Pa, so this pressure can be taken as the pressure for which all sites are saturated by CO. This procedure was used for all the catalysts, and for all of them at 133 Pa of equilibrium pressure the plateau was reached.

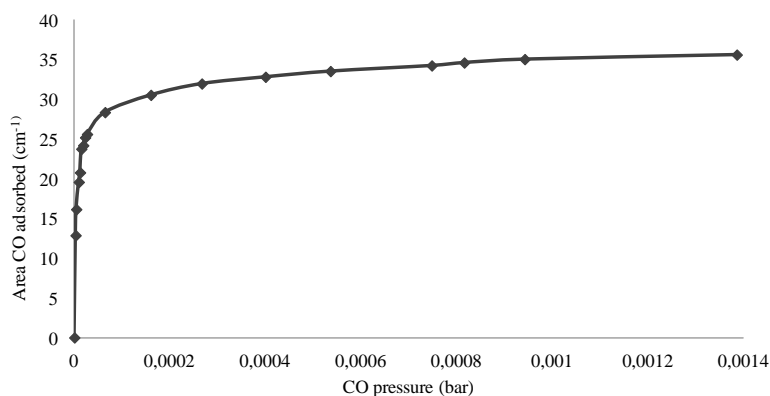


Figure IV.11. CO adsorption isotherm (T=100K) on CoMo /Al₂O₃ catalyst

2D IRIS for Mo/Al₂O₃ and CoMo/Al₂O₃ catalysts are shown in Figure IV.12. Inverse spectroscopy isotherm of Mo/Al₂O₃ highlights the presence of different sites of CO interaction with different Gibbs free energy of adsorption ($\Delta_{\text{ads}}G$). The comparison with IR spectra allows the attribution to different CO interaction sites. These sites correspond to OH group, Al³⁺ cation, M-edge sites and S-edge sites. The interaction with support sites correspond to the highest $\Delta_{\text{ads}}G$ while CO interaction with active sites presents the lowest $\Delta_{\text{ads}}G$. Similar $\Delta_{\text{ads}}G$ are detected for M-edge and S-edge although, S-edge shows slightly higher $\Delta_{\text{ads}}G$ than M-edge. The same behavior was observed for the CoMo/Al₂O₃ catalyst. Different CO interaction sites are detected with different $\Delta_{\text{ads}}G$. CO interactions with support sites present the highest $\Delta_{\text{ads}}G$, and active edge sites present the lowest $\Delta_{\text{ads}}G$. However, comparison of the $\Delta_{\text{ads}}G$ obtained on the non- and promoted sites allows distinguishing them as show Figure IV.12.b. Indeed: free Gibbs energy of adsorption is higher for non-promoted sites (Mo catalyst and M-edge of CoMo catalyst, the corresponding position in the 2D IRIS diagram is marked by a black star) than for promoted sites. Then, it appears that the presence of non promoted S-edge site contribution in the CO/CoMoS band can be discarded (the corresponding position in the 2D IRIS diagram is marked by a red cross). Finally, it has to be pointed out that the Gibbs free energy of adsorption increases for non-promoted sites (M-edge) on CoMo catalyst in comparison with the ones on Mo catalyst. Thus, it appears that totally non promoted MoS₂ nanoparticles do not exist on CoMo catalyst. Instead, it can be proposed that the

increase of $\Delta_{\text{ads}}G$ is due to the influence of Cobalt in the further neighborhood of the adsorbing non-promoted sites.

Being now focus in promoted site differentiation; small differences in free Gibbs energy of adsorption are detected between the components identified previously according to the second derivative spectra. The component at 2057 cm^{-1} shows the lowest adsorption free Gibbs energy, following by 2073 cm^{-1} , and finally by 2085 cm^{-1} . These small differences in energies can be an indication about the adsorbing site environment and it will be discussed later on.

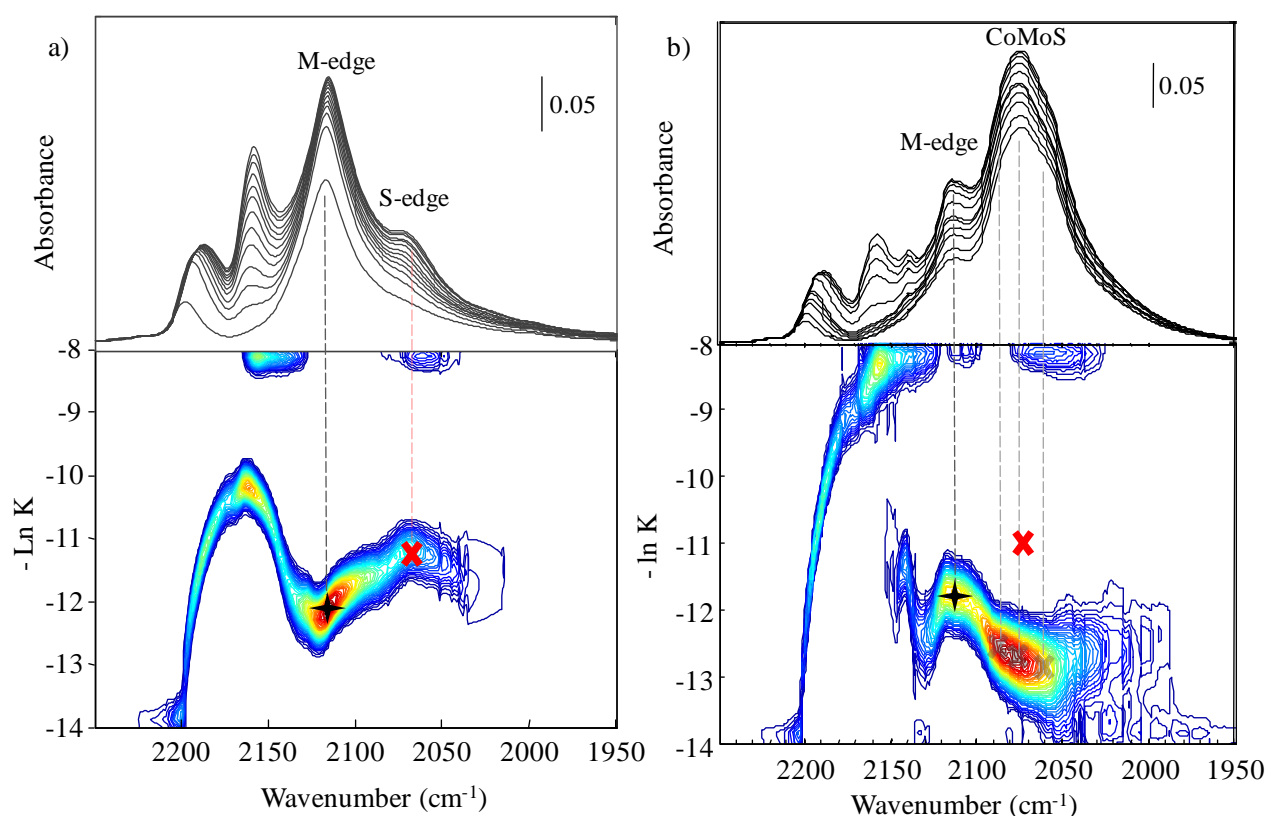


Figure IV.12. 2D-IRIS results for MoS_2 (a) and CoMoS (b) supported on Al_2O_3

From these results, it appears that for $\text{CoMo}/\text{Al}_2\text{O}_3$, the S-edge is totally promoted but what about catalyst presenting higher proportion of S-edge? In order to solve this question, 2D IRIS method was also performed on such catalysts. For that, Mo/SiO_2 and CoMo/SiO_2 catalysts were selected to carry out the study. Figure IV.13 shows the 2D IRIS obtained for non- and promoted catalysts supported on SiO_2 . Similar results than for alumina catalysts were detected for silica catalysts with similar range of Gibbs free energies of adsorption. Different CO interaction sites are detected with different Gibbs free energies of adsorption. CO interactions with the support sites present the highest $\Delta_{\text{ads}}G$, and active sites present the lowest $\Delta_{\text{ads}}G$. Similar Gibbs free energy are obtained for CO adsorption on hydroxyl groups and for physisorbed CO. M- and S-edge sites on

Mo/SiO₂ can be distinguished by both the position of the associated $\nu(\text{CO})$ band and the value of $\Delta_{\text{ads}}G$. Indeed, M-edge presents a slightly smaller adsorption Gibbs free energy than S-edge as shows Figure IV.13.a. This result is in accordance with the one obtained on Mo/Al₂O₃. Then, IRIS results for CoMo/SiO₂ are presented in Figure IV.13.b. Three different CO interaction regions with different Gibbs free energies of adsorption can be detected for CoMo/SiO₂ catalyst. The position of the $\nu(\text{CO})$ band on the IR spectra as well as the value of $\Delta_{\text{ads}}G$ allows attributing the different CO interaction sites to non-promoted sites, promoted sites, and cobalt sulfide species. CO/Cobalt sulfide species are ascribed to the band at 2065 cm⁻¹ as it is detected by the second derivative method. This contribution corresponds to the lowest adsorption Gibbs free energy. Then, CO on non-promoted M-edge sites is ascribed to the band at 2110 cm⁻¹ with a slightly higher $\Delta_{\text{ads}}G$ than in the case on non promoted catalyst. This increase of $\Delta_{\text{ads}}G$ was also detected for CoMo/Al₂O₃ catalyst and was considered as an indication of non-promoted sites formed on the same slab than CoMoS sites at the exclusion of MoS₂ nanoparticles without any cobalt decoration. Taking into account the position as well as the $\Delta_{\text{ads}}G$ range for non-promoted S-edge on Mo/SiO₂, it appears that there is no presence of Mo located in S-edge free of Co promotion for promoted catalysts.

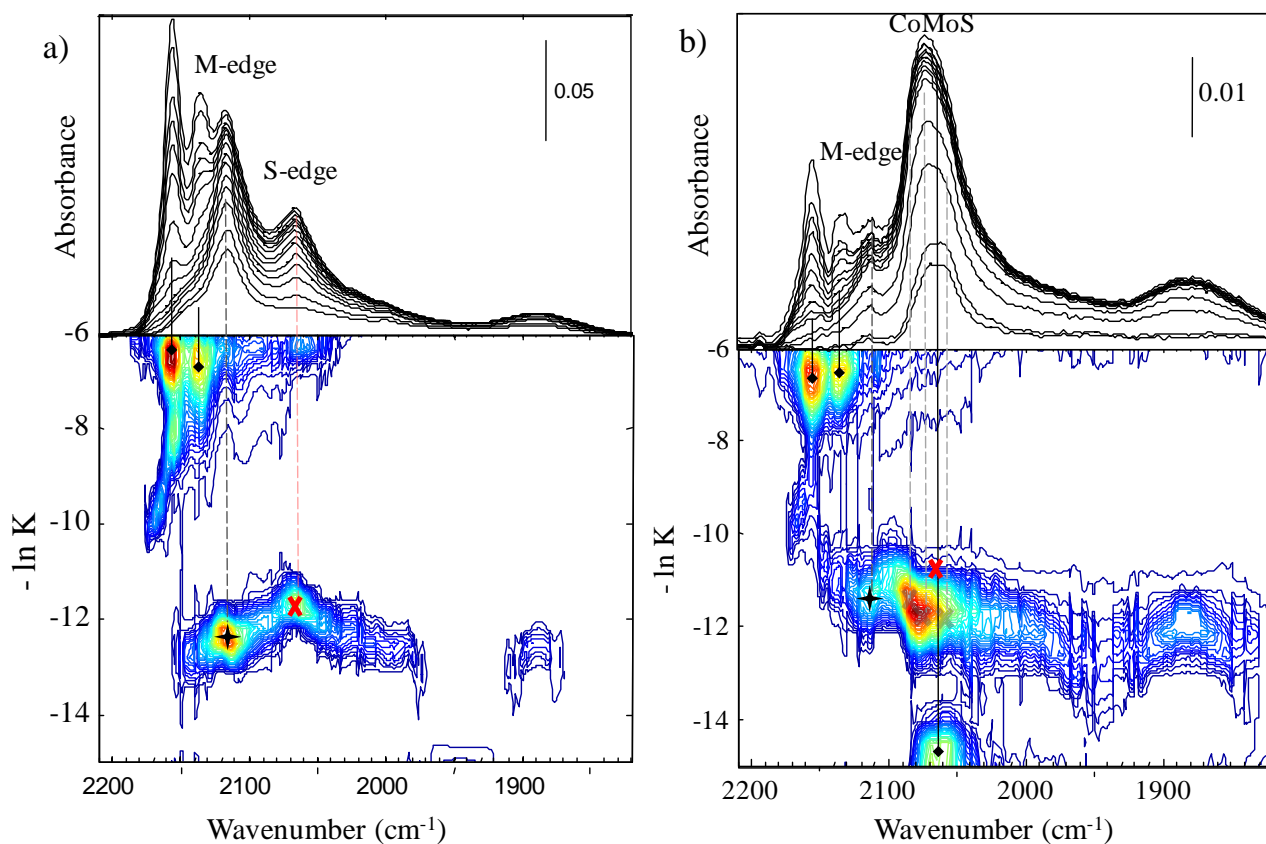


Figure IV.13. 2D-IRIS result of MoS₂ (a) and CoMoS (b) supported on SiO₂

4.3.1.2.4. Slab study by Transmission Electron Microscopy (TEM)

Transmission electron microscopy was used to determine the slab length and stacking number for promoted catalysts. A minimum of 60 images were taken for each sample to be sure about the validity of the measure.

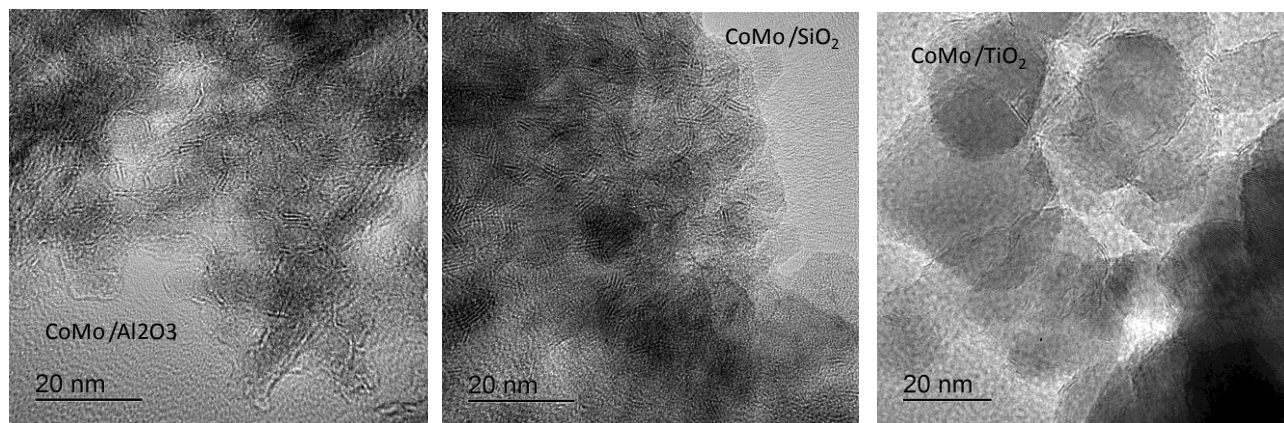
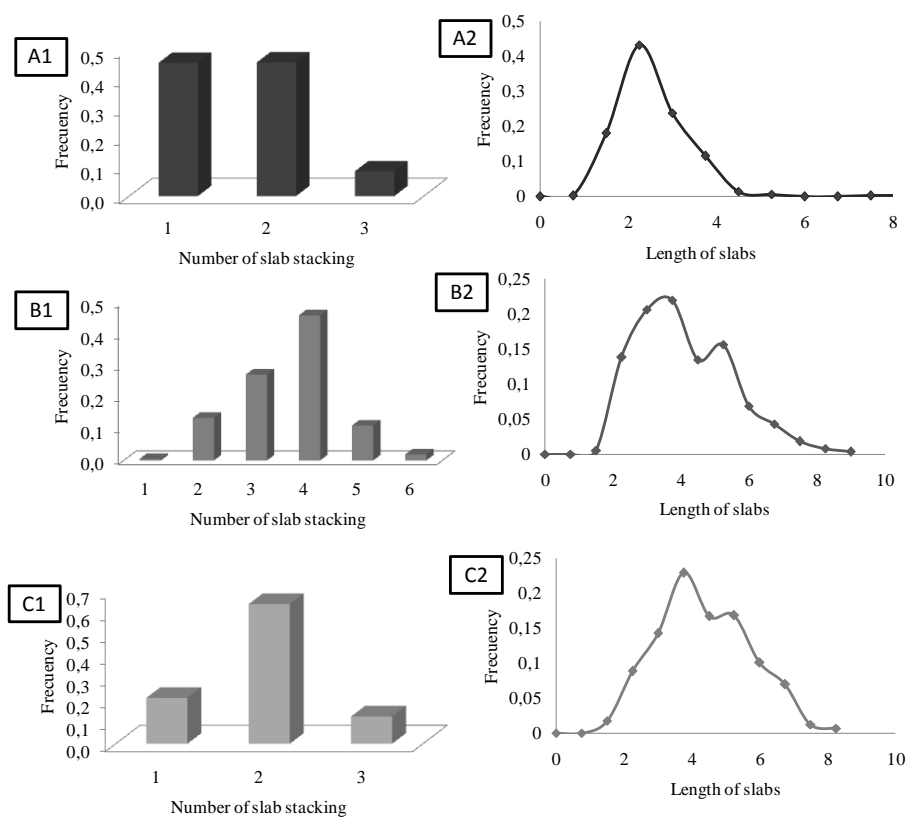


Figure IV.14. TEM images for CoMo /Al₂O₃, CoMo /SiO₂ and CoMo /TiO₂

Distribution of slabs length and stacking are shown in Figure IV.15 for promoted catalysts supported on Al₂O₃, SiO₂ and TiO₂. The average of slab length and stacking number are summarized in the table at the bottom of Figure IV.15. In order to study the variation of slab length and stacking number upon Cobalt addition, the results of non-promoted catalyst from chapter III are also added in the same table. Therefore, no significantly change was found for slab stacking number between non- and promoted catalysts. However, some change was detected for slab length after the Co addition: CoMo/Al₂O₃ catalyst shows an increase in slab length, CoMo/TiO₂ catalyst shows a decrease of slab length and CoMo/SiO₂ catalyst does not present any variation. Although, the support effect on slab length and stacking number for CoMo catalyst keeps the same tendency than for MoS₂ nanoparticles, i.e. CoMo/Al₂O₃ catalyst presents mono-stacking and the lowest slab length with an average of 2.9 nm, followed by CoMo/TiO₂ which presents a slab length of 4.7 nm and a stacking number of 1.7. However, CoMo/SiO₂ catalyst presents the highest slab stacking number with 3.3 and a slab length of 4.5 nm.



Catalysts	Stacking average		Length average (nm)	
	CoMo	Mo	CoMo	Mo
<i>(Co)Mo</i> / Al ₂ O ₃	1.4	1.3	2.9	2.0
<i>(Co)Mo</i> / SiO ₂	3.3	3.5	4.5	4.7
<i>(Co)Mo</i> / TiO ₂	1.7	2.0	4.7	6.7

Figure IV.15. Stacking on the left (1) and Length on the right (2) for CoMo catalysts supported on Al₂O₃ (A), SiO₂ (B) and TiO₂ (C). The table on the bottom summarizes the average of slabs length and stacking for Mo and CoMo catalysts supported on Al₂O₃, SiO₂ and TiO₂

4.4. Discussion

Understanding CoMoS site formation is a requirement for the catalyst improvement. For that, series of catalysts using different supports have been studied. The goal of using different supports was to obtain MoS₂ slabs with different morphologies, varying the metal-support interaction, and then to determine the Co affinity for M- and/or S-edge sites. Thus, the decoration by Co has been studied by the IR/CO method since this method allows distinguishing M- from S-edge sites for non-promoted catalysts.

4.4.1. Attribution of the components in the CO stretching range for promoted sites

Recently, IR/CO method was successfully developed for non-promoted catalysts. This technique allows the distinction of Mo located on M-edge and S-edge sites on MoS₂ nanoparticles. Studies showed that cobalt was located next to molybdenum in CoMoS sites that lead to the proposition of the CoMoS site formation by the cobalt decoration on MoS₂ edges [23]. Following this theory, IR/CO method could allow distinguishing both edge sites, M- and S-edge, decorated by Co and therefore study CoMoS site formation and their behavior in HDS reaction. Nevertheless, this study becomes difficult for promoted catalysts, i.e. CoMoS sites since such sites can vary in position (M-/S- edge), in sulfur and hydrogen coverage as well as in Co decoration level.

During decades, CoMo catalysts supported on Al₂O₃ were studied by IR/CO. These studies have shown the appearance of a CO stretching band ascribed to CO adsorption on CoMoS sites with a maximum between 2065 ~ 2070 cm⁻¹ [17,19,22,24]. Furthermore, IR/CO method distinguishes clearly two different CO adsorption domains that are ascribed to non-promoted sites and promoted sites. But, the detection of similar CO stretching range for promoted sites and Mo on S-edge sites leads to the apparition of the IR/CO method “limitation”. This limitation consists in the shortage of evidence of the presence or not of S-edge sites free of promotion in the domain ascribed to promoted sites. In order to solve this limitation, CO adsorption isotherm experiments were carried out for non- and promoted catalysts supported on Al₂O₃ to a posteriori perform the 2D inverse spectra method, which is called 2D IRIS method. The comparison of adsorption energies between non-promoted sites (Mo on M- and S-edge) and promoted sites obtained by the application of 2D IRIS method allowed to determine that only promoted sites are involved in the CO band domain characteristic of promoted sites. This result was confirmed on CoMo/SiO₂ catalyst even though the Mo/SiO₂ catalyst presents MoS₂ slabs with higher S-/M-edge ratio than Mo/Al₂O₃. In conclusion, no detection of S-edge sites free of promotion was found for promoted catalysts on both CoMo/Al₂O₃ and CoMo/SiO₂. Next, the different ν_{CO} components detected by the second derivative method can be considered to be only ascribed to CO adsorbed on promoted sites. Therefore, CoMo catalysts can present non-promoted edge, partially promoted edge or totally promoted edge as shows Figure IV.16. Non-promoted sites are located only on the M-edge since only the band at 2110 cm⁻¹ associated with coherent Gibbs free energies of adsorption was revealed by 2D IRIS method.

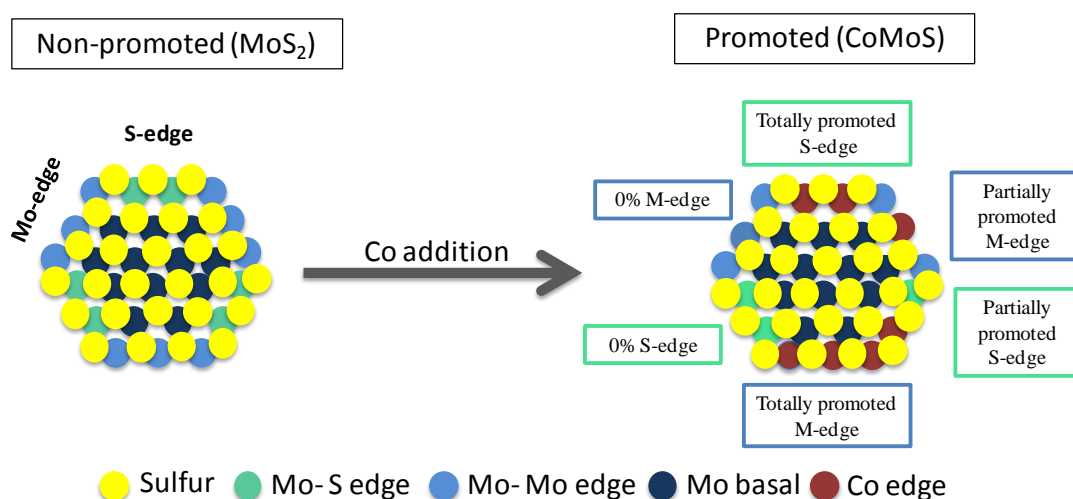


Figure IV.16. Scheme of Co decoration of MoS₂ with different promotion degree

Then the overlapping bands detected between 2020 and 2090 cm⁻¹ that are ascribed to promoted sites, have to be linked with Co location, i.e. M- or S-edge, and promotion degree i.e. totally or partially promoted edges (Figure IV.16). Recently, Chen et al. studied CoMoS site formation upon Cobalt addition using CVD method. Increasing amounts of Co(CO)₃NO were contacted with sulfide Mo/Al₂O₃ and Mo(CA/Mo=1)/Al₂O₃ catalysts as shows Figure IV.17. These two catalysts were chosen since the addition of citric acid leads to a change in the slab morphology of Mo/Al₂O₃ catalyst, i.e. the catalyst prepared with citric acid has higher S-/M-edge ratio than the one prepared without citric acid [25]. In both experiments, two CO stretching bands appear at 2055 and 2072 cm⁻¹ from the first CVD dose up to the last one. Both bands increase with Cobalt addition at the same time that the band ascribed to CO in interaction with non-promoted M-edge sites decreases. Moreover, a third band appears at 2082 cm⁻¹ with the last Co(CO)₃NO doses. This band starts to be visible earlier for Mo/Al₂O₃ catalyst than for Mo(CA)/Al₂O₃ catalyst. It can be due to the fact that MoS₂ slabs are smaller on Mo(CA/Mo=1)/Al₂O₃ and thus present higher amount of total edge sites than Mo/Al₂O₃ catalyst does [26]. Then, it indicates that the two first bands can be ascribed to partially promoted sites, and the third one can be ascribed to totally promoted sites, but without any evidence of edge site location.

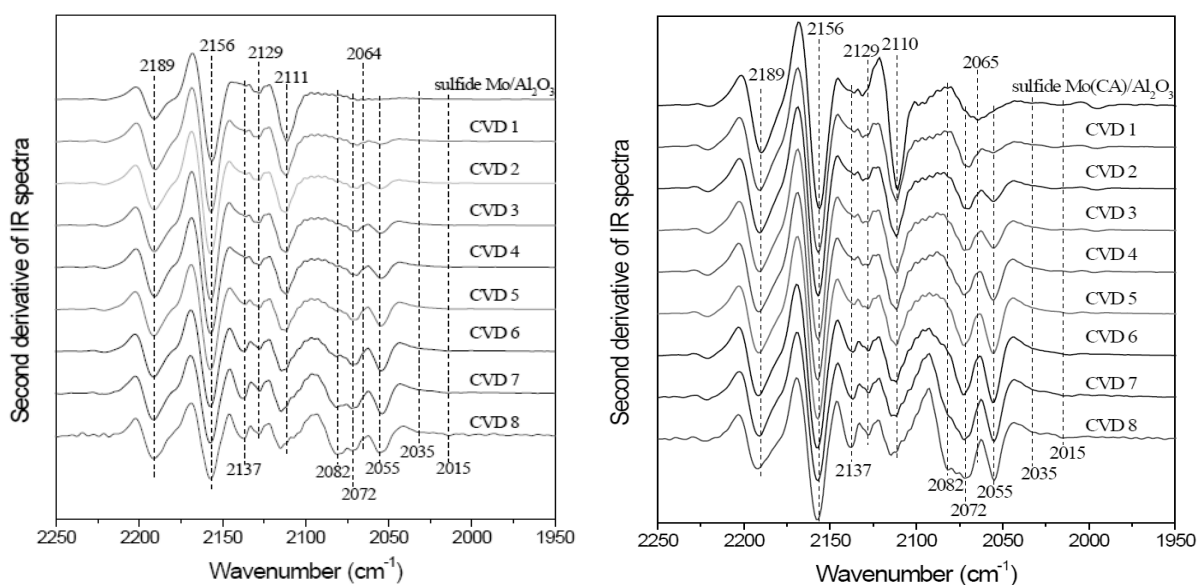


Figure IV.17. Cobalt addition by CVD method on Mo/Al₂O₃ prepared with or without Citric Acid followed by IR/CO (the experiments were performed by J. Chen during his PhD thesis) [25]

CVD method did not allow the detection of Co localization on S- or M-edge sites because the components detected in the promoted sites range increase in parallel with the decrease of the one ascribed to non-promoted sites located on M-edge sites. The decrease of the $\nu(\text{CO})$ band ascribed to non-promoted sites on M-edge sites could indicate that cobalt decorates both sites, S- and M-edge. In order to discover Co decoration, Chen et al. carried out CO adsorption on the same catalysts but prepared by wetness impregnation method. Thus, the tendency of the different components detected for promoted sites by IR/CO using catalyst with different S-/M-edge ratio, e.g. different CA/Mo ratio, was performed without any satisfactory result, since all components was increasing in parallel (Figure IV.18.a). Although a relation between the S-edge/M-edge ratio and the promoted/non-promoted sites ratio: for higher S-/M-edge ratio, higher promotion degree was detected as shows Figure IV.18.b. Thus, following the $\nu(\text{CO}/\text{promoted sites})$ components evolution with citric acid addition neither showed any indication about the Co localization.

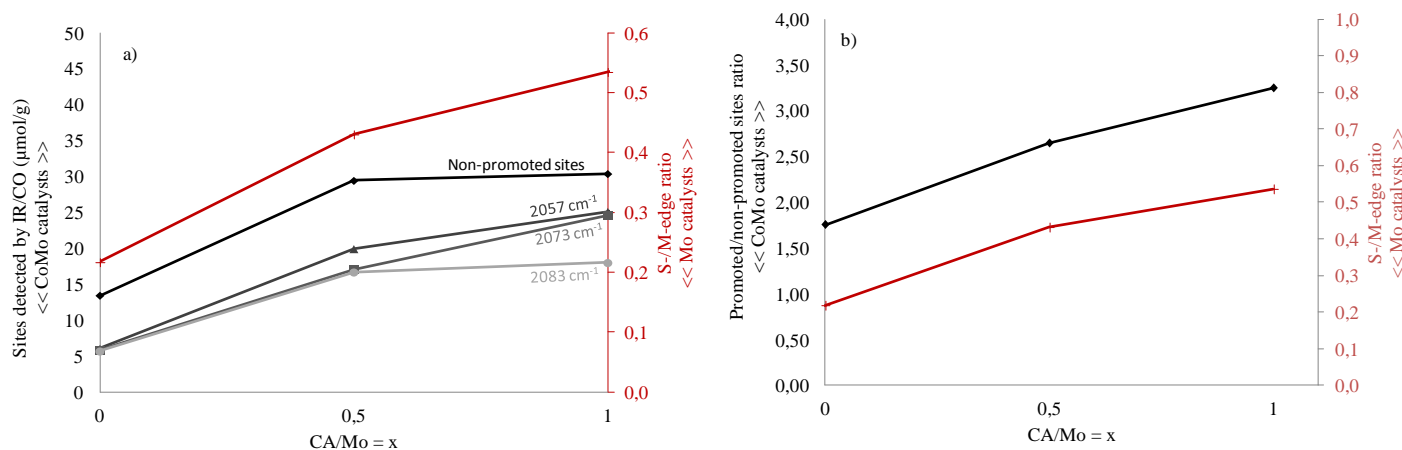


Figure IV.18. Relation of MoS₂ morphology with a) sites detected by IR/CO and b) promoted/non-promoted sites ratio for (CA/Mo=x)CoMo/Al₂O₃ catalysts

Similarly to what was obtained in the study of the promotion of (CA/Mo=x) (Co)Mo/Al₂O₃ by CVD or impregnation methods, the promoted sites/non-promoted sites ratio (promotion degree for CoMo catalysts) was plotted with the S-/M-edge ratio (morphology for the Mo catalysts) for the three supports as shows Figure IV.19.a. A relation between morphology and promotion degree was found: thus for higher S-/M-edge ratio, higher promotion degree is obtained in accordance with the results of the study on (CA/Mo=x) CoMo/Al₂O₃. Then, higher promotion degree is found for CoMo/SiO₂ followed by CoMo/Al₂O₃ and CoMo/TiO₂. It can also be noticed that the promotion degree is higher than the S-/M- edge ratio on both series: it means that Co decoration occurs on both S- and M-edge sites of MoS₂ nanoparticles. Then, the proportions of the three principal components detected by the second derivative method are represented in Figure IV.19.b. The component at 2057 cm⁻¹ follows the same trend than the S-/M-edge ratio detected for non-promoted catalyst since CoMo/SiO₂ catalyst presents the higher proportion for this component followed by CoMo/Al₂O₃ and CoMo/TiO₂. It can be an indication that this component corresponds to S-edge sites which is in agreement with the predicted band attribution (Table IV-3). Moreover, CoMo/Al₂O₃ catalysts shows the maximum proportion for the 2073 cm⁻¹ component which was ascribed to partially promoted sites and taking into account that it appears at higher wavenumber it can be linked to M-edge sites that is in agreement with the predicted band attribution (Table IV-3). On the other hand, CoMo/TiO₂ catalyst presents mainly the component detected at 2085 cm⁻¹ ascribed to totally promoted sites, and taking into account that Mo/TiO₂ was composed mostly by M-edge sites it is logical to ascribe this component to totally promoted M-edge sites in accordance with DFT calculations (Table IV-3). Additionally, a relation between the components at 2073 and 2085 cm⁻¹ can be detected, thus an increase of the proportion for totally promoted sites is related to a decrease of the proportion for partially promoted sites at 2073 cm⁻¹ and vice versa. It can be another

indication that both components (at 2073 and 2085 cm^{-1}) can be attributed to the sites to the same edge, i.e. the M-edge.

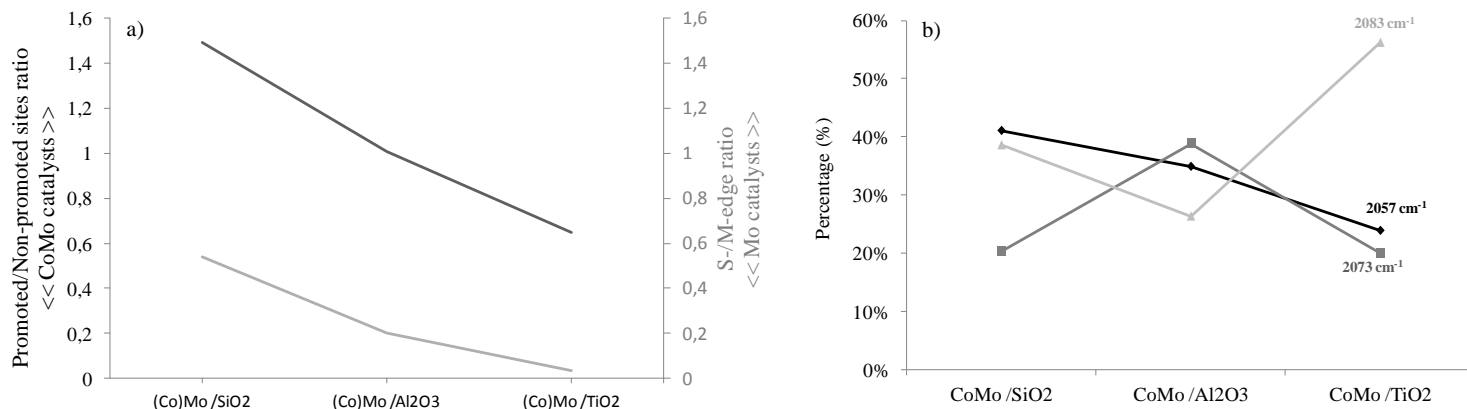


Figure IV.19. A) Comparison between MoS₂ morphology detected for non-promoted catalysts and promotion degree obtained for promoted catalysts. B) Percentage of the three $\nu(\text{CO}/\text{promoted sites})$ components detected by the second derivative for CoMo catalysts supported on Al₂O₃, SiO₂ and TiO₂

In conclusion, S-edge sites are decorated, partially or totally since any S-edge free of promotion was detected by 2D-IRIS method. CVD experiments allows us to determine that the components at 2057, and 2073 cm^{-1} can be attributed to Cobalt located in partially promoted edge while the component at 2082 cm^{-1} can be attributed to Co located in totally promoted edge. Also it was detected that non-promoted M-edge sites was decreased with Cobalt addition and the detection of high promotion degree for CoMo/TiO₂ that is formed by MoS₂ nanoparticles with small S-/M-edge ratio shows that cobalt decorates both, M- and S-edge sites. The relation between S-/M-edge ratio and promoted/non-promoted ratio indicates that S-edge sites favor Co promotion. Then, Table IV-3 shows the component attributions according to these deductions and the CO stretching vibrations calculated with DFT by Travert et al [27] versus the different promotion degree (0, 25%, 100%) and taking into account both M- and S- edges.

Table IV-3. Band attribution for components detected on the overlapping range ascribed to promoted CoMoS sites

		Co promoted sites							
<i>DFT calculations</i>									
Calculated wavenumber (cm ⁻¹)		2040	2055	2065		2076	2081	2081	2085
Attributions by DFT calculations		Mo (4c) (25% promotion) S-edge	Mo (4c) (25% promotion) M-edge	Co (25% promotion) S-edge		Co (25% promotion) M-edge	Mo (5c) (25% promotion) M-edge	Co (100% promotion) S-edge	Co (100% promotion) M-edge
<i>Experimental</i>									
Experimental wavenumber (cm ⁻¹)	2020	2038	2057	2065	2073	2083			
Attributions by DFT + experimental		Mo (4c) (partially promotion) S-edge	Co (partially promotion) S-edge	<i>Co₉S₈</i>	Co (partially promotion) M-edge	Co (totally promotion) M-edge			

4.4.2. Morphology effect on CoMoS site formation

In previous studies, metal-support interaction was reported as the main factor that influences MoS₂ slab characteristics, i.e. MoS₂ slab length, stacking and morphology, but also the slab orientation and the metal-support anchoring. In this study, different MoS₂ morphologies were obtained for Mo catalysts supported on Al₂O₃, SiO₂ and TiO₂ taking into account the IR/CO results. Thus, the strongest metal-support interaction reported for Mo/TiO₂ catalyst leads to a really low S-/M-edge ratio that corresponds to a triangle-like slab shape. Besides, the weakest metal-support interaction of Mo/SiO₂ catalyst leads to a high S-/M-edge ratio corresponding to a truncated triangular shape near to a perfect hexagon. And, catalyst with medium metal-support interaction as Mo/Al₂O₃ catalyst presents slabs of truncated triangular shape in between the two previous catalysts. The presence of different MoS₂ morphologies allows studying the Co decoration on M- and S-edge for MoS₂ nanoparticles. Hence, the study of support effect on CoMoS site formation was performed using CO adsorption followed by FTIR spectroscopy since this technique allows distinguishing non- and promoted sites as well as the location of cobalt and the promotion degree as it is predicted by DFT calculations [27]. Figure IV.20 shows IR spectra of CO at equilibrium pressure (site saturation) normalized by surface area for CoMo catalysts supported on Al₂O₃, TiO₂ and SiO₂. The highest intensity bands are detected for CoMo/TiO₂ catalyst, following by CoMo/Al₂O₃ and the lowest band intensities are detected for CoMo/SiO₂. Two different CO stretching domains ascribed to CO in interaction with edge sites are detected for the three catalysts corresponding to two kinds of sites: Non- and promoted sites. CO on non-promoted sites appears at the same stretching range for the three catalysts and corresponds to CO/M-edge sites. Similarly, the overlapping bands attributed to νCO/promoted sites appear at the same wavenumber range for the three catalysts from 2020 to 2090 cm⁻¹.

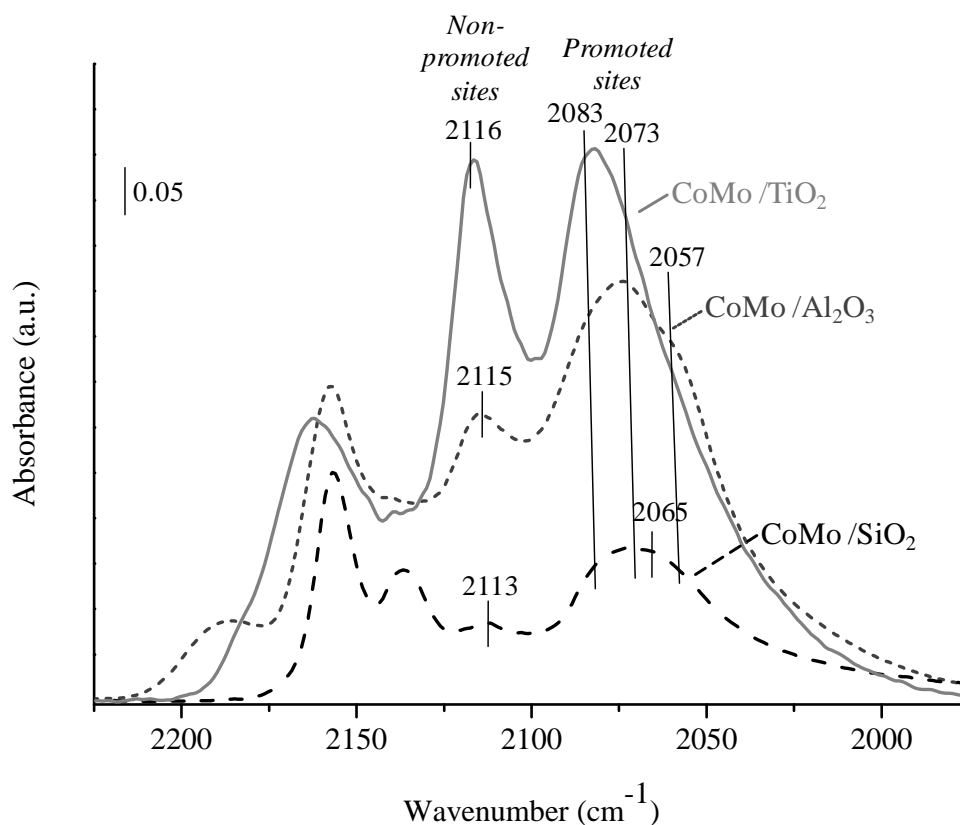


Figure IV.20. Comparison of promoted catalysts supported on Al_2O_3 , SiO_2 and TiO_2 normalized by surface area

Considering that CoMoS sites are formed through the decoration of MoS_2 nanoparticles, total edge sites detected for Mo catalysts can be compared with total edge sites detected for CoMo catalysts as shows Figure IV.21. The same tendency for total edge site concentration is detected for non- and promoted catalysts, i.e. the order from higher amount of sites detected by IR/CO to lower is $\text{TiO}_2 > \text{Al}_2\text{O}_3 > \text{SiO}_2$ catalysts. However, a slight increase of total edge sites is detected for CoMo catalysts supported on Al_2O_3 and SiO_2 compared with Mo catalysts. The increase of edge site concentration detected for CoMo/ Al_2O_3 catalyst is in controversy with the length increase detected by TEM. However, one may take in consideration that Cobalt atoms located on MoS_2 edges have lower sulfur coordination than Mo atoms; this environment change can lead to an increase in CUS site detection [7]. On the other hand, a strong decrease of total edge sites for CoMo/ TiO_2 catalyst is detected by IR/CO compared with Mo/ TiO_2 catalyst. Again, the decrease of total edge sites detected after Co addition is in controversy with the significant decrease of slab length observed by TEM upon Co addition. However, we have to mention for such consideration that we consider here the morphology of the slab unchanged between non-promoted and promoted slabs. Conversely, the decrease of edge sites for CoMo/ TiO_2 catalyst can be partially linked to a change in morphology

from triangle towards hexagon shape, which presents lower edge sites. However, one may also consider that an excess of sites was detected by IR/CO for Mo/TiO₂ catalyst compared with the TEM method. The excess of sites detected by IR/CO for Mo/TiO₂ was attributed to the slab orientation presenting an epitaxial orientation and somehow creating CUS sites. Therefore, one can propose that Co addition can modify the metal-support anchoring cancelling the epitaxial orientation for promoted slab, which lead to see a decrease of the detection of total edge sites.

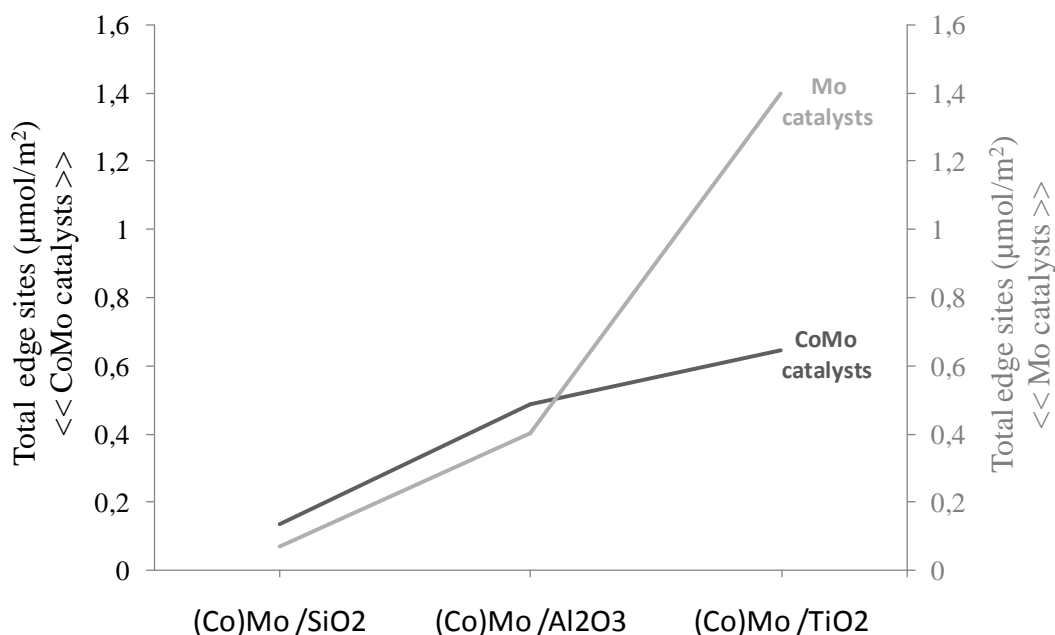


Figure IV.21. Comparison between total edge sites detected by IR/CO for non- and promoted catalysts supported on SiO₂, Al₂O₃ and TiO₂ after sulfidation

Therefore, taking into account the refined attribution of the ν_{CO} bands of CO adsorbed on promoted catalysts, the study of the morphology and location of Co promotion for the three catalysts can be performed. Thus, several calculations could be carried out and they are summarized in Table IV-4. First, total Co concentration in CoMoS sites was calculated for the three catalysts giving the highest value for CoMo/Al₂O₃ followed by CoMo/SiO₂ and CoMo/TiO₂. After, the morphology of CoMoS sites was predicted and higher S-/M-edge ratio was detected for the three catalysts in comparison with the one from Mo catalysts: Co introduction leads to a change towards more truncated triangle shape in particular for the Mo catalyst having less truncated slabs. Thus, strong change was detected for CoMo/TiO₂, followed by CoMo/Al₂O₃ and CoMo/SiO₂. This change in morphology for CoMo/TiO₂ catalyst is in accordance with the previous hypothesis to explain the high decrease of total edge site concentration as detected by IR/CO. Moreover, these changes in morphology are in agreement with the one detected by STM images that showed the

morphology change after Co addition from triangle to truncated triangle on Au support [28]. To go forward, the cobalt localization could be studied. For that as previously described, the promotion degree (promoted sites/non-promoted sites ratio) and S-/M-edge ratio (morphology of Mo catalysts) was compared for the three supported catalysts as shows Figure IV.19.a. This comparison allowed determining that Co decorates both edges, since the promotion degree was detected higher than the S-/M- edge ratio for all catalysts. Hence, the Co proportion located on S-edge for promoted sites was calculated for the three CoMo catalysts and compared with the proportion of Mo located on S-edge for Mo catalysts (see Table IV-4). Higher Co on S-edge proportion was detected for CoMo catalysts compared with Mo in S-edge catalysts for all catalysts indicating that Co decoration is favored on S-edge. This is in agreement with STM studies that detected Co decoration on S-edge sites for CoMoS phase supported on Au (111) [6]. Additionally, DFT calculations obtained more stable state for full promotion on S-edge than on M-edge [29] although more recent studies indicate that partially promoted M-edge are energetically as stable as partially or fully promoted S-edge leading to the possibility of promotion for both sites [7].

Table IV-4. Summary of the support effect on Co promotion obtained for CoMo catalysts supported on Al₂O₃, SiO₂ and TiO₂

Catalysts	Co sites in CoMoS by IR/CO (μmol/g)	S-/M-edge ratio for CoMo catalysts	S-/M-edge ratio for Mo catalysts	Co _{S-edge} /Co sites ratio for CoMo catalysts	Mo _{S-edge} /Mo _{S-edge} +Mo _{M-edge} ratio for Mo catalysts
CoMo/SiO ₂	28	0.49	0.42	0.39	0.29
CoMo/Al ₂ O ₃	49	0.32	0.20	0.35	0.17
CoMo/TiO ₂	12	0.16	0.03	0.25	0.04

4.4.3 The influence of CoMoS sites on the HDS activity

The metal-support interaction has been revealed as a factor that influences the CoMoS site nature (localization of the promoted sites and degree of promotion of the edge). Thus, the effect on catalytic activity of the different CoMoS site nature obtained on the three studied supports has to be studied. Firstly, the role of non- and promoted sites of CoMo catalysts in the catalytic activity for HDS reaction can be studied by an evolution comparison of the concentration of both edge sites and total edge sites with thiophene HDS rate as shows Figure IV.22. No clear relation is found between total edge sites and the HDS rate in particular because of the behavior of CoMo/TiO₂ catalyst showing the highest total edge site concentration but an intermediate activity between the two others catalysts. It indicates that total CUS sites concentration is an important factor but not the

unique factor for HDS activity. The comparison between non- or promoted site concentrations with the HDS rate shows a closer relation between promoted site concentration and the catalytic activity but still the behavior of CoMo/TiO₂ catalyst is not clearly explained. Indeed, CoMo/TiO₂ catalyst presents the same CoMoS sites concentration than CoMo/Al₂O₃ but a much lower activity. Thus, the differences in activity should be linked with the different CoMoS site nature that has been detected previously for the three catalysts.

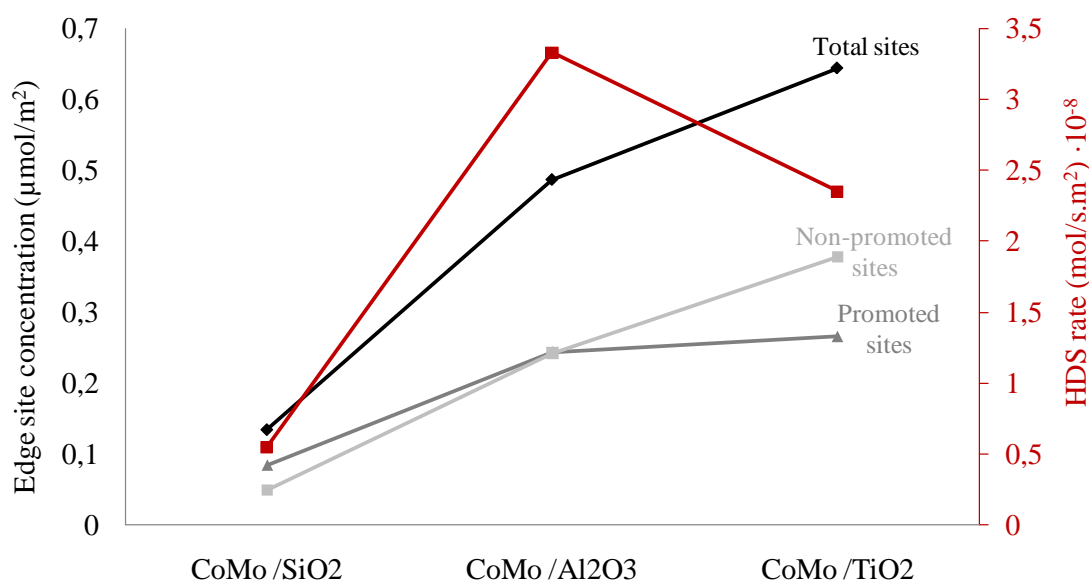


Figure IV.22. Relation between edge sites concentration detected by IR/CO and thiophene HDS rate for CoMo catalysts supported on Al₂O₃, SiO₂ and TiO₂

These differences in catalytic activity can be better studied by the TOF calculation of CoMoS sites. Thus, the TOF value for promoted sites was calculated taking into account the TOF value obtained for M-edge sites on non-promoted catalysts (see chapter III and V) and the concentration of each site, i.e. non- and promoted sites leading to $r_{\text{HDS}} = n_{\text{M-edge}} \cdot \text{TOF}_{\text{M-edge}} + n_{\text{CoMoS}} \cdot \text{TOF}_{\text{CoMoS}}$, where n is site concentration, r_{HDS} is thiophene HDS rate and TOF (turnover frequency). Table IV-5 summarizes TOF values calculated for the three catalysts. Thus, CoMo/Al₂O₃ catalyst shows the higher TOF value for promoted sites following by CoMo/TiO₂ and finally by CoMo/SiO₂. Then the origin of those different intrinsic activities can be interpreted by the Co edge location and promotion degree of the edge.

Table IV-5. TOF values of non- and promoted sites for CoMo catalysts supported on Al₂O₃, SiO₂ and TiO₂

Catalysts	TOF « M-edge* » (h ⁻¹)	TOF « CoMoS » (h ⁻¹)	TOF _{CoMoS} /TOF _{M-edge} ratio
CoMo/SiO ₂	18	224	12
CoMo/Al ₂ O ₃	20	471	24
CoMo/TiO ₂	35	269	8

* TOF value calculated on Mo catalysts characteristic of M-edge site (see chapter III, chapter V and annex II)

Then in order to understand the origin of the change of TOF values, the Co edge location and the edge promotion degree has to be studied via the components detected by IR/CO method that were attributed to Cobalt located on M- or S-edge with different promotion degree such as partially promoted edge or totally promoted edge. Figure IV.23 shows the proportion of Co on partially or totally promoted edges for the three catalysts, as well as the Co location on M- or S-edge. The calculated TOF for CoMoS sites values decreasing in the order CoMo/Al₂O₃ > CoMo/TiO₂ >> CoMo/SiO₂, no relation was found with the proportion of sites in totally or partially promoted edge or with the proportion of Co located on one specific edge, M- or S-edge. For that reason, it is proposed that the combination of both the location and the degree of edge promotion has to be taken into account to explain the TOF value of CoMoS sites. Thus, having a look to the proportion of the three components (Figure IV.19.b), a relation between TOF tendency and CoMoS sites in partially promoted M-edge is found since the highest proportion of this site was found for CoMo/Al₂O₃ catalyst, which presented the highest TOF ‘CoMoS’ value. On the other hand, CoMo/TiO₂ catalyst presented higher proportion of CoMoS sites in totally promoted M-edge that can be an indication that totally promoted M-edge sites are stronger than CoMoS sites on partially promoted S-edge. Thus, it can be conclude that Co decorated M-edge are more active than Co decorated S-edge, and additionally that sites on partially promoted M-edge are more active than sites on totally promoted M-edge. It is in agreement with *Gandubert et al.* who proposed partially promoted sites as the responsible to high intrinsic activity [30].

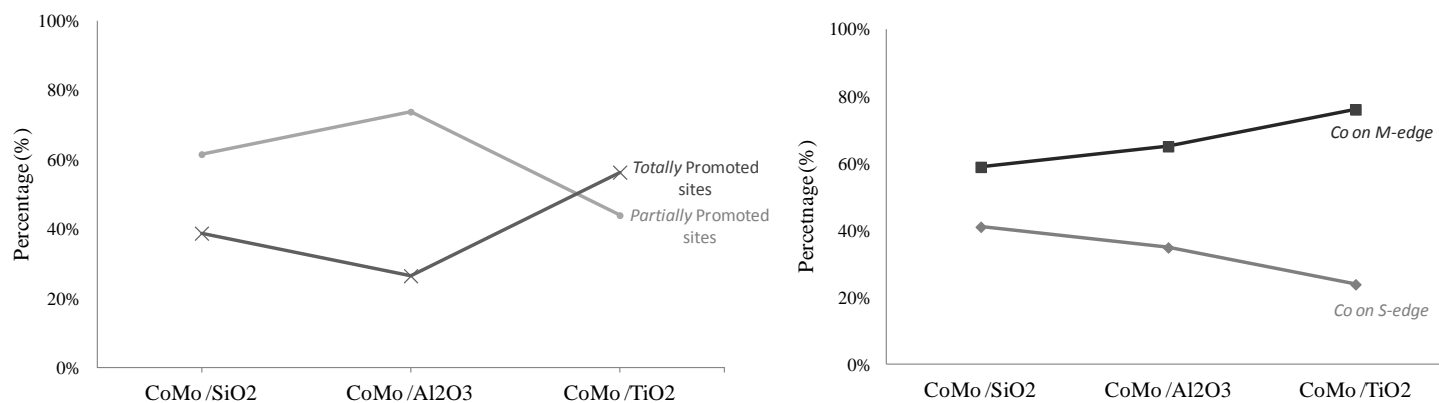


Figure IV.23. Relation between Co partially and totally promoted sites for CoMo catalysts supported on Al₂O₃, SiO₂ and TiO₂

4.5. Conclusion

In the present work, the study of CoMoS sites by IR/CO has given a step forward to the characterization of these sites in order to understand their function in the HDS reactions. The predictions of DFT calculations makes IR/CO method an interesting technique for study promoted sulfide catalysts since those calculations predicted different CO stretching vibrations for CO interacting with Co atoms localised on M- or S-edge. For that, previously, other authors studied CoMo catalysts supported on alumina using this method. The characterization of these catalysts by this method showed a “limitation” leading to not unambiguous results. This limitation appeared because the CO stretching bands ascribed to CO/promoted sites were presented at the same wavenumber region than the CO stretching bands for CO/Mo located on S-edge sites. For that, in the present work, the “limitation” of the method has been resolved using a developed method so-called 2D IRIS. This method developed by *Travert et al.* allowed revealing the absence of S-edge sites free of promotion in the sites probed by CO in the 2020-2090 cm⁻¹ range. This conclusion was based on the distinction of adsorbing sites through the Gibbs free energy of CO adsorption. M- and S-edge sites showed similar Gibbs free adsorption energies values although a small difference could be detected, higher value being obtained for S-edge than for M-edge sites. Conversely, clear differences in Gibbs free adsorption energies were detected between promoted and non-promoted sites: the value being lower for promoted sites than for non-promoted sites. The non promoted M-edge sites for CoMo catalysts appeared at the same Gibbs free energy of CO adsorption than the one detected for Mo catalysts, however, no specie was detected with the Gibbs free energy of CO adsorption and νCO wavenumber characteristics of S-edge sites. Thus, the CO stretching range

between 2020 and 2090 cm^{-1} is ascribed to CO/promoted sites for promoted catalysts prepared in the conditions described in preparation catalysts part.

After this validation step, the Co promotion can be studied using the IR/CO method. The different MoS_2 morphologies detected in the previous study (see chapter III) using different supports were used to study the preference of Co decoration on M- or S-edge sites. Hence, series of CoMo catalysts supported on alumina, silica and titania were studied by IR/CO. The CO spectra showed two different νCO domains ascribed to CO interaction with sulfide sites that are divided in non- and promoted sites. CO interacting with non-promoted sites on CoMo catalysts appeared at the same νCO wavenumber than CO interacting with M-edge sites on Mo catalysts and the attribution to CO/M-edge was corroborated by 2D IRIS method. CO interacting with promoted sites appeared in the CO stretching range between 2020 and 2090 cm^{-1} with in all cases three main components at 2057, 2073 and 2085 cm^{-1} . The comparison between Mo and CoMo catalysts allowed determining that Co decorates both M- and S-edge although it has preference to decorate S-edge sites since higher S-/M-edge ratio on Mo catalyst leads to higher promotion degree on CoMo catalyst. The Co incorporation in the MoS_2 edges showed a slight increase of total edge sites for CoMo/ Al_2O_3 and CoMo/ SiO_2 catalysts compared with its counter Mo catalysts. However, CoMo/ TiO_2 catalyst showed a strong decrease of edge sites concentration indicating a change in morphology or slab orientation promoted by the Co addition. The insight of Co promotion on M- and S-edge and a detailed study allowed the attributions of the three components ascribed to CO in interaction with promoted sites. The component that appeared at 2055 cm^{-1} was ascribed to partially promoted S-edge sites, the one at 2073 cm^{-1} was ascribed to partially promoted M-edge sites and the component at 2083 cm^{-1} was ascribed to totally promoted M-edge sites. These attributions allowed determining an explanation about the origin of the different catalytic activities found for CoMoS sites. The comparison between the total active sites (non- and promoted sites) and HDS rate detected for each catalysts lead to observe that there is not a direct relation between them indicating the importance of CoMoS nature in the catalytic activity. The order of total active sites from higher to lower is CoMo/ $\text{TiO}_2 > \text{CoMo}/\text{Al}_2\text{O}_3 > \text{CoMo}/\text{SiO}_2$, however the higher HDS rate was determined for CoMo/ Al_2O_3 followed by CoMo/ TiO_2 and CoMo/ SiO_2 . Hence, an exhaustive exam of the three components proportions revealed that the higher activity presented by CoMo/ Al_2O_3 is due to the presence of high proportion of *Co partially promoted M-edge sites*. Finally, taking into account the refined attributions the slab morphology in CoMo was predicted and a change with increasing S-/M-edge ratio was detected by the Co incorporation for all catalysts but in particular for CoMo/ TiO_2 catalyst.

4.6. References

- [1] H. Topsoe, B.S. Clausen, F.E. Massoth, *Hydrotreating Catalysis*, Springer, Berlin-Heidelberg, 1996.
- [2] H. Topsoe, B.S. Clausen, *Catal. Rev. Eng.* 26 (1984) 395–420.
- [3] H. Topsoe, B.S. Clausen, R. Candia, C. Wivel, S. M \ddot{A} ,rup, *J. Catal.* 68 (1981) 433–452.
- [4] H. Shimada, *Catal. Today* 86 (2003) 17–29.
- [5] H. Topsoe, *Appl. Catal. a-General* 322 (2007) 3–8.
- [6] F. Besenbacher, M. Brorson, B.S. Clausen, S. Helveg, B. Hinnemann, J. Kibsgaard, J. Lauritsen, P.G. Moses, J.K. Nørskov, H. Topsoe, *Catal. Today* 130 (2008) 86–96.
- [7] E. Krebs, B. Silvi, P. Raybaud, *Catal. Today* 130 (2008) 160–169.
- [8] L.S. Byskov, J.K. Nørskov, B.S. Clausen, H. Topsoe, *Catal. Letters* 64 (2000) 95–99.
- [9] H. Schweiger, P. Raybaud, G. Kresse, H. Toulhoat, *J. Catal.* 207 (2002) 76–87.
- [10] P. Stelmachowski, S. Sirotin, P. Bazin, F. Maugé, A. Travert, *Phys. Chem. Chem. Phys.* 15 (2013) 9335–42.
- [11] P. Stelmachowski, S. Sirotin, P. Bazin, F. Maugé, A. Travert, *Phys. Chem. Chem. Phys.* 15 (2013) 9335–42.
- [12] L.E. Makovsky, J.M. Stencel, F.R. Brown, R.E. Tischer, S.S. Pollack, *J. Catal.* 89 (1984) 334–347.
- [13] O. Blanco, 29 (2016) 2–6.
- [14] B. Jongsomjit, J. Panpranot, J.G. Goodwin, *J. Catal.* 204 (2001) 98–109.
- [15] H.L. Ma, J.Y. Yang, Y. Dai, Y.B. Zhang, B. Lu, G.H. Ma, *Appl. Surf. Sci.* 253 (2007) 7497–7500.
- [16] S. Dzwigaj, C. Louis, M. Breyse, M. Cattenot, V. Bellière, C. Geantet, M. Vrinat, P. Blanchard, E. Payen, S. Inoue, H. Kudo, Y. Yoshimura, *Appl. Catal. B Environ.* 41 (2003) 181–191.

- [17] F. Mauge, J.C. Lavalley, *J. Catal.* 137 (1992) 69–76.
- [18] C. Dujardin, M.A. Lelias, J. van Gestel, A. Travert, J.C. Duchet, F. Mauge, *Appl. Catal. A Gen.* 322 (2007) 46–57.
- [19] M.A. Lelias, E. Le Guludec, L. Mariey, J. van Gestel, A. Travert, L. Oliviero, F. Mauge, *Catal. Today* 150 (2010) 179–185.
- [20] M.A. Lélías, J. van Gestel, F. Maugé, J.A.R. van Veen, *Catal. Today* 130 (2008) 109–116.
- [21] M.A. Lelias, E. Le Guludec, L. Mariey, J. van Gestel, A. Travert, L. Oliviero, F. Maug??, *Catal. Today* 150 (2010) 179–185.
- [22] M.A. Lélías, J. van Gestel, F. Maugé, J.A.R. van Veen, *Catal. Today* 130 (2008) 109–116.
- [23] C. Wivel, B.S. Clausen, R. Candia, S. MÃ_rup, H. TopsÃ_e, *J. Catal.* 87 (1984) 497–513.
- [24] C. Dujardin, M.A. Lélías, J. van Gestel, A. Travert, J.C. Duchet, F. Maugé, *Appl. Catal. A Gen.* 322 (2007) 46–57.
- [25] J. Chen, F. Maugé, J. El Fallah, L. Oliviero, *J. Catal.* 320 (2014) 170–179.
- [26] J. Chen, *Catalyse D’hydrotraitement: Effet de La Pression de Sulfuration et D’agent Chélatant Sur La Morphologie et La Réactivité Des Phases Sulfures*, 2014.
- [27] A. Travert, C. Dujardin, F. Mauge, E. Veilly, S. Cristol, J.F. Paul, E. Payen, *J. Phys. Chem. B* 110 (2006) 1261–1270.
- [28] A.S. Walton, J. V Lauritsen, H. Topsoe, F. Besenbacher, *J. Catal.* 308 (2013) 306–318.
- [29] H. Schweiger, P. Raybaud, H. Toulhoat, *J. Catal.* 212 (2002) 33–38.
- [30] A.D. Gandubert, E. Krebs, C. Legens, D. Costa, D. Guillaume, P. Raybaud, *Catal. Today* 130 (2008) 149–159.

Table of contents – V Chapter

V. CHAPTER	151
5.1 Introduction.....	152
5.2 Experimental.....	153
5.3 Results.....	155
5.3.1 Study of Mo loading effect on Mo silica catalysts	155
5.3.1.1 Study of Mo/SiO ₂ catalysts in oxide form.....	155
5.3.1.1.1 Textural properties of Mo/SiO ₂ catalysts in oxidic form.....	155
5.3.1.1.2 Mo/SiO ₂ catalysts in oxidic form study by Raman spectroscopy.....	156
5.3.1.1.3 Mo/SiO ₂ catalysts in oxidic form study by UV-Vis spectroscopy.....	157
5.3.1.2 Non-promoted sulfide catalysts supported on silica.....	158
5.3.1.2.1 Catalytic activity: Thiophene HDS	158
5.3.1.2.2 Non-promoted sulfide catalysts characterization: CO adsorption by FTIR spectroscopy	159
5.3.2 Study of metal loading in promoted catalysts supported on silica	165
5.3.2.1 Catalytic activity for promoted silica catalysts – Thiophene HDS reaction	165
5.3.2.1.1 The effect of Mo loading in thiophene HDS reaction on promoted silica catalysts	165
5.3.2.1.2 The effect of Co/Co+Mo molar ratio in thiophene HDS reaction on promoted silica catalysts	166
5.3.2.2 Study of the metal loading effect in CoMoS formation by IR/CO	166
5.3.2.2.1 Mo loading effect in CoMoS site formation	167
5.3.2.2.2 Co/Co+Mo molar ratio effect in CoMoS formation	169
5.4 Discussion.....	171
5.4.1 Mo loading effect in Mo dispersion on silica surface.....	171
5.4.2 Effect of Mo loading in sulfide Mo/SiO ₂ catalysts.....	172
5.4.2.1 Effect of Mo loading in MoS ₂ slabs morphology.....	172

5.4.2.2	Effect of Mo loading in the catalytic activity for HDS thiophene	174
5.4.3	Effect of metal variation in CoMoS sites supported on silica	176
5.4.3.1	Effect of Mo loading in CoMoS sites formation.....	176
5.4.3.2	Effect of Co/Co+Mo molar ratio on CoMoS sites formation.....	178
5.4.3.3	Effect of metal variation in the catalytic activity for HDS thiophene.....	181
5.5	Conclusion	183
5.6	References.....	184

V. CHAPTER

METAL LOADING EFFECT ON

NON- AND PROMOTED CATALYSTS USING

SILICA AS SUPPORT

Abstract: Firstly, the effect of Mo loading in MoS₂ morphology for Mo/SiO₂ catalysts was studied. For that a series of non-promoted catalysts with different Mo density, 1, 2, and 3 atoms Mo per nm² were prepared and studied. Mo dispersion was studied by Raman spectroscopy. 2 atoms Mo per nm² were detected as the optimum Mo amount to get the best Mo dispersion. For this Mo concentration the catalyst presented the maximum Mo edge site concentration detected by IR/CO and whence the maximum catalytic activity. Therefore, a relation was found between activity, Mo dispersion on the surface and total edge sites concentration. Since IR/CO method allows the distinction of Mo located on M-edge and S-edge on MoS₂, the MoS₂ morphology has been studied for the series of Mo/SiO₂ catalysts. The increase of Mo loading showed an increase of S-/M-edge ratio, i.e. a change in MoS₂ morphology for Mo/SiO₂ catalysts. Slightly different TOF values have been calculated for the series of catalysts. An increase of TOF value with the increase of S-/M-edge ratio was observed. It was explained through the higher TOF value calculated for S-edge compared to M-edge on SiO₂ and Al₂O₃. The high TOF-S-edge value was ascribed to the implication of this site in the Direct Desulfurization (DDS) pathway. Secondly, the effect of metal variation, Mo or Co, on CoMoS sites formation was carried out in CoMo/SiO₂ catalysts. Three different Mo densities were studied, 1, 2 and 3 atoms Mo/nm² and constant Co/Co+Mo molar ratio equal to 0.3. Increase in promotion degree by the increase of Mo amount was detected for catalyst where Mo is well dispersed, i.e. CoMo (1) and CoMo (2). On the other hand, MoO₃ species were found as an inhibitor factor for CoMoS sites formation. Therefore, relation between S-/M-edge ratio and promotion degree was found for CoMo(1) and CoMo(2) catalysts however no relation was found for CoMo(3). Finally, four different values of Co/Co+Mo molar ratio with a constant Mo amount were used to prepare a CoMo/SiO₂ catalyst series. The optimum value was found for 0.2 Co/Co+Mo molar ratio for which the highest catalytic activity was obtained. Finally, the most active sites were shown to be the M-edge sites partially promoted by Co.

Keywords: Hydrodesulfurization (HDS), silica, CoMoS, Molybdenum disulfide (MoS₂), Slab morphology, Sulfidation, Infrared (IR) spectroscopy, CO adsorption, partially promoted, totally promoted

5.1 Introduction

The decline in available reservoirs of light oil and the continue increase of its demand especially by developing countries, requires the progressive enhancement of catalysts to remove sulfur from heavy oil. Some propose to improve the catalytic properties from some big molecules as Dibenzothiophene, is the use of some support with high surface area. Recently, there are many studies in HDS catalysts using Mesoporous silica as SBA-15, HMS, MCM-41 or some metal oxide mix as ASA [1–6]. Several studies detected higher conversion using molecule with high steric hindrance for CoMo/MCM-41 compared to CoMo/Al₂O₃ catalyst [7]. Thus, the use of material with high surface area leads to the increase of Mo dispersion and then the interaction points to carry out the reaction. The general characteristics encompassed in literature for Mo sulfide catalyst supported on silica are high intrinsic activity, low actives sites available for reaction, low Mo dispersion and easy MoO₃ formation due to the weak metal-support interaction [8–11]. Indeed the low amount of active sites detected for this family of catalysts is an artefact to carry out the reaction. Since the detection of Co decoration is favoured by S-edge sites [12], the formation of MoS₂ nanoparticles with high S-edge sites does interesting the study of these catalysts.

In the previous work, the support effect on MoS₂ formation was studied by IR/CO method (see chapter III). The comparison of the different nature of metal-support interaction using different metal oxide as support: alumina, silica and titania showed differences in MoS₂ morphology, catalytic activity, total sites available for reaction and different TOF value. Thus, this study exhibited silica as an interesting support to obtained MoS₂ nanoparticles with high S-/M-edge ratio, and high TOF value. Controversially, the high S-/M-edge ratio along with high slab length lead to observed low Mo edge sites. The high intrinsic activity that was reported in the literature [9] was attributed to the high S-edge sites present on MoS₂ nanoparticles. However, Mo/SiO₂ catalyst surface in the oxide form showed the presence of MoO₃ entities by Raman spectroscopy. On Mo/Al₂O₃, it is reported that change of the density of the impregnation solution leads to the obtaining of oxomolybdate species with different structures [13]. The interaction between the species in solution and the support surface leads after drying or calcination to the formation of oxomolybdate species as monomers, polymolybdate. It is only in presence of a large metal excess (i.e. greater than 3 atoms Mo/nm²) that MoO₃ are formed on alumina. However, the nature of the support strongly influences the structure of the oxo-species formed. Indeed, both formations of polymolybdate and molybdenum trioxide species are reported on silica for Mo/SiO₂ with 3 atoms Mo/nm² (see chapter III).

According to the previous results, the structure of the oxidic species is an important parameter that influences the morphology of the slab after sulfidation. Since oxide Mo/SiO₂ can form strongly different

oxidic entities even for limited Mo amount, we studied Mo/SiO₂ with low molybdenum density as 1 and 2 atoms Mo/nm² in the oxidic form and in the sulfided state. This study is expanded to CoMo/SiO₂ catalysts where the degree of Mo/Co dispersion on the surface can influence CoMoS sites formation. For that, a series of CoMo catalysts supported on silica varying Mo or Co loading is studied at the end of the chapter.

5.2 Experimental

5.2.1 Catalysts preparation

Mo catalysts supported on silica (506 m²/g, Merk) were prepared by wetness impregnation method of heptamolybdate tetrahydrated salt (Alfa Aesar, 99%). The support was sieved between 0.2-0.5 μm and calcined at 673K during 4h before impregnation. Then, heptamolybdate salt was dissolved into a specific volume equal to silica pore volume plus 30% in excess of deionizer water. The solution was contacted with silica during 2 hours. This maturation step allows obtaining a good dispersion of the solution inside the pores of silica. Metal density was varied from 1, 2, and 3 atoms Mo/nm² of support. After impregnation, the catalysts were dried at 383 K during 16 h, and further calcined at 673K during 4 h with a heating rate of 3K/min for both treatments. Studied catalysts are denoted as 1-Mo, 2-Mo and 3-Mo indicating the metal density. Other serial of CoMo catalysts supported on silica (506 m²/g, Merk) are prepared varying Molybdenum density (1, 2, and 3 atoms Mo per nm²) and constant cobalt molar ratio (Co/ Co+Mo equal to 0.3). Catalysts of this serial are called as CoMo (1), CoMo (2) and CoMo (3) in relation with the Mo amount per nm². The last serial of CoMo catalysts are supported on silica keeping the same metal density (2 atoms Mo /nm²) and varying Cobalt molar ratio (Co/Co+Mo = 0.1, 0.2, 0.3 and 0.4). Catalysts of this serial are called as (0.1) CoMo, (0.2) CoMo and (0.3) CoMo in relation with their cobalt molar ratio. Heptamolybdate tetrahydrated salt (Alfa Aesar, 99%) and cobalt nitrate (Alfa Aesar, 98%) were used as molybdenum and cobalt precursors respectively. The impregnation for promoted catalysts was carried out by the same procedure as was described for Mo catalysts. After impregnation, the catalysts were drying at 383 K (3 K/min) during 16 hours and then calcined at 723 K (3 K/min) during 4 hours.

5.2.2 Catalysts characterization

5.2.2.1 UV-VIS spectroscopy

Ultraviolet-visible (UV-Vis) spectra were recorded on a Carey 4000 using. The spectrum acquisition was done between 800-200 nm with a speed of 300 nm/min. The analysis was done on oxidic form of the

catalysts in order to determine the coordination symmetry of the different molybdenum oxide anions. The pure support was used as a reference spectrum. UV-Vis spectra were converted in form of the edge adsorption energy. This edge absorption energy is determined by finding the energy intercept of a straight line fitted through the low energy rise in the graphs of $[F(R) \cdot hv]^2$.vs. hv . Energy differences were compared to the average number of nearest Mo neighbours in the clusters, calculated by $N_{Mo} = 16 - 3.8 \cdot E$ [14].

5.2.2.2 Raman spectroscopy

Raman spectroscopy was used to study the structure and the dispersion of molybdenum oxide species. Raman spectroscopy was performed using a Jobin Yvon Labram 300 Raman spectrometer equipped with a confocal microscope, a Nd-YAG laser (frequency doubled, 532 nm) and a CCD detector. Spectra were recorded at room temperature in the region between 200–1000 cm^{-1} .

5.2.2.3 CO adsorption by infrared spectroscopy (IR/CO)

Sulfide (Co)Mo catalysts were characterised by CO adsorption followed by infrared spectroscopy (IR/CO). IR/CO experiments were performed in a low temperature IR cell adapted to adsorb carbon monoxide close to liquid nitrogen temperature (100K). First, oxide catalysts were pressed under the form of a disc. The wafers were activated *in situ* in the IR cell: sulfidation under 10% H_2S/H_2 flow (conventional sulfidation procedure). A post-treatment after the conventional sulfidation was performed under 2% H_2S/H_2 flow during 2 hours at 623K for Mo catalysts. The conventional sulfidation procedure was performed under 10% H_2S/H_2 flow (30 ml/min) by increasing the temperature up to 623K with a rate of 3K/min and maintaining T_s at 623K during 2 hours. Finally the catalyst was evacuated at 623K under secondary vacuum during one hour and then was cooled down to room temperature under high vacuum. The post-treatment performed after sulfidation was carried out under 2% H_2S/H_2 flow (30 ml/min) using the same protocol. After sulfidation, the catalyst was cooled down to room temperature under evacuation. After these activation procedures, the temperature was decreased to 100K under high vacuum ($1 \cdot 10^{-4}$ Pa) to perform CO adsorption. CO adsorption experiments were performed introducing successive small calibrated CO doses upon saturation using an equilibrium pressure of 133 Pa CO.

IR spectra were recorded with a Nicolet Magna 550 FT-IR spectrometer equipped with a MCT detector. All spectra were normalised to a disc of 5 mg / cm^2 . Every experiment was reproducible with an error of 6%. Spectra corresponding to CO at saturation were decomposed using OMNIC software and band shape with pseudo-voigt function.

5.2.2.4 Catalytic activity - Thiophene test

The oxide catalysts were sieved between 0.2 and 0.5 μm . The oxidic catalysts were sulfided *in situ* in the continuous reactor. Sulfurization procedure was performed by increasing the temperature up to 623K with a rate of 3K/min, under a flow of 10% $\text{H}_2\text{S}/\text{H}_2$ (30ml/min) at atmospheric pressure and maintained at 623K during 2 h. Then, thiophene reaction was performed at 623K and atmospheric pressure with a thiophene partial pressure of 8 kPa in a mixture of hydrogen (91.2 kPa) and H_2S (2.1 kPa). The outlet gas was analysed by a gas chromatograph Varian 3900 equipped with flame ionization (FID) detector. The reaction rate was calculated as $r_{\text{HDS}} = (F/m) \cdot X$, where F/m is the molar flow rate of thiophene per gram of catalyst and X is thiophene conversion that is below 5%. Thiophene reaction was running during 18h until stable reaction rate was achieved. The catalyst mass was calculated taking into account the mass before the reaction corrected by a mass loss factor calculated from the IR experiments.

5.3 Results

The support effect on the MoS_2 morphology was previously studied using Al_2O_3 , TiO_2 and SiO_2 as support. Mo/SiO_2 catalyst is characterized by being formed of MoS_2 slabs with high S-/M-edge ratio, low Mo edge dispersion, high stacking degree, high slabs length, and high “total edge” TOF value. The low Mo edge dispersion was explained by a combination between the morphology (near to perfect hexagon) and the high slabs length detected by TEM. On the other hand, the high “total edge” TOF value could be explained by the formation of MoS_2 slabs with high S-edge sites concentration since higher TOF value for S-edge than M-edge sites was calculated for $\text{Mo}/\text{Al}_2\text{O}_3$ catalysts [15]. The high S-/M-edge ratio detected for Mo/SiO_2 does an interesting catalyst to calculate the TOF values for the two edge sites for this family of catalysts. For that, the effect of metal loading on MoS_2 morphology for MoS_2 is studied. This study is extended to CoMo catalysts, therefore, at the end of the work, the effect of metal variation on CoMoS sites formation and its impact on activity is studied.

5.3.1 Study of Mo loading effect on Mo silica catalysts

5.3.1.1 Study of Mo/SiO_2 catalysts in oxide form

5.3.1.1.1 Textural properties of Mo/SiO_2 catalysts in oxidic form

Comparison of the textural properties of the Mo/SiO_2 catalysts with different Mo loadings with that of the pure support is presented in Table V-1. The deposition of molybdenum on silica leads to a strong decrease of the surface area and pore volume of the support. The increase of the amount of Mo

deposited enhances the loss of surface area and pore volume. Previous chapter (chapter III) shows that the deposition of a constant density of Mo (3 atoms Mo per nm²) on SiO₂, Al₂O₃ and TiO₂ surfaces leads to a significant decrease of surface area but only for Mo/SiO₂. This is likely related to the small pore size of silica (6 nm versus 12 nm for the two others metal oxides). Hence, the excess of metal present should block the pore and prevents a homogeneous dispersion of Mo inside the pores.

Table V-1. Textural analysis on Mo/SiO₂ oxide catalysts by N₂ adsorption

Samples	Surface area (m ² /g)	Pore volume (cm ³ /g)	Pore size (nm)
SiO ₂	506	0.7	6
1-Mo / SiO ₂	395	0.5	5
2-Mo / SiO ₂	368	0.5	5
3-Mo / SiO ₂	305	0.4	5

5.3.1.1.2 Mo/SiO₂ catalysts in oxidic form study by Raman spectroscopy

Figure V.1 shows Raman spectra for 1-Mo, 2-Mo, and 3-Mo calcined catalysts. For the three catalysts, main bands appear in the range characteristic of Mo-O vibration that is between 800 and 1000 cm⁻¹. Raman spectrum of 1-Mo catalyst shows two weak bands at 874 and 955 cm⁻¹ ascribed to Mo-O-Mo bridge vibration, and Mo=O terminal vibration, respectively [16,17]. These two main bands are characteristic of polymolybdate species. Raman spectrum of 2-Mo catalyst shows the same two bands also ascribed to polymolybdate species, and additionally two new sharp bands appears at 821 and 997 cm⁻¹ that are ascribed to MoO₃ species [13,18,19]. The formation of MoO₃ species on the surface points out a poor Mo dispersion. Raman spectrum of 3-Mo catalyst shows higher intensity for the bands species at 821 and 997 cm⁻¹, characteristic of MoO₃. Hence the optimum dispersion of oxomolybdate species on silica is reached for 2 Mo atoms per square nanometre. Greater Mo concentration leads to the development of the MoO₃ crystallites at the expense of polymolybdate phase.

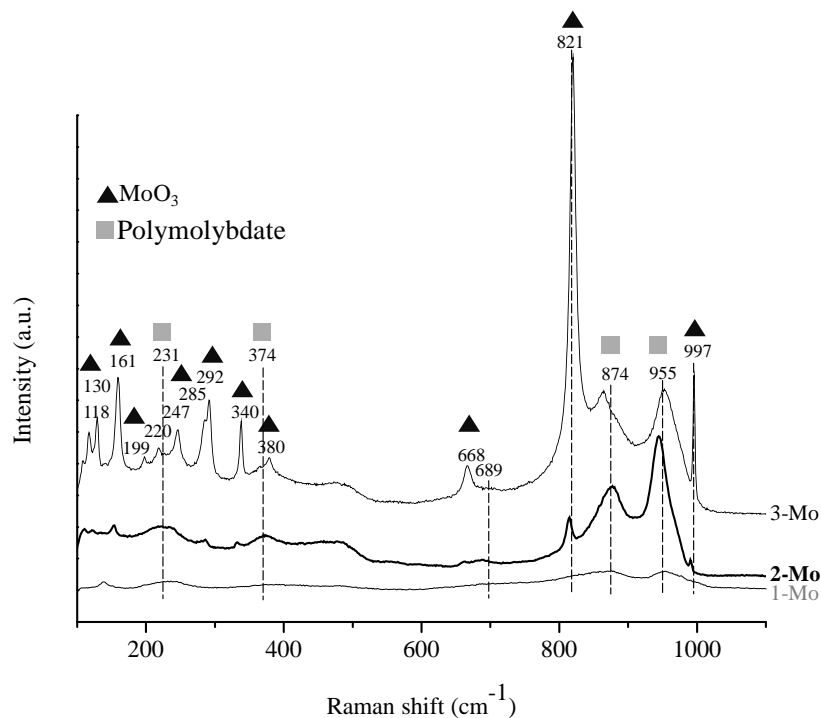


Figure V.1. Raman spectra of Mo/SiO₂ catalysts with different Mo loading

5.3.1.1.3 Mo/SiO₂ catalysts in oxidic form study by UV-Vis spectroscopy

Additional study was performed by UV-Vis spectroscopy. The edge adsorption energy was calculated for the three catalysts. As shown in Figure V.2, edge adsorption energy of the Mo/SiO₂ catalysts was compared to the average number of nearest Mo neighbours in the clusters, to predict the molybdate domain size. Different edge adsorption energies were obtained for 1-Mo, 2-Mo and 3-Mo catalysts. The increase of Mo amount leads to a decrease of the edge adsorption energy, i.e. 1-Mo: 3.66 eV, 2-Mo: 3.55 eV and 3-Mo: 3.22 eV. Hence, UV-Vis analysis shows that the number of Mo neighbours increase with the Mo amount deposited on silica. Thereby, comparison of the calculated edge adsorption energies with the references anions values indicates that 1-Mo and 2-Mo catalyst surfaces are formed of polymolybdate species as Mo₇O₂₄⁶⁻ and Mo₂O₇²⁻, with a higher proportion of heptamolybdate anions for 2-Mo catalyst. On the other hand, 3-Mo catalyst surface is formed by a mix of MoO₃ and Mo₇O₂₄⁶⁻ species. Therefore, these results are in agreement with Raman spectroscopy.

In conclusion, to optimize the dispersion of oxomolybdate on silica, Mo deposition should stay lower than to 2 atoms Mo per nm².

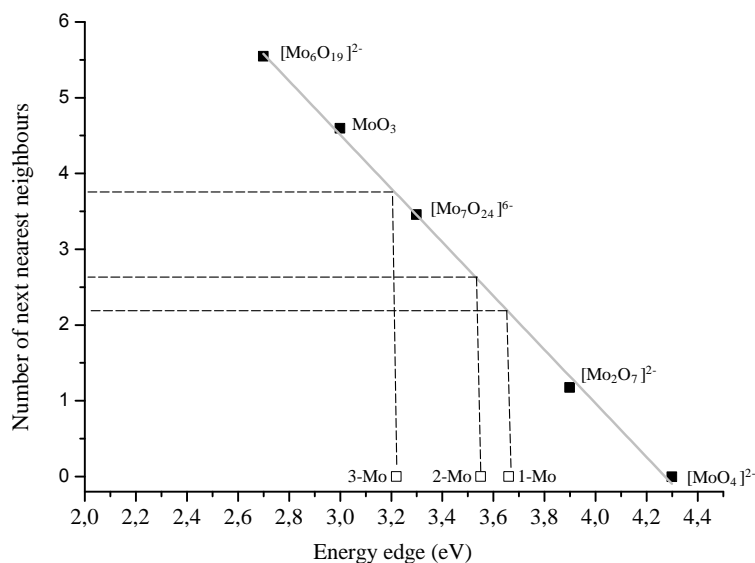


Figure V.2. Edge adsorption energy determined from UV-Vis spectra of Mo/SiO₂ with different Mo density (1, 2 and 3 Mo atoms per nm²)

5.3.1.2 Non-promoted sulfide catalysts supported on silica

5.3.1.2.1 Catalytic activity: Thiophene HDS

The catalytic activity for thiophene HDS reaction has been measured on the three Mo/SiO₂ catalysts. Figure V.3. shows that the maximum of HDS rate is found for 2-Mo catalysts followed by 3-Mo and 1-Mo catalyst.

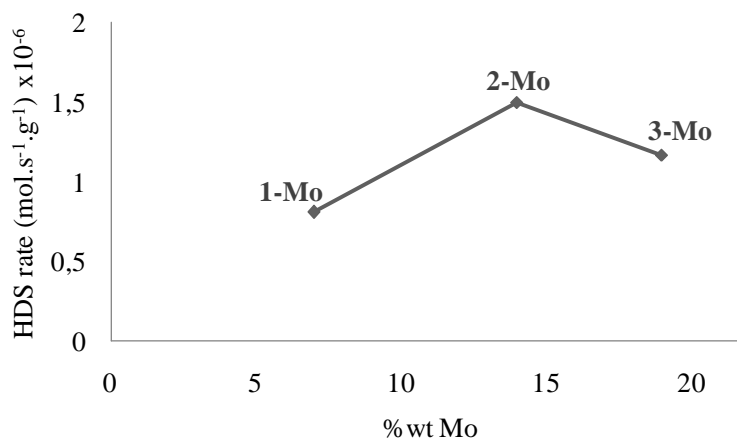


Figure V.3. HDS rate using thiophene as model molecule in Mo /SiO₂ catalysts with different Mo loading

The product distribution for HDS reaction obtained for 1-, 2- and 3-Mo/SiO₂ catalysts are presented in Figure V.4. Some differences can be noted. On the three catalysts, the amount of 2-butene

and tetrahydrothiophene stays constant. By contrast, the increase of Mo loading leads to a marked decrease of the 1-butene proportion. Furthermore, the proportion of butane is strongly increased on 3-Mo/SiO₂ catalyst. In conclusion, 1-Mo/SiO₂ and 2-Mo/SiO₂ catalysts do not present significant differences in product distribution, whereas 3-Mo/SiO₂ catalyst shows more drastic changes.

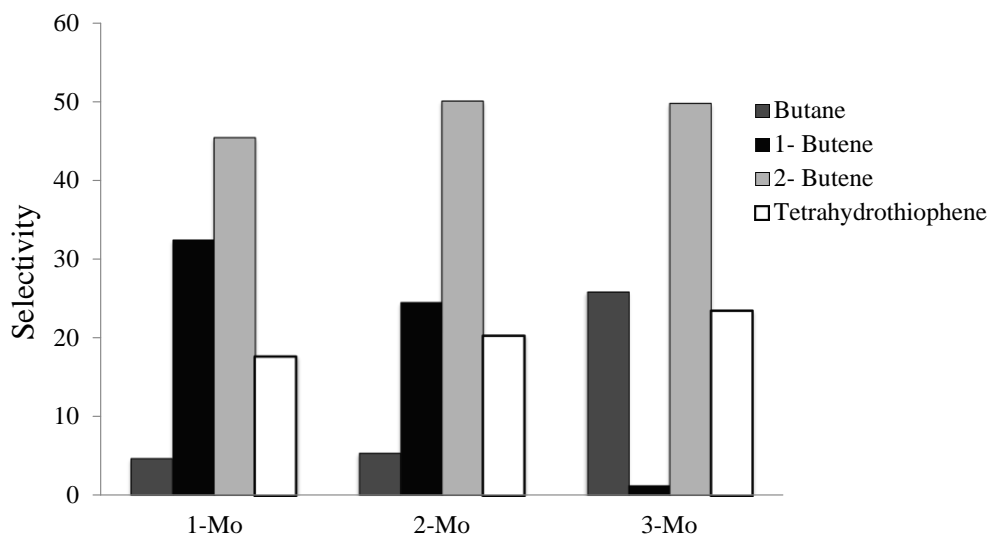


Figure V.4. Products of thiophene in hydrodesulfurization reaction for Mo/SiO₂ catalysts with different Mo loading: 1, 2 and 3 Mo atoms per nm²

5.3.1.2.2 Non-promoted sulfide catalysts characterization: CO adsorption by FTIR spectroscopy

The effect of Mo loading on the MoS₂ formation was studied by CO adsorption at low temperature followed by FTIR spectroscopy (IR/CO). Since characterization of 3-Mo catalyst was previously presented in Chapter III), the characterization of this catalyst will not be detailed in this section. Figure V.5 presents IR spectra of CO adsorption on sulfided 1-Mo catalyst from small CO doses up to sites saturation by CO adsorption at equilibrium pressure (133 Pa). In the zone characteristic of CO in interaction with silica, band at 2156 cm⁻¹ is specific of interaction with hydroxyl groups while the band at 2136 cm⁻¹ is ascribed to CO physisorbed [20–22]. In the zone specific of CO interaction with MoS₂ phase, several bands appear. Those bands are ascribed to CO in interaction with Mo located on M- and S-edge giving rise to different CO stretching bands at high and low wavenumbers respectively. The band at 2113 cm⁻¹ is ascribed to CO/Mo on M-edge. The bands at 2065, 2038, and 2021 cm⁻¹ are characteristic of CO/Mo on S-edge with different sulfur coverage. According to DFT calculations, the lower the band position, the lower the sulfur coverage. Thus, the 2065 band would correspond to a Mo site completely saturated with sulfur while the lower wavenumber bands are ascribed to CUS Mo sites with incomplete sulfur coordination [23,24]. The decrease of sulfur coverage leads to the decrease of the coordination number of Mo and then to an increase of the back-donation of Mo→CO and consequently the band

appears at lower wavenumber. Finally, the band detected at 1998 cm^{-1} is attributed to metallic molybdenum [15]. The band at 1988 cm^{-1} are assigned to Si-O-Si vibrations related to the silica structure distorted by the CO adsorption (see annex I).

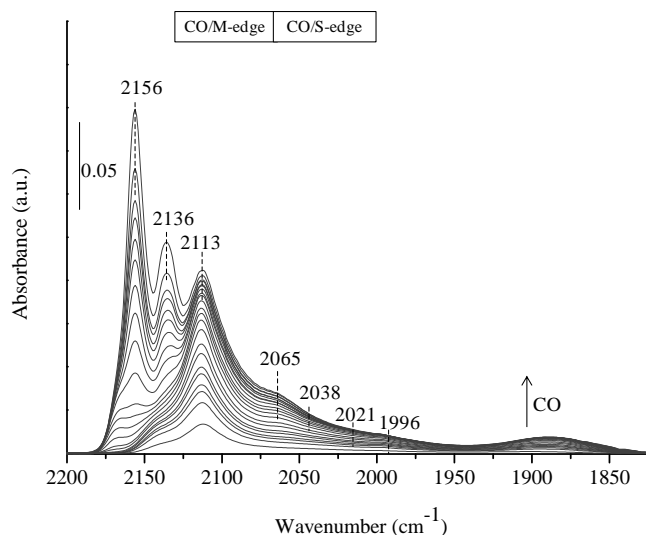


Figure V.5. IR spectra of CO adsorption from small CO doses up to saturation (133 Pa) on sulfided 1-Mo catalyst

Figure V.6 shows IR spectra of CO adsorption on sulfided 2-Mo/SiO₂. The same CO/silica bands are detected than previously. By contrast on the sulfided phase, the main stretching band of CO/Mo on M-edge is detected at 2116 cm^{-1} (instead of 2113 cm^{-1}). The CO/Mo on S-edge interactions give rise to several stretching bands at 2065, 2036, and 2021 cm^{-1} as previously reported for 1-Mo/SiO₂. However, the intensity of the band at 2065 cm^{-1} is strongly increased as well as the bands at lower wavenumber. This point out that the amount of S-edge of MoS₂ slab is increased compared to 1-Mo/SiO₂ catalyst.

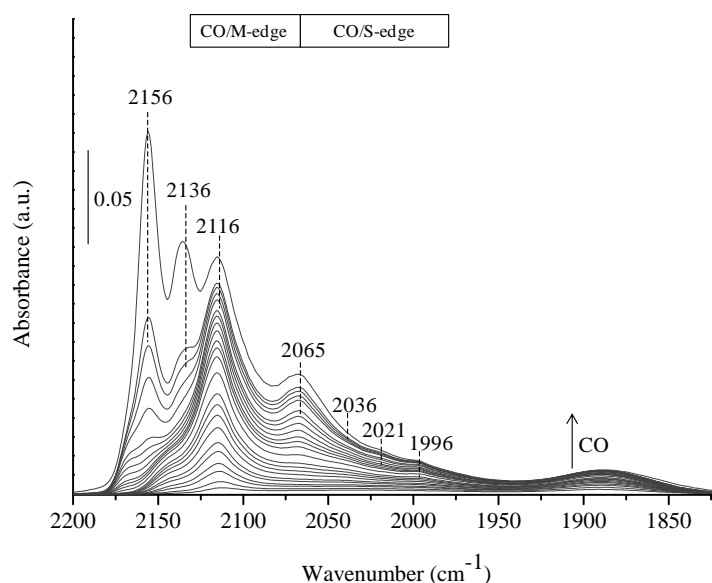


Figure V.6. IR spectra of CO adsorption from small CO doses up to saturation (133 Pa) on sulfided 2-Mo catalyst

The influence of sulfo-reductive post-treatment was studied previously (see chapter III). Chapter III showed that the sulfo-reductive post-treatment can have a strong effect on Mo sites availability; this effect depends on the nature of the support and likely on the strength of metal-support interaction. Thus, 3-Mo/SiO₂ catalyst, which is characterized by weak metal-support interaction, was shown to be very sensitive to sulfo-reductive post-treatment. For that reason, the sulfo-reductive post-treatment using 2% H₂S/H₂ reaction flow was studied for 1-Mo/SiO₂ and 2-Mo/SiO₂ catalysts. Figure V.7.a presents the IR spectra of CO adsorption after 2% H₂S/H₂ post-treatment for 1-Mo/SiO₂ sulfided catalyst from small CO pressures up to saturation using CO at equilibrium pressure (133 Pa). Similar CO band are detected than after sulfidation for CO-support interaction as well as for CO-MoS₂ interaction where bands characteristics of M- and S-edge can be observed. Figure V.7.b compares CO spectra after sulfidation (black line) and after the post-treatment (grey line) for CO at equilibrium pressure. An increase of the CO/OH band is detected likely due to the excess of H₂ in the flow that can create some hydroxyl groups. After the post-treatment, a small increase of the CO/Mo band intensity is noted only for Mo sites located on M-edge. Besides, this CO/M-edge band presents a shift of 3 cm⁻¹ to lower wavenumber in relation with the decrease in sulfur coordination of the Mo site.

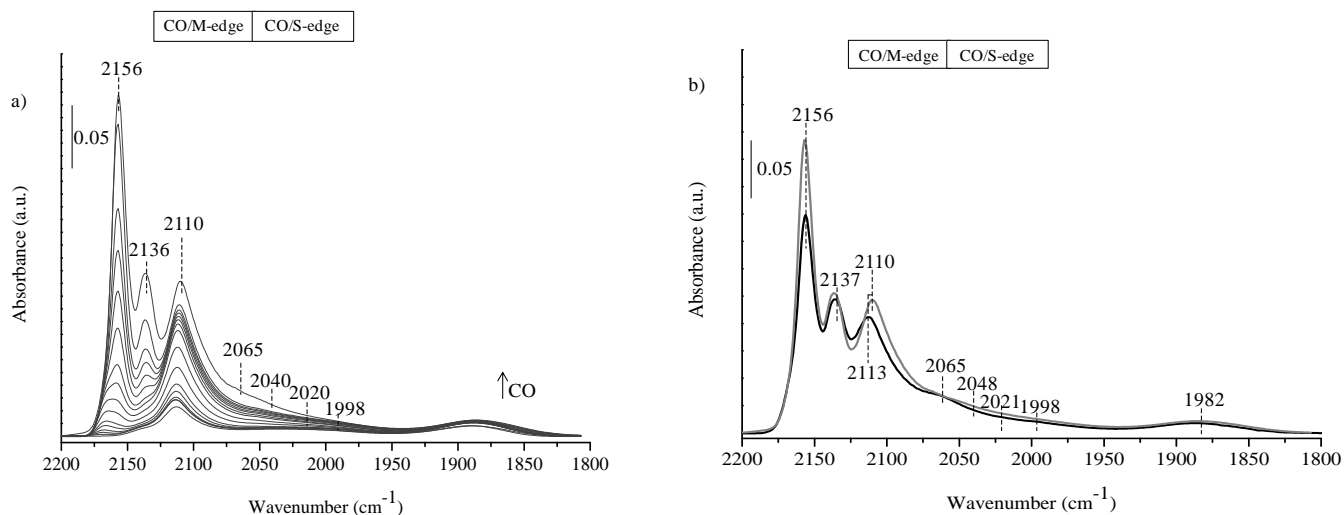


Figure V.7. IR spectra of CO adsorption on 1-Mo sulfide catalyst: a) after post-treatment under 2% $\text{H}_2\text{S}/\text{H}_2$; b) comparison of spectra obtained after sulfidation under 10% $\text{H}_2\text{S}/\text{H}_2$ (black line) and after 2% $\text{H}_2\text{S}/\text{H}_2$ post-treatment (grey line)

Figure V.8.a. shows IR spectra of CO adsorption after 2% $\text{H}_2\text{S}/\text{H}_2$ post-treatment for 2-Mo/ SiO_2 sulfided catalyst from small CO pressures up to saturation using CO at equilibrium pressure (133 Pa). Similar CO bands are detected than after sulfidation for CO-support interaction as well as for CO-MoS₂ interaction where bands characteristic of M- and S-edge can be observed. Figure V.8.b. shows the comparison between IR spectra after sulfidation (black line) and after the post-treatment (grey line) at CO equilibrium pressure. IR/CO spectrum obtained after post-treatment shows the increase of CO band intensities for Mo located in both M- and S-edge. Besides, CO/M-edge stretching vibration band presents a shift of 2 cm^{-1} to lower wavenumber due to the decrease of sulfur coverage, as well as the appearance of a shoulder at 2102 cm^{-1} . In conclusion, 2-Mo/ SiO_2 sulfide catalyst is more affected by sulfo-reductive treatment, discovering more total sites, than 1-Mo/ SiO_2 catalyst. For this reason, sites quantification after 2% $\text{H}_2\text{S}/\text{H}_2$ post-treatment was chosen as the optimum to study the MoS₂ morphology and the catalytic activity since this post-treatment gives closer information to real reaction conditions about the catalyst.

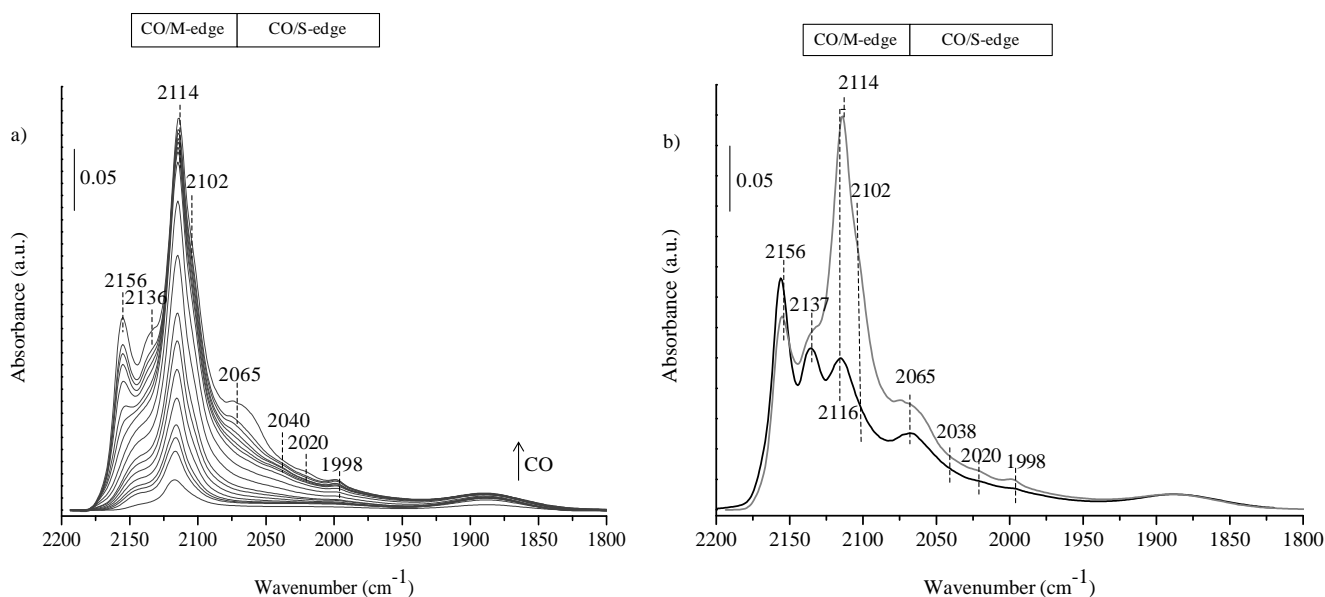


Figure V.8. IR spectra of CO adsorption on 2-Mo sulfide catalyst: a) introducing small CO doses up to saturation (equilibrium pressure, 133 Pa) after 2% $\text{H}_2\text{S}/\text{H}_2$ post-treatment and b) comparison CO equilibrium pressure after sulfidation (black line) and after 2% $\text{H}_2\text{S}/\text{H}_2$ post-treatment (grey line)

CO equilibrium spectra of the three sulfide catalysts are compared in Figure V.9. In the hydroxyl group zone, the band intensity decreases when the amount of Mo increase. This is in agreement to the increase of the coverage of the silica surface by oxomolybdate species. As for the sulfided phase band, they are strongly affected by the Mo amount. On 2-Mo/ SiO_2 , the CO/Mo bands are very strongly increased compared to 1-Mo/ SiO_2 . The band at 2065 cm^{-1} becomes now clearly visible. On 3-Mo/ SiO_2 catalyst, the CO/Mo band specific of M-edge sites present a lower intensity than on 2-Mo/ SiO_2 , whereas the intensity of the band at 2065 cm^{-1} has a similar intensity than that on this catalysts. The lower CO uptake on the MoS_2 phase of 3-Mo/ SiO_2 catalyst compared to 2-Mo/ SiO_2 catalyst account for a lower dispersion of the sulfided phase. This is in agreement with the high amount of MoO_3 crystallites detected on 3-Mo/ SiO_2 that accounts for a lower dispersion of the oxidic species. By contrast when well-dispersed oxo-Mo species are detected, the amount of sulfided edge detected is greater and depends on the Mo concentration of the catalyst.

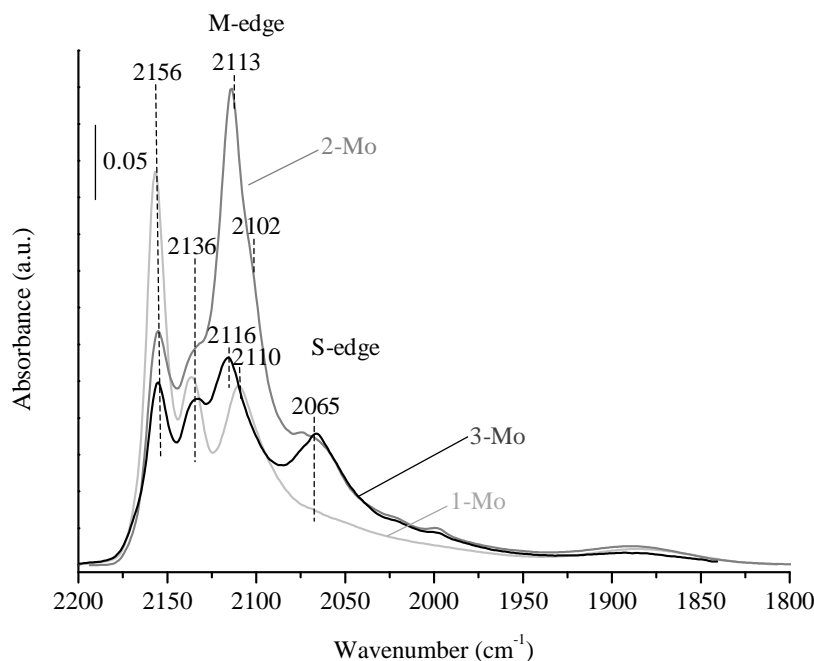


Figure V.9. Comparison of CO adsorption equilibrium (133 Pa) spectra on Mo/SiO₂ catalysts with different Mo loading after 2% H₂S/H₂ post-treatment

Mo sites quantification of the Mo/SiO₂ catalysts was performed after sulfidation and after 2% H₂S/H₂ post-treatment. The quantification is based on band area measurement after spectral decomposition and using the molar extinction absorption coefficient calculated by *Maugé et al.* [8] for Mo located on M-edge at 2110 cm⁻¹, and for Mo located on S-edge at 2065 cm⁻¹ calculated by *Chen et al.* [26]. The used coefficients were 16 ± 4 cm.μmol⁻¹ and 35 ± 4 cm.μmol⁻¹, for M-edge and S-edge respectively. The changes of intensity mentioned previously are shown in the calculated results on Table V-2. There is an increase on Mo sites concentration detected by IR/CO after 2% H₂S/H₂ post-treatment; this increase comes from the reduction of sulfur coverage on both M- and S-edge. However, the post-treatment shows higher effect in Mo on M-edge since sulfur coverage on S-edge was predicted to be more energetically stable than M-edge following DFT calculations. The order of the total Mo sites has the same order than the one discussed previously, 1-Mo < 3-Mo < 2-Mo. However, S-/M-edge ratio increases in the same order than Mo loading increases. The change of MoS₂ morphology with the increase of Mo loading was reported by *Chen et al.* [27] for Mo/Al₂O₃, where it was found that metal support interaction becomes weaker by the anchoring with neutral or less basic OH from alumina surface as surface metal concentration increases. Silica surface is formed by acid hydroxyl group, the before mentioned reasoning is unsatisfactory. For this, we propose to link the morphology change with the formation of Mo₇O₂₄⁶⁻

species. These species are characterized by higher size domain and are reported to be formed at higher metal concentrations [16].

Table V-2. Sites quantification for Mo/SiO₂ catalysts after sulfidation and after 2% H₂S/H₂ post-treatment by IR/CO

Catalysts	Conc. M-edge ($\mu\text{mol/g}$)	Conc. S-edge ($\mu\text{mol/g}$)	Total edge ($\mu\text{mol/g}$)	S-/M-edge ratio
After conventional sulfidation (10% H ₂ S/H ₂)				
1-Mo/SiO ₂	53	14	67	0.26
2-Mo/SiO ₂	59	26	85	0.44
3-Mo/SiO ₂	22	12	34	0.54
*After 2% H ₂ S/H ₂ post-treatment				
1-Mo/SiO ₂ *	60	14	74	0.23
2-Mo/SiO ₂ *	123	33	156	0.27
3-Mo/SiO ₂ *	67	28	95	0.42

5.3.2 Study of metal loading in promoted catalysts supported on silica

The study of Co promotion was carried out using silica as support. Firstly, Co promotion was studied for catalysts with different Mo density: 1 atom, 2 atoms, and 3 atoms Mo per nm², and constant Co/Co+Mo molar ratio equal to 0.3. The catalysts are named CoMo(1), CoMo(2) and CoMo(3) respectively. Secondly, Co promotion was studied keeping constant Mo amount (2 atoms Mo/nm² since it is the optimum value to get the highest Mo dispersion following the previous studies of non-promoted catalysts) and varying Cobalt molar ratio with Co/Co+Mo equal to 0.1, 0.2, 0.3, and 0.4. The catalysts are named (0.1)CoMo, (0.2)CoMo, (0.3)CoMo and (0.4)CoMo.

5.3.2.1 Catalytic activity for promoted silica catalysts – Thiophene HDS reaction

5.3.2.1.1 The effect of Mo loading in thiophene HDS reaction on promoted silica catalysts

The catalytic activity for CoMo catalysts supported on silica with different Mo density and constant Co/Co+Mo molar ratio were studied using Thiophene as model molecule for Hydrodesulfurization reaction (Figure V.10). The HDS rate increases in the order CoMo (1) < CoMo (2) < CoMo (3) i.e. with the increase of Mo density.

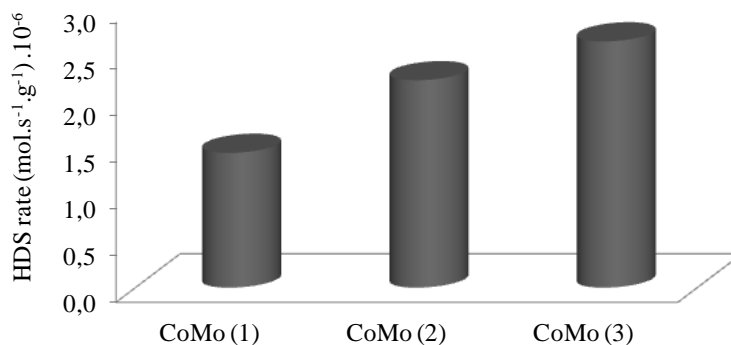


Figure V.10. HDS rate for CoMo catalysts supported on silica represented per gram of catalysts with different Mo density and constant Co/Co+Mo molar ratio

5.3.2.1.2 The effect of Co/Co+Mo molar ratio in thiophene HDS reaction on promoted silica catalysts

In addition, the study of the catalytic activity for CoMo catalysts with constant Mo density and variation of Co/Co+Mo molar ratio was also performed using Thiophene as model molecule for HDS reaction (Figure V.11). The highest catalytic activity was found for (0.2) CoMo catalyst, followed by (0.3) CoMo, (0.1) CoMo, and finally (0.4) CoMo catalysts.

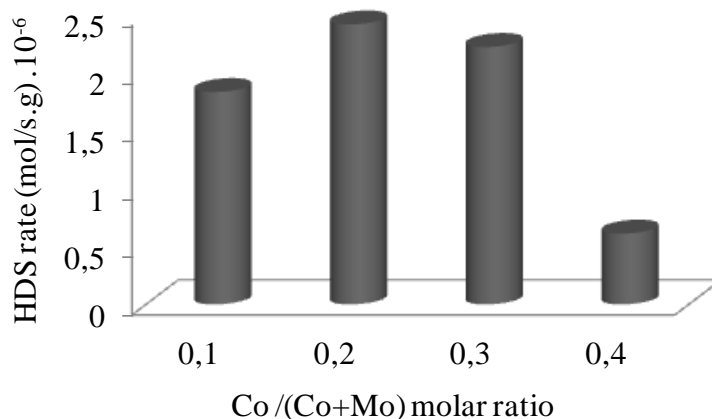


Figure V.11. Thiophene HDS rate for CoMo/SiO₂ catalysts with different Co/(Co+Mo) molar ratio and constant molybdenum density (2 atoms Mo per nm²)

5.3.2.2 Study of the metal loading effect in CoMoS formation by IR/CO

CoMoS site formation using silica as support has been studied by CO adsorption followed by FTIR spectroscopy (IR/CO). The two different series were studied: firstly, the CoMoS site formation with different Mo density and Co/Co+Mo ratio constant, and secondly, the CoMoS site formation with different Co/Co+Mo molar ratio and constant Mo density (2 atoms Mo/nm²).

5.3.2.2.1 Mo loading effect in CoMoS site formation

Since a change of MoS₂ morphology was detected for Mo/SiO₂ catalysts with different Mo density, the study of CoMoS site formation for CoMo/SiO₂ catalysts with different Mo density and constant Co/Co+Mo molar ratio was chosen to study the eventual preference of Co decoration on MoS₂ edges.

Figure V.12 shows IR spectra of CO adsorption from small CO doses up to site saturation for CoMo (1)/SiO₂ catalyst. Two different CO interaction domains are detected: CO interaction with the support and with the sulfide phase. The first domain presents two $\nu(\text{CO})$ bands at 2156 and 2134 cm⁻¹ ascribed to CO/OH stretching and $\nu(\text{CO})$ physisorbed, respectively. The second domain presents two different CO interactions, one at higher wavenumber with CO stretching range between 2090 and 2130 cm⁻¹, and another one with CO stretching range from 2000 to 2090 cm⁻¹. The CO stretching range at higher wavenumber is attributed to non-promoted Mo edge sites while the range at lower wavenumber is ascribed to promoted edge sites. For this CoMo (1)/SiO₂ catalyst, adsorption of CO on non promoted sites gives a band at 2114 cm⁻¹; instead adsorption of CO on promoted sites gives several contributions which are detected by the second derivative spectrum as shown in Figure V.12. Then, three principal components in the overlapping range are detected at 2059, 2073 and 2082 cm⁻¹. These bands and assignments are the same as the ones previously described for CoMo (3)/SiO₂ in the previous chapter (see chapter IV) except there is not the contribution of CO on Co₉S₈.

Figure V.13.a shows IR spectra of CO adsorption at site saturation on the three catalysts of the series. Surprisingly, the CoMo (2)/SiO₂ catalyst presents significantly lower band intensity for non-promoted sites than the two others catalysts even though the Co/Co+Mo molar ratio was the same.

Knowing the high sulfur coverage that can present edge sites on silica catalysts that limit the edge sites detection by IR/CO, H₂ post-treatment was performed for CoMo (2) catalyst to determine the sensibility of promoted catalyst towards sulfo-reductive conditions. Figure V.13.b shows the comparison between IR spectra of CO adsorption at equilibrium pressure after sulfidation treatment and after H₂ post-treatment. The band ascribed to non-promoted sites shows an increase in intensity, as well as a shift to lower wavenumber after H₂ post-treatment. Besides, the range of overlapping band ascribed to promoted sites shows an increase of intensity after H₂ treatment. On the other hand, the band shift detection for each component that form part of the overlapping bands ascribed to promoted sites is difficult; although, a band shift for the principal component can be detected from 2073 cm⁻¹ after sulfidation to 2070 cm⁻¹ after H₂ treatment.

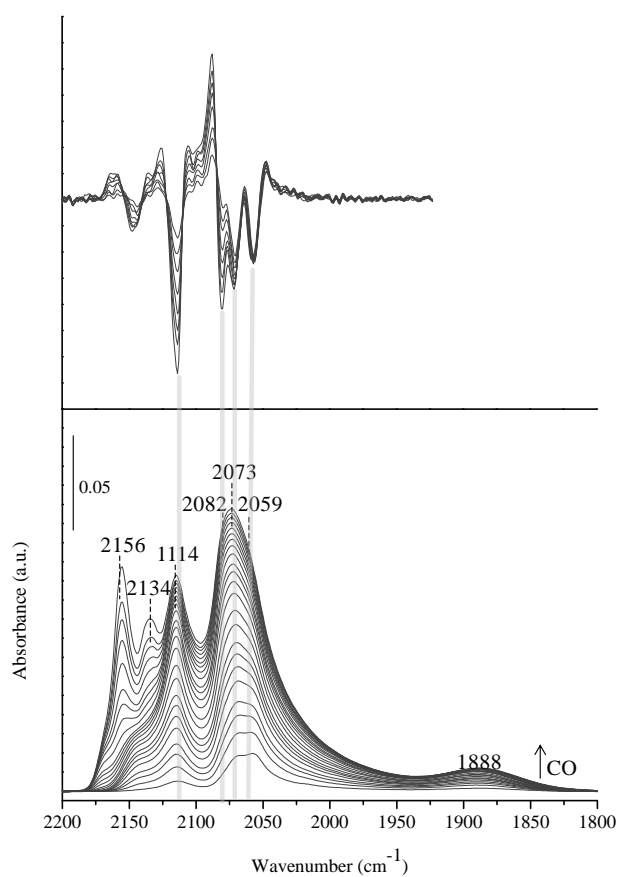


Figure V.12. IR spectra of CO adsorption from small CO pressures up to saturation using equilibrium pressure (133 Pa) for CoMo(1)/SiO₂ catalyst

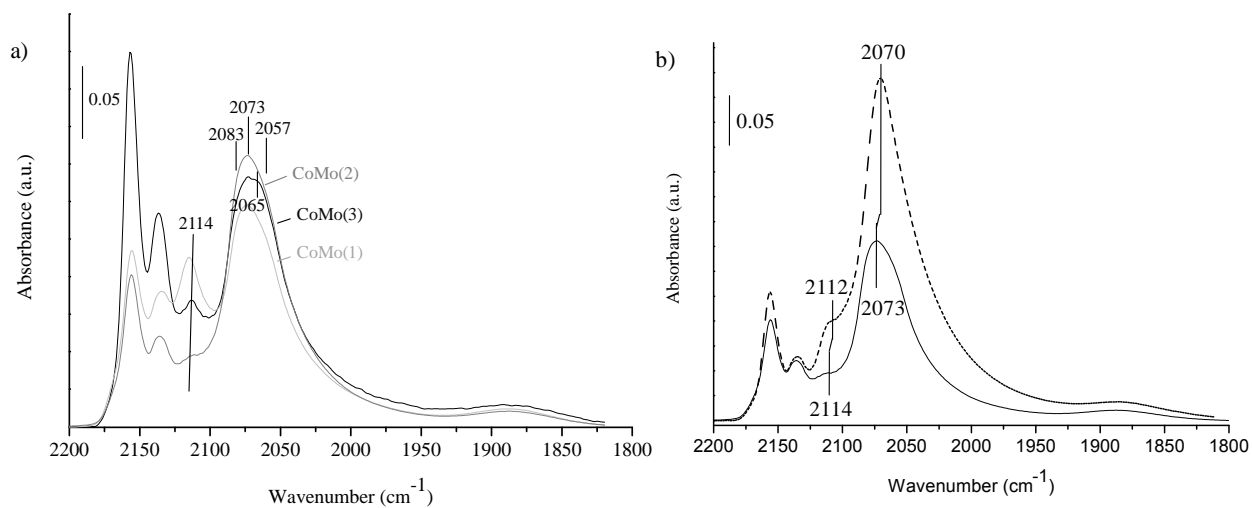


Figure V.13. CO/IR spectra at equilibrium pressure for CoMo/SiO₂ catalysts with 1, 2 and 3 Mo atoms/nm² (a), and for CoMo(2)/SiO₂ after sulfidation (full line) and after H₂ post-treatment (dotted line) (b)

Finally, CO saturated spectra of the three catalysts were decomposed and quantified using all components detected by the second derivative for each catalyst. Different molar adsorption coefficients were used to perform the calculation. Molar adsorption coefficient characteristic of M-edge sites was used for non-promoted sites due to non-promoted sites appear at the same wavenumber than M-edge sites, $16\pm 4 \text{ cm}\cdot\mu\text{mol}^{-1}$. Furthermore, another molar extinction coefficient was used for promoted sites using for all the components the same value, $43\pm 15 \text{ cm}\cdot\mu\text{mol}^{-1}$. Table V-3 summarises the sites quantification obtained for CoMo (1), CoMo (2) and CoMo (3), the total promoted site concentration is obtained making the sum of all components detected from 2020 to 2090 cm^{-1} , with the exception of the band around 2062/2065 cm^{-1} ascribed to Co_8S_9 species for CoMo (3).

Table V-3. Sites quantification for CoMo/SiO₂ catalysts with different Mo density (1, 2 and 3 Mo atoms per nm²)

Wavenumber (cm ⁻¹)	2059	2073	2083	Non-promoted sites	Promoted sites	Total sites	Promoted/non-promoted sites ratio
Concentration of sites ($\mu\text{mol/g}$)							
CoMo (1)	9	10	9	38	37	75	0.9
CoMo (2)	11	9	10	20	44	64	2.2
CoMo (3)	11	6	11	26	38	64	1.5

5.3.2.2.2 Co/Co+Mo molar ratio effect in CoMoS formation

Additionally, the study by IR/CO method of CoMoS site formation on CoMo catalysts was continued by the study of the series of CoMo catalysts supported on silica with variation of the Co/Co+Mo molar ratio at constant molybdenum density. Figure V.14.a shows IR spectra of CO adsorption at equilibrium pressure for CoMo/SiO₂ catalysts with Co/Co+Mo molar ratio equal to 0.1, 0.2 and 0.3 and molybdenum constant at 2 atoms Mo per nm². The three catalysts show the same stretching bands that can be classified in two different CO interaction domains: the CO interaction with the support and with the active sites. CO/OH stretching gives a band at 2156 cm^{-1} and it is accompanied by CO physisorbed at 2135 cm^{-1} . Active sites domain is constituted by non- and promoted sites. CO/non-promoted sites stretching vibration gives a band at 2116 cm^{-1} ascribed to M-edge sites without Co decoration. On the other hand, CO/promoted sites stretching vibration leads to a band overlapping range with components detected at 2059, 2073 and 2082 cm^{-1} . Figure V.14.b shows IR spectra of CO adsorption from small CO pressures up to saturation for (0.4) CoMo catalyst. The same CO interaction domains were detected for (0.4) CoMo catalyst than for the previous catalysts: CO interaction with the support and active sites. CO/OH stretching band is detected at 2156 cm^{-1} , as well as the νCO band at 2135 cm^{-1} ascribed to CO physisorbed. νCO /Non-promoted sites appears at 2112 cm^{-1} and is ascribed to M-edge

sites. The band overlapping ascribed to CO/promoted sites appears at the same wavenumber range than previously, from 2020 to 2090 cm^{-1} , and it is composed by several components detected by the second derivative at 2059, 2062, 2073 and 2085 cm^{-1} . Thus, one different component appears at 2062 cm^{-1} for (0.4) CoMo catalyst in comparison with the previous CoMo/SiO₂ catalysts formed by lower Co/Co+Mo molar ratio. This component can be ascribed to CO in interaction with Co₈S₉ species due to cobalt excess on the catalyst surface. In general, a decrease of sites are detected for this catalyst, it can be linked with cobalt sulfide formation. Since (0.3) CoMo catalyst did not show the presence of cobalt sulfide species, it can be considered as the limit of Co/Co+Mo molar ratio to start to form Co₈S₉ species on the surface.

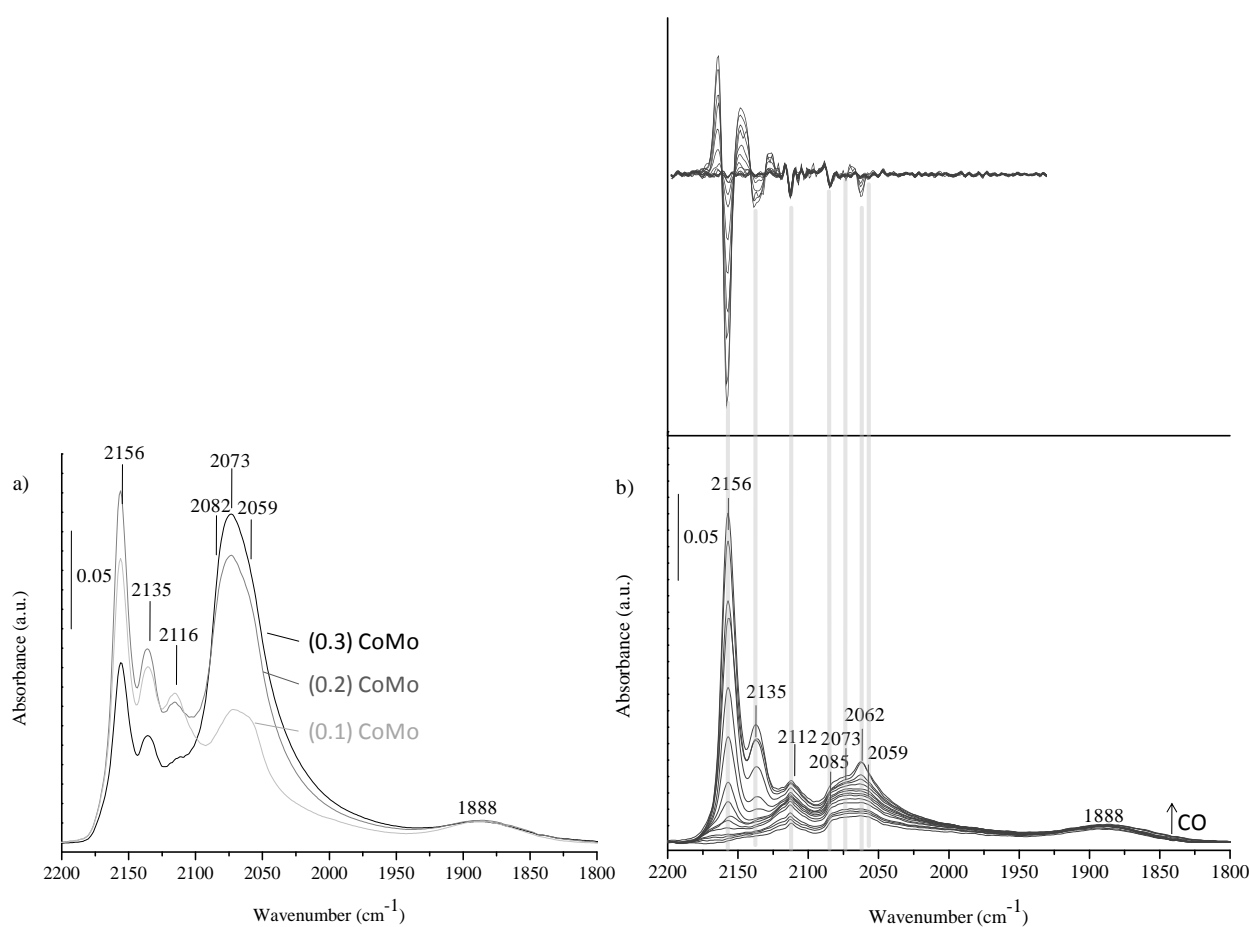


Figure V.14. a) IR/CO spectra at equilibrium pressure for CoMo/SiO₂ catalysts with Co/Co+Mo molar ratio equal to 0.1, 0.2, and 0.3 and 2 atoms Mo per nm² and b) IR/CO spectra from small CO pressure up to saturation for CoMo/SiO₂ catalyst with Co/Co+Mo molar ratio equal to 0.4 and 2 atoms Mo per nm²

Finally, CO saturated spectra of the three catalysts were decomposed and quantified using all components detected by the second derivative method for each catalyst. Table V-4 summarizes the sites quantification of non-, promoted and total sites, as well as the ratio of promoted over non-promoted sites. Molar extinction coefficient calculated by M-edge sites were used to non-promoted sites quantification ($16\pm 4 \text{ cm}\cdot\mu\text{mol}^{-1}$) and another one for promoted sites ($43\pm 15 \text{ cm}\cdot\mu\text{mol}^{-1}$); both coefficients were calculated by *Maugé et al* [25]. Note that (0.4) CoMo catalyst is not presented in the quantification since it is composed by Co/Co+Mo molar ratio above the optimum value before to form cobalt sulfide entities.

Table V-4. Quantification of sites for CoMo/SiO₂ catalysts with different Cobalt molar ratio (0.1, 0.2, and 0.3)

Wavenumber (cm ⁻¹)	2059	2073	2083	Non-promoted sites	Promoted sites	Total sites	Promoted/non-promoted sites ratio
Concentration of sites (μmol/g)							
(0.1) CoMo	6	5	3	32	19	51	0.6
(0.2) CoMo	11	11	9	29	40	69	1.4
(0.3) CoMo	11	9	10	20	44	64	2.2

5.4 Discussion

The effect of Mo loading in MoS₂ formation for non-promoted catalysts using silica as support was studied in detail in the present work. MoS₂ formation and its role in the catalytic activity have been studied by several techniques from oxide to sulfide molybdenum form, to obtain a general insight of the factors that influence the MoS₂ formation. A posterior study was performed for CoMo/SiO₂ catalysts in order to study the effect of metal loading variation, Mo or Co, in CoMoS sites formation and their role in HDS reaction.

5.4.1 Mo loading effect in Mo dispersion on silica surface

The study of metal dispersion was required in order to have a general view of the Mo loading effect in the oxomolybdate species since the Mo variation is reported to be a factor to form different oxomolybdate species [16]. Textural analysis of oxide catalysts were performed by the nitrogen adsorption method. The increase of metal amount on silica surface gave a decrease of the surface area available. This decrease of the surface area can be attributed to the small pore size characteristic of the silica used as support preventing Mo dispersion inside the pore. More detailed study was carried out by

Raman spectroscopy where two kinds of oxomolybdate species could be detected: MoO_3 and/or polymolybdate species. 1-Mo catalysts are formed by polymolybdate species that were detected in Raman spectrum with two principal vibration modes characteristic of these species: Mo=O terminal vibrational band at 955 cm^{-1} and Mo-O-Mo bridge vibrational band at 874 cm^{-1} . On the other hand, 2-Mo catalysts began to show MoO_3 species presented on the Raman spectrum characteristic by two principal vibration bands at 820 and 955 cm^{-1} ascribed to bridge and terminal vibration modes respectively; although this catalyst is mostly formed by polymolybdate species, which were detected in Raman spectrum by the same vibrational mode than 1-Mo catalyst. Finally, 3-Mo catalyst Raman spectrum is formed by band characteristic of both species: MoO_3 and polymolybdate. No difference was found for the vibration band positions compared to the previous catalysts. However some difference in band intensity ratio was detected for 3-Mo compared to 2-Mo catalysts for the vibration bands characteristic of MoO_3 species that leads to the prediction that 3-Mo catalysts are formed by larger MoO_3 species. All of this indicates the limit of the best Mo dispersion for silica catalysts is at 2 atoms of Mo per nm^2 . Additionally, UV-Vis spectroscopy was used to study the domain size of oxomolybdate species present on silica surface. The increase of metal present on the silica surface leads to a decrease of edge adsorption energy calculated from the UV-Vis spectrum. The decrease of adsorption energy is related with the increase of domain size. Edge adsorption energies were plotted with a relation line between edge adsorption energy and the nearest Mo neighbour using some oxomolybdate species as references. After the result obtained is plotted, it can be predicted that 3-Mo catalyst surface is composed by a mixture of MoO_3 and $\text{Mo}_7\text{O}_{24}^{6-}$ ion species, on the other hand, 1- Mo and 2-Mo catalysts surface are composed by a mixture of $\text{Mo}_7\text{O}_{24}^{6-}$ and $\text{Mo}_2\text{O}_7^{2-}$ species, being higher the presence of $\text{Mo}_7\text{O}_{24}^{6-}$ for 2-Mo catalyst than 1-Mo catalyst. These results are in agreement with Raman results.

5.4.2 Effect of Mo loading in sulfide Mo/SiO₂ catalysts

5.4.2.1 Effect of Mo loading in MoS₂ slabs morphology

CO adsorption at low temperature followed by FTIR spectroscopy was used to characterise non-promoted sulfide catalysts supported on silica. This technique allows a specific MoS₂ study since Mo located on M- and S-edge can be distinguished and quantified. Therefore, it gives rise to the study of MoS₂ morphology by the S-/M-edge ratio obtained by IR/CO method. Several studies were already performed modifying different factors involved in the MoS₂ morphology for Mo/Al₂O₃ catalysts such as the Mo loading [28–31]. Thus, the Mo loading effect on MoS₂ morphology was studied for non-promoted sulfide catalysts supported on silica by IR/CO method. The catalysts characterisation was performed after sulfidation and after 2% H₂S/H₂ post-treatment due to the last one is the reaction condition used to study

the HDS activity (Thiophene HDS). IR spectra after conventional sulfidation treatment showed the same CO stretching band for M- and S-edge sites on all Mo/SiO₂ catalysts independently of the Mo loading, i.e. the main ν CO band at 2113-2116 cm⁻¹ for M-edge sites and ν CO bands at 2065, 2040-2035 and 2020 cm⁻¹ for S-edge sites with different sulfur coverage. Previous study (see chapter III) showed the strong influence of the reductive post-treatment in the detection of sites by IR/CO. Hence, the 2% H₂S/H₂ post-treatment was performed for the two catalysts and it showed a strong effect on 2-Mo and weak for 1-Mo catalysts. The influence of the 2% H₂S/H₂ post-treatment was detected by an increase of band intensities ascribed to CO interaction on the edge sites and by a ν CO/M-edge band shift to lower wavenumber of 2 cm⁻¹ and the appearance of a band at 2102 cm⁻¹ for 2-Mo catalyst due to the decrease of sulfur coverage. The ν CO/S-edge site band did not show any shift indicating the high stability of these sites, and leading to conclude that M-edge sites are more sensitive to the environment conditions. The strong effect detected for 2-Mo catalyst leads to use the site concentration detected after this post-treatment since it is the most near to HDS thiophene reaction. In this way, the Mo loading effect in MoS₂ formation for Mo/SiO₂ catalysts is study by the edge site concentration detected by IR/CO as shows Figure V.15.a. The increase of Mo loading from 1 to 2 atoms Mo per nm² shows an increase in M- and S-edge site concentration, and indeed in total edge sites for Mo/SiO₂ catalysts. Moreover, the Mo loading increases from 2 to 3 atoms Mo per nm² shows a decrease of M-edge site and constant S-edge site concentration therefore the total site concentration decreases. Additionally, the increase of Mo loading shows a change in morphology detected by an increase of S-/M-edge ratio (Figure V.15.b). The change of morphology is more strongly observed for 3-Mo catalyst. The comparison between Mo/SiO₂ and Mo/Al₂O₃ shows that Mo/SiO₂ catalysts are formed by higher S-/M-edge ratio, even for low Mo loading, than Mo/Al₂O₃ catalyst [31], i.e. 12% wt Mo for Mo/Al₂O₃ gives S-/M-edge ratio equal to 0.20 while 7% wt Mo for Mo/SiO₂ gives S-/M-edge ratio equal to 0.23. It indicated that metal-support interaction is the main factor that influences the MoS₂ morphology. In conclusion, the Mo loading showed an effect in MoS₂ morphology, since higher Mo loading lead to higher S-/M-edge ratio on both Al₂O₃ and SiO₂. 2-Mo catalyst presents the highest total edge site concentration that is in relation with the optimum value to get the best Mo dispersion before to form MoO₃ species. The increase of Mo loading from 2 to 3 atoms Mo per nm² leads to observe a decrease of total edge site concentration that can be explained by the decrease of Mo dispersion forming MoO₃ species on the catalyst surface, by the increase of slab length and/or by the change of morphology to a truncated triangle with higher S-/M-edge ratio as was detected by IR/CO method leading to a decrease in Mo edge dispersion.

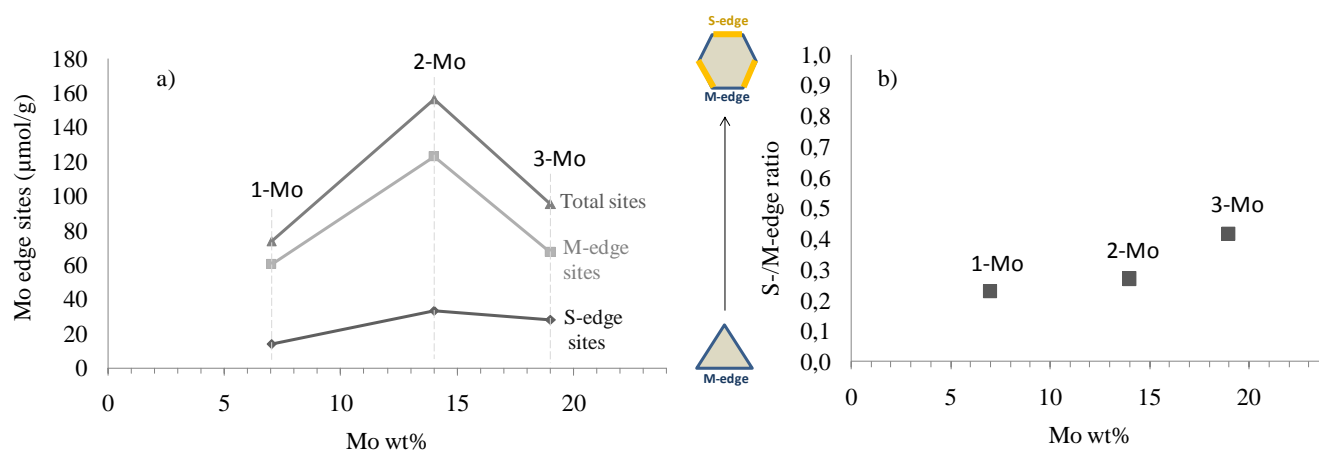


Figure V.15. a) Mo edge sites and b) MoS₂ morphology detected by IR/CO for Mo/SiO₂ after 2% H₂S/H₂ post-treatment with different Mo loading

5.4.2.2 Effect of Mo loading in the catalytic activity for HDS thiophene

The previous studies showed an effect of Mo loading in MoS₂ slab formation, i.e. Mo dispersion on the support, MoS₂ morphology, and the total available sites for reaction. Therefore, these differences induced by the effect of Mo loading have to be linked with the catalytic activity variation found in the series of catalysts. Thus, the study of Mo loading effect on HDS rate is performed by the representation of the HDS rate versus the total Mo edge site concentration for 1-Mo, 2-Mo and 3-Mo catalysts supported on silica as shows Figure V.16. Hence, a relation between the total Mo edge site concentration detected by IR/CO and HDS rate was found. 2-Mo catalyst, which presented the highest total Mo edge site concentration showed the highest catalytic activity followed by 3-Mo and 1-Mo catalysts. Therefore, the amount of sites available for reaction is the main factor involved in the catalytic activity. However, several factors can play in the amount of sites available for reaction as oxidic Mo species dispersion, MoS₂ morphology or slab length. In conclusion, when oxidic Mo species are well dispersed on the catalyst surface, the increase of Mo loading leads to an increase in total edge site concentration and then to an increase of catalytic activity. On the other hand, the too high increase of Mo loading giving a poor oxidic Mo species dispersion as was observed for 3-Mo catalyst, lead to a decrease of total edge site concentration and then to a decrease of catalytic activity.

Several studies reported that total edge site concentration and MoS₂ morphology are the main factors involved in HDS reaction [28,32]. Indeed, as previously mentioned, a relation between the total edge site concentration and thiophene HDS rate was obtained for the series of Mo/SiO₂ catalysts. In this case, the average TOF value for total edge sites obtained for the series of catalysts supported on silica was calculated to be 38 h⁻¹ (the value is obtained considering a linear equation passing by the origin and

taking into account the 3 points as shows in Figure V.16). However, some variation in the TOF values for each catalyst were detected giving rise to deduce that the proportion of M- and S-edge ratio can influence the catalytic activity. Thus, the series of Mo/SiO₂ catalysts with different Mo loading giving different S-/M-edge ratio were used to calculate the TOF values characteristic of each edge site, M- and S-edge considering that these values are the same for the three catalysts. The TOF in M-edge and TOF in S-edge denoted as TOF_{M-edge} and TOF_{S-edge} respectively, can be calculated by a linear regression using excel 2010, taking into account that both sites act individually to each other (see annex V). Thus, 18 h⁻¹ was calculated for TOF_{M-edge} and 103 h⁻¹ for TOF_{S-edge}. Note that the value of TOF_{M-edge} in silica catalysts is in the same range than the one reported for alumina catalysts, whereas the value of TOF_{S-edge} is greater for silica catalysts than for alumina catalysts [28]. Meanwhile, the higher TOF value for S-edge than for M-edge site is validated on SiO₂ catalysts. Some authors proposed that S-edge sites are involved in C-S bond cleavage whereas M-edge sites are involved in hydrogenation [33]. It could explain the high TOF value calculated by S-edge sites compared to M-edge sites. Thus, MoS₂ nanoparticles that adopt morphology near to perfect hexagon will obtain higher “total edge” TOF value due to the higher contribution of S-edge sites.

Finally, considering the products, the same product proportion was detected for 1- and 2-Mo/SiO₂ catalysts. However, 3-Mo/SiO₂ catalyst showed some variation of the product proportion compared with 1-Mo/SiO₂ and 2-Mo/SiO₂ catalysts, i.e. it favoured Butane formation. The preference for butane formation can be due to the presence of sulfide species coming from MoO₃ entities [34] presented on the surface.

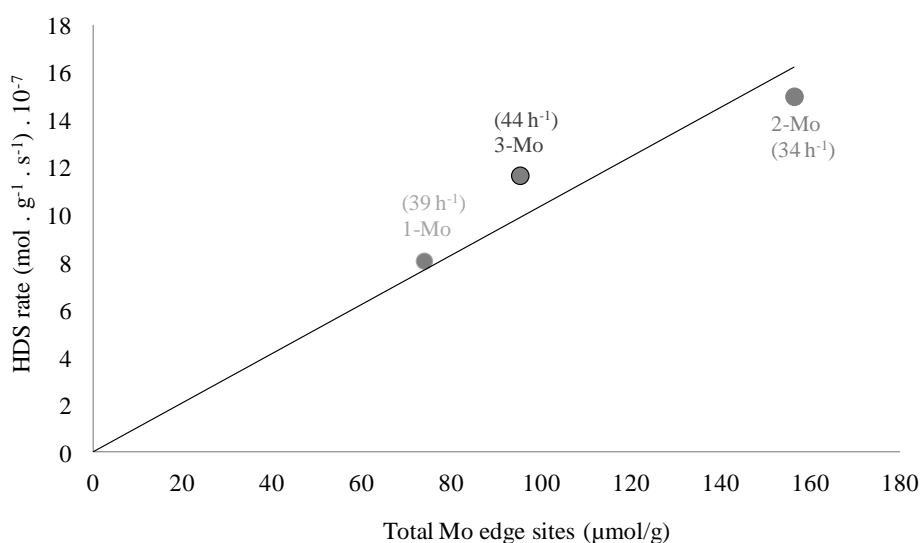


Figure V.16. Relation between thiophene HDS rate and total Mo edge site detected by IR/CO for Mo/SiO₂ catalysts. Note individual TOF values (h⁻¹) in parenthesis

5.4.3 Effect of metal variation in CoMoS sites supported on silica

5.4.3.1 Effect of Mo loading in CoMoS sites formation

The MoS₂ slab morphology was revealed as an important factor for CoMoS site formation in previous chapter (see chapter IV). Indeed, Co decoration is favoured on S-edge sites, although the relation found between the S-/M-edge ratio on the non-promoted catalyst and the promotion degree for the promoted catalyst leads to conclude that Co decorates both edge sites, M- and S-edge. Thus, it was shown that SiO₂ being the support with the lowest metal-support interaction leading to the highest S-/M-edge ratio on the non-promoted catalyst, it was the support leading to the highest promotion degree for the promoted catalyst. However, the Mo loading was also shown to be a factor that plays a role in the variation of MoS₂ morphology for Mo/Al₂O₃ and Mo/SiO₂ catalysts. Hence, the study of CoMoS site formation for CoMo/SiO₂ catalysts with different Mo density was performed in order to more carefully study the preference of Co decoration on the MoS₂ edges, M- and S-edge. Besides, the detection of MoO₃ species present on 3-Mo oxide catalyst surface leads to the requirement to know its influence in CoMoS site formation. Therefore, the effect of Mo loading variation in Co promotion was studied by IR/CO for the three catalysts with 1, 2 and 3 atoms Mo/nm². Two different CO adsorption domains can be distinguished in IR/CO spectra for the three catalysts: CO adsorbed on non- and promoted sites. All catalysts showed the same band position: a band at 2114 cm⁻¹ ascribed to vCO/non-promoted sites, which is characteristic of Mo located on M-edge site, and three components at 2057, 2073 and 2083 cm⁻¹ that formed the overlapping band detected for vCO/promoted sites. CoMo (3)/SiO₂ catalyst also showed one vCO band at 2065 cm⁻¹ that is ascribed to cobalt sulfide species. The edge site concentration variation with the Mo loading is shown in Figure V.17.a. Thus, the increase from 1 to 2 atoms Mo per nm² showed an increase of promoted sites and a decrease of non-promoted sites leading to a decrease of total edge sites. Then, the further increase, i.e. from 2 to 3 atoms Mo per nm², leads to an increase of non-promoted site concentration coming from the sulfidation of MoO₃ entities [34] and a decrease of promoted site concentration due to that the sulfide species from MoO₃ entities do not interact with cobalt. The effect of the increase of dispersed Mo amount leading to an increase of promoted sites followed by a decrease of non-promoted sites was already observed previously for CoMo/Al₂O₃ catalysts [35]. However, in this work we observe that the presence of MoO₃ or Co₂O₃ entities can also affect CoMoS sites formation. Following the theory that CoMoS sites are formed by the decoration of MoS₂ nanoparticle edges, the Co affinity for M- or S-edge can tentatively be studied by the comparison of the promotion degree with the S-/M-edge ratio detected in non-promoted catalyst as shows Figure V.17.b. The preference of Co promotion on S-edge sites is detected for CoMo (1)/SiO₂ and CoMo (2)/SiO₂ catalysts as was detected for the previous study since the higher the S-/M- ratio, the higher the promotion degree. However, the

comparison between the promotion degree (promoted/non-promoted sites ratio) and the S-/M-edge ratio lead also to conclude that cobalt decorates both sites, M- and S-edge, since the promotion degree is always higher than the S-/M- ratio. However, CoMo(3) /SiO₂ catalyst showed again a special behaviour ascribed to the presence of MoO₃ species in the oxide form of the catalyst, i.e. this catalyst presented a decrease of promotion degree compared to CoMo (2) catalyst while the MoS₂ nanoparticles are formed by higher S-/M-edge ratio.

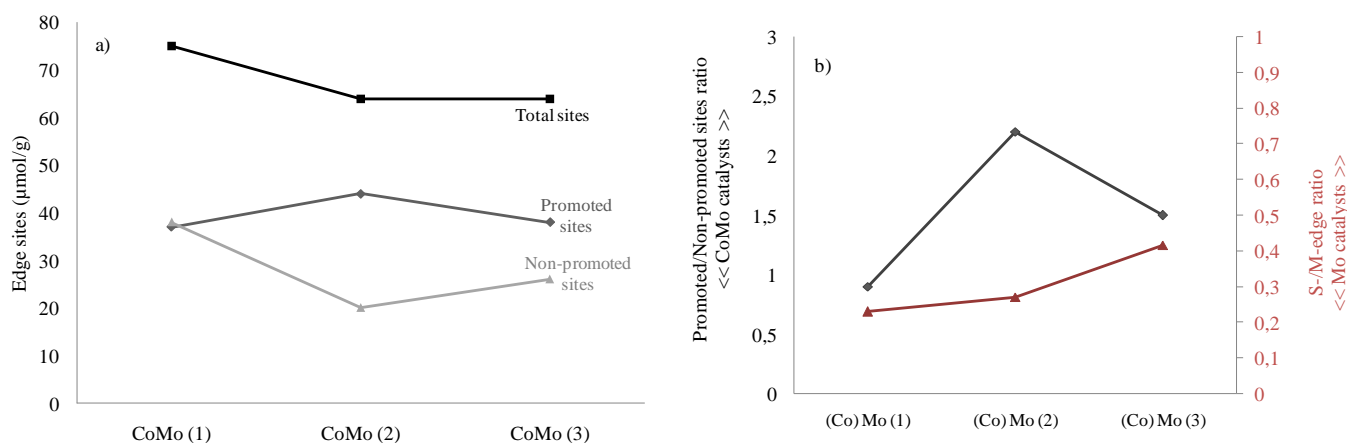


Figure V.17. a) Edge sites from CoMo catalysts and b) relation between S-/M-edge ratio from Mo/SiO₂ catalysts and Promoted/Non-promoted sites ratio from CoMo/SiO₂ catalysts with variation of Mo density (1, 2 and 3 atoms Mo/nm²)

Following that the presence of MoO₃ entities of the catalyst in oxidic form lead to a decrease of CoMoS site formation of the sulfide catalyst, the CoMo (3) catalyst is not considered for the Co localization study. Therefore, the Co localization for CoMo (1), CoMo (2) were carried out by some calculations taking in consideration the band attributions for the three components detected in promoted CO stretching range and discussed in the previous chapter (see chapter IV). Concretely, the components appeared for all catalysts at 2057, 2073 and 2083 cm⁻¹ ascribed to partially promoted S-edge site, partially and totally promoted M-edge site, respectively. Note that the H₂ post-treatment performed for CoMo (2) catalyst revealed that the component at 2073 cm⁻¹ is really sensible to reductive treatment indicating that the correct assignment of this component to M-edge site since this site showed to be strongly affected by reductive treatment. Table V-5 shows the summary of these calculations for the three catalysts, i.e. CoMo (1), CoMo (2) and CoMo (3), where, indeed, the calculations for CoMo (3)/SiO₂ catalyst do not match since the presence of MoO₃ acts as artefact. Total cobalt sites that are decorating MoS₂ edges increase for catalysts from 1 to 2 atoms Mo/nm², and as was predicted by νCO band intensity, a decrease for CoMo (3)/SiO₂ catalyst is detected. The morphology was predicted as shows Table V-5, thus an increase of S-/M-edge ratio is detected by the Co addition, as well as this increase is detected higher for CoMo (2) than for CoMo (1) catalysts. The change in morphology by the Co addition was already detected by STM

studies that detected a change from triangle to truncated triangle by the Co addition to MoS₂ nanoparticles supported on Au (111) [36]. Then, the preference of Co localization is studied by the calculation of the Co on S-edge sites amount for CoMo catalysts and it is compared with the Mo on S-edge amount detected on Mo catalysts. Thus, considering only catalysts with good metal dispersion, i.e. CoMo (1) and CoMo (2), a higher concentration of Co located on S-edge is detected compared to Mo on S-edge. This increase of Co concentration after the Co introduction showed the preferential decoration on S-edge. This preferential decoration on S-edge is in agreement with STM image where showed that the Co addition to MoS₂ nanoparticles supported on Au (111) just decorated S-edge indicating preferential decoration of this edge.

Table V-5. Summary of the effect of Mo density variation in the Co localization on CoMoS site

Catalysts	Co sites in CoMoS by IR/CO (μmol/g)	S-/M-edge ratio for CoMo catalysts	S-/M-edge ratio for Mo catalysts	Co _{S-edge} /Co sites ratio for CoMo catalysts	Mo _{S-edge} /Mo _{S-edge} +Mo _{M-edge} ratio for Mo catalysts
CoMo(1)/SiO ₂	28	0.32	0.23	0.32	0.19
CoMo(2)/SiO ₂	30	0.64	0.27	0.37	0.21
CoMo(3)/SiO ₂	28	0.49	0.42	0.39	0.29

5.4.3.2 Effect of Co/Co+Mo molar ratio on CoMoS sites formation

The effect of Co addition in CoMoS sites formation has been studied by several researchers for CoMo/Al₂O₃ catalysts [35]. Thus, the addition of increasing Co/Co+Mo molar ratio is reported to lead to an increase of the promotion degree. The optimum Mo amount to get Mo totally dispersed was previously detected to be 2 atoms Mo/nm² for Mo/SiO₂ catalysts, so the study of the effect of Co/Co+Mo ratio was performed for this Mo loading. For that, CoMo/SiO₂ catalysts constituted by 0.1, 0.2, 0.3 and 0.4 Co molar ratio were studied by IR/CO. All catalysts showed two different CO adsorption ranges, one attributed to non-promoted sites and another one to promoted sites. All of them presented the same νCO band position: non-promoted sites at 2116 cm⁻¹ ascribed to Mo located on M-edge sites, and three components on promoted sites at 2059, 2073 and 2082 cm⁻¹ ascribed to partially promoted S-edge, partially and totally promoted M-edge, respectively. However, (0.4) CoMo/SiO₂ catalyst showed another component at 2062 cm⁻¹ ascribed to cobalt sulfide species that appeared due to the increase of cobalt loading. Since Co₉S₈ formation was detected for this last catalyst indicating the limit level of Co addition is 0.3, this catalyst is not further considered in the study. Therefore, edge sites concentration detected by IR/CO for the three others catalysts, i.e. (0.1), (0.2) and (0.3) CoMo catalysts, are summarized in Figure V.18.a. The cobalt addition leads to the increase of promoted sites in parallel to the decrease of non-promoted sites. Meanwhile, Co addition increases the promotion degree as shows Figure V.18.b.

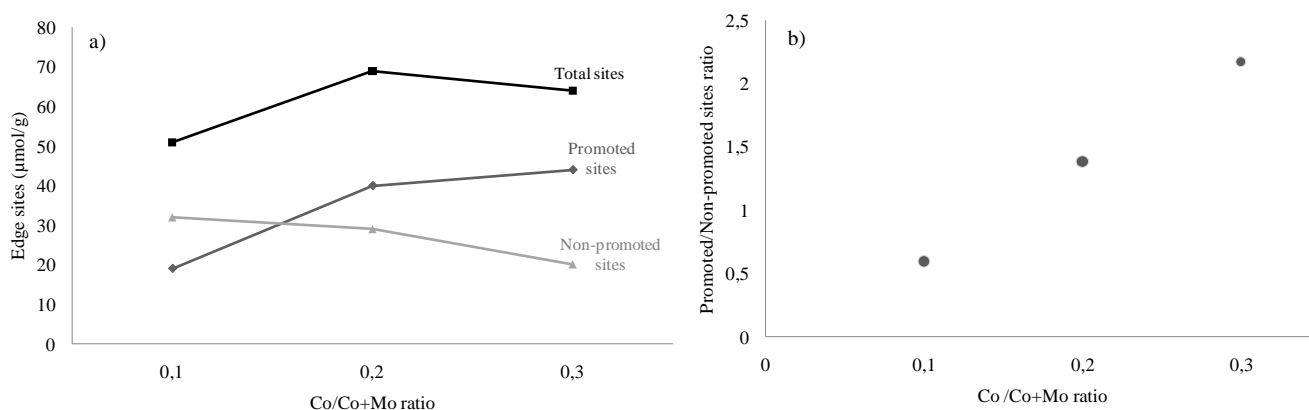


Figure V.18. Comparison the variation of Co molar ratio with a) edge sites and b) promotion degree detected by IR/CO for (0.1), (0.2) and (0.3) CoMo/SiO₂ sulfide catalysts

The sites quantification allows a detailed study about the Co decoration of MoS₂ edges by the variation of Co concentration on the catalysts. Indeed, the three components detected by the second derivative method that are present in the band overlapping range of νCO/ promoted sites, are represented in Figure V.19 for different Co/Co+Mo molar ratios. Therefore, the increase of Co/Co+Mo molar ratio from 0.1 to 0.2 leads to observe an increase of the three components at the same time, recording the lower concentration for the component at 2083 cm⁻¹ that is ascribed to M-edge sites totally promoted by Co on M-edge. The comparison between the CoMo/SiO₂ catalysts with 0.2 and 0.3 Co/Co+Mo molar ratio is an essential point to understand Co decoration. The influence of the increase of Co amount is visible for the two components ascribed to Co located on M-edge sites, i.e. M-edge partially promoted, 2073 cm⁻¹ and totally promoted, 2083 cm⁻¹. On the other hand, no variation is detected for the component at 2057 cm⁻¹ that is ascribed to S-edge sites partially promoted by Co. The increase of Co present on catalyst surface shows an increase of totally promoted M-edge sites, which is related to a decrease of the partially promoted M-edge sites. It indicates again that the component at 2073 and 2083 cm⁻¹ are related and verify the attribution proposed in chapter IV.

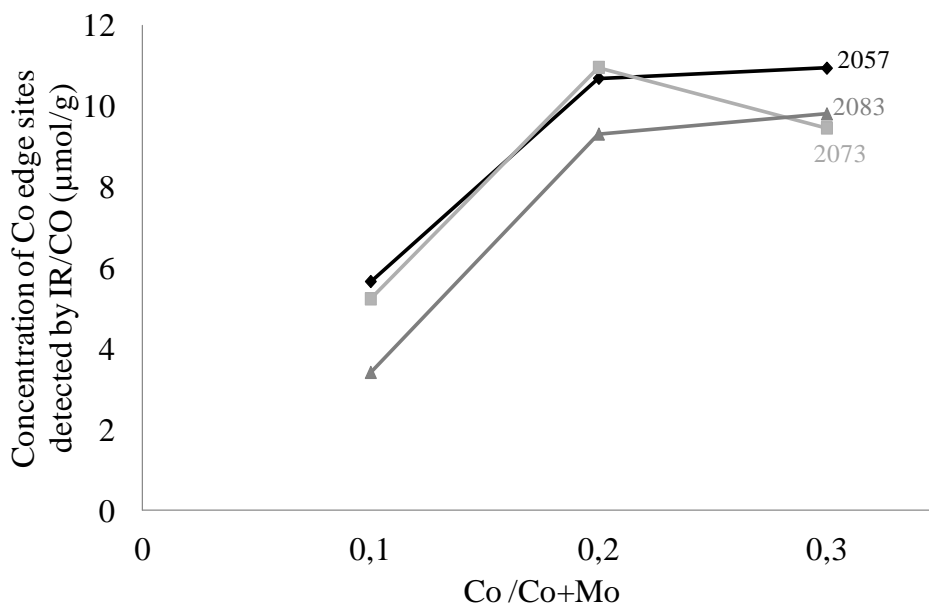


Figure V.19. Representation of the three components detected by the second derivative that compose the stretching CO band overlapping characteristic of promoted sites for CoMo/SiO₂ catalysts by different Co concentration

Therefore, the effect of the increase of cobalt amount on the Co promotion and/or localization for CoMo/SiO₂ catalysts can be studied taking into account the components attributions realised by 2057, 2073 and 2083 cm⁻¹ as Co partially promoted on S-edge sites, Co partially promoted on M-edge and Co totally promoted on M-edge, respectively. Thus, several calculations were performed as shows

Table V-6. Then, the Co amount on CoMoS site increase when the Co molar ratio increase from 0.1 to 0.2, however the increase from 0.2 to 0.3 did not show any modification. Thus, 0.2 Co molar ratio can be consider as the optimum value to CoMoS formation sites for CoMo/SiO₂ catalysts. On the other hand, the morphology was predicted showing an increase of S-/M-edge ratio when the Co molar ratio increase. Finally, the Co localization was studied by the calculation of the Co amount located on S-edge sites. Interestingly, the (0.1) CoMo catalyst showed higher Co proportion on S-edge than the others two catalysts. This increase of proportion showed the preferential Co decoration to S-edge, since the increase of Co loading showed to have more Co located on M-edge than in S-edge.

Table V-6. Summary of Co promotion study for CoMo/SiO₂ catalysts composed by 2 atoms Mo/nm² and 0.1, 0.2 and 0.3 of Co/Co+Mo ratio, as well as Mo/SiO₂ catalyst with 2 atoms Mo/nm²

Catalysts	Co sites in CoMoS by IR/CO (μmol/g)	S-/M-edge ratio for CoMo catalysts	Co _{S-edge} / Co sites ratio for CoMo catalysts	Mo _{S-edge} / Mo _{S-edge} +Mo _{M-edge} ratio for Mo catalyst
2-Mo/SiO ₂	-	0.27	-	0.21
(0.1)CoMo/SiO ₂	14	0.28	0.43	-
(0.2)CoMo/SiO ₂	31	0.41	0.36	-
(0.3)CoMo/SiO ₂	30	0.64	0.37	-

5.4.3.3 Effect of metal variation in the catalytic activity for HDS thiophene

Different CoMoS sites have been detected by the variation of the metal amount, Mo or Co. This different CoMoS sites depend on the Co localisation and promotion degree detected for CoMo/SiO₂ catalysts studied by IR/CO. Since the main factor involved in the catalytic reaction is the total edge sites amount available to be in interaction with reaction molecule, the effect of total edge sites in catalytic activity for CoMo/SiO₂ catalyst with different Mo density can be studied by the comparison of HDS rate and total edge sites detected by IR/CO as shows Figure V.20. Thus, no linear relation is found between the HDS rate and promoted edge site concentration, since the catalytic activity increases with the increase of Mo loading and promoted sites showed a decrease from 2 to 3 atoms Mo per nm². It indicates again that CoMo (3) catalyst showed a specific behaviour. Then HDS rate can be compared with the promoted sites amount when the metal is found well dispersed on the surface as CoMo (1) and CoMo (2) catalysts. In conclusion, higher Co promotion leads to higher catalytic activity for CoMo/SiO₂ catalysts with good metal dispersion, i.e. for CoMo (1) and CoMo (2) catalysts.

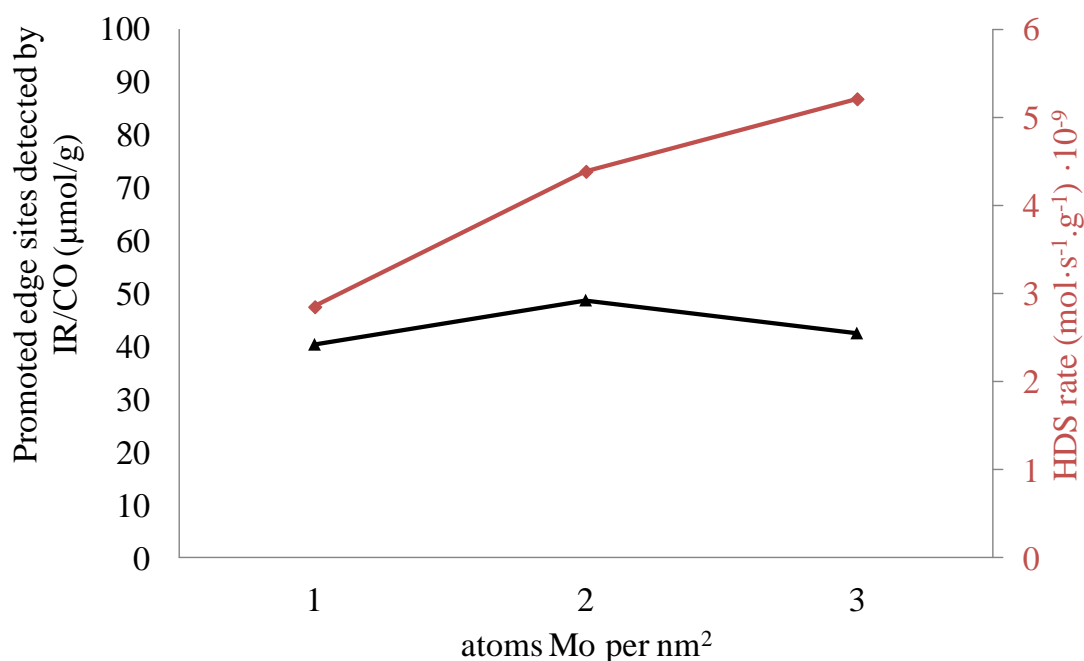


Figure V.20. Relation between catalytic activity and total sites or promoted sites detected by IR/CO

The Co loading variation was also studied to understand the Co preferential decoration on M- or S-edge site and thus, study the optimum amount of Co to obtain the highest active CoMoS sites for CoMo/SiO₂ catalysts. Figure V.21 compares HDS rate and promoted site concentration detected by IR/CO for CoMo/SiO₂ catalysts formed by different Co/Co+Mo molar ratio equal to 0.1, 0.2 and 0.3. The highest HDS rate was detected for (0.2) CoMo catalyst, however the highest promoted site concentration was detected for (0.3) CoMo catalyst leading to conclude that no clear relation exists between promoted site concentration and catalytic activity. Then looking forward, i.e. Co localization in MoS₂ edges, a relation could be found between the CoMoS sites nature and HDS rate. Thus, (0.2) CoMo catalyst presented the highest proportion of partially promoted M-edge sites (Figure V.19) indicating that the high proportion of this site in CoMo catalysts lead to high catalytic activity. This behaviour was already detected in the previous chapter (chapter IV). In conclusion, the CoMoS site formation with more proportion of Co partially promoted sites can lead to form more active sites for HDS reaction.

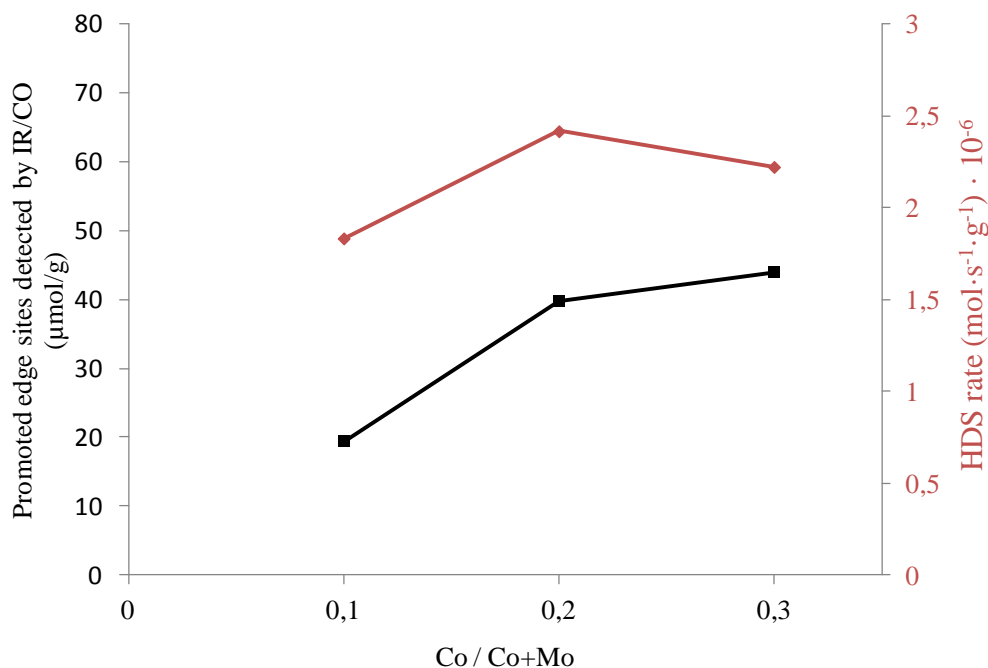


Figure V.21. Comparison between catalytic activity and total and promoted sites detected by IR/CO for CoMo/SiO₂ catalysts formed by 2 atoms Mo/nm² and 0.1, 0.2, and 0.3 of Co/Co+Mo molar ratio

5.5 Conclusion

The Mo loading effect on MoS₂ formation has been studied in detail for non-promoted catalysts supported on silica. Different MoS₂ morphologies were detected: the higher the Mo loading the higher the S-/M-edge ratio as detected by IR/CO method. The optimum Mo dispersion was found below 2 atoms Mo/nm². Consequently catalysts composed by Mo loading above this concentration showed a decrease in total active site concentration and then a decrease of catalytic activity. As a first approximation, a linear relation was found between total edge site concentration and thiophene HDS rate. However, slightly different “total edge” TOF values were calculated for the three catalysts revealing that an increase of S-/M-edge ratio leads to an increase of TOF values. Then, different TOF values for M-edge sites and S-edge sites on SiO₂ were calculated, the one for S-edge sites being higher than the one for M-edge sites in accordance with previous results on Al₂O₃. The study was continued by promoted catalysts varying the metal amount presented on the catalyst surface. The goal to study different Mo loading in CoMo catalysts was the detection of the preferential Co decoration on S- or M-edges. For that, a comparison between the morphology obtained for Mo catalysts and the promotion degree for CoMo catalysts was carried out giving the conclusion that for catalysts formed by Mo oxidic species well dispersed on the surface the increase of Mo loading lead to an increase of promotion degree. Thus, it was found for CoMo (1) and CoMo (2) that Co decorates both, M- and S-edge. On the other hand, CoMo (3) showed a specific behaviour due to the presence of MoO₃ species in the oxidic form and cobalt sulfide species in the sulfide

form. Finally, CoMo/SiO₂ catalysts with different Co/Co+Mo molar ratio (0.1, 0.2, 0.3 and 0.4) and constant Mo amount (2 atoms Mo per nm²) were studied. The optimum Co/Co+Mo molar ratio to get the higher catalytic activity was 0.2. The increase of Co/Co+Mo to 0.3 molar ratio lead to obtain more totally promoted M-edge sites leading to a decrease of the activity in comparison with the ratio of 0.2. Thus, the highly active CoMoS sites were ascribed to partially promoted M-edge sites. It is in accordance with the explanation given previously in chapter IV.

5.6 References

- [1] B. Pawelec, J.L.G. Fierro, A. Montesinos, T.A. Zepeda, *Appl. Catal. B Environ.* 80 (2008) 1–14.
- [2] T.A. Zepeda, B. Pawelec, J.L.G. Fierro, T. Halachev, *J. Catal.* 242 (2006) 254–269.
- [3] J. Ramírez, R. Contreras, P. Castillo, T. Klimova, R. Zárate, R. Luna, J. Ramírez, R. Contreras, P. Castillo, T. Klimova, *Appl. Catal. A Gen.* 197 (2000) 69–78.
- [4] E.M. Rivera-Muñoz, R. Huirache-Acuña, *Int. J. Mol. Sci.* 11 (2010) 3069–3086.
- [5] R. Huirache-Acuña, R. Nava, C. Peza-Ledesma, J. Lara-Romero, G. Alonso-Núñez, B. Pawelec, E. Rivera-Muñoz, *Materials (Basel)*. 6 (2013) 4139–4167.
- [6] V. La Parola, G. Deganello, A.M. Venezia, *Appl. Catal. A Gen.* 260 (2004) 237–247.
- [7] U.T. Turaga, C. Song, 86 (2006) 129–140.
- [8] F. Luck, 100 (1991) 781–800.
- [9] Y. Okamoto, M. Breysse, G.M. Dhar, C.S. Song, *Catal. Today* 86 (2003) 1–3.
- [10] V. La Parola, G. Deganello, C.R. Tewell, A.M. Venezia, *Appl. Catal. A Gen.* 235 (2002) 171–180.
- [11] G. Magendie, B. Guichard, A. Chaumonnot, A.A. Quoineaud, C. Legens, D. Espinat, *Appl. Catal. A Gen.* 468 (2013) 216–229.
- [12] A.S. Walton, J. V Lauritsen, H. Topsoe, F. Besenbacher, *J. Catal.* 308 (2013) 306–318.
- [13] M. Fournier, C. Louis, M. Che, P. Chaquin, D. Masure, *J. Catal.* 119 (1989) 400–414.
- [14] R.S. Weber, *J. Catal.* 151 (1995) 470–474.

- [15] J. Chen, Effet de La Pression de Sulfuration et D'agent Chélatant Sur La Morphologie et La Réactivité Des Phases Sulfures, 2014.
- [16] I.E. Wachs, *Catal. Today* 27 (1996) 437–455.
- [17] J.G. and J.P.B. S. KASZTELAN, E. PAYEN, H. TOULHOAT, *Polyhedron* 5 (1986) 157–167.
- [18] N. Chestnoy, R. Hull, L.E. Brus, *J. Chem. Phys.* 85 (1986) 2237.
- [19] L. Brus, *J. Phys. Chem.* 90 (1986) 2555–2560.
- [20] N. López, F. Illas, G. Pacchioni, *J. Mol. Catal. A Chem.* 170 (2001) 175–186.
- [21] J. Brito, amp, x, L. n, B. Griffe, *J. Mol. Catal. A Chem.* 214 (2004) 249–251.
- [22] J. Rasko, J. Kiss, *Appl. Catal. a-General* 253 (2003) 427–436.
- [23] V. Labruyere, *Structure Des Sites Sulfures Des Catalyseurs D'hydrotraitement: Approche Combinee Par Spcetroscopie IR et Modelisation Moleculaire*, Universite of Caen, 2014.
- [24] A. Travert, C. Dujardin, F. Mauge, S. Cristol, J.F. Paul, E. Payen, D. Bougeard, *Catal. Today* 70 (2001) 255–269.
- [25] F. Mauge, J.C. Lavalley, *J. Catal.* 137 (1992) 69–76.
- [26] J. Chen, E. Dominguez Garcia, L. Oliviero, F. Maugé, *J. Catal.* 332 (2015) 77–82.
- [27] J. Chen, L. Oliviero, X. Portier, F. Maugé, (2015).
- [28] J. Chen, F. Maugé, J. El Fallah, L. Oliviero, *J. Catal.* 320 (2014) 170–179.
- [29] J. Chen, E. Dominguez Garcia, E. Oliviero, L. Oliviero, F. Maugé, *J. Catal.* 339 (2016) 153–162.
- [30] J. Chen, V. Labruyere, F. Mauge, A.-A. Quoineaud, A. Hugon, L. Oliviero, *J. Phys. Chem. C* 118 (2014) 30039–30044.
- [31] J. Chen, L. Oliviero, X. Portier, F. Maugé, *RSC Adv.* 5 (2015) 81038–81044.
- [32] C. Dujardin, M.A. Lélias, J. van Gestel, A. Travert, J.C. Duchet, F. Maugé, *Appl. Catal. A Gen.* 322 (2007) 46–57.
- [33] P.G. Moses, B. Hinnemann, H. Topsoe, J.K. Norskov, *J. Catal.* 248 (2007) 188–203.

- [34] J.W. Weber, T.; Muijsers, J.C.; Van Wolput, J.H.M.C.; Verhagen, C.P.J.; Niemantsverdriet, J. *Phys. Chem.* (2017).
- [35] C. Dujardin, M.A. Lelias, J. van Gestel, A. Travert, J.C. Duchet, F. Mauge, *Appl. Catal. A Gen.* 322 (2007) 46–57.
- [36] F. Besenbacher, M. Brorson, B.S. Clausen, S. Helveg, B. Hinnemann, J. Kibsgaard, J. Lauritsen, P.G. Moses, J.K. Nørskov, H. Topsøe, *Catal. Today* 130 (2008) 86–96.

Table of contents – VI Chapter

VI.	CHAPTER.....	189
6.1	Introduction	190
6.2	Experimental	191
6.3	Results	192
6.3.1	Monometallic oxide catalysts study by Raman and UV-Vis Spectroscopies	192
6.3.2	Sulfide catalysts.....	196
6.3.2.1	Catalytic activity	196
6.3.2.1.1	Non-promoted catalysts	197
6.3.2.1.2	Promoted catalysts	197
6.3.2.2	Active sites study by IR/CO	198
6.3.2.2.1	Effect of pre-treatments on the MoS ₂ phase formation	198
6.3.2.2.2	CO adsorption on Co-promoted sulfide catalysts.....	202
6.4	Discussion	206
6.4.1	Effect of pre-treatments on MoS ₂ formation.....	206
6.4.1.1	Effect on the nature of the oxidic phase.....	206
6.4.1.2	Effect of pre-treatment on the MoS ₂ morphology	207
6.4.1.3	Effect of pre-treatment on the sulfide sites amount	208
6.4.1.4	Effect of pre-treatment on the HDS activity	209
6.4.2	The effect of pre-treatments on CoMoS sites formation.....	210
6.4.2.1	Effect of pre-treatment on the sulfide sites formation	210
6.4.2.2	Effect of pre-treatments on the sulfide sites formation of silica catalysts	211
6.4.2.3	Effect of pre-treatment on the structure of CoMoS sites	212
6.4.2.4	Effect of pre-treatment on the HDS activity	213
6.5	Conclusion.....	215
6.6	References	216

VI. CHAPTER

DRYING AND CALCINATION EFFECT ON THE STRUCTURE AND ACTIVITY OF SULFIDED (Co)Mo CATALYSTS

Abstract: The effect of the pretreatments performed before the sulfidation stage were studied in order to determine their influence on the sulfide sites formation of (Co)Mo catalysts supported on Al₂O₃, SiO₂ or TiO₂. A series of catalysts were prepared by wetness impregnation method keeping constant Mo amount (3 atoms Mo/nm²) and with addition of cobalt with a molar ratio of Co/(Mo + Co) = 0.3. A detailed study was performed on the impact of drying and calcination on the species formed on oxide and sulfide non-promoted and promoted catalysts. At the oxidic stage, the strongest effects were observed for Mo/SiO₂ catalyst since Mo was found well-dispersed on dried Mo/SiO₂ catalyst while on calcined catalyst MoO₃ crystallites were detected. Finally, the morphology of the MoS₂ particles was characterized measuring the S-/M-edge ratio using IR/CO method. For the sulfided Mo/Al₂O₃ and Mo/TiO₂ catalysts, no changes in MoS₂ morphology were detected on dried or calcined samples. By contrast, dried Mo/SiO₂ catalysts showed MoS₂ nanoparticles with higher S-/M-edge ratio than the calcined catalyst. Total Mo edge sites were found as the principal factor influencing the thiophene HDS activity. Thus, the highest active sites concentration detected by IR/CO corresponds to the highest catalytic activity. The highest catalytic activity was detected for Mo/TiO₂, followed by Mo/Al₂O₃ and Mo/SiO₂.

On the other hand, stronger variations with the pre-treatment condition were reported for CoMoS sites formation. An improvement of the promotion degree is observed on dried CoMo/SiO₂ catalyst that can be related to the increase of Mo dispersion on the oxidic state. By contrast, calcination stage favors CoMoS sites formation for CoMo/Al₂O₃ catalyst. And finally, the same proportion of CoMoS sites were found for dried and calcined CoMo/TiO₂ catalysts, although, the dried CoMo/TiO₂ catalyst presents higher amount of non-promoted sites.

Keywords: Hydrodesulfurization (HDS), preparation pre-treatments, dry, calcined, Infrared (IR) spectroscopy, CO adsorption, Molybdenum disulfide (MoS₂), Slab morphology, M-edge, S-edge, CoMoS sites, Co promotion, promotion degree, partially promoted, totally promoted.

6.1 Introduction

Molybdenum sulfide promoted by cobalt and supported on Al_2O_3 is the conventional catalyst for hydrodesulfurization reaction [1]. To meet the very restrictive legislative demands the urge for catalysts with improved activity is still a challenge. This leads to the requirement of a detailed understanding of both, the formation of active sites and the behavior of HDS catalyst during the reactions. Previous studies (see literature as well as results presented in chapter IV and V) showed the influence of the nature of oxomolybdate species present on the oxidic form of the catalyst in the subsequent sulfide sites formation. The presence of MoO_3 species limits obtaining sulfide phase with good dispersion and high promotion level. This observation makes important to avoid MoO_3 formation before the sulfidation stage. Several parameters of the preparation stage monitor the nature and dispersion of oxomolybdate species as the nature of the metal precursors, the synthesis method, e.g. impregnation, sol-gel, chemical vapor deposition, etc, as well as drying and calcination treatments [2,3]. Considering the conventional preparation method, i.e. wetness impregnation, and heptamolybdate as Mo precursor [2,4,5], the main parameter that influences the formation of oxomolybdate species is the pre-treatment step i. e. drying with or without calcination calcination steps [6–8]. These treatments can indeed strongly modify the mode of interaction between oxomolybdate species and the support surface that is fundamental in the formation of specific oxomolybdate species.

Therefore in this work, a thorough investigation was carried out applying several characterization techniques to study the influence of drying and calcination of the oxidic catalyst precursor on the formation of active sites by sulfidation. For that, a series of (Co)Mo catalysts supported on Al_2O_3 , SiO_2 and TiO_2 were prepared. The impact of drying and calcination on the nature and dispersion of species formed on the oxidic catalysts was studied by Raman and UV-Vis spectroscopies. The consequences of these two pre-treatments on the structure of sulfided catalysts were studied by CO adsorption at low temperature followed by FTIR spectroscopy (IR/CO). This technique accounts for the nature, dispersion of the sulfided phase as well as for the distinction of Mo located on M- and S-edge [9]. In addition, IR/CO method also informs about the influence of pre-treatments on the formation of CoMoS sites on sulfided CoMo catalyst. Thiophene HDS tests were also performed to complete the spectroscopic results.

6.2 Experimental

6.2.1 Catalysts preparation

A series of non- and promoted catalysts with different supports were prepared using wetness impregnation method with the constant molybdenum density (3 atoms Mo per nm²) and the Co/(Co + Mo) ratio equal to 0.3. Heptamolybdate tetrahydrated salt (Alfa Aesar, 99%) and cobalt nitrate (Alfa Aesar, 98%) were used as molybdenum and cobalt precursors, respectively. Al₂O₃ (250 m²/g, Sasol), SiO₂ (506 m²/g, silica gel, Merk) and TiO₂ (59 m²/g, anatase and rutile mix, Degussa) were used as support after being sieved with a specific particles size between 0.2-0.5 μm, and calcined before impregnation. Cobalt and/or molybdenum precursors were dissolved in a detailed water volume (support pore volume + 30%) and dispersed inside the pores of the support by a maturation step of 2 hours. To study the effect of drying and calcination, the impregnated catalysts were dried at 383K (3K/min) during 16h. This step is followed or not by a calcination at 673K or 723K (3K/min) during 5h under air for Mo or CoMo catalysts, respectively.

6.2.2 Catalysts Characterization

7.2.2.1. Raman Spectroscopy

Raman spectroscopy was used to study the dispersion of molybdenum and cobalt oxide species, of oxidic catalysts. Raman spectroscopy was performed using a Jobin Yvon Labram 300 Raman spectrometer equipped with a confocal microscope, an Nd-YAG laser (frequency doubled, 532 nm) and a CCD detector. Spectra were recorded at room temperature in the region between 200–1000 cm⁻¹.

6.2.2.2 UV-Vis Spectroscopy

Ultraviolet-visible (UV-Vis) spectra were recorded with a Cary 4000 from Varian equipped with a praying mantis from Harrick for diffuse reflection. The spectrum acquisition domain was between 800-200 nm with a speed of 300 nm /min. The analysis was done on the oxide catalysts under atmospheric conditions, and taken each support as reference. UV-Vis spectra (F(R) vs λ) were converted in [F(R) · hv]² vs hv in order to get the edge adsorption energy. The edge absorption energy is determined by finding the energy intercept of a straight line fitted through the low energy rise in the graphs of [F(R) · hv]² vs hv.

6.2.2.3 Infrared Spectroscopy

Infrared characterizations were performed in a cell adapted for CO adsorption at liquid nitrogen temperature (100K). Before adsorption, the catalyst wafer was activated *in situ* at 623K under 10%

H₂S/H₂ flow during 2 hours with a rate of 3K/min adapting the conventional sulfidation procedure. After 2 hours under sulfidation condition, the catalyst was flushed with Ar during 10 minutes and leaving under vacuum at 623 K for 1 h and finally it was cooled down to room temperature. The CO adsorption was performed under high vacuum (1.10^{-4} Pa) by cooling down to 100K and introducing small doses of CO. CO adsorption experiments were performed introducing small CO doses calibrated upon saturation using equilibrium pressure (133 Pa). IR spectra were recorded with a Nicolet Magna 550 FT-IR spectrometer equipped with a MCT detector. All spectra were normalised to a disc of 5 mg /cm². All experiments were duplicated, with an error of 5%. Saturated spectra were taken to decompose it using OMNIC program and pseudo-voigt function.

6.2.2.4 Catalytic activity: thiophene test

The oxide catalysts were sieved to maintain the particle size between 0.2-0.5 μ m and subsequently subjected to sulfurization procedure under the flow of 10% H₂S/H₂ (30 ml/min) at atmospheric pressure at 623K for 2 h. The thiophene tests were carried out in a continuous flow-reactor at 623K and atmospheric pressure with a thiophene partial pressure of 8 kPa in a mixture of hydrogen (91.2 kPa) and H₂S (2.1 kPa). The products were analysed by Varian 3900 gas chromatograph equipped with flame ionization detector (FID). The reaction rate was calculated as $r_{\text{HDS}} = (F/m) \cdot X$, where F/m is the molar flow rate of thiophene per gram of catalyst and X is thiophene conversion which is below 5%. Thiophene reaction was running during 18h to take a stable reaction rate. The mass after sulfurization was corrected by mass loss calculates with infrared experiments.

6.3 Results

6.3.1 Monometallic oxide catalysts study by Raman and UV-Vis Spectroscopies

Some modification in Raman spectra are reported in the literature for dried and calcined catalysts [2,3]. The differences between the treatments are related to the changes in metal-support interactions. Dried catalysts show weaker interaction between the metal and the support than calcined catalysts do, and this behavior is reflected in the Mo=O_{terminal} vibration band which is shifted to higher wavenumber as it is explained in chapter II. The different interaction with the support leads to changes in oxomolybdate structure found on the support surface. Then, in order to study this change in structure, Raman spectroscopy was performed for dried and calcined non-promoted catalysts deposited on the different supports.

Figure VI.1 shows Raman spectra for dried and calcined Mo/Al₂O₃ catalysts. Raman spectrum of calcined Mo/Al₂O₃ was already discussed in chapter III. It presents bands at 220, 363, 856 and 958 cm⁻¹ which are characteristics of polymolybdate species. On dried Mo/Al₂O₃ catalyst the high frequencies bands appear at 900 and 947 cm⁻¹. These bands are ascribed to Mo=O terminal vibration modes of monomeric and polymeric species, respectively [3]. Note that the Mo=O band of polymolybdate species is observed at 947 cm⁻¹ after drying and at 958 cm⁻¹ after calcination. This shift of Mo=O vibration toward higher wavenumber is related to the increase of number of Mo-O bonds of the polymeric species [3]. Note that such interpretation is in agreement with the low wavenumber of Mo=O band of monomeric molybdate species detected on dried catalyst. Additionally, one band can be detected at 560 cm⁻¹ for dried catalyst. This band is characteristic of AlMo₆ entities and it is reported in the literature that it appears for dried Mo/Al₂O₃ catalysts with the same Mo density than in this work [2].

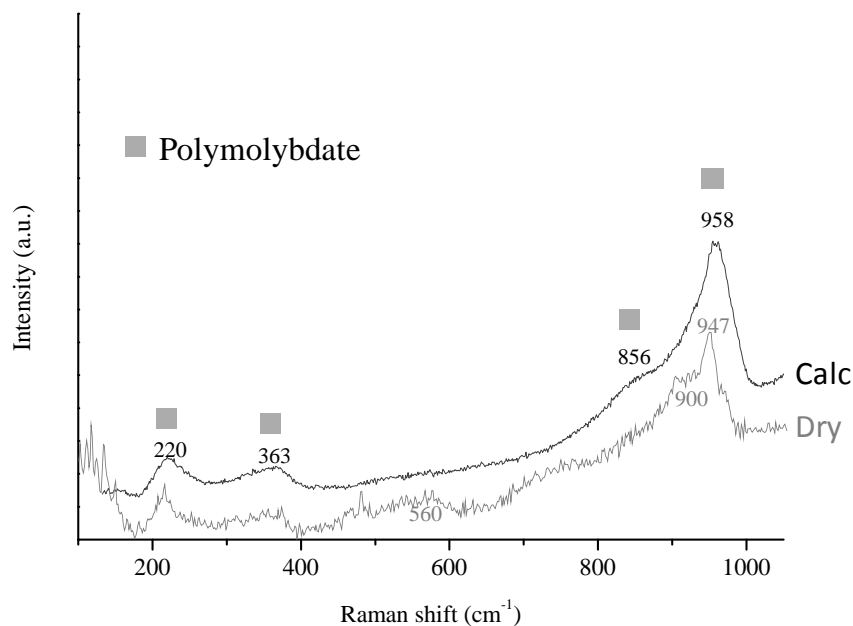


Figure VI.1. Raman spectra of dried (grey line) and calcined Mo/Al₂O₃ catalyst (black line)

Figure VI.2 shows the Raman spectra of the dried and calcined Mo/SiO₂ catalysts. Interestingly, the calcined catalyst showed intense bands at 821 and 997 cm⁻¹ which are the characteristic bands for the formation of MoO₃ species, several bands at lower wavenumbers from 100 to 400 cm⁻¹ as well as one at 668 cm⁻¹ confirm the formation of MoO₃ [10]. Bands characteristic of polymolybdate species are also observed at 220, 866 and 955 cm⁻¹. A shoulder is also detected on dried Mo/SiO₂, indicating the presence of some monomeric molybdate species; Furthermore, additional bands were observed at 965 and 978 cm⁻¹ which are attributed to the

formation of silicomolybdic acid [3,11]. Polymeric and monomeric molybdate species appear at similar wavenumbers as those observed on calcined Mo/Al₂O₃ catalyst [3]. It should be mentioned that any bands characteristics of MoO₃ species are observed on the dried Mo/SiO₂ catalyst. This confirms that the calcination stage strongly changes the nature of oxo-species on silica supported catalyst.

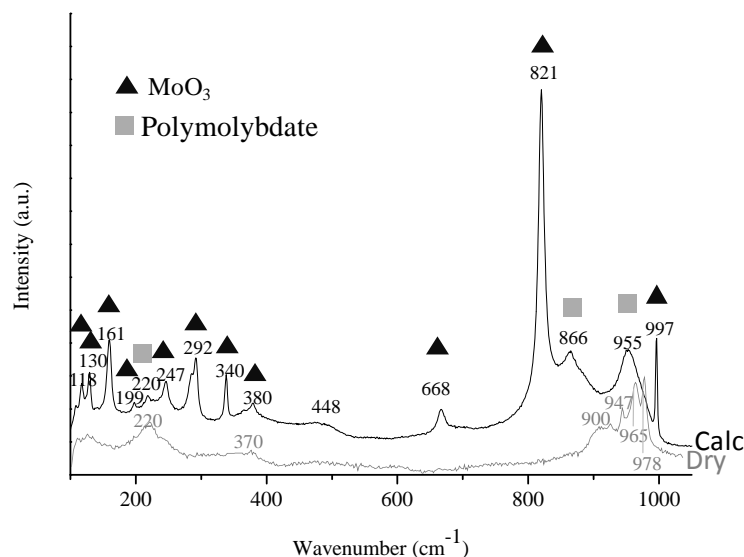


Figure VI.2. Raman spectra of dried (grey line) and calcined Mo/SiO₂ catalyst (black line)

Figure VI.3 shows the XRD patterns of the dried and calcined Mo/SiO₂ catalysts and the pure silica. It can be seen very clearly that the MoO₃ phase is formed after calcination of Mo/SiO₂ catalyst but not after drying. This confirms Raman results and indicates that MoO₃ particles formed by calcination are sufficiently large to be detected by XRD.

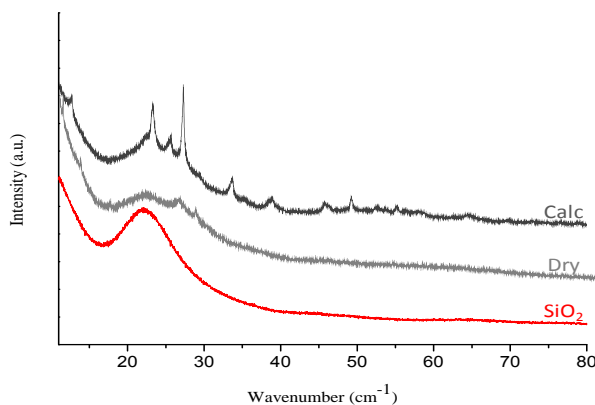


Figure VI.3. XRD pattern of silica gel, calcined and dried Mo/SiO₂ catalysts

Finally, dried and calcined Mo/TiO₂ catalysts were also studied by Raman spectroscopy. Raman spectra of both catalysts are shown in Figure VI.4. Vibration modes characteristics of titania appear at low wavenumber at 147, 199, 324, 396, 517, 638 and 798 cm⁻¹ attributed to anatase phase and 244, and 446 cm⁻¹ corresponding to rutile phase [12]. In addition to these intense bands, dried and calcined Mo/TiO₂ catalysts present bands characteristics of polymolybdate species at 874, 965 and 974 cm⁻¹. The Mo=O terminal vibration band is detected at 965 cm⁻¹ for both pre-treatment while the component at 974 cm⁻¹ is only present for dried catalyst. This point is not yet clarified. The most significant difference between dried and calcined catalysts is the band intensity of Mo=O_{terminal} vibration since dried catalyst presents higher intensity than calcined catalyst for similar intensity of the bands ascribed to anatase and rutile phases. This can be an indication about and oxo-species that occur from the drying stage. This can be an indication about the strong interactions between support and oxo species for titania catalysts that can lead to the so-called wetting effect [13].

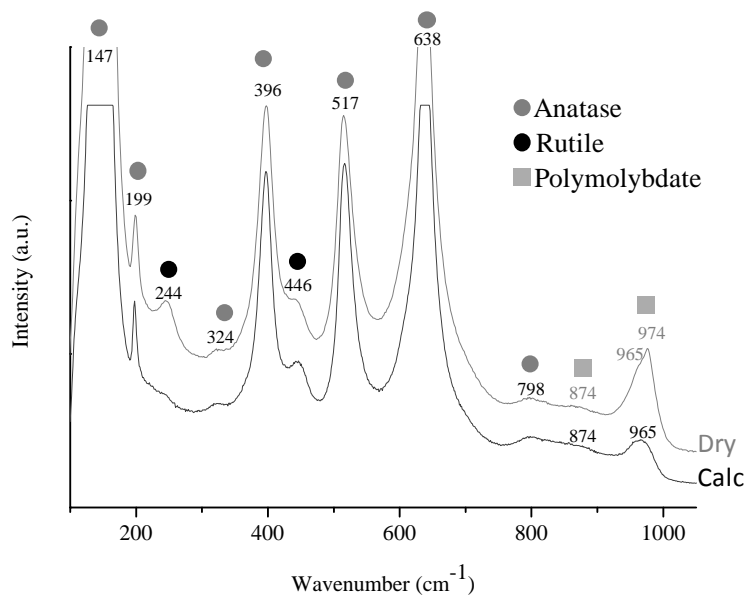


Figure VI.4. Raman spectra of dried (grey line) and calcined Mo/TiO₂ catalyst (black line)

The non-promoted catalysts were further characterized by UV-visible spectroscopy to have detailed insights about the different molybdenum oxide species that could be formed on the catalyst surface upon drying or calcination. The absorption edge energy calculated from the UV-Vis spectrum can be directly related to the size of the MoO_x (oxomolybdate species) domain. Thus, to determine the size of the domains present on the catalyst surface (dried and calcined), several molybdenum oxides in solutions were used as reference. Figure VI.5 shows the correlation between

the sizes of MoO_x domain i.e. the number of next nearest neighbors, and the absorption edge energy for a series of molybdenum oxides. This correlation was used to predict the size of the MoO_x domain formed on the catalyst surface upon the different treatments.

Then, $\text{Mo}/\text{Al}_2\text{O}_3$ catalyst presents same edge adsorption energy after drying and calcinations treatments. After both treatments, $\text{Mo}/\text{Al}_2\text{O}_3$ catalysts are formed mostly by dimolybdate anions. By contrast, on calcined Mo/SiO_2 catalyst, heptamolybdate anions and MoO_3 species are predicted to be present, while a mixture of dimolybdate and heptamolybdate anions is predicted to be present on the dried Mo/SiO_2 catalyst. Finally, Mo/TiO_2 catalysts show low adsorption edge energy indicating a great number of neighbors. Dried catalyst presents somewhat lower adsorption edge energy than calcined catalyst, suggesting even larger oxo-Mo particles.

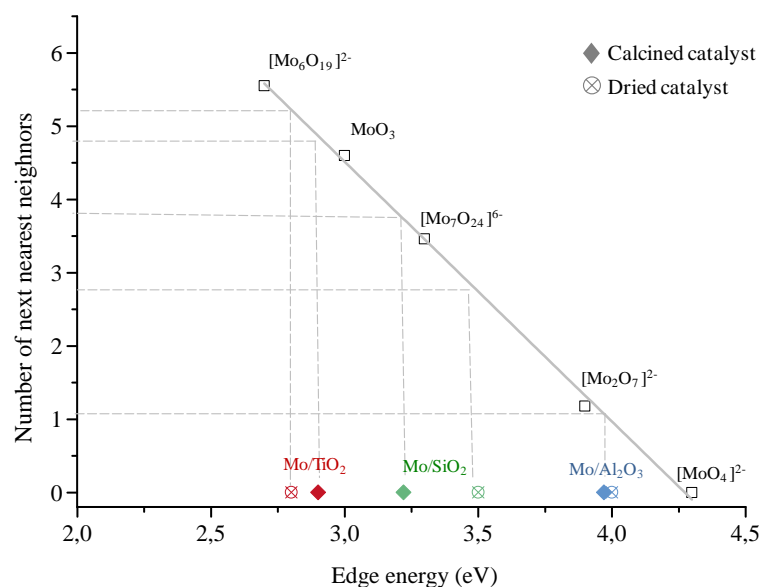


Figure VI.5. Relation between the absorption edge energy and the number of next nearest neighbors in MoO_x for dried and calcined catalysts supported on Al_2O_3 , SiO_2 and TiO_2

6.3.2 Sulfide catalysts

6.3.2.1 Catalytic activity

The effect of drying and calcination of the oxidic catalyst on the catalytic activity of Mo and CoMo sulfided catalysts was studied using thiophene as a model reaction of hydrodesulfurization reaction.

6.3.2.1.1 Non-promoted catalysts

The thiophene HDS rates per gram and per surface area of the non-promoted MoS₂ catalysts supported on Al₂O₃, SiO₂ and TiO₂ are shown in Figure VI.6.a and b. The black bars represent the HDS rates obtained over calcined catalysts whereas the grey bars represent the rates over dried catalysts. It can be observed that Mo/SiO₂ does not show any significant differences in the HDS rates per gram upon catalyst pre-treatment while, some differences were observed for Mo/Al₂O₃ and Mo/TiO₂ upon catalyst pre-treatment. The HDS rate was slightly higher for dried Mo/Al₂O₃ catalyst compared to the calcined one while Mo/TiO₂ showed the reverse effect. However, it must be mentioned that, among all, the catalytic activity of Mo/TiO₂ per unit surface area is significantly greater (more than 3 times) than that of the other two systems. In conclusion, the pre-treatment conditions have a more limited effect on HDS activity of non-promoted catalysts than the support nature has.

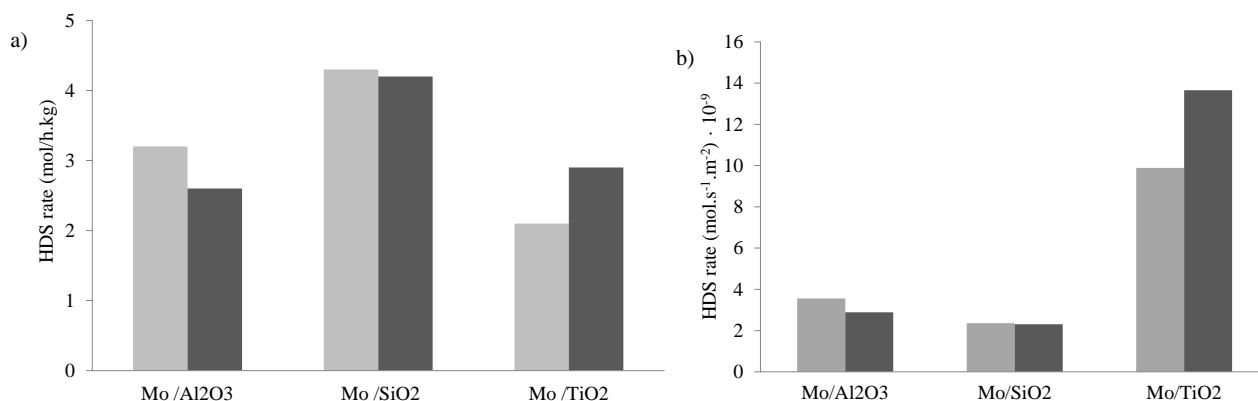


Figure VI.6. HDS rate on dried (grey bars) and calcined (black bars) over non-promoted catalysts per gram (a) and surface area (b)

6.3.2.1.2 Promoted catalysts

The thiophene HDS rates per gram and per unit surface area over the three Co-promoted MoS₂ catalysts supported on Al₂O₃, SiO₂ and TiO₂ are shown in Figure VI.7a and b. The black bars represent the HDS rates over calcined catalysts whereas the grey bars represent the HDS rates over dried catalysts. Unlike the case of non-promoted catalysts, the HDS rates of promoted catalyst appear to be significantly dependent over the catalyst pre-treatment. For instance, the catalytic activity of the calcined CoMo/Al₂O₃ was significantly higher than that of the dried system while, the calcination decreased the corresponding activities for CoMo/SiO₂ and CoMo/TiO₂. Again, the HDS rates per unit surface area are higher for CoMo/TiO₂ system. In conclusion, the HDS rates over promoted catalysts are clearly dependent on the support nature but also on the catalyst pre-treatment.

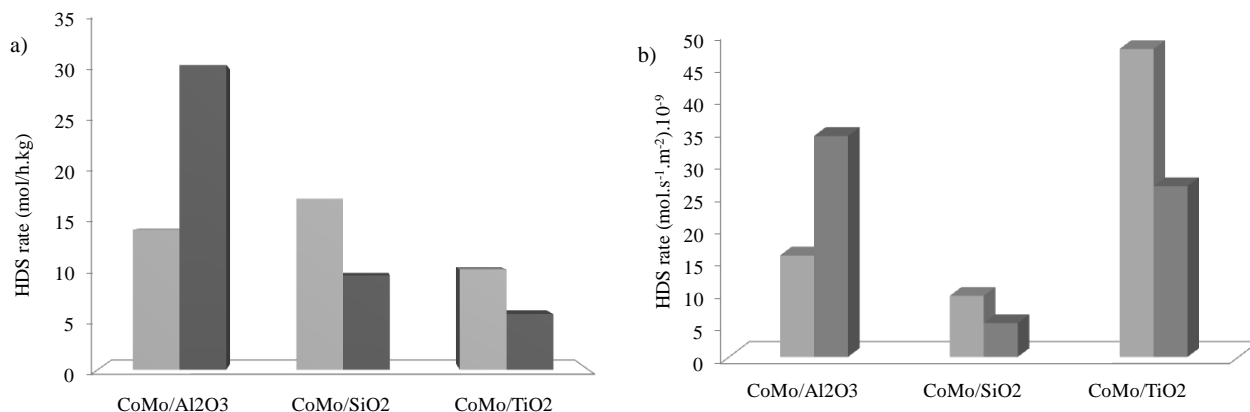


Figure VI.7. HDS rate on dried (greybars) and calcined (black bars) promoted catalysts per gram (a) and surface area (b)

6.3.2.2 Active sites study by IR/CO

As discussed in the previous chapters, the development of the IR/CO methodology allowed great insight into the nature and amount of the surface species of the sulfide catalysts which are directly involved in the catalytic reactions. Here, this methodology was applied to understand the effect of the pre-treatment, on the sulfided Co-promoted and non-promoted Mo catalysts supported on Al₂O₃, SiO₂ and TiO₂.

6.3.2.2.1 Effect of pre-treatments on the MoS₂ phase formation

Figure VI.8 shows the IR spectra of CO adsorption at equilibrium pressure (133 Pa) for dried and calcined catalysts. The IR spectra of CO adsorbed on sulfided Mo/Al₂O₃ pre-treated by drying or calcination present similar bands. CO interaction with the CO/Al³⁺ is characterized by the vibration frequency at 2187 cm⁻¹, while, CO/OH vibration frequency appears at 2157 cm⁻¹. The interaction of CO with MoS₂ nanoparticles is characterized by the CO stretching frequency at 2114 cm⁻¹ and 2070 cm⁻¹ (shoulder) which are ascribed as CO/M-edge and CO/S-edge vibration bands, respectively. The most significant difference is that dried catalyst presents higher intensity for M-edge band than the calcined one.

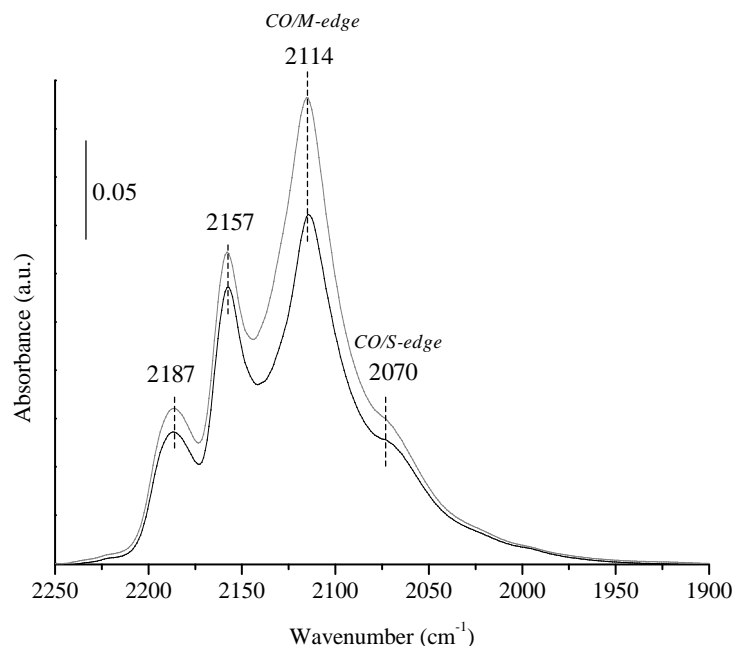


Figure VI.8. IR spectra of CO (133 Pa) on $\text{MoS}_2/\text{Al}_2\text{O}_3$ sulfided after drying (grey line) or calcination (black line)

Figure VI.9 shows the comparison of IR spectra of CO adsorption at equilibrium pressure (133 Pa) on sulfided Mo/SiO_2 catalyst dried and calcined after standard sulfidation (a) or after standard sulfidation followed by a 2% $\text{H}_2\text{S}/\text{H}_2$ post-treatment. As previously, IR/CO spectra show two different domains: CO in interaction with the support and with MoS_2 nanoparticles. The spectra are composed of several bands: 2156 cm^{-1} characteristic of $\nu\text{CO}/\text{OH}$, 2137 cm^{-1} corresponds to CO physisorbed, 2116 cm^{-1} ascribed to $\nu\text{CO}/\text{M-edge}$, as well as a band at 2065 cm^{-1} and weakly intense bands at 2039 cm^{-1} and 2018 cm^{-1} ascribed to $\nu\text{CO}/\text{S-edge}$ with different sulfur coverages, the CO stretching band at 1998 cm^{-1} is ascribed to metallic Mo [9,14,15], and the band at 1888 cm^{-1} to structural band characteristic of silica materials (see annex I). All these vibration frequencies appear at the same wavenumber independently of the pre-treatment or the sulfidation conditions. However whatever the sulfidation treatments, the bands characteristic of MoS_2 phase of the dried catalyst present lower intensities compared to those of the calcined catalyst. The nature and amount of sites of the catalysts detected after the post-treatment under 2% $\text{H}_2\text{S}/\text{H}_2$ is particularly interesting since this treatment is representative of the atmosphere present under reaction conditions. After this post-treatment, an increase of the $\nu\text{CO}/\text{OH}$ band intensity is detected on calcined catalyst. In addition, the post-treatment increases the $\nu\text{CO}/\text{M-edge}$ and $\nu\text{CO}/\text{S-edge}$ band intensities for both dried and calcined catalysts. Note that previous studies showed a strong influence of sulfo-reductive treatments on the amount of sulfided sites detected by IR/CO on SiO_2 supported catalyst.

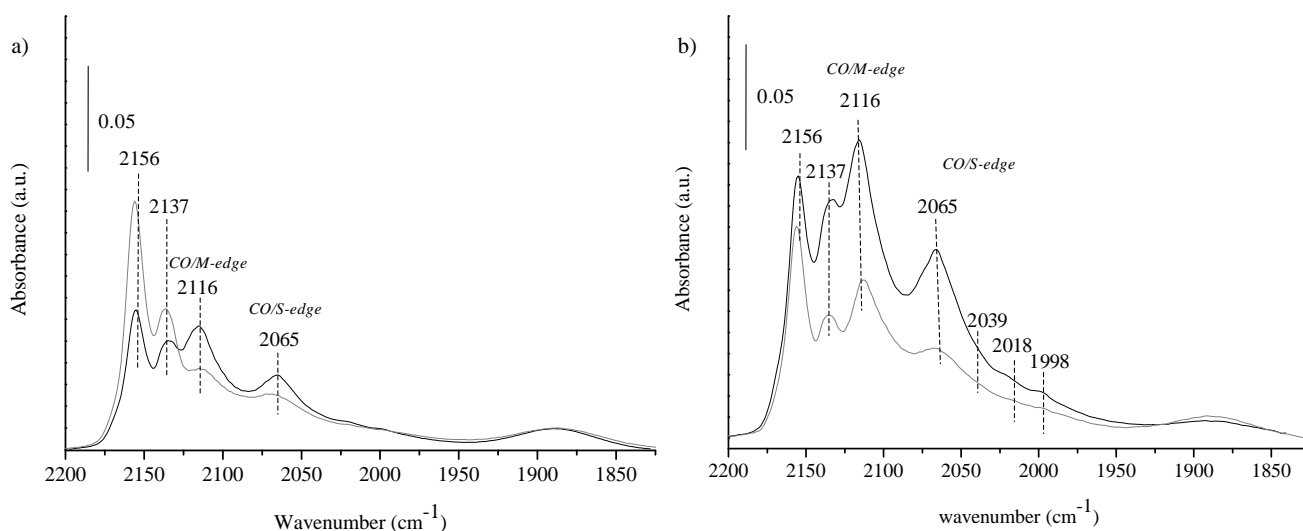


Figure VI.9. IR spectra of CO (133 Pa) on $\text{MoS}_2/\text{SiO}_2$. Catalyst sulfided after drying (grey line) or calcination (black line): a) after sulfidation treatment (623K/2h) and b) after 2% $\text{H}_2\text{S}/\text{H}_2$ post-treatment (623K/2h)

Figure VI.10 shows the comparison of IR spectra for CO adsorption at equilibrium pressure (133 Pa) for dried and calcined Mo/TiO_2 catalysts. The CO stretching frequencies associated with the interaction with the support are detected at the same position for dried and calcined catalyst. The CO/Ti^{4+} interaction appear at 2172 cm^{-1} , while CO/OH interaction can be observed at 2162 and 2155 cm^{-1} . The νCO band detected at 2162 cm^{-1} is assigned to interaction with OH groups but perturbed by the sulfidation of the titania surface (see results presented in chapter III). The interaction of CO with MoS_2 nanoparticles is characterized by a main band ascribed to $\nu\text{CO}/\text{M-edge}$ at 2116 or 2118 cm^{-1} for dried or calcined catalysts, respectively. In addition, a small shoulder is detected at 2070 cm^{-1} that accounts for $\nu\text{CO}/\text{S-edge}$. It can be observed that, for dried and calcined catalysts, the M-edge is largely predominant indicating an almost pure triangular shape of MoS_2 slabs. On dried catalyst, the intensity of the $\nu\text{CO}/\text{M-edge}$ band is lower as well as slightly shifted toward lower wavenumbers. Note that for this dried catalyst, the decrease of the νCO band intensity ascribed to OH group has to be mentioned since it can be linked with the $\text{MoS}_2\text{-TiO}_2$ anchoring.

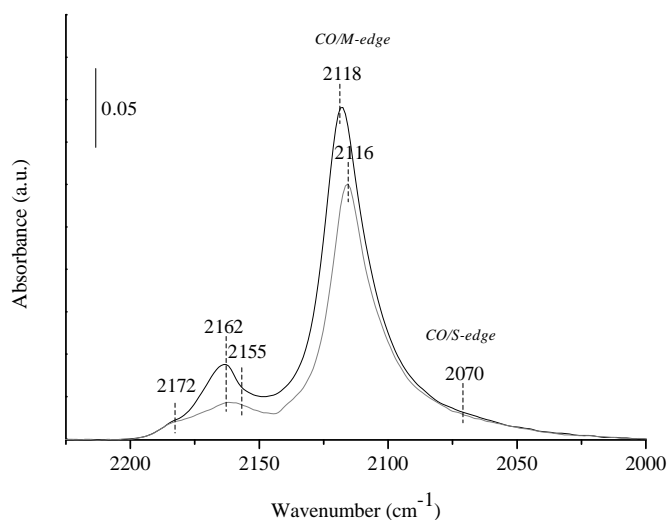


Figure VI.10. IR spectra of CO (133 Pa) on MoS₂/TiO₂ sulfided after drying (grey line) or calcination (black line)

The CO adsorption sites were quantified after spectral decomposition. The molar adsorption coefficients for M-edge ($16 \pm 4 \text{ cm} \cdot \mu\text{mol}^{-1}$) and for S-edge ($35 \pm 9 \text{ cm} \cdot \mu\text{mol}^{-1}$) were previously determined by Maugé et al. and Chen et al. respectively [16,9]. The sites quantifications are summarized in Table VI-1. It can be seen that the pre-treatments has different effects on each catalyst. On Mo/Al₂O₃ catalyst, the calcination pre-treatment leads to a decrease in the concentration of M-edge sites whereas there is no effect on the S-edge sites. For Mo/SiO₂ catalysts, the calcination causes an increase of both M- and S-edge sites. While, for Mo/TiO₂ catalyst, the concentration of M-edge sites increased upon calcination but no changes in the S-edge sites amount is measured. Thus, S-/M-edge ratio was calculated for all catalysts and no significant differences were found for Mo/Al₂O₃ and Mo/TiO₂ catalysts between dried and calcined catalysts. Conversely, Mo/SiO₂ catalysts showed a change in MoS₂ morphology with lower S-/M-edge ratio for the calcined catalyst.

Table VI-1. Effect of drying and calcination on the amount of M- and S-edge sites of MoS₂ slabs

Catalysts	Conc. M-edge (μmol/g)	Conc. S-edge (μmol/g)	Total edge sites (μmol/g)	S-/M-edge ratio
<i>Mo/Al₂O₃ dry</i>	106	17	123	0.16
Mo/Al ₂ O ₃ calc	83	17	100	0.20
<i>Mo/SiO₂ dry *</i>	32	17	49	0.53
Mo/SiO ₂ calc *	67	28	95	0.42
<i>Mo/TiO₂ dry</i>	56	3	59	0.05
Mo/TiO ₂ calc	79	3	82	0.03

* after 2% H₂S/H₂ post-treatment

6.3.2.2.2 CO adsorption on Co-promoted sulfide catalysts

The effect of pre-treatments of Co-promoted Mo catalysts deposited on different support has also been studied by IR/CO method.

Figure VI.11 compares the IR/CO spectra of CoMo/Al₂O₃ catalyst dried (grey line) or calcined (black line) before sulfidation. As previously detailed, the IR spectra show two different CO adsorption domains. $\nu(\text{CO})$ at 2187 cm⁻¹ correspond to interaction with Lewis acid sites (Al³⁺) and $\nu(\text{CO})$ at 2157 cm⁻¹ to interaction with acidic OH groups of alumina. These $\nu(\text{CO})$ band intensities are affected by pre-treatment conditions. The band associated to the CO-Lewis acid site interaction is lowered upon calcination likely due to the formation of CoAl₂O₄ while, the intensity associated with the $\nu\text{CO}/\text{OH}$ band is enhanced upon calcination. In the zone corresponding to CO in interaction with sulfided sites, one can detected a band at 2115 cm⁻¹ on calcined catalyst characterizing $\nu\text{CO}/\text{M-edge}$ of unpromoted Mo phase and bands in the range of 2000-2090 cm⁻¹ associated with CO in interaction with CoMoS sites. The CO in interaction with promoted sites leads to several νCO components at 2059, 2073, and 2085 cm⁻¹ that are observed for both pre-treatments. The positions of these bands remained almost unchanged after drying or calcination. Only the $\nu\text{CO}/\text{M-edge}$ band shows a slight shift down to 2111 cm⁻¹ on dried catalyst. Otherwise, the calcined catalyst shows greater intensities of the bands corresponding to CO in interaction with the promoted and non-promoted Mo sites.

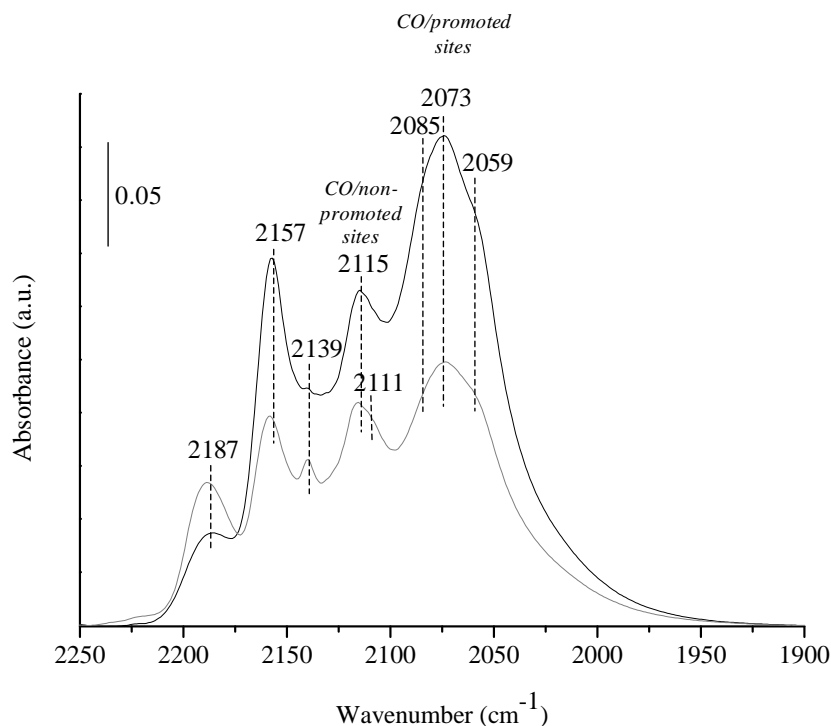


Figure VI.11. IR spectra of CO (133 Pa) on CoMo/Al₂O₃ sulfided after drying (grey line) or calcination (black line)

Figure VI.12 compares the CO adsorption IR spectra at equilibrium pressure (133 Pa) of sulfided CoMo/SiO₂ dried (grey line) or calcined (black line) catalysts. Silica surface is only composed of weakly acidic OH groups. Hence, one sharp and intense ν CO/OH band appears at 2155 cm⁻¹. CO physisorbed was observed at 2137 cm⁻¹. The intensity of ν CO/OH band was lower on the dried catalyst. In the second domain, the ν CO band at 2112 cm⁻¹ is associated to non-promoted MoS₂ sites and the bands at 2000-2090 cm⁻¹ are associated to CO interaction with promoted sites. Compared to calcined catalyst, the dried catalyst shows a lower ν CO band intensity for CO in interaction with non-promoted sites whereas higher ν CO band intensities for CO in interaction with promoted sites. As on alumina, CO in interaction with the promoted sites leads to three ν CO components. A ν CO band at 2065 cm⁻¹ which is ascribed to the cobalt sulfide species, is only detected over calcined catalyst.

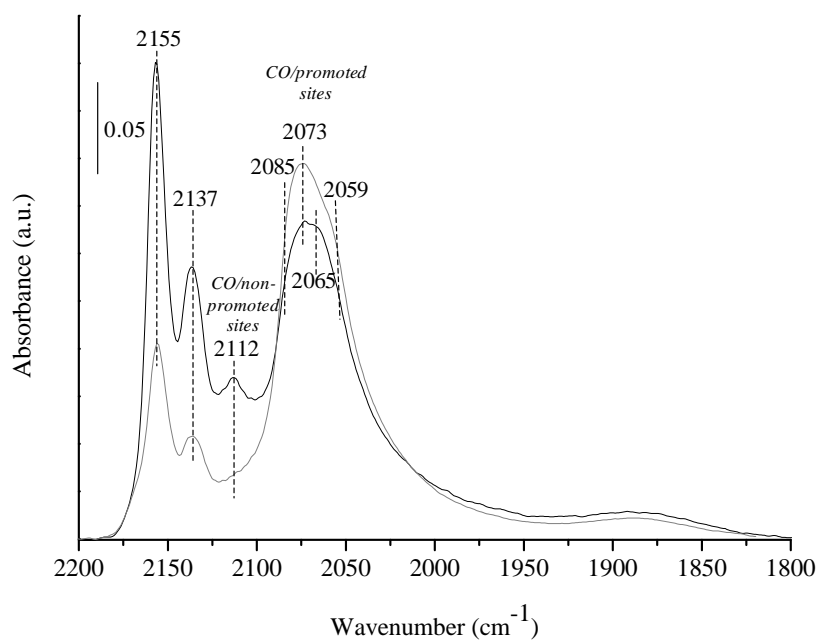


Figure VI.12. IR spectra of CO (133 Pa) on CoMo/SiO₂ sulfided after drying (grey line) or calcination (black line)

Figure VI.13 compares IR spectra of CO adsorption at equilibrium pressure (133 Pa) of sulfided CoMo/TiO₂ dried (grey line) and calcined (black line) catalysts. Titania surface exhibits both Lewis acid sites and hydroxyl groups. Accordingly, ν CO bands detected at 2182, 2160 and 2139 cm⁻¹ are associated to Lewis acid sites, CO/OH interaction and CO physisorbed, respectively. Unlike the alumina and silica catalysts, after drying the CoMo/TiO₂ catalyst mainly presents non-promoted MoS₂ sites (ν CO/M-edge at 2116 cm⁻¹). The amount of unpromoted Mo sites decreased on the calcined sample. No band shift was detected for dried and calcined samples. As noted for the other supports, the ν CO massif of CO in interaction with the promoted sites is composed of several bands at 2057, 2073, and 2085 cm⁻¹ and only small shifts and very limited intensity changes were observed between calcined and dried catalysts.

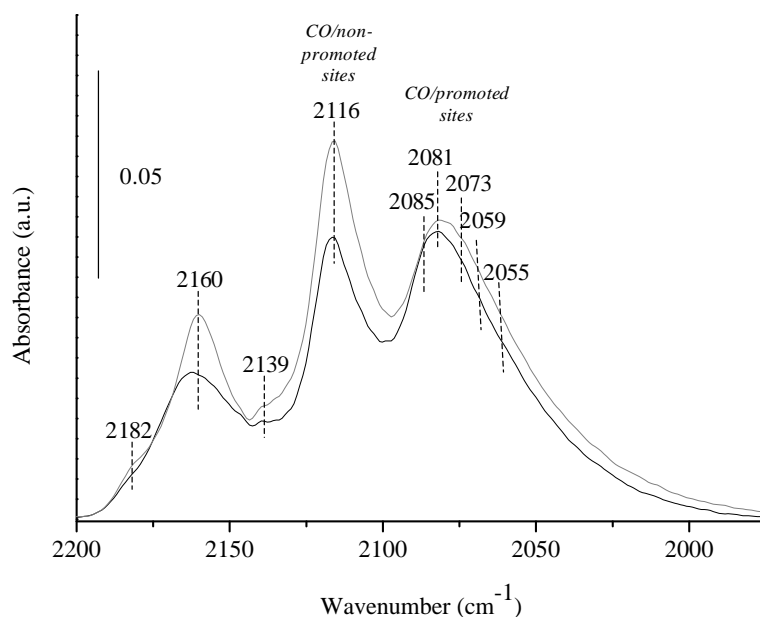


Figure VI.13. IR spectra of CO (133 Pa) on CoMo/TiO₂ dried sulfided after drying (grey line) or calcination (black line)

CO adsorption spectra for Co-promoted catalysts were decomposed in order to quantify the total, non-promoted and promoted sites using respective molar absorption coefficient. The molar adsorption coefficients for non-promoted ($16 \pm 4 \text{ cm} \cdot \mu\text{mol}^{-1}$) and for promoted ($43 \pm 15 \text{ cm} \cdot \mu\text{mol}^{-1}$) sites were previously determined by Maugé et al. [16]. The sulfided sites quantification according to pre-treatment and supports is summarized in Table VI-2. It is clear that the pre-treatment influences the concentration of promoted and non-promoted sulfide sites. The calcination increases the total number of sulfide sites on CoMo/Al₂O₃ and CoMo/SiO₂ catalysts. For CoMo/Al₂O₃, this augmentation is due to an increase of both promoted and non-promoted sites while, for CoMo/SiO₂ catalyst, calcinations caused an increase of the non-promoted sites while the amount of promoted sites stays almost constant. For CoMo/TiO₂, the amount of non-promoted sites decreased upon calcination but no significant changes were observed for promoted sites.

Table VI-2. Effect of drying and calcination on the amount probed by IR/CO of sulfided sites of CoMo supported on Al₂O₃, SiO₂, and TiO₂

CATALYSTS	Non-promoted sites (μmol/g)	Promoted sites (μmol/g)	Total sites (μmol/g)	Promoted/non-promoted sites ratio
<i>CoMo/Al₂O₃</i> <i>DRY</i>	42	34	76	0.8
<i>CoMo/Al₂O₃</i> <i>CALC.</i>	61	62	123	1.0
<i>CoMo/SiO₂</i> <i>DRY</i>	8	39	47	4.9
<i>CoMo/SiO₂</i> <i>CALC.</i>	26	38	64	1.5
<i>CoMo/TiO₂</i> <i>DRY</i>	33	14	47	0.4
<i>CoMo/TiO₂</i> <i>CALC.</i>	23	14	37	0.6

6.4 Discussion

Results presented in previous chapters (chapters III and IV) provided evidence for the influence of the nature of the support on the MoS₂ morphology and on the CoMoS sites formation. These differences can be mainly interpreted in term of strength of the sulfide-support interaction. However, the results presented in this chapter show that, for a same support, the characteristics of the supported phase in its oxidic or sulfided forms, can be strongly influenced by the pre-treatment conditions such as drying or calcination after impregnation [17]. The study of these effects was performed in order to understand the influence of the nature and dispersion of oxomolybdate entities on MoS₂ formation and Co promotion of the sulfided slabs.

6.4.1 Effect of pre-treatments on MoS₂ formation

6.4.1.1 Effect on the nature of the oxidic phase

Before sulfidation process, molybdenum is present on the surface as oxidic form. These oxides species include crystalline MoO₃, monomers or polymolybdate species such as Mo₂O₇²⁻, Mo₆O₁₉²⁻ or Mo₇O₂₄⁶⁻. From the previous discussions based on Raman spectroscopy (Chapter II), it is evident that the support nature as well as the pre-treatment conditions i.e. drying or calcination,

allows a control of the oxidic species formed on the support before the sulfidation stage. The nature and dispersion of these oxidic phases impact nature, dispersion and promotion of the HDS catalyst.

On dried Mo/Al₂O₃, polymolybdate, AlMo₆ and some isolated monomeric molybdate species are detected on Raman spectrum. Polymolybdate and monomeric species are characterized by a Mo=O terminal band at 947 cm⁻¹ and at 900 cm⁻¹, respectively. AlMo₆ entities give rise to a band at 952 cm⁻¹ that appears in the oxomolybdate vibration region, but also to a characteristic band, out of this range, at 560 cm⁻¹ that indicates undoubtedly the presence of this species on the surface [2]. After calcination of Mo/Al₂O₃, no more monomeric and AlMo₆ species are detected, however polymolybdate species are present and characterized by a Mo=O terminal vibration band at 958 cm⁻¹. On dried Mo/SiO₂, polymolybdate as well as some isolated monomeric molybdate and silicomolybdic species are detected. Calcination leads to strong modifications as the formation of large crystallites of MoO₃, and the disappearance of monomeric molybdate and silicomolybdic species. Some polymolybdate species are still detected after calcination. UV-Vis data confirms the co-existence of MoO₃ and polymolybdate species on silica-supported catalyst after calcination. Both dried and calcined Mo/TiO₂ catalysts present only polymolybdate species. The main effect of calcination is a decrease of the intensity of Mo=O band that could be interpreted as a change in the structure of polymolybdate by calcination. UV-Vis data points out the large size of the polymolybdate species formed on this support compared to species formed on alumina and silica. These results clearly show that calcination effect strongly depends on the support nature. In the case of silica, the calcination leads to the creation of MoO₃ species. By contrast, the polymolybdate species formed on silica after drying resist to calcination. Similar features are observed for Mo/Al₂O₃, as the transformation of monomeric species into polymeric species by calcination, and only polymolybdate species are detected after calcination. Mo/TiO₂ catalysts show different behaviors upon pre-treatments. Only polymolybdate species are detected on dried and calcined samples with the two characteristic Raman bands appearing at higher wavenumber compared with Mo/Al₂O₃ and Mo/SiO₂. This shift to higher wavenumber can be linked with the strong interaction between oxomolybdate species and titania support.

6.4.1.2 Effect of pre-treatment on the MoS₂ morphology

Effect of the pre-treatment on the Mo sulfided phase formation on the various supports was followed by IR/CO. For Mo/Al₂O₃ and Mo/SiO₂, bands characteristic of M- and S-edges sites are detected (Figure VI.8 and Figure VI.9). Change of the pre-treatment conditions does not induce any shift of the νCO bands specific of Mo sites on these catalysts. Indeed CO on M-edge sites is observed at 2114 cm⁻¹ on Mo/Al₂O₃ and 2116 cm⁻¹ on Mo/SiO₂ whatever the pre-treatment.

Similarly, the νCO band on S-edge sites is detected at 2070 cm^{-1} for $\text{Mo}/\text{Al}_2\text{O}_3$ and at 2065 cm^{-1} for Mo/SiO_2 whatever the pre-treatment. For Mo/TiO_2 catalysts, mostly M-edge sites are detected and a shift, although limited, is observed from dried to calcined catalysts since νCO is detected at 2116 and 2118 cm^{-1} , respectively. This band shift can be explained by a stronger MoS_2 - TiO_2 interaction on calcined titania supported catalyst. Stronger interaction with the support will lead to a decrease in $\text{Mo}\rightarrow\text{CO}$ back-donation leading to a νCO band shift to higher wavenumbers. The distinction of M- and S- edge sites of MoS_2 slabs accounts about the impact of drying and calcination on the MoS_2 slab morphology. It was found that the S-/M- edge ratio followed the order $\text{Mo}/\text{SiO}_2 > \text{Mo}/\text{Al}_2\text{O}_3 > \text{Mo}/\text{TiO}_2$ for both dried and calcined catalysts. Interestingly, for $\text{Mo}/\text{Al}_2\text{O}_3$ and Mo/TiO_2 catalysts, these shapes are almost not modified by pre-treatments (Table VI-1). This can be related to the absence of any dramatical change in oxomolybdate species of the oxidic form after drying or calcination. By contrast for Mo/SiO_2 catalysts, the MoS_2 shape is significantly modified by pre-treatment conditions. Dried Mo/SiO_2 catalyst presented higher S-/M-edge ratio than the calcined one (Table VI-1 - dried: S/M=0.53; calc.: S/M=0.42). This change can be related to the important modifications in nature of oxo-Mo species that are under the forms of mono- and polymolybdate species after drying and mainly under the form of MoO_3 crystallites after calcination. In conclusion, on Mo/TiO_2 , MoS_2 nanoparticles present a shape close to a pure triangle exposing almost exclusively M- edges. On $\text{Mo}/\text{Al}_2\text{O}_3$ MoS_2 nanoparticles are under the form of truncated triangles, whereas on Mo/SiO_2 they have an almost regular hexagonal shape with a proportion of S-edge greater after drying than after calcination.

6.4.1.3 Effect of pre-treatment on the sulfide sites amount

Table VI-1 shows that pre-treatment impacts the amount of sulfide edge sites. On $\text{Mo}/\text{Al}_2\text{O}_3$, calcined catalyst has a lower total Mo sites available than the dried one (-19%). By contrast, on Mo/SiO_2 and Mo/TiO_2 calcination leads to an increase of the amount of sulfide sites (+93% and +39%, respectively). On $\text{Mo}/\text{Al}_2\text{O}_3$, the monomeric MoO_x species detected by Raman and UV experiments on dried oxidic catalyst should generate smaller MoS_2 slabs than the calcined one explaining the slightly increase in total Mo sites. Mo/SiO_2 catalyst showed a very strong increase of MoS_2 sites detected after calcination. This can be at least partially explained by the MoS_2 slabs with less truncated triangular form on calcined (S-/M-edge=0.42) than on dried (S-/M-edge=0.55), leads, considering a constant slab length, to a greater amount of edge sites. Finally on titania, the only in the structure of oxidic species change upon pre-treatment is the decrease of $\text{Mo}=\text{O}$ band intensity that could indicate a wetting effect after calcination. From literature, the wetting effect has an impact creating sulfur vacancies. This could explain at least partially the increase of CO uptake

after calcination. However, since the slab length of sulfide slab has only been measured on calcined catalysts, we cannot discuss further the influence of this parameter on the edge site amount.

In conclusion, we observed that pre-treatment has an impact on the amount of edge sites but a limited effect on sulfide slab morphology. The question now is: what is the pre-treatment effect on HDS activity.

6.4.1.4 Effect of pre-treatment on the HDS activity

Previous studies showed that the amounts of edge sites as well as the MoS₂ morphology play a determining role in the catalytic activity. The thiophene HDS activity is compared to the total amount of Mo edge sites detected by IR/CO on Mo catalysts after drying and calcination on Figure VI.14. The relationship confirms that Mo edge sites detected by CO are active in thiophene HDS. Hence, the highest activity is obtained for catalysts presenting the greater amount of sulfur vacancies per square nanometer. The best results are obtained on calcined Mo/TiO₂. Figure VI.14 reports also the calculated activity taking into account the amount of Mo sites on M- and S-edges for dried and calcined catalysts (Table VI-1) and the TOF values of M- and S-edge sites previously determined on calcined catalysts (Table VI-3). A very good agreement appears between calculated (cross symbols) and experimental values except for dried Mo/SiO₂. Hence, the pre-treatment does not change the TOF values of alumina and titania Mo catalysts.

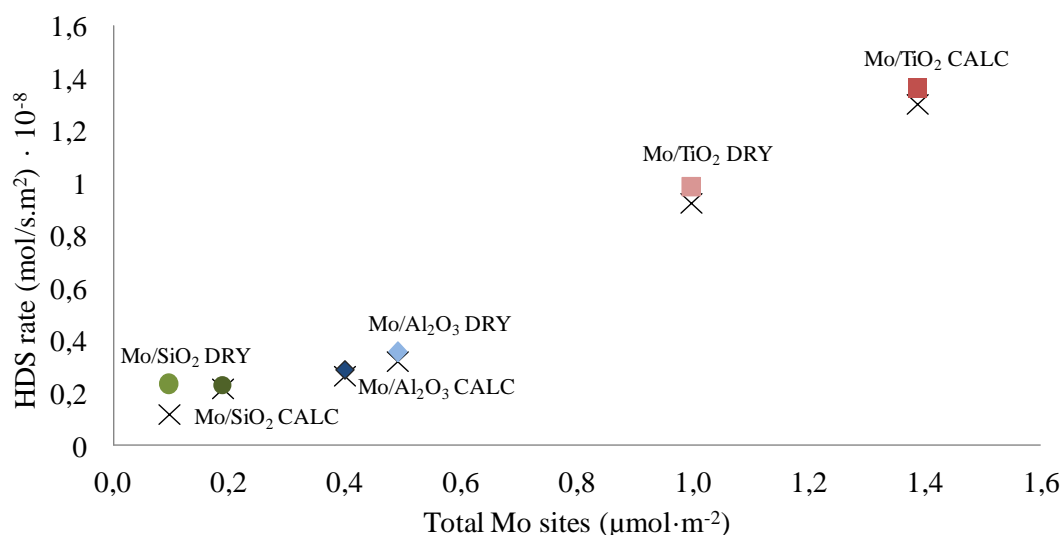


Figure VI.14. Relation between the Mo sites amount and the HDS rate for Mo supported catalysts sulfided after drying or calcination. Cross symbols calculated HDS rate

Table VI-3. TOF values of M- and S-edge sites previously determined on Mo catalysts supported on alumina, silica and titania sulfided after calcination

Calcined catalysts	TOF _{M-edge}	TOF _{S-edge}	Ref.
Mo/Al ₂ O ₃	20 ± 2	35 ± 4	[9]
Mo/SiO ₂	18 ± 10	103 ± 35	Annex II
Mo/TiO ₂	35 ± 4	-	Chapter III

6.4.2 The effect of pre-treatments on CoMoS sites formation

6.4.2.1 Effect of pre-treatment on the sulfide sites formation

IR/CO results point out that the effects of the pre-treatment conditions on the amount of sulfided sites depend on the nature of the support (Figure VI.11 to Figure VI.13– Table VI-2). For instance, calcination increases the CoMoS sites amount on CoMo/Al₂O₃. On the other hand, drying or calcination almost does not change the CoMoS site amount of CoMo catalysts supported on SiO₂ and TiO₂. The support nature also impacts the variation of unpromoted Mo sites concentration after drying and calcination. An increase of Mo sites concentration is detected after calcination on CoMo/Al₂O₃ and CoMo/SiO₂ whereas a decrease is measured on CoMo/TiO₂. Thus, no general trend appears in the effect of drying and calcination on the variation of promoted and unpromoted sites concentration.

Previous chapters showed that CoMoS sites formation strongly depends on the S-/M- edge ratio of unpromoted Mo catalysts. Hence, Figure VI.15 reports the promotion rate of CoMo catalysts and the S/M edge ratio of Mo catalysts for sulfided samples after drying and calcination. As was discussed in the chapter IV for calcined catalysts, the amount of CoMoS sites formed on the promoted catalyst varies in the same way than that of the S-/M- edge ratio of unpromoted Mo catalysts. Similarly, a good agreement appears also for dried catalysts between these two parameters (open symbols on Figure VI.15). Hence, the Co promotion rate followed the order CoMo/SiO₂ > CoMo/Al₂O₃ > CoMo/TiO₂, whereas the S-/M-edge ratio of non-promoted Mo catalysts followed the same order i.e. Mo/SiO₂ > Mo/Al₂O₃ > Mo/TiO₂. Therefore, this confirms that the MoS₂ morphology is an important factor that influences the Co promotion ability.

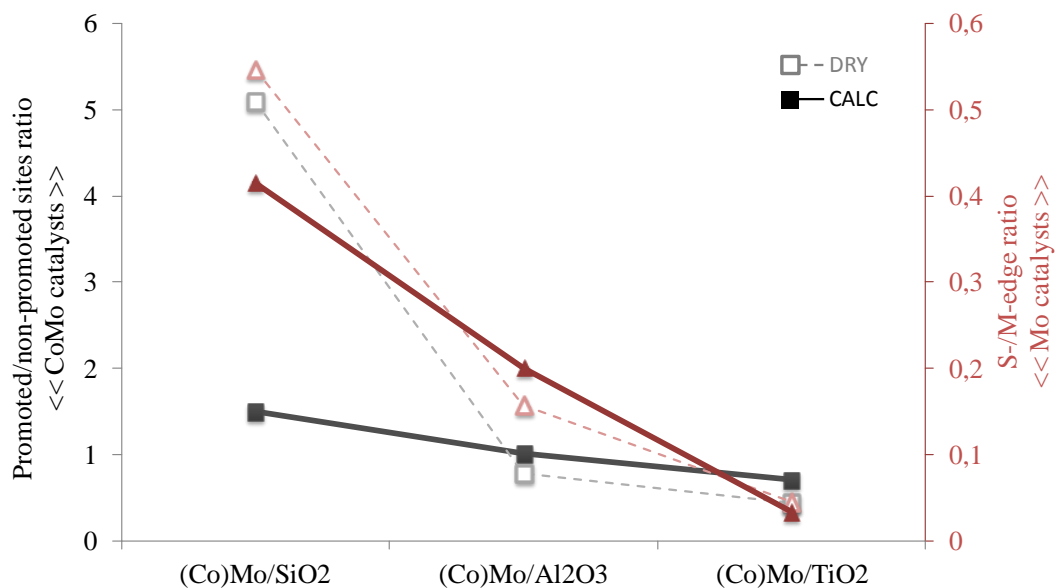


Figure VI.15. Effect of the support nature on the S-/M-edge ratio of sulfided Mo catalysts (red line), and on CoMoS/Mo sites ratio of sulfided CoMo catalysts (black line). The catalysts were dried (open symbol) or calcined (full symbol) before sulfidation

6.4.2.2 Effect of pre-treatments on the sulfide sites formation of silica catalysts

To establish more strongly the relationship between amount of S-edge sites and degree of promotion, and since the morphology of MoS₂ phase can be only significantly varied on silica catalysts, a series of (Co)Mo/SiO₂ was studied. These silica-supported catalysts present different coverages in Mo (1, 2 and 3 at. Mo per nm²) and a constant Co/Mo atomic ratio of 0.3. Their study was detailed in Chapter V. Figure VI.16 reports the promotion rate of CoMo/SiO₂ catalysts and the S-/M- edge ratio of Mo/SiO₂ catalysts after drying and calcination. First, it appears that the increase of the amount of molybdenum increases the S-/M-edge ratio of the sulfided Mo silica catalysts. This change of morphology with Mo content is in good agreement with the results reported by Chen et al on Mo supported on alumina with different Mo loadings [18]. In addition, Figure VI.16 shows once more the importance of MoS₂ morphology on the formation of active CoMoS sites. Increase of S-/M- edge site ratio leads to an increase of the promotion rate on the whole silica series, except for the calcined CoMo catalyst with 3 Mo atoms/nm². Conversely to what was expected, the calcined 3-CoMo catalyst presents a high S-/M-edge ratio but a weak promotion rate. It should be remind that, at the oxidic state, this catalyst is the unique sample of the series discussed in this chapter that exhibits a large amount of MoO₃ phase. MoO₃ is known to be difficult to sulfide. It can be proposed that during the sulfidation stage, MoO₃ forms intermediate species that inhibits the promotion by

Co. Thus, the drying enhances Mo dispersion and avoids MoO₃ formation leading to an increase in promotion degree as shows dried CoMo/SiO₂ (3 at. Mo per nm²).

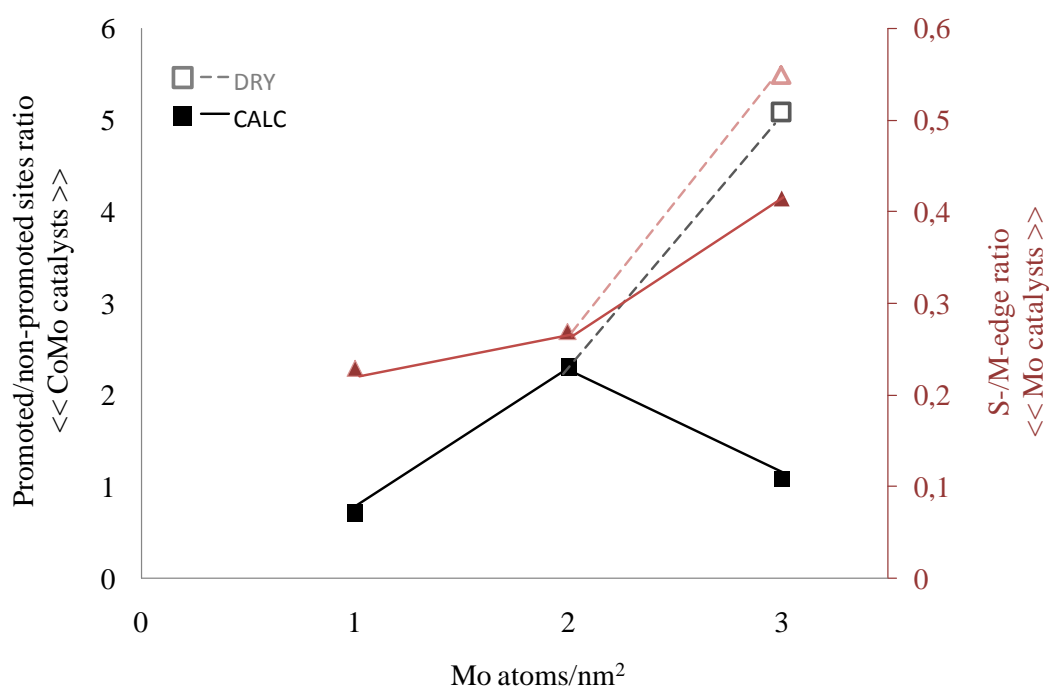


Figure VI.16. Effect of the Mo amount on the S-/M-edge ratio of sulfided Mo/SiO₂ (red line), and on CoMoS/Mo sites ratio of sulfided CoMo/SiO₂ (black line). The catalysts were dried (open symbol) or calcined (full symbol) before sulfidation

6.4.2.3 Effect of pre-treatment on the structure of CoMoS sites

Chapter IV presented a detailed analysis of the IR/CO massif of the zone 2085-2055 cm⁻¹. At least three different components can be distinguished at 2083, 2073 and 2057 cm⁻¹. These νCO bands characterize CoMoS sites with different structures and locations. As discussed in the previous chapter, parallel between spectroscopic data and DFT calculation allowed us to propose that these three bands correspond to CO adsorbed on CoMoS sites on M-edge completely promoted (2083 cm⁻¹), on CoMoS sites on M-edge partially promoted (2073 cm⁻¹), and on CoMoS sites on S-edge partially promoted (2057 cm⁻¹).

To determine the impact of drying and calcination on these three species, the ratio of the area of each of these three bands over the total area of the CoMoS bands was calculated and reported on Figure VI.17 for CoMo catalysts supported on Al₂O₃, SiO₂, and TiO₂ after the two pre-treatments. First, Figure VI.17.a shows that the proportion of the band at 2057 cm⁻¹ does not change after drying and calcination. This behavior is in good agreement with the assignment of this band to CoMoS sites on S-edge. Indeed, the ratio of 2057 cm⁻¹ band area followed the same trend than S-

edge proportion detected on Mo catalysts on different support and after various pre-treatment. Figure VI.17.b and Figure VI.17.c shows that drying and calcination have stronger influence of the proportion of $\nu(\text{CO})$ bands at 2073 and 2083 cm^{-1} ascribed to partially and totally promoted M-edge, respectively. For CoMo/ Al_2O_3 drying and calcination does not change markedly the promotion of these bands. By contrast, on catalysts supported on silica and titania, pre-treatments induce strong changes and leads to the same types of variation. For these two catalysts, calcination decreases the proportion of the band at 2073 cm^{-1} compared to drying, while it increases the proportion of the band at 2083 cm^{-1} . The opposite variation of these two bands confirms their assignments to sites on partially and completely promoted same edge (M-edge). These results show that on titania and silica CoMo catalysts, sulfidation directly after drying favors the formation of partially promoted M-edge.

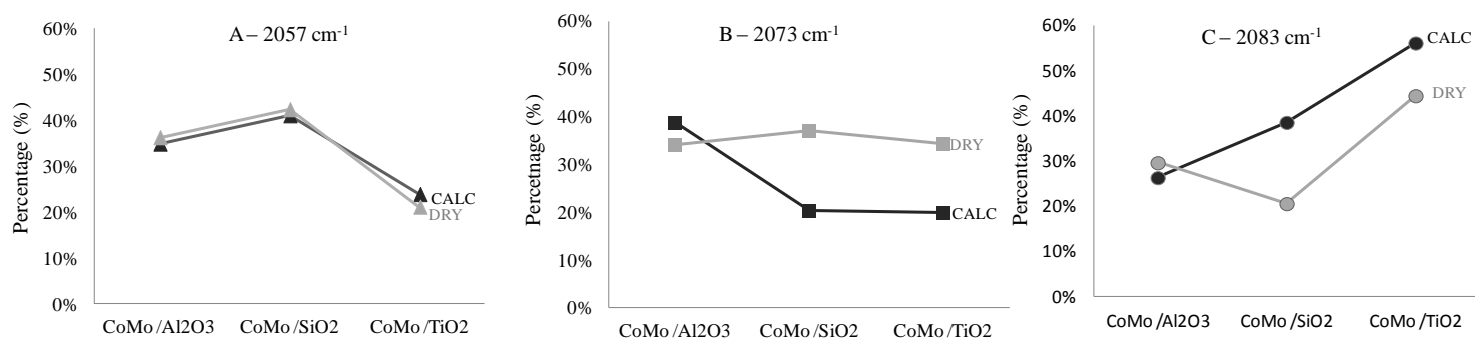


Figure VI.17. Variation of the area (in percentage) of the three $\nu(\text{CO})/\text{CoMoS}$ bands for sulfided CoMo catalysts sulfided after drying (grey) or after calcination (black)

6.4.2.4 Effect of pre-treatment on the HDS activity

Figure VI.18 reported the HDS rates versus the amount of promoted sites of sulfided CoMo catalysts deposited on different supports and after the various pre-treatments. As a general manner HDS activity increases with the amount of CoMoS sites, even if there is no direct relationship for all the catalysts. For example CoMo/TiO₂ dried is clearly above the tendency line while after calcination CoMo/TiO₂ and CoMo/SiO₂ catalysts are below the tendency line.

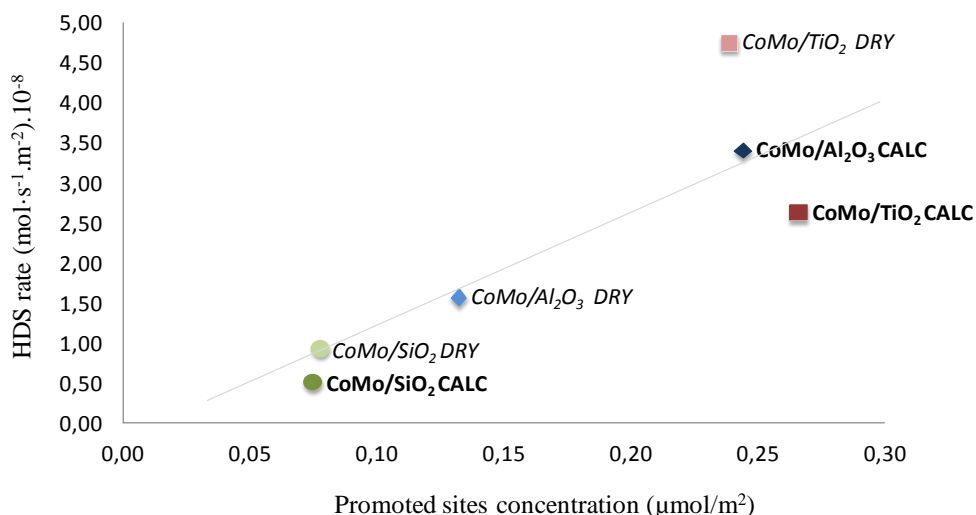


Figure VI.18. Relation between the promoted sites amount and the HDS rate for CoMo supported on alumina, silica and titania sulfided after drying or calcination

To go further, TOF values of the CoMoS sites of these different catalysts were calculated taking into account the amount of CoMoS sites (Table VI-4) and the contribution of the unpromoted Mo sites to the global activity. Activity of unpromoted Mo sites is calculated according to the equation:

$$r_{\text{unpromoted Mo}} = n_{\text{unpromoted Mo}} \times \text{TOF}_{\text{unpromoted Mo}}$$

considering $n_{\text{unpromoted Mo}}$ presented in Table VI-2 and $\text{TOF}_{\text{unpromoted Mo}}$ values for M-edge calculated in previous studies and recall in Table VI-3 and Table VI-4.

Close TOF values are obtained for CoMo/Al₂O₃ catalysts whatever the pre-treatment and for dried CoMo/SiO₂. An almost value of half is obtained for the TOF of calcined CoMo sites on silica and on TiO₂. These changes in TOF values can be interpreted as a change in the CoMoS site structure i.e edge location of Co and degree of promotion of the edge. Indeed, a parallel appears between the variation of the three components of the vCO/CoMoS sites (Figure VI.17) and the changes of the TOF values (Table VI-4). The decrease of the TOF value detected after calcination of CoMo on silica and on titania can be related to the decrease of the proportion of the band at 2073 cm⁻¹. This points out that the sites located on partially promoted M-edge present a specifically strong intrinsic activity. This is in accordance with previous conclusion.

Table VI-4. TOF values of sulfided CoMo catalysts supported on alumina, silica and titania. Effect of drying and calcination

Catalysts	TOF «M-edge» (h ⁻¹)	TOF «CoMoS» (h ⁻¹)	TOF _{CoMoS} / TOF _{M-edge} ratio
<i>CoMo</i> /Al ₂ O ₃ dry	20	401	24
CoMo /Al ₂ O ₃ calc		483	24
<i>CoMo</i> /SiO ₂ dry	18	433	24
CoMo /SiO ₂ calc		238	13
<i>CoMo</i> /TiO ₂ dry	35	636	18
CoMo /TiO ₂ calc		307	9

6.5 Conclusion

On unpromoted catalyst, no influence of pre-treatment was detected on MoS₂ morphology for Mo/Al₂O₃ and Mo/TiO₂ in agreement with the absence of change in oxo-Mo that stays as polymolybdate after drying or calcination. On the other hand, slab morphology of Mo/SiO₂ catalyst depends on pre-treatment. Calcination leads to a decrease in S-/M-edge ratio. This can be related to the modification of oxo-Mo dispersion that changes from polymolybdate species after drying to MoO₃ crystallites formation after calcination. These results corroborate that the principal factor for monitoring the MoS₂ morphology is the metal-support interaction.

Pre-treatment strongly affects the CoMoS sites formation on the different supports. Although calcination strongly increases the amount of CoMoS on alumina, the effect of pre-treatment is very limited on silica and titania. Nevertheless as previously shown, it appears that the promotion rate of CoMo catalysts strongly depends on the ratio S-/M-edge sites generated on the Mo catalysts. As for HDS activity, a relation exists between the global amount of CoMoS (promoted) sites detected by IR/CO and the thiophene HDS rate. However the structure of the CoMoS sites has also to be considered, since the three types of CoMoS sites do not present the same activity. Hence, it appears that a greater proportion of CoMoS sites on partially promoted M-edge (band at 2073 cm⁻¹) leads to a higher intrinsic activity.

In conclusion, the catalytic activity depends both on the amount of CoMoS sites and on their quality. The more active catalysts should present a high concentration of CoMoS partially promoted and located on M-edge.

6.6 References

- [1] H. Topsøe, B.S. Clausen, F.E. Massoth, *Hydrotreating Catalysis*, Springer, Berlin-Heidelberg, 1996.
- [2] P. Blanchard, C. Lamonier, A. Griboval, E. Payen, *Appl. Catal., A* 322 (2007) 33–45.
- [3] E. Payen, J. Grimblot, S. Kasztelan, *J. Phys. Chem. J. C. Adv. Chem. Ser* 91 (1987) 6642–6648.
- [4] M.J. Vissenberg, L.J.M. Joosten, M.M.E.H. Heffels, A.J. van Welsenens, V.H.J. de Beer, R.A. van Santen, J.A.R. van Veen, *J. Phys. Chem. B* 104 (2000) 8456–8461.
- [5] S. Kasztelan, J. Grimblot, J.P. Bonnelle, E. Payen, H. Toulhoat, Y. Jacquin, *Appl. Catal.* 7 (1983) 91–112.
- [6] I.E. Wachs, *Catal. Today* 27 (1996) 437–455.
- [7] L. Le Bihan, P. Blanchard, M. Fournier, E. Payen, V. Cedex, *J. Chem. Soc., Faraday Trans.* 94 (1998) 937–940.
- [8] E. Le Guludec, L. Oliviero, J.P. Gilson, F. Mauge, M. Rebeilleau, V. De Grandi, S. van Donk, *Catal. Sci. Technol.* 5 (2015) 835–842.
- [9] J. Chen, E. Dominguez Garcia, L. Oliviero, F. Maugé, *J. Catal.* 332 (2015) 77–82.
- [10] M. Fournier, C. Louis, M. Che, P. Chaquin, D. Masure, *J. Catal.* 119 (1989) 400–414.
- [11] W. Banares, Hu, (1994).
- [12] H.L. Ma, J.Y. Yang, Y. Dai, Y.B. Zhang, B. Lu, G.H. Ma, *Appl. Surf. Sci.* 253 (2007) 7497–7500.
- [13] D. Costa, C. Arrouvel, M. Breysse, H. Toulhoat, P. Raybaud, *J. Catal.* 246 (2007) 325–343.
- [14] E.C. Decanio, D.A. Storm, *J. Catal.* 132 (1991) 375–387.

- [15] A. Travert, C. Dujardin, F. Mauge, S. Cristol, J.F. Paul, E. Payen, D. Bougeard, *Catal. Today* 70 (2001) 255–269.
- [16] F. Mauge, J.C. Lavalley, *J. Catal.* 137 (1992) 69–76.
- [17] I.E. Wachs, *Catal. Today* 27 (1996) 437–455.
- [18] J. Chen, L. Oliviero, X. Portier, F. Maugé, *RSC Adv.* 5 (2015) 81038–81044.

ANNEX I. Supported data for support effect on non-promoted catalysts

1. Textural analysis: Support versus catalyst

Structure analysis of the supports (Al_2O_3 , SiO_2 , and TiO_2) was performed by X-Ray diffraction. XRD patterns are shown in Figure 1, Alumina shows a typical diffraction of gamma-alumina, so this structure can be considered for alumina used in this work. Silica shows a typical diffraction form of amorphous structure, and finally Titania presents a diffraction of a mix phase, rutile and anatase. The analysis was completed with the catalysts after impregnation and calcination treatment at 673K during 4h. No diffraction of molybdenum trioxide was found for $\text{Mo}/\text{Al}_2\text{O}_3$ and Mo/TiO_2 , the same diffraction was found than before the impregnation, but MoO_3 structure was detected for Mo/SiO_2 .

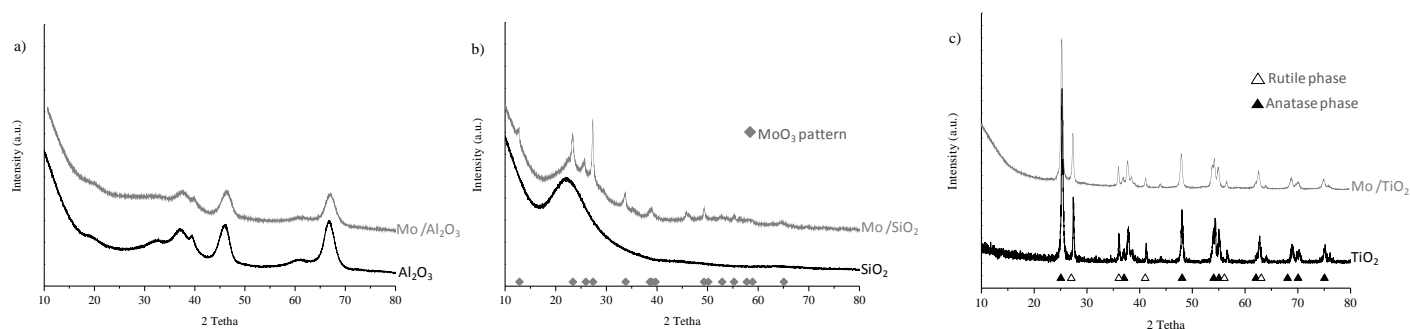


Figure 1. XRD pattern of the support (black line) and the catalyst (grey line) on: Al_2O_3 (a), SiO_2 (b), and TiO_2 (c)

Nitrogen adsorption isotherms are represented in Figure 2 for Al_2O_3 (a), SiO_2 (b), TiO_2 (c) and their Mo catalysts respectively. $\text{Mo}/\text{Al}_2\text{O}_3$ present a light decrease of the surface area, pore size and volume in comparison with the one without molybdenum. This decrease is normal because of the metal deposition on the alumina surface. However, Mo/SiO_2 catalyst presents a high decrease of the surface in relation with the one detected for silica without molybdenum. Half of the surface is lost; it is attributed to the small pore size of 6 nm in comparison with Al_2O_3 of 12 nm, and then additional immobilization of heptamolybdate anions results in a further decrease of the surface area. Instead, Mo/TiO_2 catalyst does not present any change in the surface area but an increase in the pore size and volume revealed by

a change in the hysteresis after molybdenum deposition on the surface. No change in the hysteresis was found after molybdenum deposition on alumina and silica.

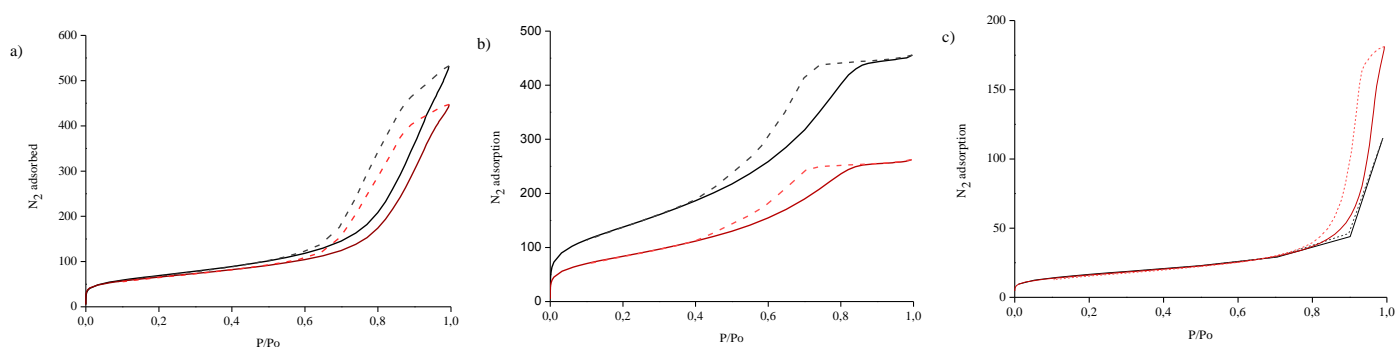


Figure 2. Nitrogen adsorption isotherm represented support in black line and catalyst in red line as well as full line for adsorption and discontinue line for desorption on: a) Al_2O_3 versus Mo / Al_2O_3 , b) SiO_2 versus Mo / SiO_2 , and c) TiO_2 versus Mo / TiO_2 .

2. CO stretching of silica structure

IR spectra of CO adsorption for silica present different stretching domains: OH range, CO stretching, Si-O-Si range and Si=O range as shows Figure 3. The first one is characteristics of hydroxyl group stretching range between 3800 and 3400 cm^{-1} in which appear a band at 3750 cm^{-1} of isolated hydroxyl group on silica surface [1]. Also appear a band at 3660 cm^{-1} characteristic of CO in interaction with OH group, when this band is increasing stretching band of hydroxyl group (3750 cm^{-1}) decrease. The second range is CO stretching in the domain from 2250 to 2000 cm^{-1} , with the characteristic CO gas band at 2043 cm^{-1} [2]. The third and fourth ranges are characteristic of silica structure. The third domain is between 2000 - 1500 cm^{-1} and the fourth range is between 1300 and 1000 cm^{-1} which correspond to Si-O-Si and Si=O stretching respectively [3–5].

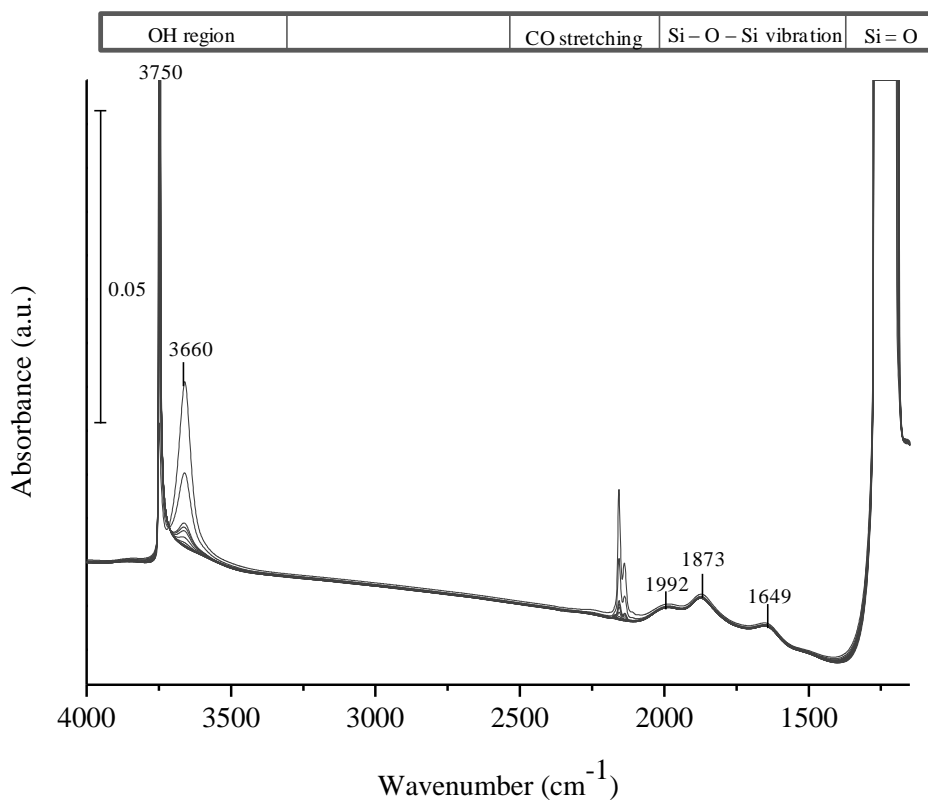


Figure 3. IR spectra of CO adsorption on silica gel after heating treatment at 673K

The existence of the stretching range of Si-O-Si that is near to CO stretching leads to obtain a distortion band of the Si-O-Si stretching during CO adsorption spectra. This distortion band can be shown more clearly in Figure 4, which represents CO adsorption on Mo /SiO₂ catalyst. CO/S-edge stretching appears really close to Si-O-Si stretching bands, then the subtraction of the reference with the corresponding CO adsorption spectrum leads to a distortion coming from the band at lower wavenumber around 1882 cm^{-1} .

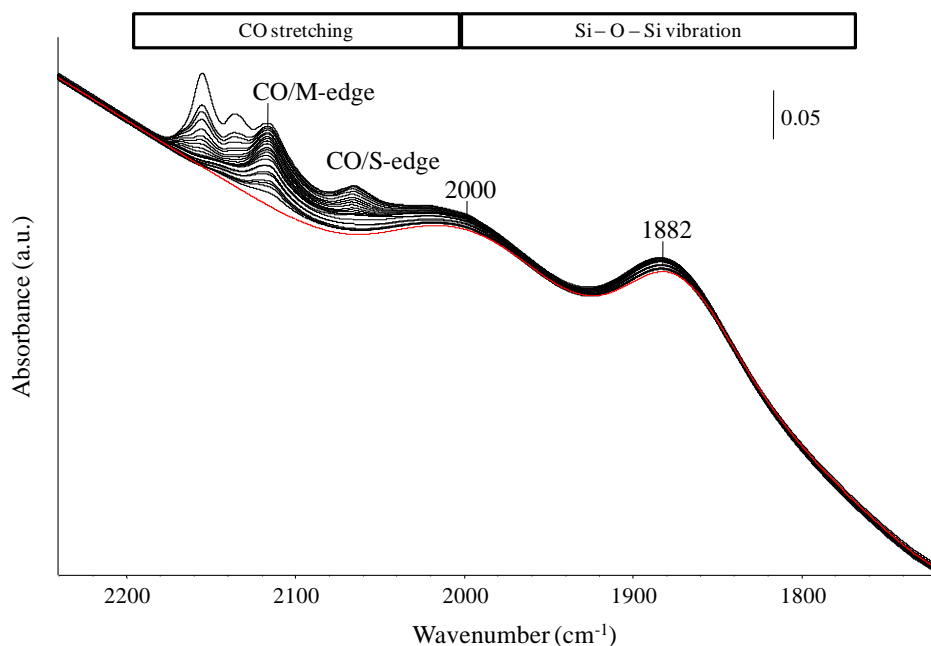


Figure 4. IR spectra of CO adsorption introducing doses upon equilibrium pressure on Mo /SiO₂ catalyst after sulfidation at 623K. Red line represents IR spectrum before CO adsorption

3. Molar extinction coefficient of CO/M-edge stretching for Mo/ Al₂O₃ and Mo/ TiO₂ catalysts

The addition of small CO doses by using a standard volume allow the discrimination of some CO stretching i.e. CO only interacts with Mo on M-edge in the first CO introduction. Then, this band discrimination allows to the quantification of the molar extinction coefficient for some components.

Molar extinction coefficient was calculated for Mo /Al₂O₃ and Mo /TiO₂ catalysts for the component at 2110 cm⁻¹ ascribed to Mo located on M-edge. The three first doses (0.25, 0.5, and 0.5 torr) were taken to calculate the molar extinction coefficient by the slope straight of the band area versus CO introduced per pellet surface. Figure 5 shows molar extinction coefficient calculation for Mo /Al₂O₃. On the left, IR spectra of CO adsorption of the three first doses show the contribution of one CO band at 2113 cm⁻¹ ascribed to Mo on M-edge. On the right is represented introduced CO amount per pellet surface (2.01 cm²) versus the band area of adsorbed CO. The slope obtained for the straight line passing by the origin (0,0) corresponds to the molar extinction coefficient.

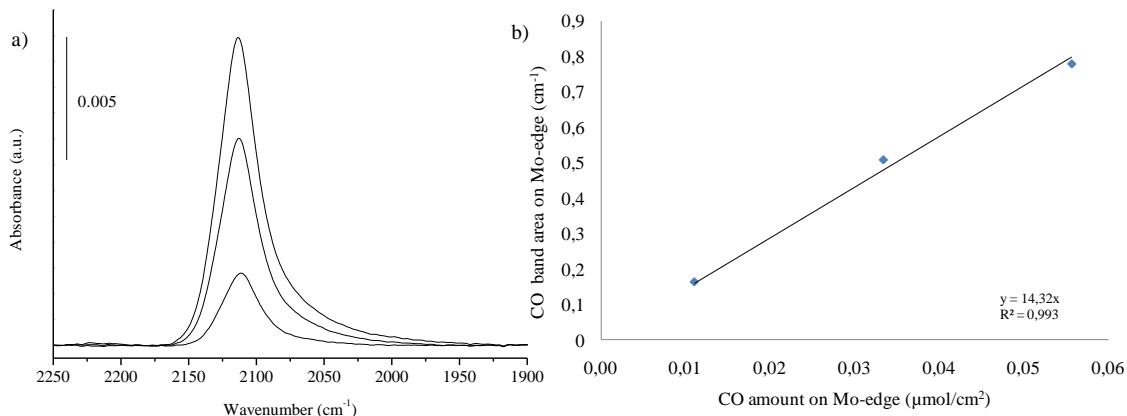


Figure 5. Molar extinction coefficient of the band at 2110 cm⁻¹ attributed to Mo located on M-edge for Mo /Al₂O₃ catalyst

Figure 6 shows molar extinction coefficient calculation for Mo /TiO₂. On the left, IR spectra of CO adsorption for the three first doses (1 torr each one) show the contribution of one CO band at 2118 cm⁻¹ ascribed to Mo on M-edge. On the right is represented introduced CO amount per pellet surface (2.01 cm²) versus the band area of adsorbed CO. The slope obtained by the straight line passing by the origin (0,0) corresponds to the molar extinction coefficient. The molar extinction coefficient obtained for both catalysts was 14 μmol⁻¹cm, which is in the same order than the one calculated by Maugé et al. for Mo /Al₂O₃ [6]. Since the same molar extinction coefficient was calculated for Mo /Al₂O₃ and Mo /TiO₂, we can take the value calculated by Maugé et al. as good one and use it for every MoS₂ catalyst for this band.

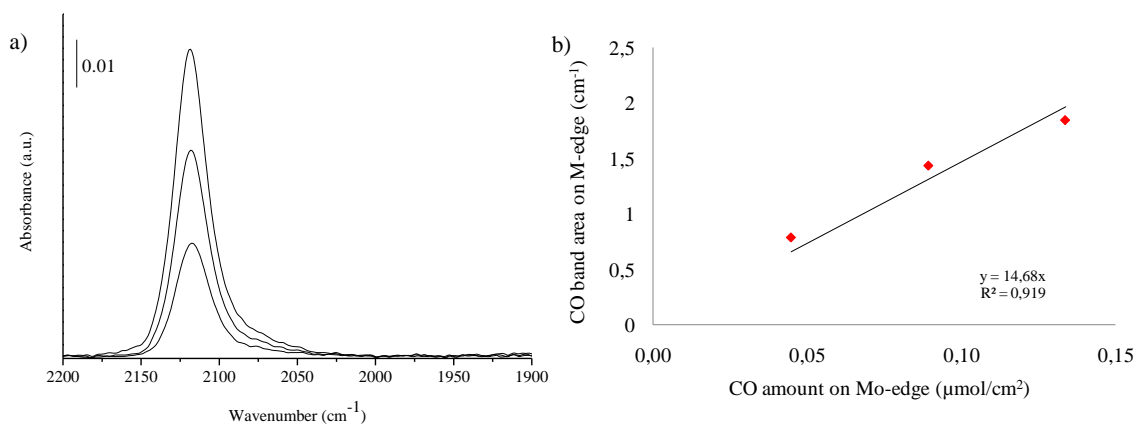


Figure 6. Molar extinction coefficient of the band at 2110 cm⁻¹ attributed to Mo located on M-edge for Mo /TiO₂ catalyst

Mostly Mo on M-edge sites is detected for Mo /TiO₂ by IR/CO. Additionally molar extinction coefficient was calculated for CO/M-edge stretching appearing for sulfided Mo/TiO₂ catalysts at 2118 cm⁻¹. H₂ post-treatment reacts with sulfur presents on MoS₂ edges, and then it has a direct effect on the sulfur coverage at edge of MoS₂ clusters. The reduction of sulfur coverage leads to the increase of the component at lower sulfur coverage that appears at 2108 cm⁻¹ for Mo /TiO₂. Usually, the same molar extinction coefficient is used for this band than for the ν(CO/M-edge) band at for M-edge with higher sulfur coverage. However, the correct utilization of molar extinction coefficient always leads to an intense debate. Thus since Mo /TiO₂ allows calculate molar extinction coefficient in M-edge component with lower sulfur coverage, the calculation could be preformed after H₂ post-treatment with the three first CO doses as shown previously. Figure 7 shows the calculation of this for Mo /TiO₂ after H₂ post-treatment. On the left, IR spectra of CO adsorption of the three first doses (1 torr each one) are shown. On the right, molar extinction coefficient is calculated as the slope of the straight line linking the area of the CO band at 2108 cm⁻¹ with the introduced CO amount per pellet surface area. As it was reported for the molar extinction coefficient of the ν(CO/S-edde) band and as expected, the decrease in wavenumber leads to an increase of the molar extinction coefficient (from 14 to 21 μmol⁻¹cm).

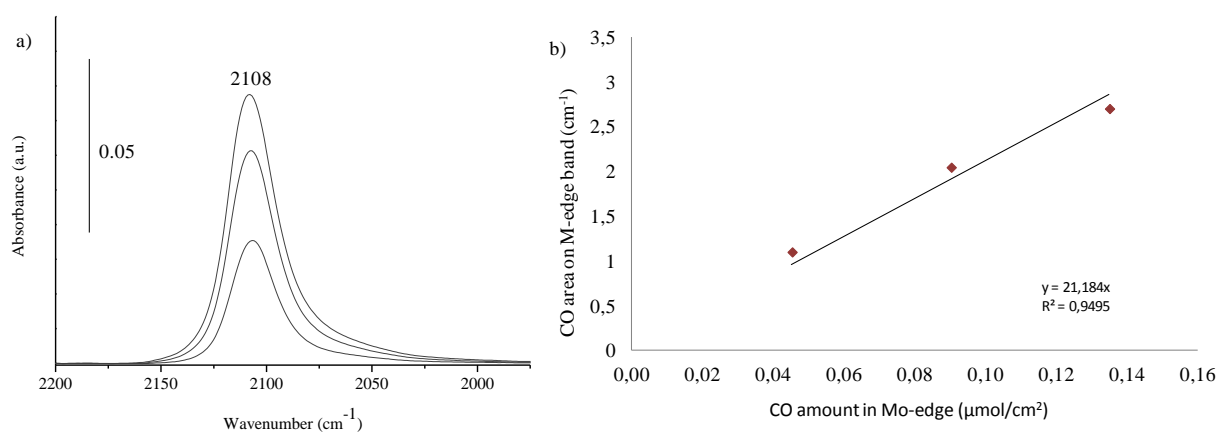


Figure 7. Molar extinction coefficient of the band at 2108 cm⁻¹ attributed to Mo located on M-edge with lower sulfur coverage (37.5%) for Mo /TiO₂ sulfided catalyst after H₂ post-treatment

4. References

- [1] J. T.P. BEEBE, P. GELIN * and J.T. YATES, *Surf. Sci.* 148 (1984) 1–9.
- [2] K.I. Hadjiivanov, G.N. Vayssilov, *Adv. Catal.* 47 (2002) 307–511.
- [3] V. F., (2013).
- [4] J.P. Gallas, J.M. Goupil, A. Vimont, J.C. Lavalley, B. Gil, J.P. Gilson, O. Miserque, *Langmuir* 25 (2009) 5825–5834.
- [5] L. A.P., *The Surface Properties of Silicas*, 1998.
- [6] F. Mauge, J.C. Lavalley, *J. Catal.* 137 (1992) 69–76.

ANNEX II. The Mo loading effect on HDS catalysts supported on MCM-41 and TOF calculation for Mo/SiO₂ catalysts

1. Introduction

To face the decline in availability of fossil oil reserve and to the continue increase of fuel demand, efficiency of the processes for sulfur removal have to be improved. One way is to enhance the surface area of the hydrotreatment catalysts and specifically of the support, to be able to deposit greater amount of sulfide phase with a good dispersion. For that, this annex presents the study of Mo sulfided catalysts deposited on MCM-41 that presents a very high surface area compared to the classical silica (MCM-41: 945 m²/g, SiO₂: 506 m²/g).

2. MCM-41: synthesis and characterization

2.1. Synthesis of MCM-41

In recent years, the synthesis of hexagonal mesoporous silica (HMS, MCM-41 and SBA-15) by cooperative assembly of silica and surfactants has attracted a great interest for their technical applications as catalysts and catalyst supports [1–4]. The principal characteristic of these mesoporous silica is a high surface area (around 1000 m²/g), and high thermal stability at temperature up to 1073 K.

Mesoporous silica, MCM-41, was synthesized according to the procedure reported by Meynen et al [5]. The molar composition is: 1 SiO₂ : 0.25 Cetyltrimethylammonium (CTAB) : 0.2 Tetraethylammonium hydroxide (TEAOH) : 39.36 H₂O.

Cetylmethylammonium (CTAB, Across Organic) was added to deionized water under stirring at room temperature. When the Cetylmethylammonium was dissolved, Tetraethylammonium hydroxide 20% (TEAOH, Sigma-Aldrich) was added. After, fumed silica (Sigma-Aldrich) was added to the solution under stirring at 70°C during 2h. The stirring was maintained during 24h and later the viscous solution was introduced into an autoclave and heated to 150°C for 48h. The recovered product was filtered, transferred into an autoclave with a little amount of water just for cover the solid in the autoclave and heated, a second

time, to 150°C for 72h. The final product was filtered, washed with deionized water and dried at 100°C overnight. Finally, the template was removed by calcination step at 550°C during 6h.

Since in this synthesis, a template was used to get the desired structure, it had to be removed in the calcination step. Thermogravimetry technique was used to select the correct calcination condition. Figure 1 shows TGA, and DTA obtained for dried MCM-41 synthesized material. TGA shows two main peaks: one peak at 200°C and the other one around 300°C, the first one corresponding to the removal of the main template fraction. In DTA result, there is a notable exothermic peak around 350°C. So, the template is removed between 200°C and 400°C and thus calcination process was carried out with a very low temperature ramp (0.25K/min) in this temperature domain.

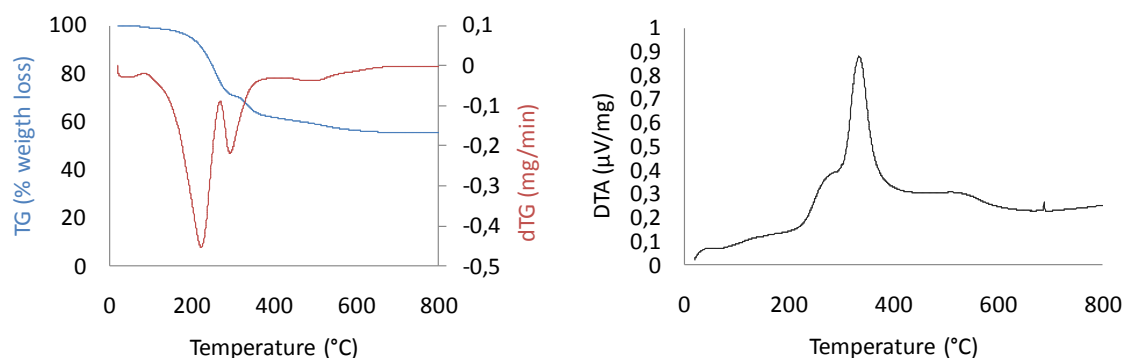


Figure 1. TGA and DTA of MCM-41 material

The template elimination by calcination was checked by IR spectroscopy. First, IR spectrum of cetyltrimethylammonium template was measured as reference. It is reported in Figure 2. Similar bands with lower intensities appeared in the spectrum correspond to dried MCM-41 material. After calcination, the template bands were completely eliminated

Typical silica vibrations appear in two different IR region: one corresponding to SiOH group between 3000 cm^{-1} to 3800 cm^{-1} and the other characteristic of Si-O vibration around 700 cm^{-1} to 1200 cm^{-1} [2].

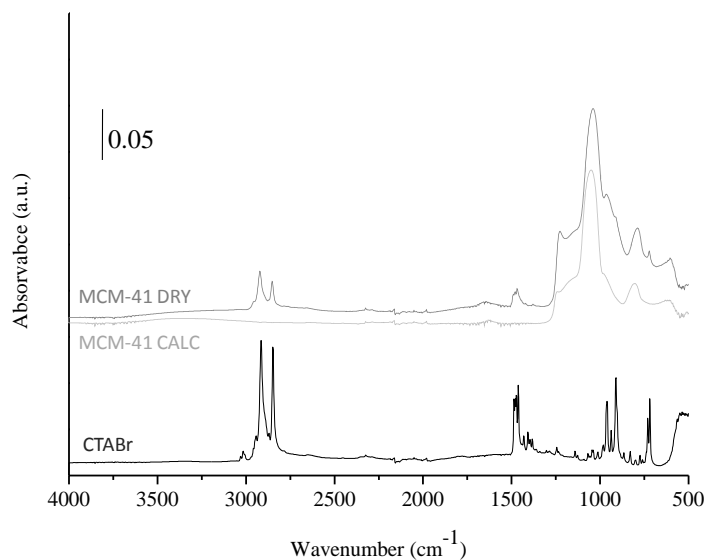


Figure 2. IR spectra of the template, CTABr (dark line), dried and calcined MCM-41 material (grey line and light grey line respectively)

2.2. Structural and textural characterizations of MCM-41

Finally, template-free MCM-41 was studied by X-Ray Diffraction (XRD) and nitrogen adsorption. Figure 3 shows the adsorption isotherm obtained for synthesized MCM-41 material. The isotherm is type IV as the one characteristic of mesoporous materials. Also the hysteresis is typical of this kind of material.

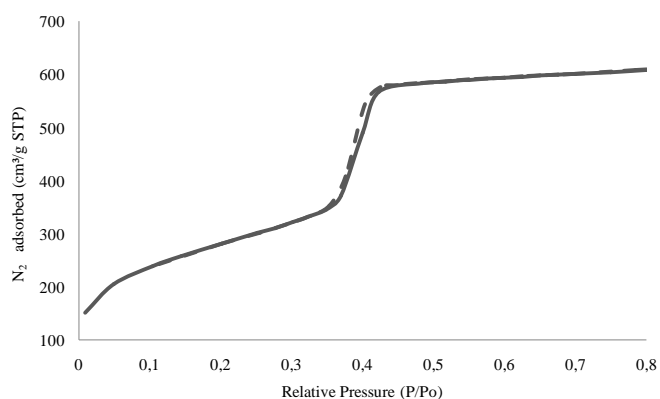


Figure 3. Nitrogen adsorption isotherm for MCM-41

X-Ray Diffraction at small angle was performed as shown in Figure 4. The diffractogram shows the peaks typical of MCM-41 material [6,7], as the intense one at $1.7\ 2\theta$ and smaller two other peaks at 3 and $3.5\ 2\theta$.

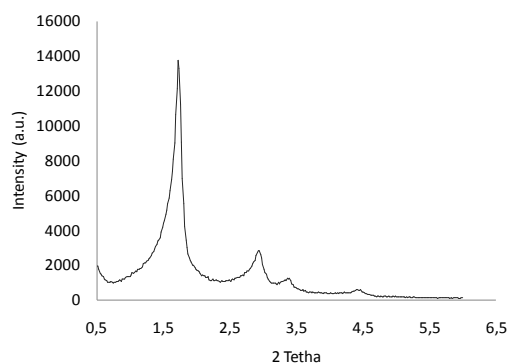


Figure 4. XRD small angle pattern for MCM-41

Finally, Transmission Electron Microscopy (TEM) was used to check the structure of the synthesized material (Figure 5).

All of these results confirm the quality of MCM-41 material synthesized, that can be used as support for HDS catalysts.

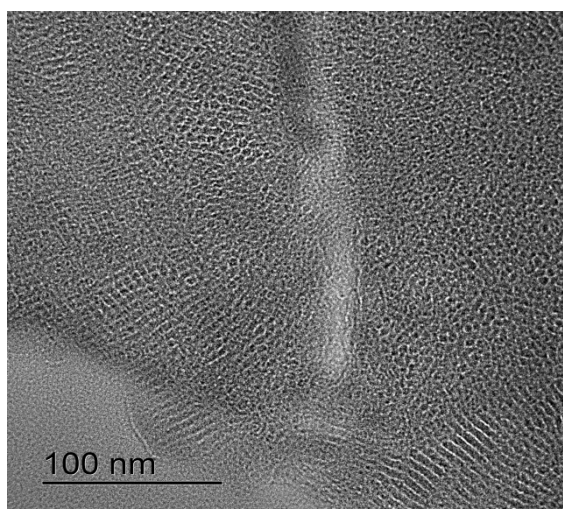


Figure 5. TEM image from MCM-41

2.3. Hydroxyl groups of MCM-41 and commercial silica

IR spectroscopy of CO adsorption at low temperature (IR/CO) was performed to characterize the hydroxyl group of the synthesised MCM-41. IR/CO spectra obtained for MCM-41 and silica were compared (Figure 6). The left and right parts of the figure show that OH groups of MCM-41 and silica materials have the same acidity: perturbation of SiOH by CO of $\sim 90\text{ cm}^{-1}$ and CO/OH stretching band appear at 2157 cm^{-1} for both materials. A CO physisorbed vibration band appears at 2137 cm^{-1} . Accordingly, no change of CO band position was detected for both silica materials and neither difference in OH group density.

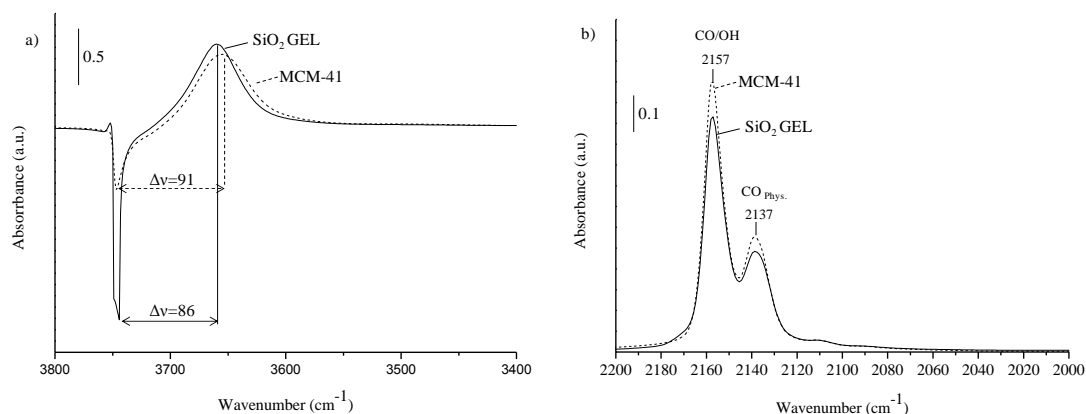


Figure 6. IR spectra of CO adsorption at equilibrium pressure (133 Pa) after heating at 673K/2h for commercial silica (full line) and MCM-41 (dotted line): a) OH region and b) CO stretching vibrations region. Spectra are normalized to surface area

The effect of sulfidation treatment on the MCM-41 surface was also studied. Thus CO spectra at equilibrium pressure after heating and after sulfidation treatments are shown in Figure 7. No change was found after sulfidation treatment so it can be concluded that H_2S/H_2 treatment does not impact in the hydroxyl group for silica surface.

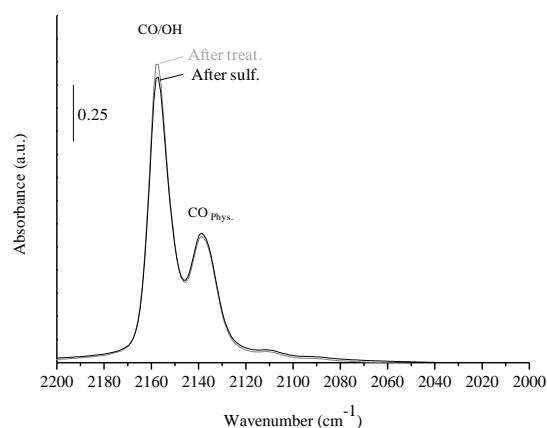


Figure 7. IR spectra of CO adsorption at equilibrium pressure (133 Pa) of MCM-41 after heating treatment at 623K/2h (grey line) and after sulfidation treatment at 623K/2h under 10% H_2S/H_2 (black line)

3. Mo/MCM-41 catalysts

3.1. Oxidic Mo/MCM-41 catalysts

3.1.1. Textural properties

Table 1 summarised the surface area, pore volume and pore size for 1-Mo/MCM-41, 2-Mo/MCM-41 and 3-Mo/MCM-41 oxide catalysts, as well as for pure MCM-41. The three catalysts exhibit a strong decrease of surface area compared with the pure support. That decrease is greater when the Mo amount presented on the catalyst surface is maximum. The pore volume also is decreased, however pore size remains unaltered.

Table 1. Textural study of calcined Mo/MCM-41 catalysts by N₂ adsorption

Samples	Surface area (m ² /g)	Pore volume (cm ³ /g)	Pore size (nm)
MCM-41	945	1.1	4
1-Mo/MCM-41	543	0.6	4
2-Mo/MCM-41	503	0.6	4
3-Mo/MCM-41	338	0.4	4

3.1.2. Raman spectroscopy

Oxidic 1-Mo, 2-Mo and 3-Mo catalysts supported on MCM-41 were studied by Raman spectroscopy (Figure 8). Raman spectrum for 1-Mo/MCM-41 shows two main bands in the vibration domain characteristic of Mo-O vibrations, at 875 and 954 cm⁻¹ ascribed to Mo-O-Mo bridge vibration and Mo=O terminal vibration. These two bands are characteristic of the polymolybdate species. Note that two narrow band at 820 and 995 cm⁻¹ characteristic of MoO₃ are also detected. Raman spectrum for 2-Mo/MCM-41 shows the same bands that indicate that this catalyst is mainly formed by polymolybdate species. However, two low intensity bands at 820 and 995 cm⁻¹ characteristic of MoO₃ species are observed. Raman spectrum for 3-Mo/MCM-41 shows vibration bands at 875 and 954 cm⁻¹ ascribed to polymolybdate species and the vibration bands at 820 and 995 cm⁻¹ characteristic of MoO₃ species. Therefore, it is assumed that 1-Mo and 2-Mo present a great proportion of polymolybdate species on MCM-41, showing a good Mo dispersion. Main species on 3-Mo catalyst are MoO₃ crystallites; this indicates a poor dispersion of oxo-Mo species. These

results are close to the results obtained on commercial silica where the optimum Mo dispersion is reached for 2 atoms Mo/nm² (Chapter V-Figure V.1).

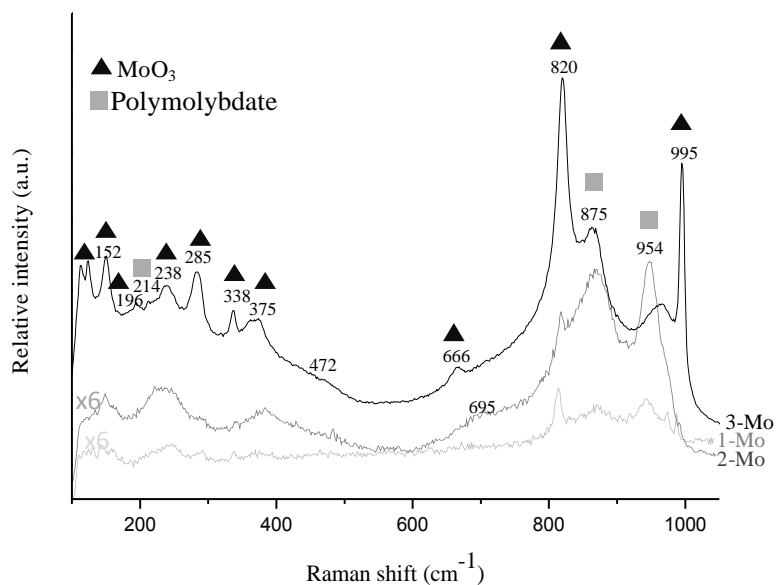


Figure 8. Raman spectra of catalysts in oxidic form for 1-Mo, 2-Mo and 3-Mo supported on MCM-41

3.2. Sulfide Mo/MCM-41 catalysts

3.2.1. Catalytic activity

The effect of Mo loading on HDS catalytic activity for Mo/MCM-41 catalysts was studied using thiophene as model molecule. Figure 9 shows the HDS rate obtained for the three sulfide catalysts, and the ranking of the HDS rate is 1-Mo < 3-Mo < 2-Mo. Similar ranking is observed for Mo/MCM-41 catalysts and for Mo/SiO₂ catalysts (Chapter V). Therefore, it appears that the key parameter is the Mo density of the catalyst not the texture of the silica used as support.

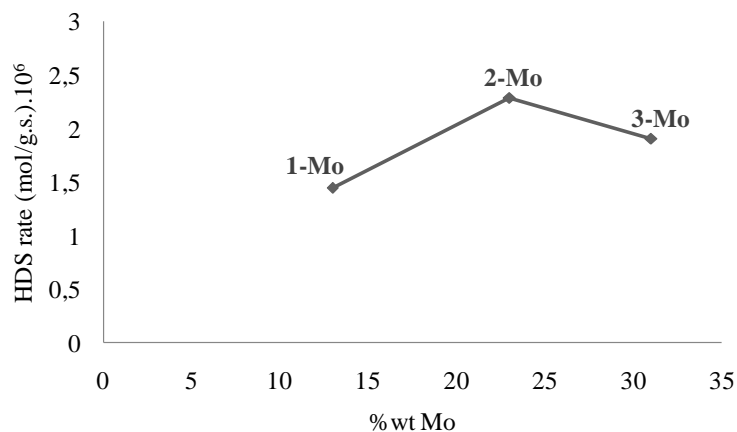


Figure 9. HDS rate on sulfided catalysts supported on MCM-41 with 1 atom Mo, 2 atoms and 3 atoms Mo per nm²

3.2.2. IR/CO characterization

The effect of Mo loading in MoS₂ formation for Mo/MCM-41 sulfide catalysts is studied by the IR/CO method. IR spectra of CO adsorption from small CO pressure up to saturation of CO sites using equilibrium pressure (133 Pa) is shown in Figure 10 for sulfide 1-Mo/MCM-41. Spectra show two types of CO adsorption domains, one related with the support and the other one to MoS₂ sites. CO/OH band appears at 2156 cm⁻¹, as observed on the parent support. CO physisorbed band appears at 2135 cm⁻¹. As for MoS₂ sites, the main νCO band is detected at 2120 cm⁻¹. Besides, several νCO bands appear at lower wavenumber at 2075, 2068, 2040, 2026 cm⁻¹ that can be ascribed to Mo located on S-edge sites with different sulfur coverage. Two main νCO bands located at 2120 and 2075 cm⁻¹ can be ascribed respectively to M-edge sites and to S-edge sites with high sulfur coverage. In addition, CO stretching band at 1998 cm⁻¹ can be assigned to of metallic molybdenum. Furthermore, the band at 1882 cm⁻¹ characterized Si-O vibrations of the sub-surface silica that are perturbed by CO adsorption.

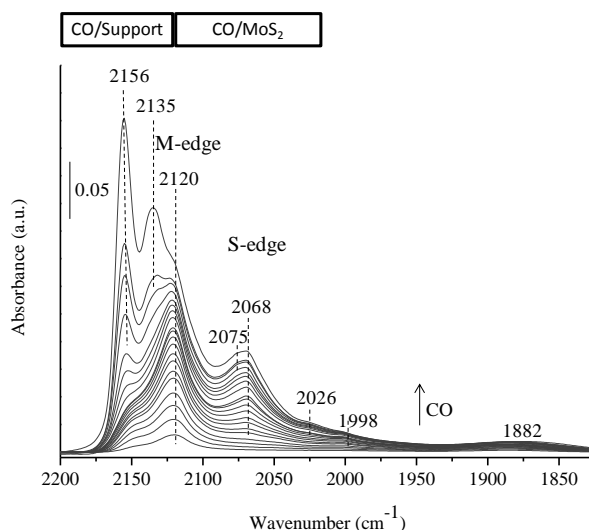


Figure 10. IR spectra of CO adsorption from small CO doses up to saturation at equilibrium pressure (133 Pa) for MoS₂/MCM-41 with 1 Mo atom per nm² (1-Mo)

IR spectra of CO adsorption on sulfide 2-Mo/MCM-41 are shown on Figure 11.a. similar bands are observed : One main ν CO band at 2120 cm⁻¹ ascribed previously to M-edge sites, and several ν CO bands at 2076, 2068, 2040 and 2025 cm⁻¹ that are ascribed to Mo located on S-edge with different sulfur coverage. It has to be noted that the MoS₂ phase bands develop differently with CO doses and at saturation present different intensities and different ratio compared to 1-Mo catalyst.

In the zone 2130-210 cm⁻¹, a main band at 2120 cm⁻¹ ascribed to M-edge sites is detected from the first CO dose introduced. However, one cannot exclude the presence of other species. Indeed, one cannot be ignored that CO stretching band for oxysulfide species appear between 2120 and 2130 cm⁻¹[8]. To clarify the presence or not of these oxysulfide species 2-Mo/MCM-41 catalyst was sulfided at 673K. IR spectra of CO adsorption on 2-Mo/MCM-41 catalyst sulfided at 673K is shown in Figure 11.b. Comparison with spectra obtained after sulfidation at 623 K is presented in dotted line. The same CO bands position are detected for catalyst sulfided at 623 or 673 K. No changes are detected on the first CO doses spectra. Hence, no oxysulfide species are present on this catalyst.

Note that the increase of sulfidation temperature has an effect on the M-edge sites detection, i.e. ν CO band of M-edge sites shows a decreased intensity after the increase of sulfidation temperature. Additionally, no effect in band intensity or position was detected for S-edge sites. This decrease on M-edge sites by the increase of sulfidation temperature was already detected for Mo/Al₂O₃ catalysts and is attributed to a change in MoS₂ morphology [9].

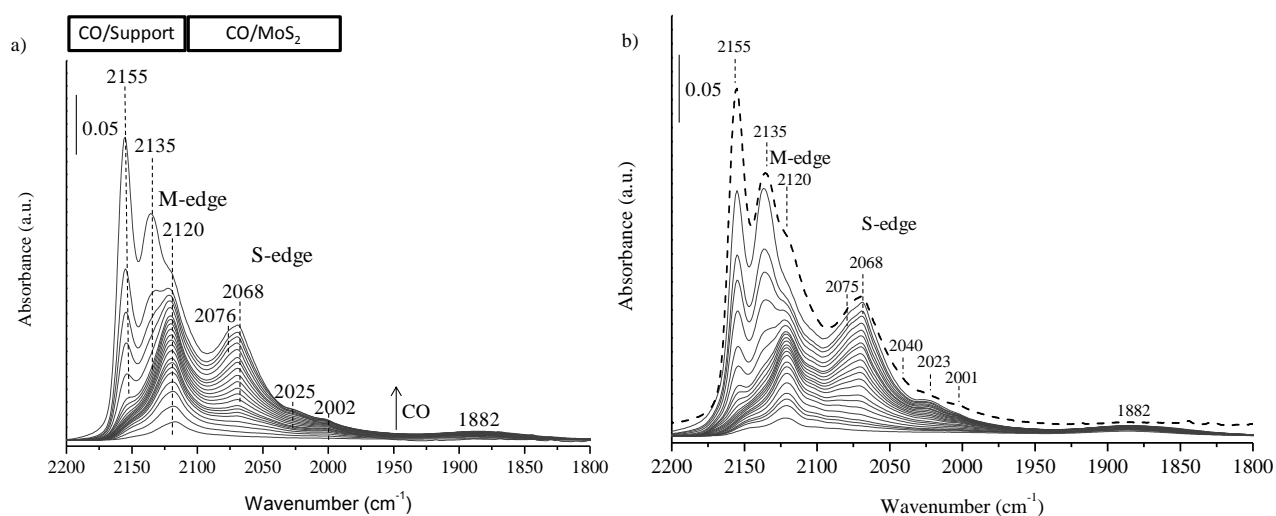


Figure 11. IR spectra of CO adsorption from small CO doses up to saturation using equilibrium pressure (133 Pa) after sulfidation at 623K/2h (a) and after sulfidation at 673K/2h (b) for MoS₂/MCM-41 with 2 atoms Mo per nm² (2-Mo). Note that dotted line represents IR spectra at CO equilibrium pressure after sulfidation at 623K/2h

Finally, 3-Mo/MCM-41 sulfide catalyst was studied by IR/CO method (Figure 12.a). Thus, the same CO stretching bands are detected for CO/support and CO/MoS₂ interaction than on previous catalysts. Additionally, H₂ post-treatment was carried out after conventional sulfidation treatment of 3-Mo/MCM-41 sulfide catalyst to study the effect in the of H₂ treatment on the creation of sulfur vacancies [10,11]. The IR spectra of CO adsorption at equilibrium pressure for sulfided 3-Mo catalyst before and after H₂ post-treatment is shown in

Figure 12.b. The comparison shows that H₂ post-treatment has a strong effect on the position of the IR/CO band (shift from 2120 to 2114 cm⁻¹) and on the amount of sulfided sites. Indeed, the band intensity is four times greater after than before the H₂ post-treatment. Besides, the increase of the band intensity is much more strong for M-edge sites than S-edge sites. This behaviour is characteristic of M-edge sites since 50 % sulfur coverage for M-edge is the most energetically stable. On the other hand 100% of sulfur coverage is the most energetically stable calculated for S-edge sites. This stability can explain the strong influence of H₂ post-treatment, due to M-edge that present after sulfidation 100% of sulfur coverage will tend to adopt the more stable state, 50% of sulfur coverage.

The decrease in sulfur coordination of the Mo edge sites increases the accessibility of Mo sites since CO cannot probe M-edge sites with 100% of sulfur coverage [10,12]. The decrease in sulfur coverage is also confirmed by the band shift toward lower wavenumber of the band characteristic of M-edge sites of the main band and the appearance of a band at 2102

cm^{-1} for M-edge sites. This new νCO band at 2102 cm^{-1} is ascribed to M-edge sites with lower than 50% of sulfur coverage (37%). No shift can be detected for S-edge site band due to the limited sulfur coordination change and due to the overlapping caused by the high band intensity of M-edge sites.

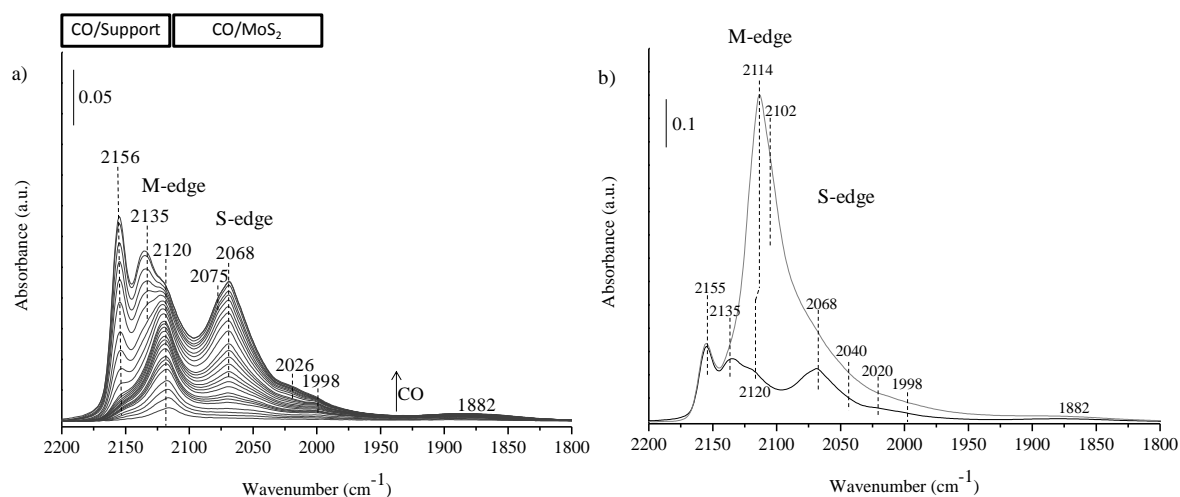


Figure 12. IR spectra of CO adsorption from small CO doses up to saturation at equilibrium pressure (133 Pa) after standard sulfidation at 623K/2h (a), and IR spectra of CO at equilibrium pressure (133 Pa) after standard sulfidation (dark line) and sulfidation followed by H_2 treatment (light line) (b) for Mo/MCM-41 with 3 atoms Mo per nm^2 (3-Mo)

To go further, IR spectra were decomposed and Mo sites were quantified using the molar adsorption coefficient for M-edge and S-edge as $16 \pm 4\text{ cm} \cdot \mu\text{mol}^{-1}$ and $35 \pm 9\text{ cm} \cdot \mu\text{mol}^{-1}$ respectively [13,14]. The concentrations of Mo sites located on M- and S-edge, as well as the total amount of Mo sites after the different activation treatments are summarized in Table 2.

On the catalysts sulfided in standard conditions ($623\text{K}/2\text{h}/10\%\text{H}_2\text{S}/\text{H}_2$), spectra present close frequencies of CO/Mo bands but bands develop differently with CO doses and at saturation they present different intensities. Hence, one can conclude that increasing the Mo loading of MCM-4, increase the S- over M- edge ratio and thus change the sulfide slab morphology. Similar results were obtained for Mo supported on silica (Chapters 3 and 5).

Note that after standard sulfidation, are observed different ratio that likely reveals difference of morphology.

On the Mo catalyst classically sulfided and post-treated under 2% $\text{H}_2\text{S}/\text{H}_2$ at 623 K, spectra present CO/Mo bands at close frequencies than after standard sulfidation; however at

saturation they present some difference in intensities. The change of amount of S- and M-edge sites detection due to the modification of sulfidation procedure is not yet clear. Nevertheless, as previously, data showed that Mo amount increase leads also to an increase of the S- over M- edge ratio.

The pure H₂ post-treatment of sulfided 3-Mo/MCM-41, leads to very strong increase of the amount of Mo sites that is much more important for M-edge sites. This indicates that M-edge is much more sensitive to the reductive environment. This is confirmed by the appearance of a band at 2102 cm⁻¹ that is characteristic of Mo on M-edge with low sulfur coverage.

Table 2. Sites quantification after different treatments: conventional sulfidation (10% H₂S/H₂), 2% H₂S/H₂, and H₂ treatments

Catalysts	Conc. S-edge (μmol/g)	Conc. M-edge (μmol/g)	Total conc. (μmol/g)	S-/M-edge ratio
1-Mo /MCM41	31	63	94	0.49
2-Mo /MCM 41	33	48	82	0.68
3-Mo /MCM 41	35	37	72	0.97
<i>After 2% H₂S/H₂ treatment</i>				
<i>1-Mo /MCM41*</i>	<i>18</i>	<i>77</i>	<i>95</i>	<i>0.23</i>
<i>2-Mo /MCM 41*</i>	<i>33</i>	<i>87</i>	<i>120</i>	<i>0.38</i>
<i>3-Mo /MCM 41*</i>	<i>28</i>	<i>57</i>	<i>85</i>	<i>0.50</i>
<i>After H₂ treatment</i>				
<i>3-Mo /MCM 41**</i>	<i>62</i>	<i>334</i>	<i>396</i>	<i>0.19</i>

The question that arises now is: what are the activation conditions that are representative of the catalyst in reaction conditions i.e. that give sulfide slab morphology and amount of sites equivalent to that of the working catalyst ?

Since the HDS reaction is performed under a flow of 2% H₂S/H₂, since the conversion is maintained below 5%, the spectroscopic data relevant for comparison with catalysis are those obtained on the catalysts sulfided and post-treated under 2% H₂S/H₂. Therefore, the sites quantification after 2% H₂S/H₂ post-treatment were taken into account to study the MoS₂ morphology and total sites available for reaction since this condition is the one near to reaction condition using in this work.

Figure 13 showed a relation between Mo loading and S-/M-edge ratio. Thus, higher Mo loading showed higher S-/M-edge ratio indicating a change in MoS₂ morphology from

truncated triangle to truncated triangle more near to a perfect hexagon. Since commercial silica and MCM-41 have different surface area, Mo catalysts with the same Mo density presented different Mo wt%. Hence, Figure 13 has also collected the S-/M-edge ratio detected for Mo/SiO₂ catalysts (commercial silica). The comparison between Mo catalysts supported on SiO₂ and MCM-41 showed a relation between Mo loading and MoS₂ morphology for Mo supported on silica catalysts.

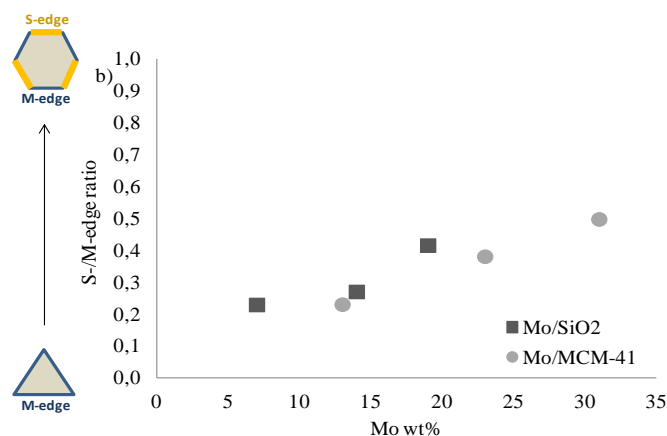


Figure 13. Relation between S-/M-edge ratio and Mo loading for Mo supported on MCM-41 and commercial silica

3.2.3. HDS Activity

Total sites detected by IR/CO after 2% H₂S/H₂ post-treatment and HDS rate for Mo/SiO₂ and Mo/MCM-41 catalysts are represented in Figure 14. This representation showed a relation between the amount of Mo sites available for reaction and the catalytic activity. However, there is not a linear relation due to another factor that also influences in the catalytic activity as the MoS₂ morphology. Previously was shown that Mo loading has an effect in MoS₂ morphology, and then the influence of this parameter in the catalytic activity can be studied by the calculation of TOF values. For that, Figure 15 relates TOF values and MoS₂ morphology, i.e. S-/M-edge ratio, leading to show a relation between them: the highest S-/M-edge ratio showed the highest TOF value.

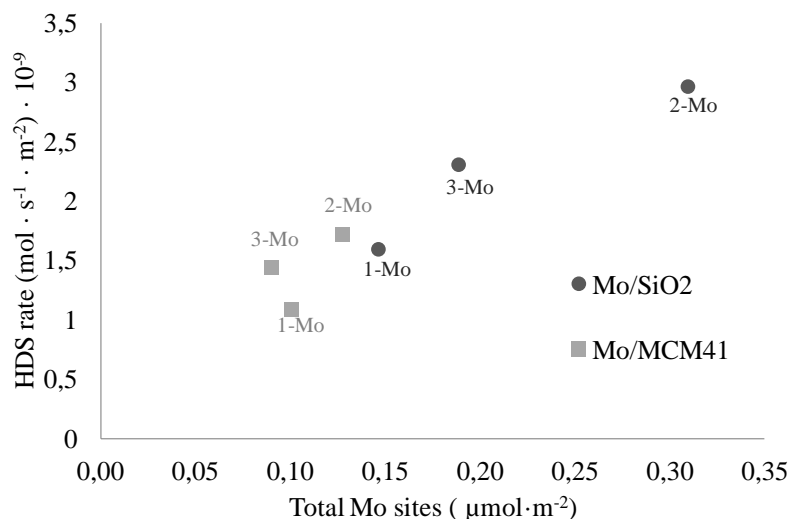


Figure 14. Relation between HDS rate and total sites detected by IR/CO after 2% H₂S/H₂ post-treatment for Mo supported on commercial silica (SiO₂) and MCM-41

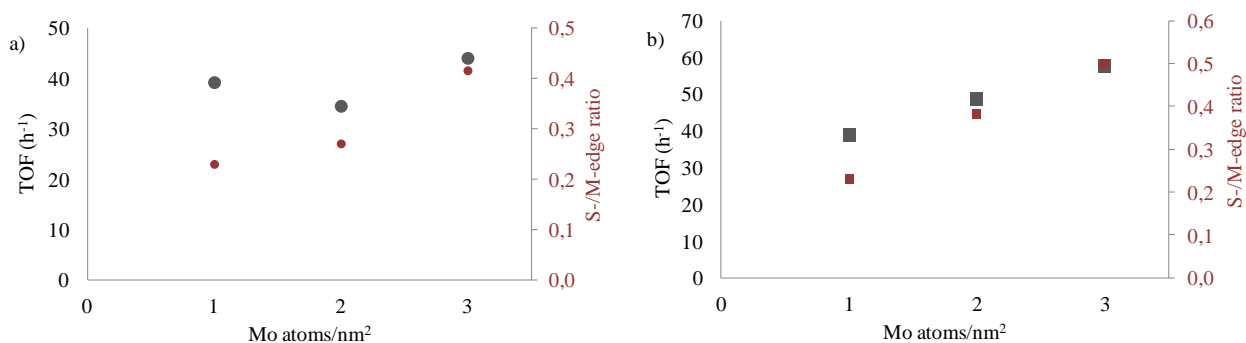


Figure 15. Relation between TOF value and S-/M-edge value for Mo/SiO₂ catalysts (a) and Mo/MCM-41 catalysts (b)

3.3. Calculation of TOF_{M-edge} and TOF_{S-edge} for Mo supported on silica

The quantification of Mo sites by IR/CO allows the TOF calculation. Generally the equation used to study TOF is showed bellow:

$$r_{\text{HDS}} = n \cdot \text{TOF}$$

where r_{HDS} is the thiophene HDS rate, n is concentration of active sites, TOF is the activity per site.

Recently, we develop a method allowing to distinguish the “total” TOF from the TOF of Mo located on M-edge (TOF_{M-edge}) and TOF from Mo located on S-edge (TOF_{S-edge}) using

a serial of Mo/Al₂O₃ catalysts with changes in S-/M-edge ratio [15]. Therefore, the previous equation can be refined by including these two components:

$$r_{\text{HDS}} = n_{\text{M-edge}} \cdot \text{TOF}_{\text{M-edge}} + n_{\text{S-edge}} \cdot \text{TOF}_{\text{S-edge}}$$

where $n_{\text{M-edge}}$ and $n_{\text{S-edge}}$ are the concentration of Mo sites on M-edge and S-edge, respectively.

The series of Mo/SiO₂ catalysts with different Mo density (1, 2, and 3 atoms Mo per nm²) and different S-/M-edge ratio allow calculating the TurnOver Frequency (TOF) characteristic from M-edge (TOF_{M-edge}) and S-edge (TOF_{S-edge}). The calculation was performed using Microsoft excel 2010 with the multi -actor line regression tool.

Table 3. Summary of the data used to calculate the TOF on M-edge and on S-edge for Mo catalysts supported on silica and MCM-41

Catalysts	Thiophene rate (μmol/g.h)	Concentration M-edge sites (μmol/g)	Concentration S-edge sites (μmol/g)
1-Mo/SiO ₂	2900	60	14
2-Mo/SiO ₂	5400	123	33
3-Mo/SiO ₂	4200	67	28
1-Mo/MCM41	3700	77	18
2-Mo/MCM41	5850	87	33
3-Mo/MCM41	4900	57	28

Note: Edge sites detected by IR/CO after the 2% H₂S/H₂ post-treatment

Table 4 shows the parameters obtained for the linear regression for the calculation of TOF on M-edge and S-edge for silica catalysts. Then, It is obtained that TOF_{M-edge} is 18 ± 10 cm·μmol⁻¹ and TOF_{S-edge} is 103 ± 35 cm·μmol⁻¹ for the series of Mo/SiO₂ catalysts and TOF_{M-edge} is 15 ± 2 cm·μmol⁻¹ and TOF_{S-edge} is 141 ± 6 cm·μmol⁻¹ for the series of Mo/MCM-41 catalysts. Close values were obtained for the two series; however high error of the calculation for Mo/SiO₂ catalysts was obtained due to there is a point out of the tendency as shows Figure 15. This figure relations TOF value with S-/M-edge ratio showing a linear relation for Mo/MCM-41 catalysts but the first point of the series of Mo/SiO₂ is out of the tendency explaining the error obtained for calculations.

Table 4. Calculation results of TOF_{M-edge} and TOF_{S-edge} by Microsoft 2010

	<i>Coefficients</i>	<i>Error</i>	<i>t</i>	<i>P</i>
Mo/SiO₂ catalysts				
TOF _{M-edge}	18	10	1.7	0.2
TOF _{S-edge}	103	35	2.9	0.1
Mo/MCM-41 catalysts				
TOF _{M-edge}	15	2	7	0.02
TOF _{S-edge}	141	6	24	0.001

<i>Catalysts</i>	Mo/SiO ₂	Mo/MCM-41
<i>Regression line parameters</i>		
Multiple R	0.998	0.999
R Square	0.996	0.999
Adjusted R Square	0.494	0.499
Standar Desviation (SD)	339	74
Observation	4	4

Note: (0,0) was also used as a point in order to reduce the error

4. Conclusion

In the present annex, Mo supported on mesoporous silica, MCM-41 was studied and compared to Mo/silica. Firstly, the pure MCM-41 present a much greater specific area (945 m²/g) than silica (506 m²/g). However, the density of silanol groups as well as their acidic properties is similar for both supports.

Comparison of Mo/MCM-41 and Mo/SiO₂ with the same Mo density shows that on oxidic catalysts, the optimum Mo dispersion is obtained for 2 atoms Mo per nm². Besides on the sulfide catalysts supported on MCM-41 and silica, the increase of Mo loading leads an increase on S-/M-edge ratio. In both cases, the morphology goes from a truncated triangle (1 Mo at.nm²) to more near to a perfect hexagon (3 Mo at.nm²) (Figure 13).

The highest catalytic activity as well as the highest amount of Mo sites was detected for 2-Mo catalysts. By contrast, the 3-Mo catalyst presents a lower activity as well as a lower amount of Mo sites, that is a consequence of the lower dispersion of the Mo phase at the oxidic stage.

It has to be mentioned that for the two series of catalysts, a similar relationship was found between Mo sulfided sites amount and the catalytic activity. Additionally, a relation between the S-/M-edge ratio and TOF value was found, i.e. the higher the S-/M-edge ratio, the higher the TOF value (Figure 15). Indeed, higher TOF value was detected for S-edge sites than M-edge sites. Note that for the two series of catalysts, the TOF values calculated are close.

The drawback of silica supported catalysts is that when a high density of Mo is introduced, Mo phase presents a poor dispersion. A way to overcome this problem is the use of high surface area silica as MCM-41. This work shows that similar behaviors are observed between Mo supported on silica or on MCM-41 while higher Mo amount can be introduced on MCM-41 materials.

5. References

- [1] H. Shimada, *Catal. Today* 86 (2003) 17–29.
- [2] A. Taguchi, F. Schuth, *Microporous Mesoporous Mater.* 77 (2005) 1–45.
- [3] D. Trong On, D. Desplandier-Giscard, C. Danumah, S. Kaliaguine, *Appl. Catal. A Gen.* 253 (2003) 545–602.
- [4] A. Truel, *Microporous Mesoporous Mater.* 27 (1999).
- [5] V. Meynen, P. Cool, E.F. Vansant, *Microporous Mesoporous Mater.* 125 (2009) 170–223.
- [6] C.-Y. Chen, S.L. Burkett, H.-X. Li, M.E. Davis, *Microporous Mater.* 2 (1993) 27–34.
- [7] W. Zhang, M. Fröba, J. Wang, *J. Am. Chem. Soc.* 7863 (1996) 9164–9171.
- [8] V. Labruyere, *Structure Des Sites Sulfures Des Catalyseurs D'hydrotraitment: Approche Combinée Par Spectroscopie IR et Modélisation Moléculaire*, 2014.
- [9] J. Chen, V. Labruyere, F. Mauge, A.-A. Quoineaud, A. Hugon, L. Oliviero, *J. Phys. Chem. C* 118 (2014) 30039–30044.

- [10] A. Travert, C. Dujardin, F. Mauge, S. Cristol, J.F. Paul, E. Payen, D. Bougeard, *Catal. Today* 70 (2001) 255–269.
- [11] A. Travert, H. Nakamura, R.A. van Santen, S. Cristol, J.F. Paul, E. Payen, *J. Am. Chem. Soc.* 124 (2002) 7084–7095.
- [12] A. Travert, C. Dujardin, F. Mauge, E. Veilly, S. Cristol, J.F. Paul, E. Payen, *J. Phys. Chem. B* 110 (2006) 1261–1270.
- [13] F. Mauge, J.C. Lavalley, *J. Catal.* 137 (1992) 69–76.
- [14] J. Chen, E. Dominguez Garcia, L. Oliviero, F. Maugé, *J. Catal.* 332 (2015) 77–82.
- [15] J. Chen, Effet de La Pression de Sulfuration et D'agent Chélatant Sur La Morphologie et La Réactivité Des Phases Sulfures, PhD, University of Caen, 2014.

Annex III. Effect of Mo loading and titania structure on the MoS₂ morphology of Mo/TiO₂ catalysts

1 Introduction

In the previous study (see chapter III), Mo sulfide catalysts (3 at Mo/nm²) supported on Al₂O₃, SiO₂ and TiO₂ were studied. Mo/TiO₂ catalyst showed the highest catalytic activity compared to Mo/Al₂O₃ and Mo/SiO₂. This high activity could be related to a large amount of sulfide sites but also to their high TOF. Note also that Mo/TiO₂ presents greater hydrogenation properties than the other catalysts. Hence, these previous results show a specific behaviour for catalyst supported on TiO₂. It was proposed that the origin come from a strong metal-support interaction on this catalyst. To establish this point, several questions have to be answered:

- Is this particular behavior detected for Mo-3/TiO₂, a specific case or is it typical of Mo/TiO₂ catalysts? To go further, a series of Mo/TiO₂ catalysts with different Mo loadings (2, 3 and 4 at Mo/nm² denoted as 2-Mo, 3-Mo and 4-Mo) were studied

- The TiO₂ used as support in this study (chapter III) is formed by a mixture of anatase (80%) and rutile (20%) phases. It will be denoted in the present annex as TiO₂-A. The question that arises is: Has the small proportion of rutile an influence on MoS₂ slabs? In order to answer this question, a commercial TiO₂ formed exclusively by anatase structure and denoted as TiO₂-B was used. Mo/TiO₂-B catalyst with the Mo density of 3 atoms Mo per nm² was prepared and compared to the Mo/TiO₂-A (see Chapter III).

2 Effect of Mo loading on Mo/TiO₂-A

2.1 Oxidic Mo/TiO₂-A

The effect of Mo loading in Mo dispersion on Mo/TiO₂-A oxide catalysts was studied using Raman spectroscopy. Because TiO₂-A is formed by anatase and rutile phases, some vibration modes characteristic of Titania structure were detected in all Raman spectra at low

wavenumbers. Anatase phase presents some characteristic vibration modes at 147, 244, 324, 396, 517, 638, and 798 cm^{-1} ; while, rutile phase presents some characteristic vibration modes at 199, and 446 cm^{-1} [1]. The intensities of these characteristic vibration modes are higher than those of oxomolybdate vibration bands. In order to have a better insight of the oxomolybdate species, the three Raman spectra of $\text{MoO}_x/\text{TiO}_2$ with 2, 3 and 4 Mo %wt are represented in the range of oxomolybdate vibrations, i.e. between 800 and 1000 cm^{-1} in Figure 1. All three Raman spectra show principally two vibration bands at 965 and 876 cm^{-1} ascribed to Mo=O terminal vibration mode and Mo-O-Mo bridge vibration mode, respectively[2]. Moreover, the Raman spectrum of 4-Mo catalyst shows an intense band at 995 cm^{-1} . This band could be ascribed to MoO_3 species. MoO_3 species in general present two characteristic vibration bands at 820 and 995 cm^{-1} attributed to Mo-O-Mo bridge vibration mode and Mo=O terminal vibration mode, respectively[3–5]. The band at 820 cm^{-1} for 4-Mo catalyst in Figure IV seems to be highly overlapped due to the high intensity structural vibrations thus, very difficult to interpret. However, the MoO_3 species formation for Mo/TiO_2 catalyst composed by 4 Mo atoms/ nm^2 was reported in the literature [2]. Thus, it can be taken as consideration to determine that 4- Mo/TiO_2 catalyst presents MoO_3 species on its surface. In conclusion, polymolybdate species are detected in the three oxide catalysts. Mo is good dispersed down to 3 Mo atoms/ nm^2 , however above this Mo concentration, MoO_3 species were detected indicating worse Mo dispersion.

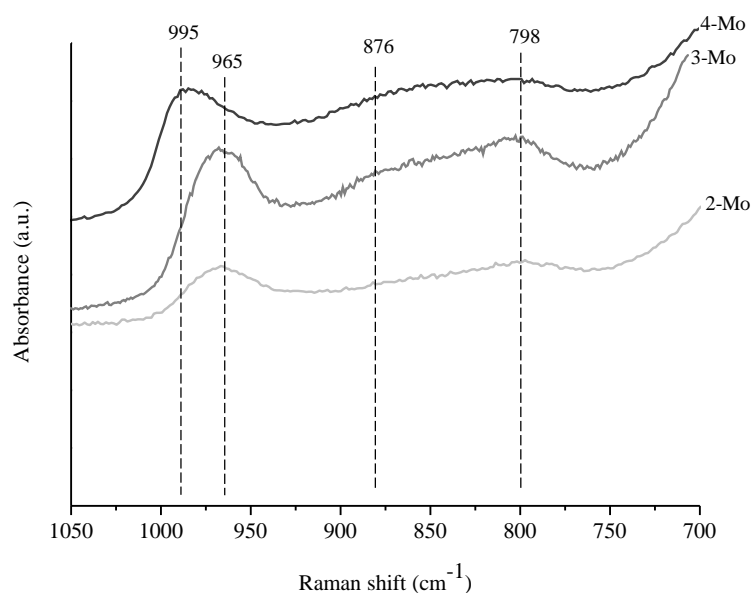


Figure 1. Raman spectra of $\text{Mo}/\text{TiO}_2\text{-A}$ calcined catalysts in oxidic form with different Mo density: 2 at. Mo/nm^2 (2-Mo, light grey line), 3 at. Mo/nm^2 (3-Mo, grey line) and 4 at. Mo/nm^2 (4-Mo, black line)

Additionally, UV-Vis experiments were performed for $\text{MoO}_x/\text{TiO}_2$ catalysts in order to calculate the absorption edge energy of the three catalysts and thus predict the domain size of molybdenum oxide species formed on the catalyst surfaces with the Mo loading variation [5]. The relation between number of next nearest neighbour of $\text{MoO}_x/\text{TiO}_2$ catalysts and the absorption edge energy is shown in Figure 2. Similarly the absorption edge energies are calculated for different Mo loadings on $\text{MoO}_x/\text{TiO}_2$ catalysts, i.e. 3.05, 2.9 and 2.8 eV for 2-Mo, 3-Mo and 4-Mo catalysts respectively. Thus, the Mo loading caused decrease in the absorption edge energy and the increase of the oxomolybdate domain size.

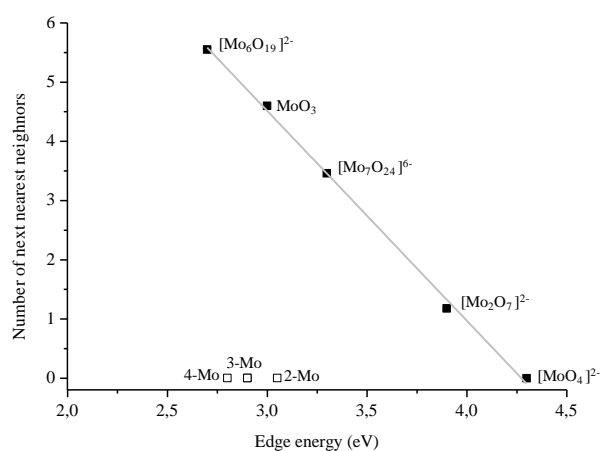


Figure 2. Relation between the Absorption Edge energy calculated by UV-VIS spectroscopy and number of next nearest neighbour predict for some references for Mo/TiO_2 oxide catalysts with different Mo density (2, 3, and 4 at. Mo per nm^2)

The small absorption edge energy variation detected for different Mo loadings is an indication of the strong metal-support interaction detected in the previous study (see chapter III).

2.2 Sulfided $\text{Mo}/\text{TiO}_2\text{-A}$

The Mo loading effect in the MoS_2 morphology for $\text{Mo}/\text{TiO}_2\text{-A}$ catalysts was studied by CO adsorption at low temperature followed by FTIR spectroscopy (IR/CO). Three different Mo densities used are: 2, 3 and 4 at. Mo per nm^2 . The sulfide catalyst with 3-Mo/ TiO_2 was studied in detail in the previous study (see chapter III), therefore the IR/CO spectra of this catalyst is not re-shown in this work. The IR spectra of CO adsorption from small CO pressure up to sites saturation using equilibrium pressure (133 Pa) for 2-Mo and 4-Mo/ $\text{TiO}_2\text{-A}$ sulfide catalysts are shown in Figure 3.a and Figure 3.b, respectively. IR/CO spectra of 2-Mo/ $\text{TiO}_2\text{-A}$ catalyst show

two different CO adsorption domains: CO adsorption on the titania surface and CO adsorption on MoS₂, active sites. The first one concerns the CO interaction with the support and appears at higher wavenumbers, between 2140 and 2200 cm⁻¹. The CO interactions with Titania surface give two main bands at 2182 and 2162 cm⁻¹ that correspond to Lewis acid sites (Ti⁴⁺) and hydroxyl group distorted by SH⁻ species, respectively. The νCO/OH band distorted by SH⁻ species were ascribed in the previous study where the sulfidation effect on titania surface was studied by IR/CO indicating a strong sulfidation influence in Lewis acid sites and hydroxyl group (see chapter III). On the other hand, CO stretching bands from the interaction with MoS₂ nanoparticles appear in a low wavenumber region between 2000 and 2130 cm⁻¹. One principal νCO band is detected at 2118 cm⁻¹ ascribed to M-edge sites with a shoulder at 2070 cm⁻¹ ascribed to S-edge sites. The CO stretching bands were detected in the same position for 4-Mo/TiO₂-A sulfide catalyst than 2-Mo/TiO₂-A catalyst. Although, the main νCO/M-edge band shows lower intensity for 4-Mo/TiO₂-A catalyst compared to 2-Mo/TiO₂-A catalyst.

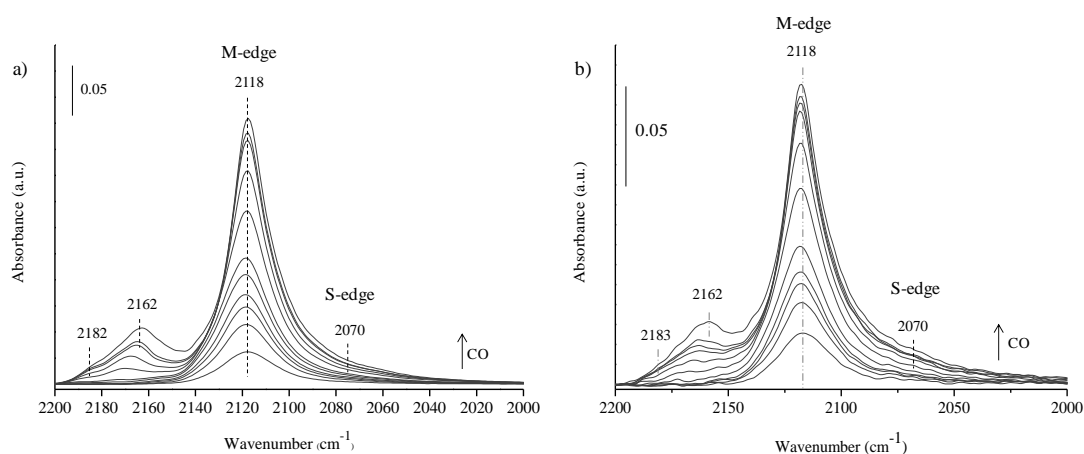


Figure 3. IR spectra of CO adsorption at low temperature from small CO pressure up to sites saturation for Mo/TiO₂-A catalysts: a) 2 atoms Mo/nm² and b) 4 atoms Mo/nm²

The study of the Mo loading effect in MoS₂ morphology for Mo/TiO₂-A catalysts is carried out by the comparison of IR/CO spectra at CO equilibrium pressure (133 Pa) for the three sulfide catalysts as shows Figure 4. The same CO stretching bands are detected for the three catalysts, i.e. νCO bands at 2162 and 2184 cm⁻¹ that correspond to hydroxyl group distorted by SH⁻ species and Lewis acid sites respectively, and the two νCO bands at 2070 and 2118 cm⁻¹ correspond to Mo located on S-edge and M-edge respectively. However, the Mo loading increase leads to a decrease of the band intensity of the νCO/M-edge band. The decrease of sites can be linked with the increase of slabs length by the increase of Mo amount

on the Titania surface. The Mo loading increase is related with the decrease of $\nu\text{CO}/\text{Ti}^{4+}$ band and also the decrease of $\nu\text{CO}/\text{OH}$ band for 4-Mo/ TiO_2 -A catalyst that can be attributed to the excess of Mo on the surface forming MoO_3 species as was detected by Raman spectroscopy.

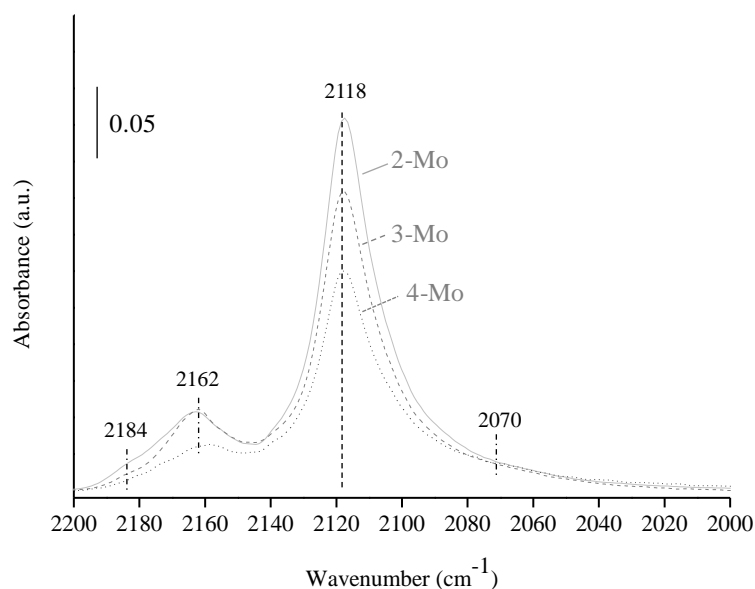


Figure 4. IR spectra of CO adsorption at equilibrium pressure (133 Pa) for Mo/ TiO_2 -A catalysts with different Mo density (2, 3 and 4 at. Mo per nm^2)

The quantification of M-edge and S-edge sites detected by IR/CO using their respective molar extinction coefficients (16 and $35 \text{ cm} \cdot \mu\text{mol}^{-1}$ for M-edge and S-edge respectively [6,7]) are summarized in Table 1. Total sites are formed by the sum of both Mo edges sites detected by IR/CO. Therefore, the increase of Mo loading shows a decrease of total sites probe by CO as was predicted previously. On the other hand, no change in MoS_2 morphology is detected by the increase of Mo loading because MoS_2 nanoparticles are formed mostly by M-edge sites, more than 95% of the total sites detected.

Table 1. Sites quantification detected by IR/CO for Mo/TiO₂-A catalysts with 2, 3 and 4 Mo % wt

Catalysts	Conc. M-edge (μmol/g)	Conc. S-edge (μmol/g)	Total edge (μmol/g)	% M-edge	% S-edge
2-Mo/TiO ₂	101	3	104	97%	3%
3-Mo/TiO ₂	80	3	83	96%	4%
4-Mo/TiO ₂	65	3	68	96%	4%

The morphology for MoS₂ in Mo/TiO₂-A catalysts can be predicted as triangular in shape formed by M-edge sites as shows Figure 5 and is independent of Mo loading. The decrease in sites with Mo loading can be explained by the corresponding increase of MoS₂ slabs length which in turn leads to a decrease of metal dispersion on the edge[8]. Interestingly, the higher amount of Mo sites detected by IR/CO is not related with the higher Mo dispersion amount detected by Raman spectroscopy, i.e. 3-Mo catalyst that presents the higher Mo dispersion on the surface, showed lower Mo sites probed by CO compared to 2-Mo catalyst. It indicates the increase of Mo leads to form large MoS₂ slabs decreasing Mo sites available for reaction.

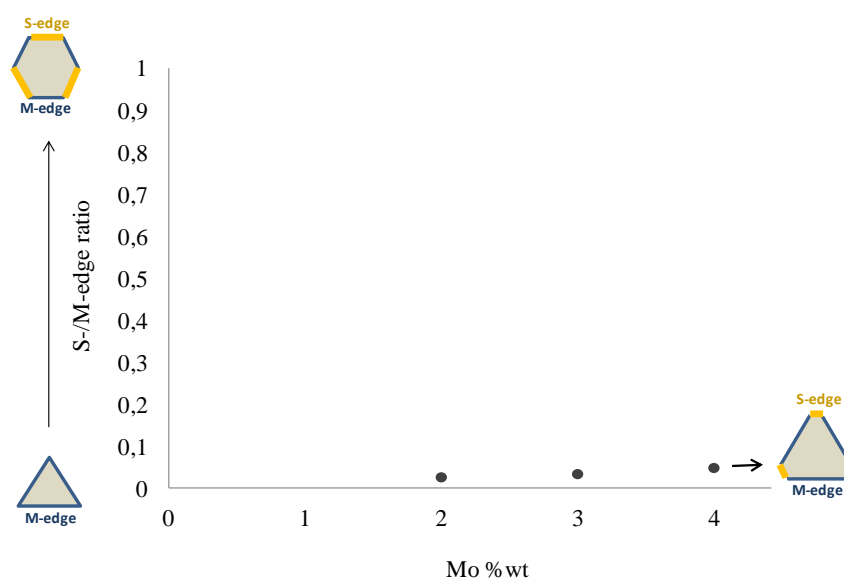


Figure 5. Relation between MoS₂ morphology and Mo loading on Mo/TiO₂-A

2.3 Conclusion

In conclusion, polymolybdate species are detected on the three calcined oxide catalysts. Mo has a good dispersed up to 3 Mo atoms/nm², however above this Mo concentration, MoO₃ species were detected indicating worse Mo dispersion. Mo-O bridge and terminal mode vibrations are detected at constant wavenumbers - 874 and 965 cm⁻¹ respectively - whatever the Mo loading. These bands appeared at high wavenumber compared to Mo supported on alumina and silica catalysts, indicating a strong metal-support interaction characteristic of Mo/TiO₂ catalysts. On sulfided Mo/TiO₂, the increase of Mo loading did not lead to any change in sulfide slab morphology, thus the triangular slabs with exposed M-edge sites is observed for the three Mo/TiO₂ catalysts. This effect is ascribed to the strong MoS₂-TiO₂ interaction that was found to be characteristic of the titania-supported catalysts.

3 Effect of TiO₂ structure on Mo/TiO₂

3.1 Oxidic Mo/TiO₂-A and Mo/TiO₂-B

The Raman spectra for Mo/TiO₂-A and Mo/TiO₂-B oxide catalysts with the same Mo density (3 atoms Mo/nm²) are compared in Figure 6. Raman spectrum of Mo/TiO₂-B catalyst shows the typical vibration modes of anatase phase at low wavenumber range: 147, 199, 324, 396, 517, 638 and 798 cm⁻¹. The comparison of both Raman spectra at low wavenumber region shows that TiO₂-B catalyst is only formed by anatase phase while TiO₂-A is formed by both anatase and rutile phases that is in agreement with the XRD patterns for each support before impregnation. Besides, Raman spectrum of Mo/TiO₂-B catalyst shows two main vibration bands in the vibration range of oxomolybdate at high wavenumber, i.e. between 800 and 1000 cm⁻¹. These two bands are detected at 965 and 874 cm⁻¹ assigned to Mo=O terminal vibration mode and Mo-O-Mo bridge vibration mode, respectively. Those bands appear at the same wavenumber that the one for Mo/TiO₂-A catalyst thus the same metal-support interaction can be proposed for Mo-TiO₂-A and -TiO₂-B catalysts. Additionally, MoO₃ species formation is not detected for Mo/TiO₂-B catalyst, therefore, Mo can be considered as dispersed on TiO₂-B surface since just vibration bands characteristic of polymolybdate species were detected. Note the same band shift to higher wavenumber was detected for Mo/TiO₂-B than Mo/TiO₂-A for Mo-O vibration modes compared to Mo/Al₂O₃ and Mo/SiO₂ catalysts. It indicates the strong metal-support interaction for all Mo/TiO₂ catalysts.

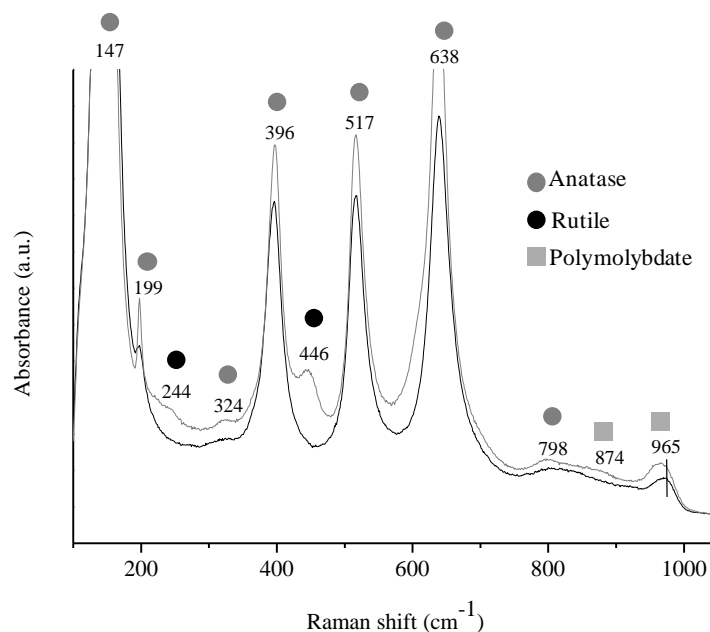


Figure 6. Raman spectra of calcined Mo catalysts supported on TiO₂-A (grey line) and TiO₂-B (black line)

The absorption edge energy was calculated for Mo/TiO₂-B catalyst by UV-Vis spectroscopy and found to be 3 eV that is in the same range than the one calculated for Mo/TiO₂-A (2.9 eV). In conclusion, Mo catalysts supported on TiO₂ are characterised by the same absorption edge energy and then the same oxomolybdate species. A band shift to higher wavenumber is found for those catalysts in relation with others such as Mo/Al₂O₃ or Mo/SiO₂. This shift can be link with the strong support-metal interaction that presents all Mo/TiO₂ catalysts.

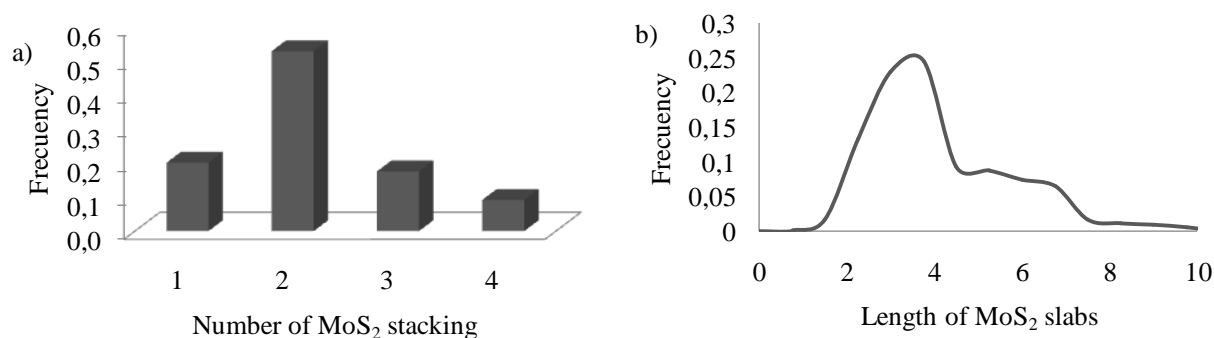
3.2 Sulfided Mo/TiO₂-A and Mo/TiO₂-B

3.2.1 Transmission Electron Microscopy (TEM)

The stacking and length of MoS₂ slabs present on Mo/TiO₂-B catalyst surface were determined by Transmission electron microscopy and shown in Figure 7.a and b respectively. Thus, Mo/TiO₂-B catalyst mostly present slabs with stacking 2, and, in less extent, stacking 1 and 3, as well as, large slabs length between 2 and 8 nm, with the maximum at 4 nm.

The average slab length and stacking for Mo/TiO₂-B and Mo/TiO₂-A catalysts (from chapter III) are summarised in the table presented on the bottom of the Figure 7. Similar

stacking are detected for both Mo/TiO₂ catalysts (stacking 2), but the slab length for Mo/TiO₂-B (4.6 nm) was found smaller than Mo/TiO₂-A catalyst (6.7 nm).



Catalysts	Average stacking	Average length
Mo/TiO ₂ (A)	2	6.7
Mo/TiO ₂ (B)	1.8	4.6

Figure 7. Stacking and length of MoS₂ slabs on Mo/TiO₂ (B) catalysts. The bottom table summarized the length and stacking averages for sulfided Mo supported on TiO₂-A and TiO₂-B

3.2.2 Study by IR/CO

The IR spectra of CO adsorption from small CO pressure up to sites saturation for Mo/TiO₂-B catalyst after sulfidation treatment are shown in Figure 8.a. IR spectra show two different CO adsorption domains: CO adsorption on Titania surface and CO adsorption on the active sites, MoS₂. CO interactions with Titania surface give several CO stretching bands: the principal one at 2168 and 2163 cm⁻¹ ascribed to OH group perturbed by SH⁻ species from the sulfidation treatment; and two small ones at 2184 and 2192 cm⁻¹ ascribed to Lewis acid sites[9]. On the other hand, CO interacts with MoS₂ nanoparticles giving a principal band at 2120 cm⁻¹ ascribed to Mo sites located in M-edge. Hence, the νCO/M-edge stretching band at high wavenumber, i.e. around 2118-2120 cm⁻¹, can be consider as a characteristic of MoS₂ nanoparticles in interaction with titania surface. The strong MoS₂-TiO₂ interaction reduces the Mo→CO back donation which leads to a band shift to higher wavenumber. Additionally, the study of H₂ post-treatment in the Mo sites detection by IR/CO was also performed for this catalyst. IR spectra of CO adsorption after H₂ post-treatment from small CO pressure up to sites saturation for Mo/TiO₂-B catalyst is shown in Figure 8.b. The CO interaction with TiO₂-B surface gives several vibration bands with the maximum detected at 2181 and 2163 cm⁻¹ that are ascribed to Lewis acid sites and hydroxyl group, respectively. However, the CO interaction

with MoS₂ nanoparticles gives rise a main vibration band at 2112 cm⁻¹ with a shoulder at 2102 cm⁻¹, which are ascribed to M-edge sites with different sulfur coverage. Further, other small vibration band is detected at low wavenumber at 2065 cm⁻¹ that is ascribed to Mo located on S-edge sites.

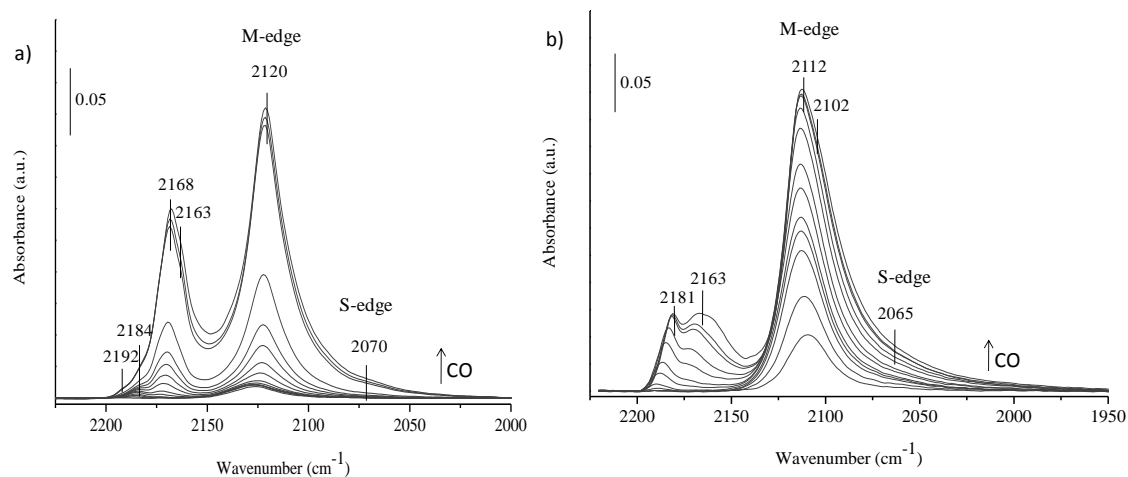


Figure 8. IR spectra of CO adsorption from small doses up to saturation at equilibrium pressure (133 Pa) after sulfidation at 623K/2h under 10% H₂S/H₂ (a) and after post-treatment at 623K/2h under H₂ (b) for Mo/TiO₂-B catalyst

Figure 9 shows the IR spectra of CO adsorption at equilibrium pressure (133 Pa) before and after H₂ post-treatment for Mo/TiO₂-B catalyst. The H₂ post-treatment effect is evident in all CO adsorption domains. The intensity of ν CO/Ti⁴⁺ band at 2181 cm⁻¹ increased after the post-treatment due to the elimination of SH⁻ species that react with H₂ to form H₂S. In the opposite way, CO/OH stretching perturbed by SH species appeared at 2168 cm⁻¹ shows a decreased intensity due to the elimination of SH species. On the other hand, the main ν CO/M-edge band shifted to lower wavenumber from 2120 to 2112 cm⁻¹ and a new ν CO band appeared at lower wavenumber, at 2102 cm⁻¹. The sulfur removal from the MoS₂ edges due to the H₂ post-treatment decreases the sulfur coverage leading to the lower wavenumber shift of ν CO/Mo sites bands. Thus, the band at 2102 cm⁻¹ is ascribed to M-edge sites with 37% of sulfur coverage [7,10]. On the other hand, the band shift detected for the main ν CO/M-edge sites is also ascribed to the decrease of the electron density effect of TiO₂-B surface to MoS₂ nanoparticles. Thus, H₂ post-treatment has an effect in the electron density reduction from the support to MoS₂ nanoparticles. Besides, the band shift from 2070 to 2065 cm⁻¹ for ν CO/S-edge is also detected by the sulfur removal due to the H₂ post-treatment. In general, a slightly

increase of the availability of Mo sites was observed after H₂ post-treatment being in agreement with the result obtained previously for Mo/TiO₂-A.

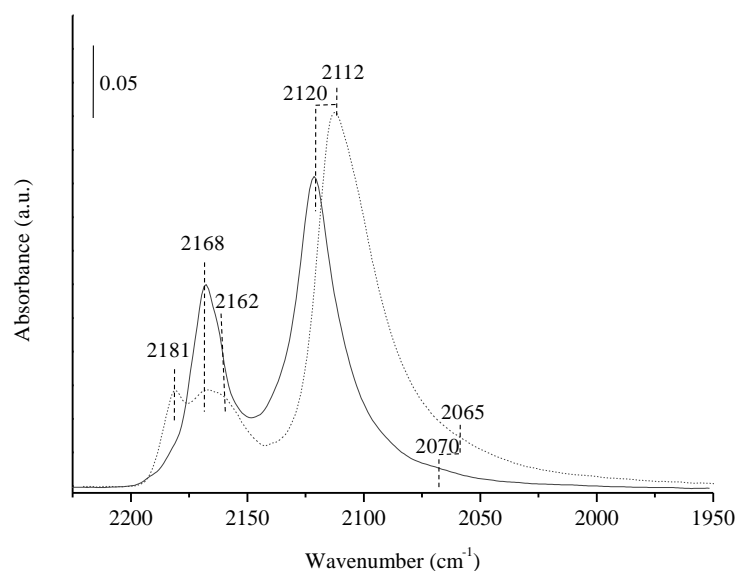


Figure 9. IR spectra of CO adsorption at equilibrium pressure (133 Pa) after sulfidation at 623K/2h under 10% H₂S/H₂ (black line) and after post-treatment at 623K/2h under H₂ (grey line) for Mo/TiO₂-B catalyst

Mo located on M- and S-edge can be discriminated and quantified using the respective molar extinction coefficient (16 ± 4 and 35 ± 6 respectively) [6,7] and shown in Table 2 as along with the percentage of Mo located in both M- and S-edge. The H₂ post-treatment does not show a strong effect in Mo/TiO₂ catalysts indicating the strong metal-support interaction that is characteristic of these kinds of catalysts. Mostly M-edge sites were detected for all Mo/TiO₂ catalysts therefore the MoS₂ morphology is predicted as truncated triangular shape close to perfect triangle formed by M-edge sites.

Table 2. Mo sites quantification after sulfidation (10% H₂S/H₂) and after H₂post-treatment for Mo catalysts supported on TiO₂-A and TiO₂-B with 3 atoms Mo/nm²

Catalysts	Conc. M-edge (μmol/g)	Conc. S-edge (μmol/g)	Total edge (μmol/g)	% M edge	% S edge	S-/M-edge ratio
Mo/TiO ₂ (B)	92	1	93	99%	1%	0.01
Mo/TiO ₂ (B) After H ₂ treatment	135	10	145	93%	7%	0.08
Mo / TiO ₂ (A)	80	3	82	97%	3%	0.03
Mo / TiO ₂ (A) After H ₂ treatment	100	7	107	93%	7%	0.10

3.2.3 Activity and TOF calculation

Since mostly M-edge sites are present on MoS₂ slabs of Mo/TiO₂ catalysts, the MoS₂ morphology has not to be considered for explaining change in HDS rate. Indeed, a good correlation appears between total Mo sites and HDS rate both for Mo/TiO₂-A and Mo/TiO₂-B catalysts (Figure 10). A linear relationship is found between total Mo sites detected by IR/CO and HDS rates per area unit. Total TOF values are shown in parentheses for both catalysts. Close TOF values are obtained for Mo-3 supported on TiO₂-A and TiO₂-B, 35 h⁻¹ and 44 h⁻¹, respectively. Hence, the TOF value for Mo/TiO₂ catalysts are greater than those measured on Mo/Al₂O₃ and Mo/SiO₂ catalysts. This points out the specificity of Mo sites when supported on titania.

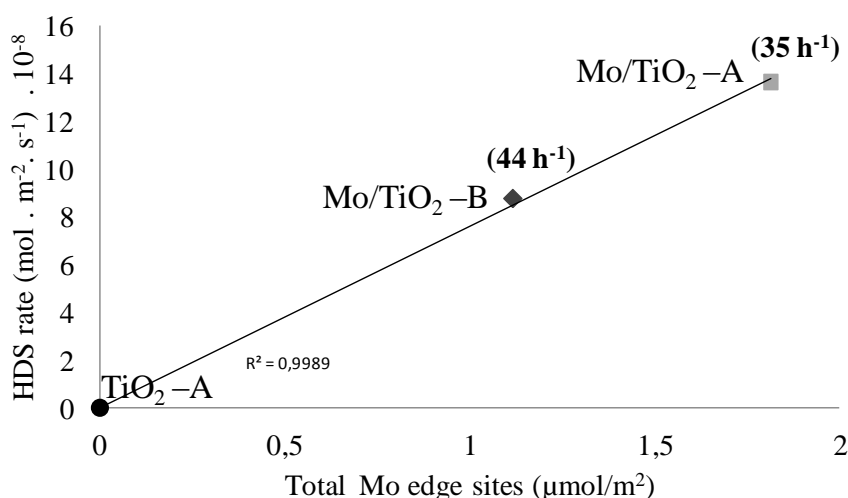


Figure 10. Relationship between thiophene HDS activity and total edge sites detected by IR/CO for sulfided Mo/TiO₂-A and Mo/TiO₂-B catalysts. TOF values are presented in parenthesis

3.3 Conclusion

In conclusion, Mo was found dispersed on Mo/TiO₂-B catalyst in oxidic form. Besides, polymolybdate species was detected by the terminal vibration band at 965 cm⁻¹ and bridge vibration band at 874 cm⁻¹ for the oxidic catalyst. Mostly M-edge sites are detected by IR/CO method for MoS₂/TiO₂ catalysts. Then, triangle shape is proposed as the MoS₂ morphology typical of Mo catalysts supported on TiO₂ whatever the titania structure. The CO adsorption on M-edge sites presents a specific stretching band between 2118 and 2120 cm⁻¹ for Mo supported on TiO₂-A and TiO₂-B catalysts. This band position recorded at higher wavenumber compared to νCO/M-edge bands for other catalyst, e.g. Mo/Al₂O₃ or Mo/SiO₂ (see chapter III) that is ascribed to the specific electron density that present titania surface leading to strong Mo-TiO₂ interaction. This strong interaction reduces the back donation from Mo to CO and then showing a band shift to higher wavenumber. This strong metal-support interaction could be detected by Raman spectra since Mo-O mode vibrations appear at higher wavenumber compared to Mo supported on alumina and silica catalysts.

4 Conclusion

Two series of Mo/TiO₂ catalysts were studied from their oxide to sulfided form in order to have a more insight about the so-called metal-support interaction. In this part, two parameters were modified in order to study their effect on MoS₂ formation: Mo loading and the structure of the support. For all Mo/TiO₂ catalysts, mainly one IR/CO band is detected at 2118 (2120 cm⁻¹ for Mo/TiO₂-B) ascribed to M-edge sites. Hence, the spectroscopic characterization provides evidence that sulfided Mo supported on TiO₂ are formed by triangular shaped MoS₂ slabs exposing M-edge sites whatever the Mo loading and the titania structure.

Comparison with Mo supported on silica and alumina shows some main differences:

(1) CO on Mo/M-edge band present a constant wavenumber (2118 cm⁻¹) whatever the Mo loading, and is located at higher wavenumber on Mo/TiO₂ than on Mo-3/SiO₂ (2110 cm⁻¹) and Mo-3/Al₂O₃ (2111 cm⁻¹).

(2) A striking feature is the absence of any change of morphology of the MoS₂ slab with Mo loading for sulfided Mo/TiO₂ catalysts whereas increase of Mo amount leads to a development of S-edge at the expense of M-edge on Mo supported on silica and alumina,

(3) The value of TOF Mo/M-edge is clearly greater for Mo supported on titania A and B (Mo/TiO₂:35-40 h⁻¹) than for Mo/SiO₂ (18 h⁻¹) and Mo/Al₂O₃ (22 h⁻¹).

These specific behaviours of sulfided slabs on titania can be explained by a very strong metal-support interaction that prevents any change of morphology by Mo addition. The very strong interaction between sulfided phase and titania that changes the electronic properties of the Mo sites, should be at the origin of the greater TOF and other specific behaviour of Mo/TiO₂ as detailed in Chapter III.

5 References

- [1] H.L. Ma, J.Y. Yang, Y. Dai, Y.B. Zhang, B. Lu, G.H. Ma, *Appl. Surf. Sci.* 253 (2007) 7497–7500.
- [2] S. Dzwigaj, C. Louis, M. Breysse, M. Cattenot, V. Bellière, C. Geantet, M. Vrinat, P. Blanchard, E. Payen, S. Inoue, H. Kudo, Y. Yoshimura, *Appl. Catal. B Environ.* 41 (2003) 181–191.
- [3] N. Chestnoy, R. Hull, L.E. Brus, *J. Chem. Phys.* 85 (1986) 2237.
- [4] L. Brus, *J. Phys. Chem.* 90 (1986) 2555–2560.
- [5] M. Fournier, C. Louis, M. Che, P. Chaquin, D. Masure, *J. Catal.* 119 (1989) 400–414.
- [6] F. Mauge, J.C. Lavalley, *J. Catal.* 137 (1992) 69–76.
- [7] J. Chen, E. Dominguez Garcia, L. Oliviero, F. Maugé, *J. Catal.* 332 (2015) 77–82.
- [8] S. Kasztelan, H. Toulhoat, J. Grimblot, J.P. Bonnelle, *Appl. Catal.* 13 (1984) 127–159.
- [9] a. Travert, O. V. Manoilova, a. a. Tsyganenko, F. Mauge, F. Maugé, J.C. Lavalley, *J. Phys. Chem. B* 106 (2002) 1350–1362.
- [10] C. Dujardin, M.A. Lelias, J. van Gestel, A. Travert, J.C. Duchet, F. Mauge, *Appl. Catal. A Gen.* 322 (2007) 46–57.

- [11] D. Costa, C. Arrouvel, M. Breyse, H. Toulhoat, P. Raybaud, *J. Catal.* 246 (2007) 325–343.

ANNEX IV. Decomposition

1. Decomposition of IR spectra at CO equilibrium pressure for non-promoted catalysts from chapter III

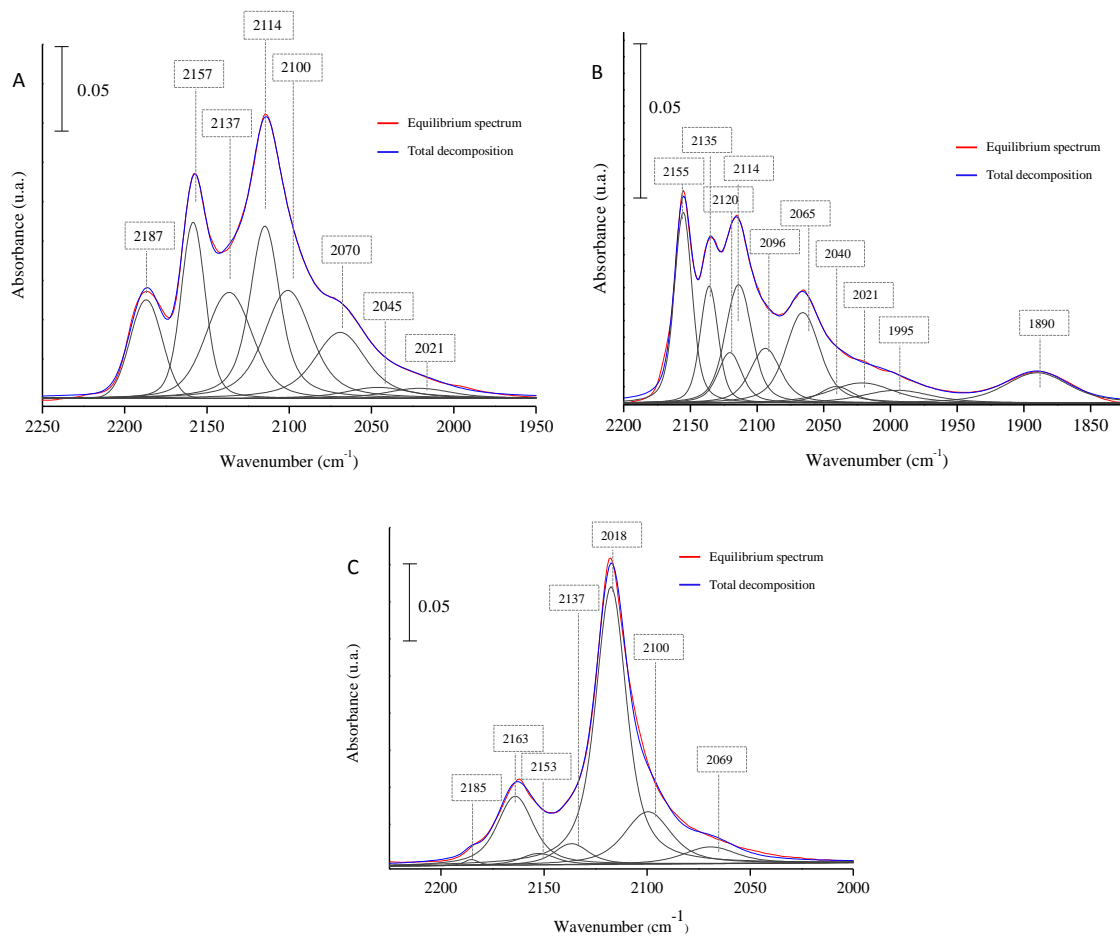


Figure 1. Decomposition of IR spectra at CO equilibrium pressure for a) Mo/Al₂O₃, b) Mo/SiO₂ and c) Mo/TiO₂ after conventional sulfidation condition (10% H₂S/H₂)

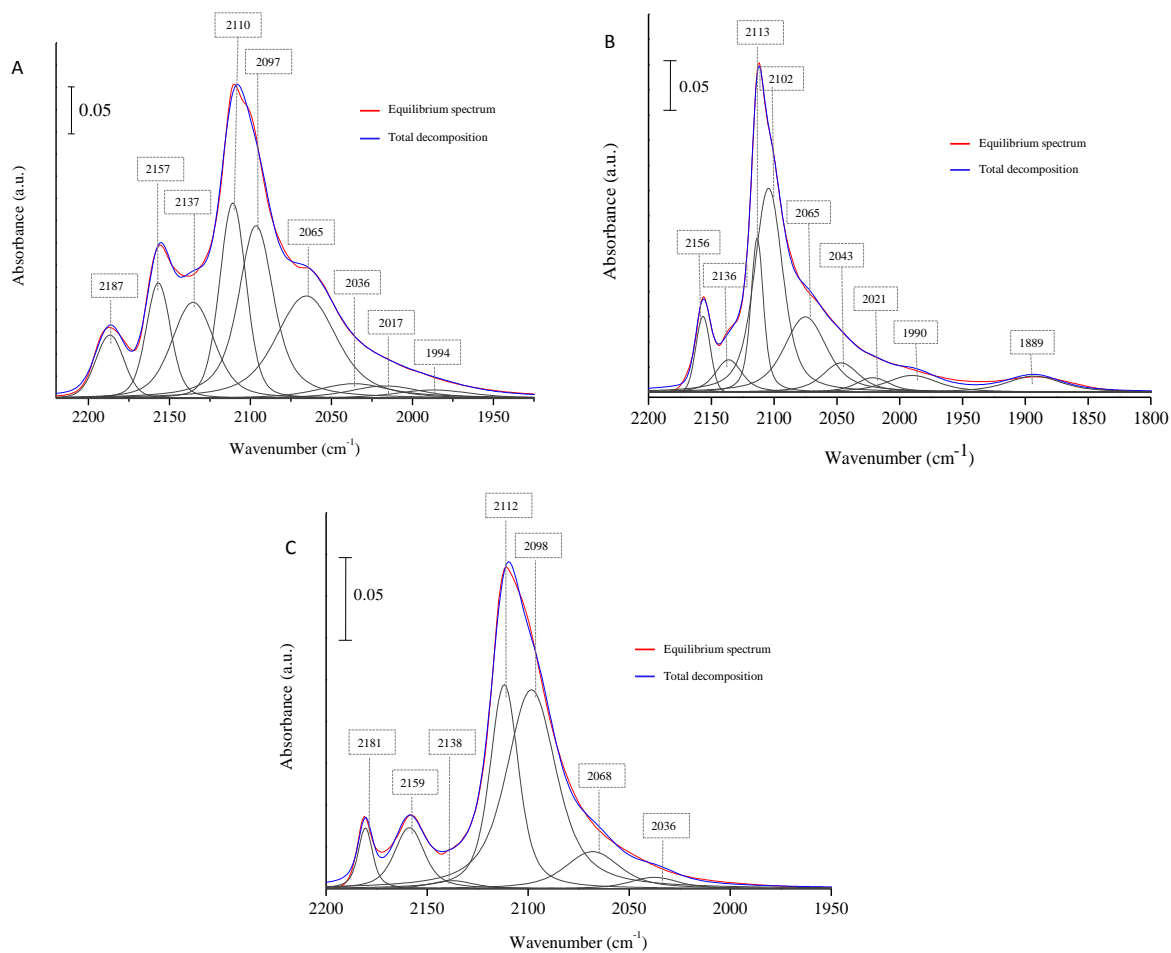


Figure 2. Decomposition of IR spectra at CO equilibrium pressure for a) Mo/Al₂O₃, b) Mo/SiO₂ and c) Mo/TiO₂ after H₂ post-treatment

2. Decomposition of CO saturated spectra on promoted catalysts from chapter IV

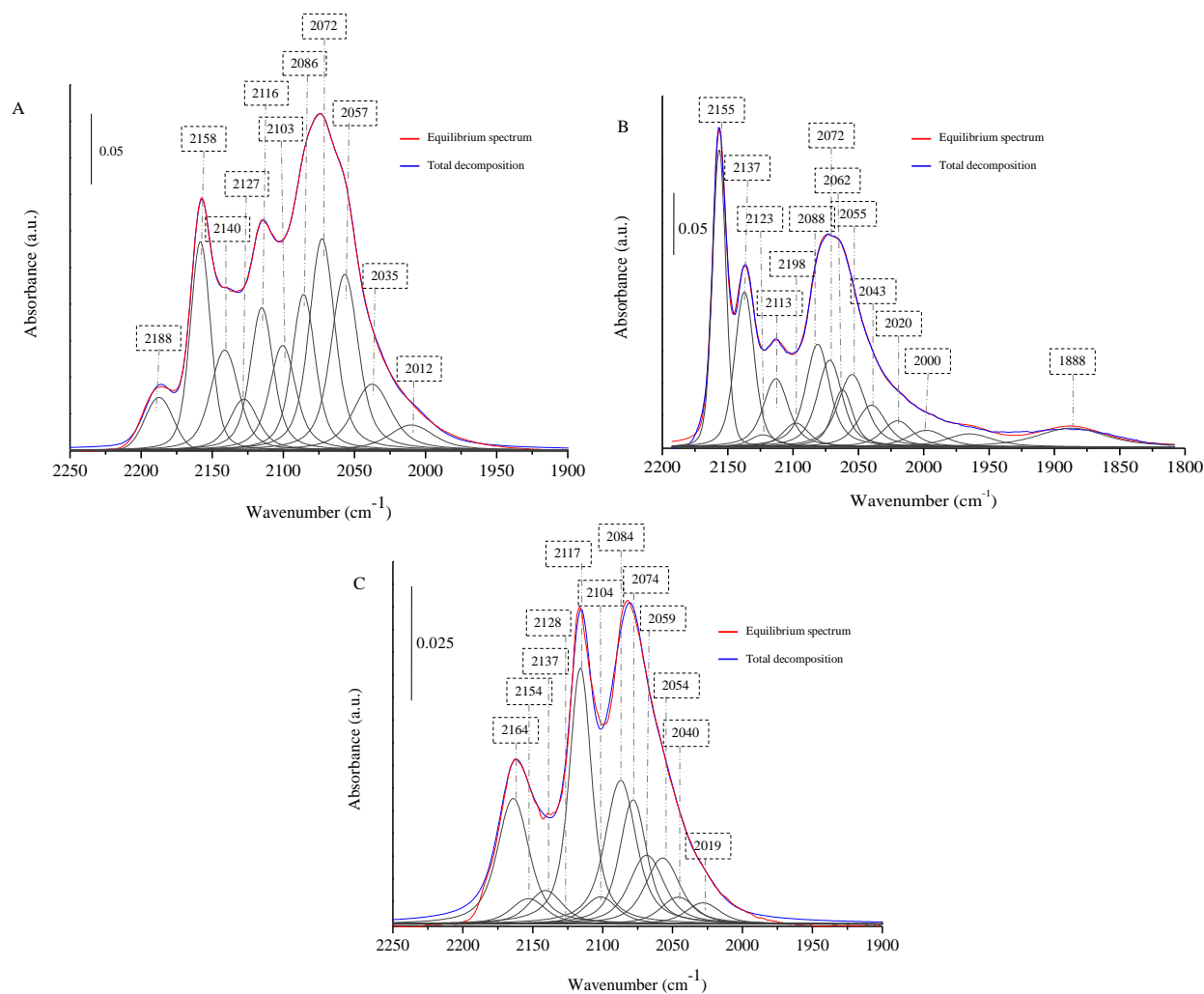


Figure 3. Decomposition of IR spectra at CO equilibrium pressure (133 Pa) for a) CoMo/Al₂O₃, b) CoMo/SiO₂ and c) CoMo/TiO₂ after conventional sulfidation condition (10% H₂S/H₂)

GENERAL CONCLUSION

This manuscript presents a deep molecular insight into sulfide Mo and CoMoS sites of industrial type hydrotreatment catalysts. The objective of this work was to identify factors that determine the sulfided phase morphology as well as the formation of CoMoS sites on supported (Co)Mo catalysts. Main parameters investigated are support nature, influence of Mo amount and effect of pre-treatment.

At the oxidic stage, catalysts were mainly characterized by Raman and UV-Vis spectroscopies. After sulfidation, the catalysts were deeply investigated by CO adsorption at low temperature followed by FTIR spectroscopy (IR/CO). This technique gives accurate information about the nature, structure and amount of sulfide sites. In addition, IR/CO spectral data were analyzed by 2D-IRIS, a new technique developed at LCS laboratory. The sulfide catalysts were also characterized by Transmission Electron Microscopy (TEM), and tested in thiophene hydrodesulfurization (HDS).

On unpromoted Mo catalyst, the study of Mo deposited on various supports as alumina, silica (commercial silica and MCM-41), and TiO₂ (anatase with a fraction of rutile, and pure anatase) points out that the strength of the metal(sulfide)-support interaction is a key factor. The nature of the support affects both the dispersion of the oxidic phase, the morphology of the sulfided phase as well as the concentration of the MoS₂ edge sites.

The influence of the strength of interaction with the support is observed from the oxidic stage. Indeed study of oxidic catalysts with a constant Mo density (3 at. Mo/nm²) shows the appearance of MoO₃ crystallites for Mo/SiO₂, whereas only polymolybdate species are detected for Mo/Al₂O₃ and Mo/TiO₂. In addition, drying or calcination does not change the oxidic species formed on Mo/Al₂O₃ and Mo/TiO₂ whereas on Mo/SiO₂ it influences the amount of MoO₃ formed. This provides evidence for the weak interaction with the silica support.

The influence of strength of interaction with the support is much more striking at the sulfide stage. Indeed, for a constant Mo density (3 at. Mo/nm²), IR/CO shows that the support strongly influences the S-/M-edge ratio. It varies such as Mo/SiO₂ > Mo/Al₂O₃ > Mo/TiO₂,

indicating a change of MoS₂ slabs morphology. Thus, Mo/SiO₂ is formed by MoS₂ nanoparticles with a near hexagonal shape, while MoS₂ slabs present truncated-triangular shape on Mo/Al₂O₃ and triangular shape on Mo/TiO₂.

The effect of Mo loading on silica and titania supported catalysts was studied in this work, and on alumina supported catalysts in a previous work¹. The Mo loading also influences the MoS₂ morphology of Mo/SiO₂ and Mo/Al₂O₃ catalysts. The morphological changes with Mo amount are more important on silica than on alumina. On Mo/TiO₂ catalysts, the Mo loading does not change the morphology of sulfide phase. This absence of modification points out the strong interaction between MoS₂ and titania. These results confirm that metal-support strength controls the sulfide phase morphology.

In order to determine the influence of the reaction atmosphere on the MoS₂ edges, the sulfide catalysts were post-treated under various conditions: under pure H₂ or under 2% H₂S/H₂ at 623 K. Note that this last post-treatment mimics the thiophene HDS atmosphere. Both treatments increase the amount of CUS Mo sites on all the catalysts. It should be noted that the CUS sites creation is more important on M-edges than on S-edges. Interestingly, the augmentation very strongly depends on the support nature, it is more important on sulfided phase supported on silica than on alumina than on titania. For this last support, the variation is almost negligible. Since the treatment under 2% H₂S/H₂ is representative of the reaction conditions, the amount of sites and the S-/M-edge ratio measured in this condition will be used for comparison with thiophene HDS results.

Then, a parallel appears between the total amount of Mo sites and the HDS rate. Comparison at a constant surface area shows that Mo supported on titania is the most active in agreement with its greater amount of sites. To go further intrinsic activity of M and S-edge sites has been calculated considering the amount of each type of sites on the different catalysts. First, TOF of S-edge sites is greater than TOF of M-edge sites. On M-edge sites, TOF is similar on silica and alumina catalysts but significantly greater on titania ones.

It has to be mentioned some specific behaviors of titania supported catalysts as: (1) the high amount of CUS Mo sites compared to the amount of Mo exposed deduced from TEM, (2) the stability of the supported phase regarding pre-treatment as well as post-treatment, (3) the detection of almost exclusively M-edge sites, (4) the high TOF value. All these features can be accounted for a strong MoS₂-Titania interaction.

In conclusion, these results show that chosen morphology of MoS₂ phase can be obtained by properly choosing the support nature and in a more limited way the pre-treatment conditions and the Mo amount.

On sulfide Co-promoted catalysts, it is well-known that IR/CO allows distinguishing unpromoted Mo sites from promoted sites. However, in the IR signal generally assigned to CoMoS sites at least three components can be distinguished. Several questions are raised: what is their specific assignment? Do they indeed characterize CoMoS sites since in the same region CO in interaction with Mo sites located on S-edge can appear? Hence, in order to answer this question, a new method of spectra treatment called 2D Infrared Inverse Spectroscopy (2D-IRIS) has been applied. This method took in consideration the different CO absorption energies. 2D-IRIS allows excluding the presence of band characteristic of unpromoted Mo sites on S-edge sites in the CoMoS massif. Thanks to this finding, the question of the location of Co promoter on the MoS₂ edges can be addressed. For the three supports, a nice parallel appears between the S-/M- edge sites ratio of Mo catalysts and the promotion degree (CoMoS/MoS₂ sites) of CoMo catalysts. This evidences that the more S-/M- edge ratio, the greater the promotion degree. Thus, S-edges are favorable to anchor promoter. This is in agreement with DFT calculation and STM observation on model catalysts. However, since the promotion degree is greater than the S-/M-edge sites ratio of the various catalysts, it points out that Co promoter also anchored on M-edge sites.

The detection of three IR/CO components at 2057, 2073 and 2083 cm⁻¹ i.e. in the zone characteristic of promoted sites can be linked to different structures of CoMoS as location on S- or M- edges. Taking into account the frequencies predicted by DFT calculation², the detection of the three components versus Co introduction on MoS₂ by CVD experiments using Co(CO)₃NO³, and the variation of the three components on the CoMo catalysts on the different supports, assignments of the three bands can be proposed. Hence, these bands can be ascribed to Co on partially promoted S- edge (band at 2057 cm⁻¹), Co on partially promoted M-edge (band at 2073 cm⁻¹) and Co on totally promoted M-edge (band at 2083 cm⁻¹).

The morphologies of promoted catalyst can be deduced from the area of these various CoMoS sites as well as of the band characteristic of Mo sites on M-edges. It appears that the S-/M- edge ratio of promoted catalysts slightly increases with Co addition. This

morphological change by promotion of the MoS₂ slabs is in agreement with DFT calculation prediction and STM observation.

There is a parallel between the total amount of promoted sites and thiophene HDS rate but without linear relationship. This indicates that the different CoMoS sites present different intrinsic activity. In particular, it appears that the CoMoS sites located on partially promoted M-edge (characterized by a band at 2073 cm⁻¹) present a higher TOF than the two other CoMoS sites.

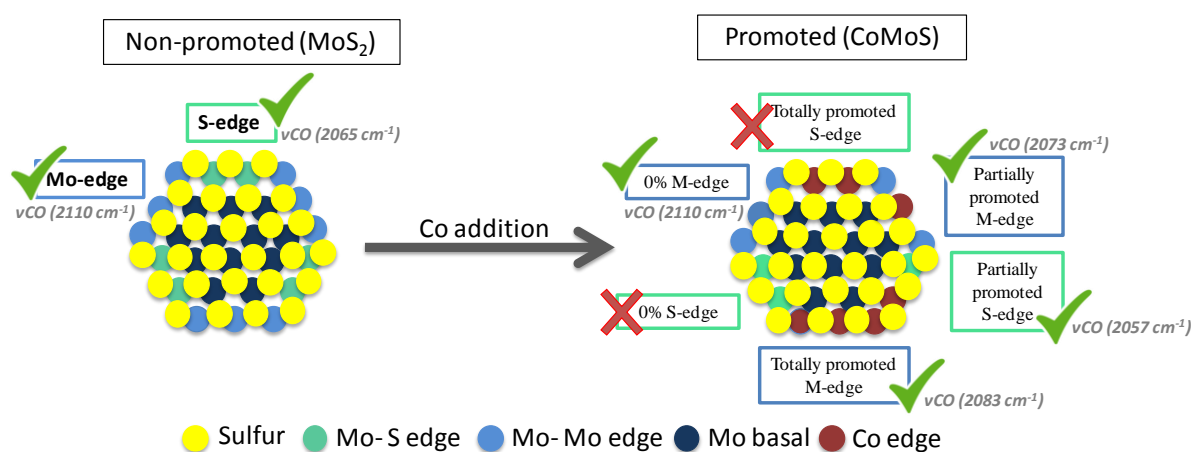


Figure 1. Scheme of the Co decoration on MoS₂ edges detected in the present work

The differentiation of S-edge and M-edge sites by IR/CO is a real step forward that opens the road to the fine characterizations of the morphology of (Co)Mo catalysts and of the various structures of CoMoS sites. These specific characterizations show that the structure of CoMoS sites strongly influences its intrinsic activities. From these data, optimized sulfided Mo catalysts are obtained when metal-support interactions are very strong (as on titania) whereas optimized CoMo catalyst required medium metal-support interaction (as on alumina).

References

1. Chen, J., Oliviero, L., Portier, X. & Maugé, F. On the morphology of MoS₂ slabs on MoS₂/Al₂O₃ catalysts: the influence of Mo loading. *RSC Adv.* **5**, 81038–81044 (2015).
2. Travert, A. *et al.* CO Adsorption on CoMo and NiMo Sulfide Catalysts: A Combined IR and DFT Study. *J. Phys. Chem. B* **110**, 1261–1270 (2006).
3. Chen, J. *Catalyse d'hydrotraitement: effet de la pression de sulfuration et d'agent chélatant sur la morphologie et la réactivité des phases sulfures.* PhD, Université de Caen (2014).

RESUME

Parmi les différentes étapes du raffinage du pétrole, l'hydrotraitement est une étape clé consistant à éliminer de la charge les hétéroatomes S, N, O, et les métaux en présence d'hydrogène. On distingue alors l'hydrodésulfuration (HDS), l'hydrodézazotation (HDN), l'hydrodéoxygénation (HDO) et l'hydrodémétallation (HDM). Les carburants obtenus après hydrotraitement doivent répondre à des normes de plus en plus sévères sur les teneurs en soufre tout en conservant leurs spécifications respectives. Le renforcement des normes ainsi que l'extraction de pétroles de plus et plus lourds nécessitent une bonne connaissance des catalyseurs industriels afin d'améliorer sélectivement leurs performances.

Les catalyseurs d'hydrotraitement associent un élément du group VI (Mo) et un élément du groupe VIII (Co) sous leur forme sulfure. Ces phases sont dispersées sur un support le plus souvent de type alumine. Le cobalt agit en élément promoteur. Le catalyseur est préparé sous la forme oxyde par imprégnation au volume poreux d'une solution d'un sel métallique par co-imprégnation suivie d'une étape de séchage et/ou de calcination. Le teneur en molybdène déposé sur alumine peut varier entre 9% et 20% MoO₃. La quantité de promoteur est généralement ajustée de manière à obtenir un rapport atomique effet de synergie, c'est-à-dire les éléments métalliques constituant la phase active induisent une activité supérieure à la somme des activités des métaux séparés. Dans le précurseur oxyde, le molybdène est sous forme MoO₃ ou MoO_x anions. Il est transformé en sulfure MoS₂ par un processus complexe à la fois de sulfuration et de réduction. Industriellement, sulfuration peut être effectuée de manière in-situ par les composés sulfurés ou de manière ex-situ. La sulfuration par un mélange H₂/H₂S n'est appliquée industriellement mais est très utilisée dans les études académiques. Les processus de sulfuration peut se résumer selon ces différentes étapes : adsorption de composés soufrés en surface, échange oxygène-soufre jusqu'à la sulfuration complète et on obtient le MoS₂ promu ou non par le cobalt. MoS₂ est la phase active des catalyseurs non promus. La structure du MoS₂ est un empilement de feuillets hexagonaux. Dans ces feuillets, l'atome de molybdène est situé au centre d'un prisme trigonal formé par les anions sulfures. De un autre côté, des catalyseurs promus sont formés par des phases actives CoMoS. Alors, le cobalt peut être présent sous 3 formes : en promotion des feuillets de MoS₂, en sulfure de cobalt Co₉S₈ ou en forme spinelle dans l'alumine, CoAl₂O₄.

Cependant, la localisation du cobalt a donné lieu au développement de nombreux modèles afin d'expliquer la particularité du site promu. Modèles géométriques de la structure du MoS₂ ont proposé que MoS₂ peut adopter différentes morphologies comme des morphologies triangulaires, hexagonales, rhomboïdes ou en chaîne. Récemment, l'observation de MoS₂ déposé sur Au (111) par microscopie à effet tunnel (STM) montre des feuillets triangulaires ou triangle tronqué en fonction des conditions de sulfuration. La modélisation moléculaire permet d'approcher la description au niveau local ou atomique de la structure. Les récents développements de techniques de modélisation moléculaire comme la théorie fonctionnelle de densité (DFT) ont été appliqués aux catalyseurs sulfures. Les feuilles de MoS₂ est alors décomposé en deux entités représentant le bord molybdène (10-10) et le bord soufre (-1010). La modélisation moléculaire permet de calculer la géométrie des surfaces thermodynamiquement stables de ces 2 bords en fonction de la température et du rapport P (H₂)/P(H₂S) de l'atmosphère environnante. Cependant, la localisation du cobalt reste difficile à simuler par les études de DFT. Bien que certaines études aient été réalisées simulant plusieurs pourcentages de promotion (50 et 100%) dans les deux sites, bord M et S. Les calculs ont montré que les sites 50% promus du bord M et 50 et 100% du bord S sont thermodynamiquement stables sur les conditions d'hydrodésulfuration indiquant que le bord S promu est légèrement plus favorisé pour la promotion. Ces résultats sont en relation avec ceux obtenus par STM, le feuillet retrouve une forme triangle tronqué par la présence de cobalt et cependant une décoration du cobalt uniquement sur les bords de type soufre. Pourtant, la connaissance de la formation des sites CoMoS est essentielle pour l'amélioration continue du catalyseur. Pour cela l'utilisation d'autres techniques pour la meilleure compréhension de ces sites. La technique de caractérisation IR/CO a récemment montré de grands résultats satisfaisants basés sur l'étude MoS₂. La méthode IR/CO a permis de distinguer Mo situé au bord M ou S et donc de prédire la morphologie du MoS₂. La distinction de Mo situé sur le bord M et le bord S par IR/CO pour les catalyseurs non promus conduit à la possibilité d'étudier l'affinité de la décoration Co sur les sites de bord M ou S. Par conséquent une série de catalyseurs non promus et promus soutenus dans trois supports différents ont été préparés et étudiés.

Ce manuscrit présente une étude approfondie des sites Mo et CoMoS de catalyseurs d'hydrotraitement de type industriel. L'objectif de ce travail était d'identifier les facteurs qui déterminent la morphologie de la phase sulfure ainsi que la formation et la structure des sites CoMoS des catalyseurs (Co)Mo supportés. L'étude a porté sur l'étude de la nature du support, l'influence de la quantité de Mo introduit et l'effet du pré-traitement (séchage seul ou suivi d'une calcination).

Les catalyseurs sous forme oxyde ont été caractérisés par spectroscopies Raman et UV-Vis. Après sulfuration, les catalyseurs ont été étudiés de manière approfondie par adsorption de CO à basse température suivie d'une spectroscopie FTIR (IR/CO). Cette technique donne des informations précises sur la nature, la structure et la quantité de sites sulfures. De plus, les données spectrales IR/CO ont été analysées par 2D-IRIS, une technique nouvellement développée au LCS. Les catalyseurs sulfure ont également été caractérisés par microscopie électronique à transmission (TEM) et testés dans la réaction d'hydrodésulfuration au thiophène (HDS).

Sur le catalyseur de Mo non-promu, l'étude du Mo déposé sur différents supports comme l'alumine, la silice (silice commerciale et MCM-41) et le TiO₂ (anatase avec une fraction de rutil, et anatase pure) indique que la force de l'interaction métal (sulfure)-support est un facteur clé. La nature du support affecte à la fois la dispersion de la phase oxyde, la morphologie de la phase sulfure ainsi que l'accessibilité des sites de bord MoS₂.

La force de l'interaction avec le support est un paramètre important même à l'état oxyde. L'étude de catalyseurs Mo supportés sur différents oxydes avec une densité de Mo constante (3 at. Mo.nm⁻²) montre la formation de cristallites de MoO₃ sur Mo/SiO₂, alors que seules des espèces polymolybdates sont formées sur Mo/Al₂O₃ et Mo/TiO₂. De même, le séchage ou la calcination influence la quantité de MoO₃ formée sur Mo/SiO₂ alors que les espèces oxydées formées sur Mo/Al₂O₃ et Mo/TiO₂ ne sont pas modifiées par le pré-traitement. Ces résultats montrent que l'interaction phase supporté – silice est faible.

L'influence de la force de l'interaction avec le support est beaucoup plus frappante sur le catalyseur sulfure. En effet, pour une densité de Mo constante (3 at Mo.nm⁻²), l'IR/CO montre que le support influence fortement le rapport entre les bords S- et les bords M-. Ce

ratio varie ainsi : $\text{Mo/SiO}_2 > \text{Mo/Al}_2\text{O}_3 > \text{Mo/TiO}_2$, et montre une modification de la morphologie des feuillets de MoS_2 . Ainsi, Mo/SiO_2 est formé par des nanoparticules MoS_2 de forme quasi hexagonale, tandis que les feuillets de MoS_2 présentent une forme triangulaire tronquée sur $\text{Mo/Al}_2\text{O}_3$ et une forme triangulaire sur Mo/TiO_2 .

L'effet de la teneur en Mo des catalyseurs supportés sur la silice et l'oxyde de titane a été étudié dans ce travail, et l'effet a aussi été étudié sur des catalyseurs supportés l'alumine dans un travail antérieur. La teneur en Mo influence aussi la morphologie des feuillets de MoS_2 des catalyseurs Mo/SiO_2 et $\text{Mo/Al}_2\text{O}_3$. A noter que les changements de morphologie sont plus importants sur silice que sur alumine. Sur les catalyseurs Mo / TiO_2 , la teneur en Mo ne modifie pas la morphologie de la phase sulfure. Cette absence de modification souligne la forte interaction entre le MoS_2 et l'oxyde de titane. Ces résultats confirment que l'importance de la force de l'interaction avec le support dans le contrôle de la morphologie de la phase sulfure.

Afin de déterminer l'influence de l'atmosphère réactionnelle sur les structure des bords des feuillets sulfures, les catalyseurs sulfurés ont été post-traités dans différentes conditions: sous H_2 pur ou sous 2% $\text{H}_2\text{S/H}_2$ à $T=623$ K. Ce dernier post-traitement est équivalent à l'atmosphère qui règne lors de la réaction d'HDS du thiophène. Sur tous les catalyseurs, ces deux post-traitements augmentent la quantité de CUS Mo. Il faut noter que la création de sites CUS est plus importante sur les bords de type M que ceux de type S. Autre point à noter, l'augmentation de CUS dépend très fortement de la nature du support, puisqu'elle est plus importante pour les phases sulfure supportée sur silice que sur l'alumine et que sur oxyde de titane. Dans ce dernier cas, la variation est quasiment négligeable. Le traitement sous 2% $\text{H}_2\text{S/H}_2$ étant représentatif des conditions de réaction, la quantité de sites et le rapport bord S-/M- mesurés dans ces conditions seront utilisés pour la comparaison avec les résultats d'HDS du thiophène.

Un parallèle apparaît entre la quantité totale de sites Mo et le vitesse de réaction en HDS. La comparaison à surface constante montre que le Mo supporté sur dioxyde de titane est le plus actif en accord avec sa plus grande quantité de sites. Pour aller plus loin l'activité intrinsèque des sites des bords M- et S- (TOF) a été calculée en considérant la quantité de chaque type de sites sur les différents catalyseurs. Premièrement, le TOF des sites S- est supérieur au TOF des sites M-. Sur les sites M-, le TOF est similaire sur les catalyseurs à base

de silice et d'alumine, mais significativement plus élevé sur les catalyseurs à base de dioxyde de titane.

On note des comportements spécifiques des catalyseurs supportés sur le dioxyde de titane: (1) la quantité élevée de sites CUS Mo comparée à la quantité de Mo exposée déduite du TEM, (2) la stabilité de la phase supportée quelque soit le prétraitement ou le post-traitement, (3) la détection presque uniquement de sites M-, (4) la valeur élevée du TOF. Toutes ces caractéristiques peuvent être expliquées par une forte interaction du MoS₂ avec le titane.

En conclusion, ces résultats montrent que la morphologie de la phase MoS₂ dépend principalement de la nature du support et de façon plus limitée des conditions de pré-traitement et de la quantité de Mo introduite.

Sur les catalyseurs promus par le Co, il est bien connu que la spectroscopie IR du CO adsorbée permet de distinguer les sites Mo non promus des sites promus. Cependant, dans le massif IR/CO généralement attribués aux sites CoMoS, trois composantes au moins peuvent être distinguées. Plusieurs questions se posent: quelle est leur attribution ? Caractérisent-elles les sites CoMoS ou des sites Mo puisque dans la même région, peut apparaître une bande CO caractéristique des sites Mo situés sur les bords S-? Aussi, afin de répondre à cette question, une nouvelle méthode de traitement des spectres appelée 2D Infrared Inverse Spectroscopy (2D-IRIS) a été appliquée. Cette méthode prend en compte les différentes énergies d'adsorption du CO. Le 2D-IRIS permet d'exclure la présence d'une bande caractéristique des sites Mo non-promus sur les bords S- dans le massif CoMoS. Grâce à cette conclusion, la question de la caractérisation IR de la localisation du promoteur Co sur les bords MoS₂ peut être abordée. Pour les trois supports, un parallèle apparaît entre le rapport bords S / bords M des catalyseurs Mo et le degré de promotion (sites CoMoS/MoS₂) des catalyseurs CoMo. Cela indique que plus le rapport des bords S / M est élevé, plus le degré de promotion est élevé. Ainsi, la présence de bords S est favorable pour ancrer le promoteur. Ceci est en accord avec les calculs DFT et les observations STM sur des catalyseurs modèles. Cependant, puisque le degré de promotion est supérieur au rapport des bords S/M des différents catalyseurs, ceci montre que le promoteur Co peu également être ancré sur les sites des bords M.

Dans la zone IR caractéristique des sites promus, trois bandes sont détectées à 2057, 2073 et 2083 cm⁻¹. La détection de ces composantes doit la présence de 3 structures de sites CoMoS différentes comme la localisation sur les bords S ou M-. En tenant compte des

fréquences prédites par le calcul DFT, de la détection des ces composants en fonction de l'introduction de Co sur MoS₂ par des méthodes CVD en utilisant Co (CO)₃NO, et de la variation de ces trois composants sur les catalyseurs CoMo déposés sur les différents supports, des attributions pour ces trois bandes ont pu être proposées. Ces bandes peuvent être attribuées aux Co sur le bord S partiellement promu (bande à 2057 cm⁻¹), au Co sur le bord M partiellement promu (bande à 2073 cm⁻¹) et au Co sur le bord M totalement promu (bande à 2083 cm⁻¹).

Les morphologies des catalyseurs promus ont pu être déduites de l'intensité des bandes caractéristiques de ces différents sites CoMoS ainsi que celle de la bande caractéristique des sites Mo sur les bords M. Il apparaît que le rapport des bords S/M des catalyseurs promus augmente un peu avec l'addition de Co par rapport au catalyseur non promu. Ce changement de morphologie avec la promotion des feuillettes de MoS₂ est en bon accord avec la prédiction de calcul DFT et l'observation STM.

Un parallèle apparaît entre la quantité totale de sites promus et la vitesse de réaction en HDS du thiophène mais la relation n'est pas linéaire. Il est probable que les différents sites CoMoS présentent une activité intrinsèque différente. Ainsi, il apparaît que les sites CoMoS situés sur les bords M partiellement promus (caractérisés par une bande à 2073 cm⁻¹) présentent une activité par site nettement plus élevée que les deux autres sites CoMoS.

En conclusion, la détection spécifique par IR/CO des sites des bords S et des bords M a permis un véritable pas en avant qui ouvre la voie à des caractérisations fines de la morphologie des catalyseurs (Co)Mo et des différentes structures des sites CoMoS. Ces caractérisations ont permis de mettre en évidence que la structure des sites CoMoS influence fortement leurs activités intrinsèques. Ces résultats montrent que les catalyseurs Mo auront des performances maximum lorsque l'interaction métal-support est très forte (comme sur l'oxyde de titane) alors que pour le catalyseur CoMo, une activité maximum sera obtenue lorsque l'interaction métal-support est intermédiaire (comme sur alumine).

